A Nonlinear Neural Network-Based Model Predictive Control for Industrial Gas Turbine

by

Ibrahem Mohamed Atia IBRAHEM

THESIS PRESENTED TO ÉCOLE DE TECHNOLOGIE SUPÉRIEURE
IN PARTIAL FULFILLMENT FOR THE DEGREE OF
DOCTOR OF PHILOSOPHY
Ph.D.

MONTREAL, OCTOBER 22, 2020

ÉCOLE DE TECHNOLOGIE SUPÉRIEURE
UNIVERSITÉ DU QUÉBEC

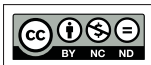

BOARD OF EXAMINERS

THIS THESIS HAS BEEN EVALUATED

BY THE FOLLOWING BOARD OF EXAMINERS

Mrs. Ouassima Akhrif, Thesis Supervisor
Department of Electrical Engineering, École de technologie supérieure

M. Hany Moustapha, Co-supervisor
Department of Mechanical Engineering, École de technologie supérieure

M. Pierre Bélanger, President of the Board of Examiners
Department of Mechanical Engineering, École de technologie supérieure

Mrs. Lyne Woodward, Member of the jury
Department of Electrical Engineering, École de technologie supérieure

M. David May, External Independent Examiner
Siemens Energy Canada Limited

M. Guchuan Zhu, External Examiner
Department of Electrical Engineering, Ecole Polytechnique de Montreal

THIS THESIS WAS PRESENTED AND DEFENDED

IN THE PRESENCE OF A BOARD OF EXAMINERS AND THE PUBLIC

ON OCTOBER 15, 2020

AT ÉCOLE DE TECHNOLOGIE SUPÉRIEURE

ACKNOWLEDGEMENTS

The present document, resulting of three years of research, would not have been possible without the help, encouragements and support of many persons. I thank all of them and I present them all my gratitude.

Firstly, I would like to acknowledge my direct supervisors Professor Ouassima Akhrif and Professor Hany Moustapha for their enthusiasm, inspiration, and huge efforts to explain things clearly and simply. I would have never finished this thesis without their constant support, encouragement, and stimulating advice. All of these helped me a lot in maintaining my confidence to continue my research. I would also like to thank the project leader Mr. Martin.Staniszewski at Siemens Energy Canada Limited for helping and supporting me. He generously gave much time and effort to help me.

I would like to thank the Egyptian Ministry of defense for funding me and École de technologie supérieure for accepting me in its graduate program and motivating me to do this work. Also, I thank Siemens Energy Canada Limited R & D center for providing me the opportunity to use their products to perform my simulations and helping me to fill out the gap between academia and industry. I cannot end without thanking my engineering friends for sharing their knowledge regarding the electric department.

Finally, My deepest thanks to who enlighten my life with happiness, my lovely wife Reham and my son Asser for their love, patience, encouragement, and support. I am indebted to my mother, my father, and my sisters for their support that they offered me over my studying years. And here in, I wish my sister Ghada to be proud of me.

Commande prédictive non linéairebasée sur un réseau neuronal pour une turbine à gaz industrielle

Ibrahem Mohamed Atia IBRAHEM

RÉSUMÉ

Les turbines à gaz sont largement utilisées actuellement dans l'aviation, les applications pétrolières et gazières et la production d'électricité. Avec cette utilisation croissante dans une large gamme d'applications, les turbines à gaz sont conçues pour fonctionner dans une large plage de fonctionnement. Typiquement, la température ambiante peut varier considérablement d'une chaude journée d'été à une froide nuit d'hiver. Aussi, différents types de carburant peuvent être utilisés. De plus, les performances d'un turbomoteur se détériorent à l'usage en raison de la dégradation des composants provoquée par l'érosion et la corrosion. Ces exigences pour garantir des niveaux de performance élevés tout en maintenant la stabilité et un fonctionnement sûr avec un coût global minimal imposent de grands défis à la conception du système de commande. Dans cette thèse, de nouvelles approches pour la modélisation de turbines à gaz et la conception de contrôleurs avancés multivariables sont étudiées. Une approche de contrôle prédictif non linéaire (NMPC) basée sur un ensemble de réseaux neuronaux récurrents (NN) est utilisée pour atteindre les objectifs de contrôle d'un moteur à turbine à gaz aérodérivé à trois bobines Siemens SGT-A65 utilisé pour la production d'électricité. Une nouvelle méthode d'ensemble est proposée, qui aboutit à un modèle NN adaptatif. Les résultats de la simulation montrent une amélioration de la précision et de la robustesse en utilisant l'approche de modélisation proposée. En outre, un autre gain important est le temps d'exécution très faible (40,5 μs), qui peut permettre de nombreuses applications en temps réel qui nécessitent une conception de contrôle basée sur un modèle.

Pour la commande en boucle fermée, un contrôleur prédictif non linéaire (NMPC) à entrées multiples et sorties multiples (MIMO) et avec contraintes est développé sur la base de l'algorithme de contrôle prédictif généralisé (GPC) en raison de sa capacité à gérer les problèmes MIMO dans un même algorithme. Dans ce contrôleur, une nouvelle approche de compromis entre l'utilisation d'un modèle non linéaire et des approches de linéarisation successives est utilisée afin de réduire l'effort de calcul et en même temps d'augmenter la robustesse du contrôleur. L'estimation des réponses libres et forcées du GPC est réalisée sur la base du modèle NN de la turbine à chaque instant d'échantillonnage. En outre, la procédure de programmation quadratique (QP) de Hildreth est utilisée pour résoudre le problème d'optimisation quadratique du contrôleur NNGPC, qui offre simplicité et fiabilité dans la mise en œuvre en temps réel. Une comparaison entre les performances du contrôleur proposé (NNGPC) et du contrôleur actuel du moteur SGT-A65 (le contrôleur min-max) est effectuée. Les résultats de la simulation montrent que le NNGPC donne des réponses de sortie supérieures avec moins de comportement oscillatoire et des actions de contrôle plus douces aux variations soudaines de la charge électrique que celles observées pour le contrôleur min-max existant. De plus, le contrôleur NNGPC nécessite moins d'effort de contrôle que le contrôleur min-max pour atteindre les objectifs souhaités. La minimisation de l'effort de commande a des répercussions pratiques importantes car elle

réduit l'intensité de l'usure mécanique des actionneurs, ce qui conduit à une augmentation de la sécurité fonctionnelle, de la durée de vie et de l'économie du processus contrôlé. De plus, le temps de calcul nécessaire pour résoudre le problème d'optimisation était suffisamment plus rapide que la fréquence d'échantillonnage, ce qui rend possible une implémentation en temps réel du contrôleur NNGPC.

Mots-clés: Modèle NARX, Turbine à gaz, Modélisation, Réseaux de neurones, Ensemble, GPC, NMPC, NNGPC.

A Nonlinear Neural Network-Based Model Predictive Control for Industrial Gas Turbine

Ibrahem Mohamed Atia IBRAHEM

ABSTRACT

Gas turbines are now extensively used in aviation, oil and gas applications and power generation. With this increasing use in a diverse range of applications, gas turbine engines are designed to operate in a wide operating envelope. Typically, the ambient temperature can vary substantially from a hot summer day to a cold winter night. In addition, different fuel types may be used. Furthermore, the performance of a turbine engine deteriorates with use because of component degradation caused by erosion and corrosion. These requirements for guaranteed high performance levels while maintaining stability and safe operation with minimum overall cost impose severe challenges on control system design. In this dissertation, new approaches for gas turbine engine modelling and multivariable advanced controller design are investigated. A nonlinear model predictive control (NMPC) approach based on an ensemble of recurrent neural networks (NN) is utilized to achieve the control objectives for a Siemens SGT-A65 three spool aeroderivative gas turbine engine used for power generation. A novel ensemble method is proposed, which results in an adaptive NN model. The simulation results show improvement in accuracy and robustness by using the proposed modelling approach. Also, another important gain is the very rapid execution time (40,5 μs), which can support many real time applications that require model-based control design.

For the closed-loop control, a constrained multi-input multi-output (MIMO) nonlinear model predictive controller (NMPC) is developed based on the generalized predictive control (GPC) algorithm because of its ability to handle MIMO problems in one algorithm. In this controller, a novel trade-off approach between the usage of a non-linear model and successive linearization approaches is used in order to reduce the computation effort and at the same time increase the robustness of the controller. Estimation of the free and forced responses of the GPC are performed based on the NN model of the plant at each sampling time. In addition, the Hildreth's Quadratic Programming (QP) procedure is utilized to solve the quadratic optimization problem of the NNGPC controller, which offers simplicity and reliability in real-time implementation. A comparison between the performance of the proposed controller (NNGPC) and the current controller of the SGT-A65 engine (min-max controller) is performed. The simulation results show that the NNGPC has demonstrated superior output responses with less oscillatory behavior and smoother control actions to sudden variations in the electric load than those observed in the existing min-max controller. Furthermore, the NNGPC controller requires less control effort than the min-max controller to achieve the desired objectives. The minimization of control effort has significant practical repercussions because it reduces the intensity of mechanical wear of the actuators, which leads to an increase in the functional safety, lifetime, and economics of the controlled process. In addition, the computation time required to solve an optimization problem was sufficiently shorter than the sampling period which makes a real-time implementation of the NNGPC controller possible.

Keywords: NARX model, Gas turbine, Modelling, Neural Networks, Ensemble, GPC, NMPC, NNGPC.

TABLE OF CONTENTS

LIST OF TABLES

Page

LIST OF FIGURES

Page

LIST OF ABREVIATIONS

ADGTE	Aero-derivative gas turbine engine
GTE	Gas turbine engine
DLE	Dry low emission
LPC	Low pressure compressor
IPC	Intermediate pressure compressor
HPC	High pressure compressor
LPT	Low pressure turbine
IPT	Intermediate pressure turbine
HPT	High pressure turbine
LP	Low pressure
IP	Intermediate pressure
HP	High pressure
PT	Power turbine
CC	Combustion chamber
ECS	Engine control system
NGV	Nozzle guide vanes
OGV	outlet guide vane
CMF	Constant mass flow iterative method
ICV	Inter-component volume method

NN	Neural network
ANN	Artificial neural network
ARX	Autoregressive with exogenous inputs
NARX	Non-linear autoregressive with exogenous inputs
trainbr	Bayesian regularization training algorithm
trainlm	Levenberg-Marquardt training algorithm
trainscg	Scaled conjugate gradient training algorithm
RUL	Remaining useful life
MPC	Model predictive control
LMPC	Linear model predictive control
NMPC	Non-linear model predictive control
NLP	Non-linear programming
GPC	Generalized predictive control
NNGPC	Neural network generalized predictive control
SISO	Single-input single-output
MIMO	Multiple-input multiple-output
MISO	Multiple-input single-output
SQP	Sequential quadratic programming
HDWM	Hybrid dynamic weighting method
BEM	Basic ensemble method

DWM	Dynamic weighting method
QP	Quadratic programming
PI	Proportional plus integral
CPU	Central processing unit

LISTE OF SYMBOLS AND UNITS OF MEASUREMENTS

WF	Fuel flow in ppm
LPBOV	Low pressure bleed-off valves position %
VIGV	Variable inlet guide vanes position %
IPVSV	Variable stator vanes position %
IPBOV	Number of opened intermediate pressure bleed off valves
HPBOV	Number of opened High pressure bleed off valves
NOx	Nitrogen oxide
M	Mach number
B	Bleed fraction
LHV	Fuel heating value
N	Relative spool speed
T	Stagnation temperature
P	Stagnation pressure
W	Work
W_T	Work of turbine
W_C	Work of compressor
PW_{dem}	Power demand
U	Internal energy
f	Frequency

H	Altitude
J	Polar moment of inertia
c_{p_a}	Specific heat at constant pressure of air
c_{p_g}	Specific heat at constant pressure of gas
c_v	Specific heat at constant volume
ΔPR_{in}	Inlet pressure losses
ΔPR_{CC}	Combustor pressure losses
ΔPR_{ex}	Exhaust nozzle pressure losses
γ_a	Specific heat ratio of air
γ_g	Specific heat ratio of combustion gas
R	Universal gas constant
β	Beta value
η_{th}	Thermal efficiency
θ	Corrected temperature
δ	Corrected pressure
π	Pressure ratio
$m^{\bullet}$	Mass flow rate
d	Droop percentage of the engine generator
$\hat{y}$	The predicted output
w	The reference output

u	The Manipulated input
N_2	The maximum prediction horizon
N_1	The minimum predictive horizon
N_u	The control horizon
T_s	The sampling time
Λ	The control-weighting factor
λ	The Lagrangian multiplier
$\boldsymbol{y}_{constr}$	The constraint output vector
y_{contr}	The controlled output vector
kg	Kilogram
s	Second
ms	Milliseconds
K	Kelvin
MW	Mega watt
ppm	Parts per million
pph	Pounds per hour
rpm	Revolution per minute
Hz	Hertz
$T^{\bullet}$	The rate of change of temperature
$P^{\bullet}$	The rate of change of pressure
$U^{\bullet}$	The rate of change of internal energy

INTRODUCTION

Gas Turbine is a complex system with highly nonlinear dynamics and a large operating range. Gas turbine engines and their related technologies represent one of the most efficient forms of propulsion and power generation, with applications in various areas: as prime movers in planes, in power plants for electricity generation, ground-based vehicle and marine ships for propulsion. Increasing demands for gas turbine engines usage in many fields have caused different design requirements such as, improving performance, more efficiency, reliability, and the reduction of development costs and time. As a result, the cost of research, development and implementation of new technology in gas turbine systems is becoming prohibitively expensive. Moreover, one of the main reasons of this high development cost is the need to perform many hardware tests of the physical engine. Therefore, the needs for exploring the performance of gas turbine engines to reduce the initial cost of designing new engines and improve the performance has led to the raise of research on modelling and simulation of gas turbine engines. Effective simulation models can be developed without any prototypes being needed at the very early stages of the design. In addition, modelling of gas turbine engines can be used in the design of engine's controller. Based on the fact that gas turbine engines are highly non-linear and operate very close to their thermal and mechanical limits, many layers of complexity are added to the controller design operation which emphasizes the need for sophisticated control systems. Also, modifications to the control system become the desired path in the development field of gas turbines because it is easier to change the control logic and the corresponding code rather than to redesign, re-manufacture, and reinstall new engine components. The objective of the control system is to achieve good thrust or shaft power response qualities while maintaining critical engine outputs within safety limits. The design of controllers capable of delivering this objective represents a challenging problem (Richter, 2011).

Problem Statement

Gas turbine engine, as mentioned above, is a highly non-linear plant due to the large range of operation conditions and the power levels experienced during a typical mission. Also gas turbine engine operation is restricted due to the following constraints as shown in Figure 0.1.

1. Mechanical limitation.
2. Aerodynamic limitation.
3. Thermal limitation.
4. Flow limitation.

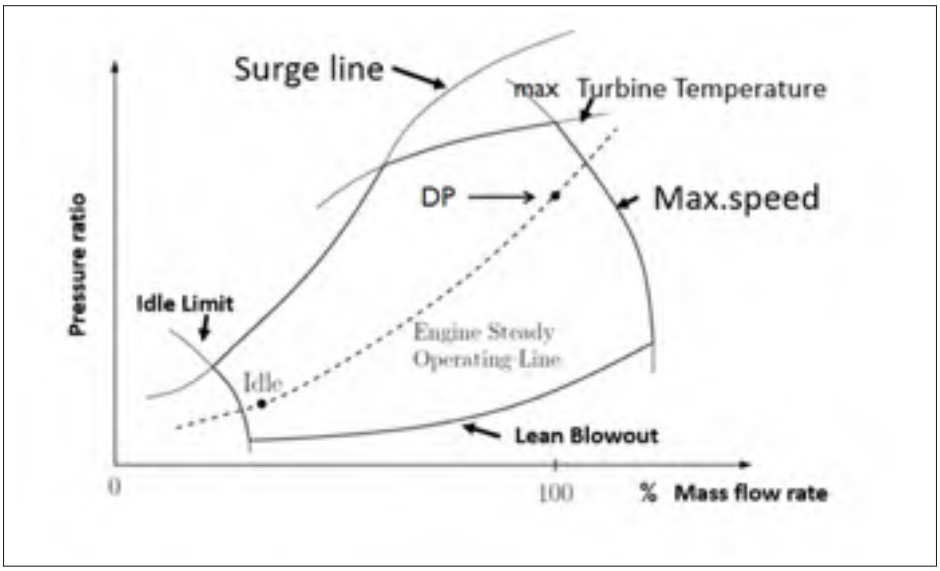

Figure 0.1 Gas turbine engine operation envelope

Based on gas turbine engine operating envelope, there are many challenges in the area of gas turbine engine's controller design to ensure the safe operation of the engine and at the same time get the maximum performance. **The first challenge** is the change of the surrounding conditions. The performance of the gas turbine engine is dependent on the mass of air entering

the engine. At a constant speed, the compressor pumps a constant volume of air into the engine with no regard for air mass or density. If the density of the air decreases, the same volume of air will contain less mass, so less power is produced. If air density increases, power output also increases as the air mass flow increases for the same volume of air. Atmospheric conditions affect the performance of the engine since the density of the air will be different under different conditions [-60^oC to 40^oC air temperature]. On a cold day, the air density is high, so the mass of the air entering the compressor is increased. As a result, higher horsepower is produced. In contrast, on a hot day, or at high altitude, air density is decreased, resulting in a decrease of output shaft power.

The second challenge is quick engine start. Quick engine starts and rapid accelerations are also desirable. To provide higher power with low specific fuel consumption and acceptable starting and acceleration characteristics, it is necessary to operate as close to the surge region as possible. To prevent compressor stall or surge, fuel flow must be properly metered during the start and acceleration cycle of any gas turbine engine. To accomplish this, we need a very accurate engine controller.

The third challenge: On the emissions side, the challenge is to increase turbine inlet temperatures while at the same time reduce peak flame temperature in order to achieve lower NOx emissions and meet the latest emission regulations. In addition, reliable fuel switching capabilities in industrial gas turbine engines should be taken in consideration.

The fourth challenge: With respect to components lifetime, and performance degradation, there are big challenges in this area because customers need to increase components lifetime in order to decrease the cost but at the same time ensure the safe, reliable and high performance of the engine operation. Therefore, these requirements put more complexity on the design operation of the gas turbine engine controller. In addition, every gas turbine engine has its own signature even for the same engine's configuration over time. The gas turbine engine

controller should take into consideration the effect of performance degradation due to repair and maintenance of the engine.The controller must therefore be re-tuned after any maintenance operation to recover the engine performance. Customers needs this tuning operation of the engine controller to be automated to save time and money and have high engine performance at the same time.

The fifth challenge: The engine control system must handle some engine monitoring functions. Traditionally, engine monitoring functions have been a part of the modern control system functionality. To monitor engine health state and maintain high engine availability, an engine monitoring system must be able to detect incipient failures and predict how much longer the engine can operate with the "known" degradation before the failure becomes so severe that the engine performance becomes unacceptable (Jaw & Mattingly, 2009).

The concept of a more intelligent gas turbine engine aims at actively controlling engine operation to increase efficiency, durability and safety, while maintaining the high level of reliability required for aeronautic and industrial applications. Today engine manufacturers are investigating the potential of intelligent technologies for the next engine generation to meet the previous challenges. The design of controllers capable of satisfying the previous requirements represents a challenging problem (Figure 0.2) ; classical feedback is no longer suitable as a paradigm for the development of advanced propulsion control concepts.

Research objectives

The research project is based on Siemens requirements, which include:

1. Real-time model based control.

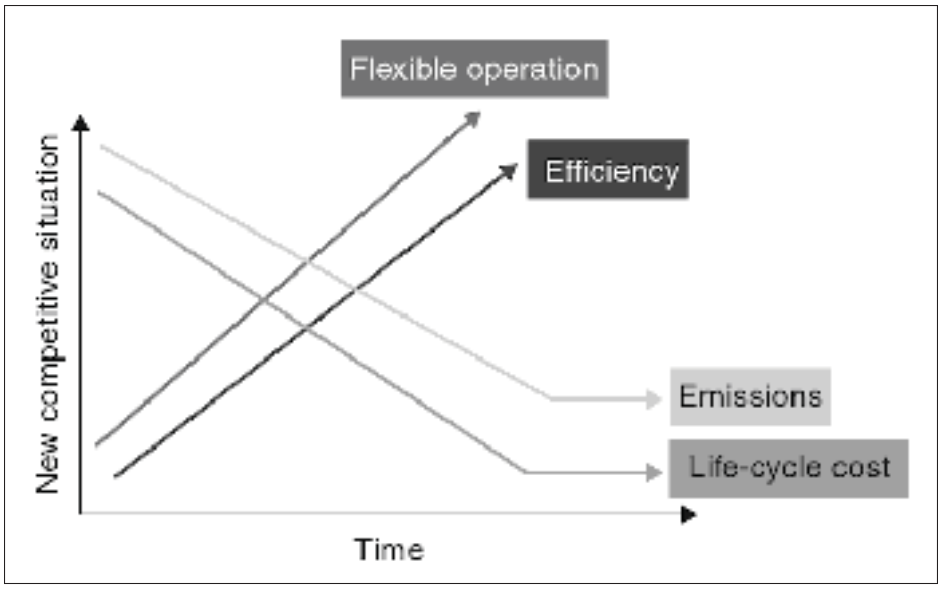

Figure 0.2 New competitive area of gas turbine engine control system

Run good fidelity transient thermodynamic models of its GT in a real-time machine, which is to be connected in real-time to the engine controller in order to improve overall reliability (soft sensors) and also open new possibilities with model based control.

2. Machine learning and physics based hybrid models.

   Couple physics based thermodynamic models with AI/machine learning in order to optimize their fidelity (self-tuning) and explore letting AI/machine learning algorithms take control over portions of the engine to optimize performance and emissions.

We can see that Siemens's objectives are to address the above five challenges. Therefore, we can summarize our research objective by the following points:

- **Objective (1)**: Demonstration of the capability of data based model approach in capturing complex non-linear dynamics of gas turbines.

- **Objective (2)**: Development of advanced controller based on good fidelity transient models of Gas Turbines (GT) in order to improve the performance and overall reliability of the machine.
- **Objective (3)**: Implementation of these benefits in real time using working prototypes of Siemens GT and their edge-computing platform.

Methodology

Different approaches are used and proposed throughout this thesis. In the following, the main methodologies are categorized:

1. To address objective 1, Chapter 3 presents a novel data-driven neural networks based model approach, which is used for modelling of a three-spool aero-derivative gas turbine engine (ADGTE) used for power generation during its loading and unloading conditions. An ensemble of MISO NARX models is used to develop this model in MATLAB environment using operational closed-loop data collected from Siemens (SGT-A65) ADGTE. The following procedure is used during the modelling operation:
    a. Data preprocessing and estimation of the order of these MISO models were performed.
    b. A computer program code was developed to perform a comparative study and to select the best NARX model configuration, which can represent the system dynamics.
    c. The most accurate MISO-NARX model with minimum *RMSE* during testing operation is selected.
    d. A homogeneous ensemble for each output parameter of the engine is generated based on the best selected structure of the MISO-NARX model from the last step, and diver-

sity among them is ensured by altering the training datasets which represent different operation conditions.

e. The major challenge of the ensemble generation is to decide how to combine results produced by the ensemble's components. In this study, a novel hybrid dynamic weighting method (HDWM) is proposed. The verification of this method was performed by comparing its performance with three of the most popular basic methods for ensemble integration: basic ensemble method (BEM), median rule, and dynamic weighting method (DWM).

f. Finally, the generated ensembles of MISO NARX models for each output parameter were evaluated using unseen data (testing data).

2. To address objective 2, Chapter 4 presents a novel approach to implement the constrained MIMO NMPC based on neural network model. The implementation of NMPC of ADGTE in real time has two challenges: Firstly, the design of an accurate non-linear model which can run many times faster than real time. Secondly, the usage of a rapid and reliable optimization algorithm to solve the optimization problem in real time. To solve these issues, the following approaches are proposed:

a. The NN model of the engine obtained using methodology 1 presented above was used as a base model of the NMPC to predict the process output. As shown in the results from Step 1-f of methodology 1, the ensemble of MISO-NARX models can represent the ADGTE during the full operating range with good accuracy even with different input scenarios from different operation conditions. This proves the high generalization characteristic of the ensemble. Also, another important gain was the very low execution time, which can support many real time applications like model based controller design.

b. A constrained MIMO NMPC is developed based on the generalized predictive control (GPC) algorithm because of its simplicity, ease of use, and ability to handle problems in one algorithm. The usage of a non-linear model within GPC changes the optimization problem from a convex quadratic problem to a nonconvex non-linear one. As a consequence of that, there is no guarantee that the global optimum can be found especially in real-time control when the optimum solution has to be obtained in a prescribed time. To overcome this issue, a novel trade-off approach between the usage of a non-linear model and successive linearization approaches is used in order to reduce the computation effort and at the same time increase the robustness of the controller. Estimation of the free and forced responses of the GPC are performed based on the NN model of the plant each sampling time. It reduces the neural network generalized predictive control (NNGPC) optimization problem to a linear optimization problem at each sampling step. Therefore, the optimization problem can be solved using quadratic programming which will improve the computation time and reliability of the solution.

c. The Hildreth's Quadratic Programming (QP) procedure is utilized to solve the quadratic optimization problem of the NNGPC controller, which offers simplicity and reliability in real-time implementation. The maximum number of iterations within this algorithm is calculated by trial and error and is limited to 100 iterations to avoid increasing of computation time. This implies that in some cases the optimum solution may not be reached and the algorithm will use a suboptimal solution.

d. The NNGPC tuning parameters have a great effect on the performance and computation effort of the controller. The computation effort decreases with the decrease in the prediction horizon. However, the response speed and the computation effort increase with increasing prediction horizon. Consequently, a trade-off is required to find the

effective values of the tuning parameters. In this study, a trial and error method is employed to find the best values of the tuning parameters.

3. To address objective 3, Chapter 5 presents a comparison between the performance of the NNGPC controller developed in this study and the existing min-max controller of the engine and is performed to demonstrate the effectiveness of this advanced controller. This test is performed in MATLAB/Simulink environment. As a result of the current epidemic (Covid-19) situation, implementation of the NNGPC controller in real time using working prototypes of Siemens GT and their edge-computing platform is replaced by validation in MATLAB/Simulink environment using experimental data.

Thesis Contribution

Guided by the research objectives and using the methodologies proposed above, this thesis presents the following important and novel contributions:

1. Proposing a novel methodology for the development of data driven based model of ADGTE, in order to simulate the dynamic performance of the ADGTE during the full operating range in real time. Inspired by the way biological neural networks process information and by their structure which changes depending on their function, MISO NARX models with different configurations were used to represent each of the ADGTE output parameters with the same input parameters.

2. Proposing a novel approach for the real time performance prediction of ADGTE through system identification using ensemble methods.

3. Proposing a novel hybrid dynamic weighting method (HDWM) to combine results produced by the ensemble's components.

4. Proposing a novel approach to implement the constrained MIMO NMPC based on ensemble of neural network models, in order to control an ADGTE during its loading and unloading conditions.

5. Proposing a novel method to estimate the free and forced responses of the GPC based on the NN model of the plant each sampling time. It reduces the NNGPC optimization problem to a linear optimization problem at each sampling step and improves the computation time and reliability of the solution.

6. Using Hildreth's quadratic programming algorithm to solve the quadratic optimization problem within the NNGPC controller, which offers simplicity and reliability in real-time implementation. Furthermore, Hildreth's method may be useful to implement on non-PC platforms like programmable logic controllers or embedded machine which do not support linear algebra libraries.

Outline of the thesis

This thesis consists of five Chapters. **Chapter 1** presents the basic aero-thermodynamic principles of gas turbines in general, and of ADGTEs in particular. It also includes the mathematical model of a three spool SGT-A65 Siemens ADGTE used for power generation. **Chapter 2** presents a comprehensive overview of the most significant researches in the field of modelling, simulation and control of ADGTEs. It covers both physics based and data driven based models of ADGTEs. In addition, it presents a survey of the historical development of GTE control and the most significant publications in the field of advanced controller design for industrial GTEs. In **Chapter 3**, a novel data-driven neural networks based model approach is used for modelling of a three-spool aero-derivative gas turbine engine (ADGTE) used for power generation during its loading and unloading conditions. An ensemble of MISO NARX models is used to develop this model in MATLAB environment using operational closed-loop data collected

from Siemens (SGT-A65) ADGTE. **Chapter 4** provides a novel approach for the design of a constrained MIMO NMPC based on neural networks. **Chapter 5** presents the development of NNGPC controller for the three spool SGT-A65 ADGTE based on ensembles of MISO NARX models of that engine. Finally, the conclusion and suggestions for future work are presented at the end of the thesis.

CHAPTER 1

GAS TURBINE - OVERVIEW

1.1 Introduction

This chapter provides an overview of gas turbine engine technology and principle of operation with reference to several research publications in this field. Firstly, the basic aero-thermodynamic principles of gas turbines in general and in particular that of ADGTEs are introduced. This includes the mathematical model of Siemens SGT-A65 three spool ADGTE used for power generation.

1.2 Gas turbine principle of operation

Gas turbine is a type of internal combustion engine, which converts chemical energy to mechanical work by rotating shafts in power generation plants or thrust for propulsion. The thermodynamic working cycle for the GTE is based on Brayton cycle, which consists of four processes, including compression, heat addition, expansion and heat rejection as shown in Figure 1.1 .

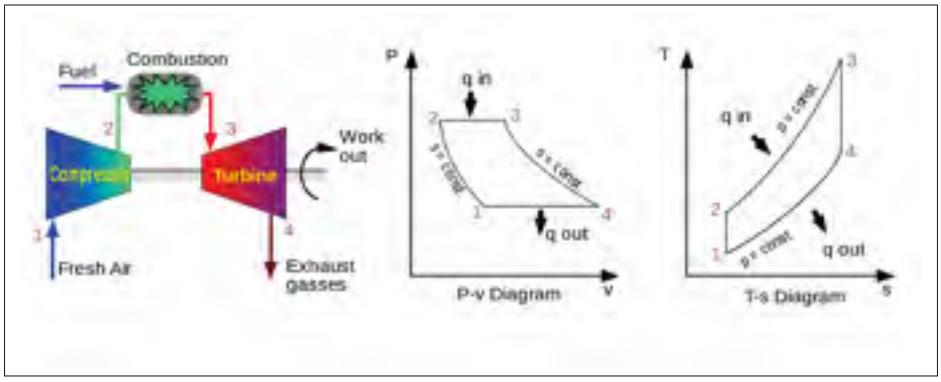

Figure 1.1 Gas turbine cycle and $T-s$ and $p-V$ diagram for Brayton cycle
Taken from Asgari & Chen (2015)

Gas turbine engines consists of three main components, compressor, combustion chamber, and turbine. The set of these components is called engine core or gas generator. As shown in Figure 1.2, air from intake enters the compressor and air is compressed through passing the compressor. Then, the hot and compressed air enters the combustor. In combustor, fuel is mixed with air and ignited. The hot gases that are the product of combustion are forced into the turbine that provides the required energy for rotation of compressor and other auxiliary systems that need mechanical power. In 1930, Sir Frank Whittle was awarded his first patent for using a gas turbine to produce a propulsive jet. Sir Frank Whittle made the first ground run of his W.1 (Figure 1.3) engine in April 1937 (Royce, 2015).

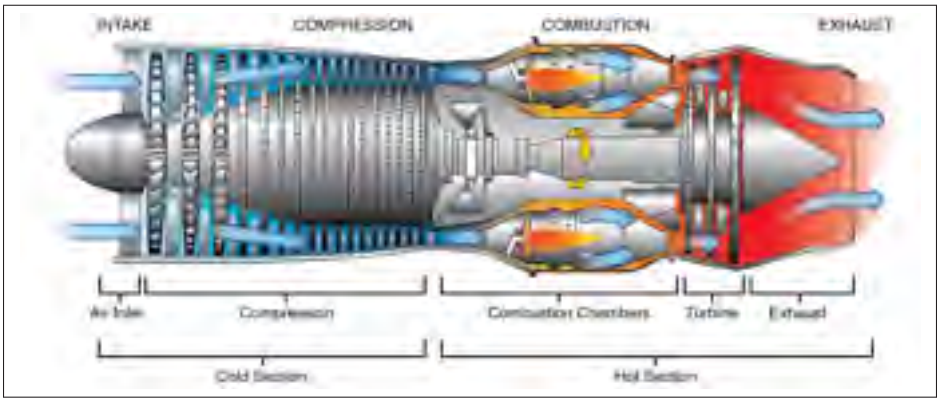

Figure 1.2 Gas turbine engine components
Taken from Administration (2011)

Gas turbine engines can be classified into two main types, aero-gas turbine engines and stationary (or industrial) GTEs. In aero-gas turbines, gas turbine is used as propulsion system to generate thrust and move an airplane through air. There exist four types of aero-gas turbine engines: Turbojet, Turbofan, Turbo shaft and Turboprop engine as shown in Figure 1.4. In stationary gas turbines, gas turbine is used as prime mover to generate a mechanical power required to rotate electrical generator, pump or compressor. If the main shaft of the stationary gas turbine is connected to an electrical generator (i.e. constant speed operation of the load), it can be used to produce electrical power. On the other hand, if the main shaft of the stationary gas turbine is connected to pump or process compressor (where the speed of the driven equipment

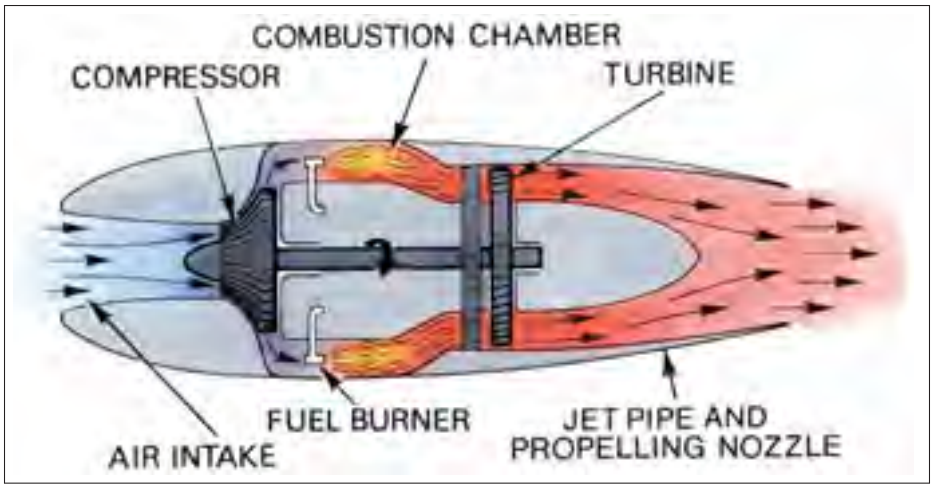

Figure 1.3 A Whittle-type turbo-jet engine
Taken from Royce (2015)

can vary with load), it can be used in mechanical drive applications (pumping applications for gas and oil transmission pipelines). There exist two big markets for stationary gas turbines (Effiom *et al.*, 2017). One for heavy duty gas turbines (100-570 MW output power and 30 - 46 % efficiency) designed for land based applications and found in large power generation units. The other is aero derivative gas turbine engines (up to 200 MW output power and 35-45% efficiency) which characterized by its light weight and compact size.

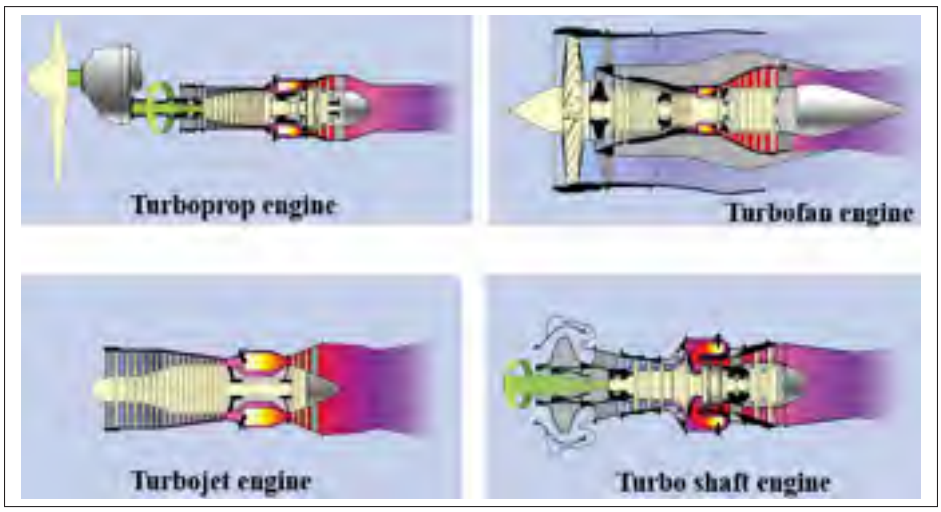

Figure 1.4 Types of gas turbine engines

1.3 Aero-derivative gas turbine engine

The ADGTEs were created from aero-gas turbine engines, which give them lighter weight, faster response and a smaller footprint compared with their heavy duty GTE counterparts. They can operate on a very wide range of fuels (natural gas and liquid fuel) with low NOx emissions (below 25 ppm) using DLE combustors or water injection (Gülen, 2019). They are usually offered as packaged units with prefabricated accessory modules for rapid installation. Their modular design also enhances their operability and maintainability. ADGTEs are often seen as a good choice in smaller-scale (up to 200 MW) energy generation.

The conversion from aero GTE to ADGTE is accomplished simply in a single shaft GTEs by replacing the nozzle with a free turbine, for example the Rolls-Royce Avon (Fletcher, 1963). In two shaft turbofan GTEs, the conversion operation includes removal of the fan, modification of the LPC to overtake the duty of the removed fan, modify the LPT to drive the modified LPC, and add a new power turbine as shown in Figure 1.5, for example the LM 5000 ADGTE based on the CF6-50 turbofan GTE (Haaser & Casper, 1991). However, the conversion of a big three shaft turbofan GTE has followed another approach. In this approach, the intermediate pressure and high pressure cores are retained, the LPC is redesigned (essentially taking the place of fan root and the original LPC), and a new LPT is redesigned to act as a drive for the new LPC and the load (Horlock, 1997). The three shaft Siemens SGT-A65 ADGTE which was derived from Rolls Royce RB211 Trent 60 represents an example to this approach.

As can be seen, the objective of the conversion operation is to keep as high commonality with the original aero GTE. This will minimize the number of parts that need to be redesigned and hence reduce the cost of conversion. In addition, less modification from the parent engine means less conversion time, which may accelerate the supply chain and benefits both the manufacturer and customers.

The gas generator of ADGTE generates a high-energy gas stream that can be used to provide shaft power which is determined by fuel flow and the management of airflow through the compressor stages. The engine control system must ensure that the desired power output is

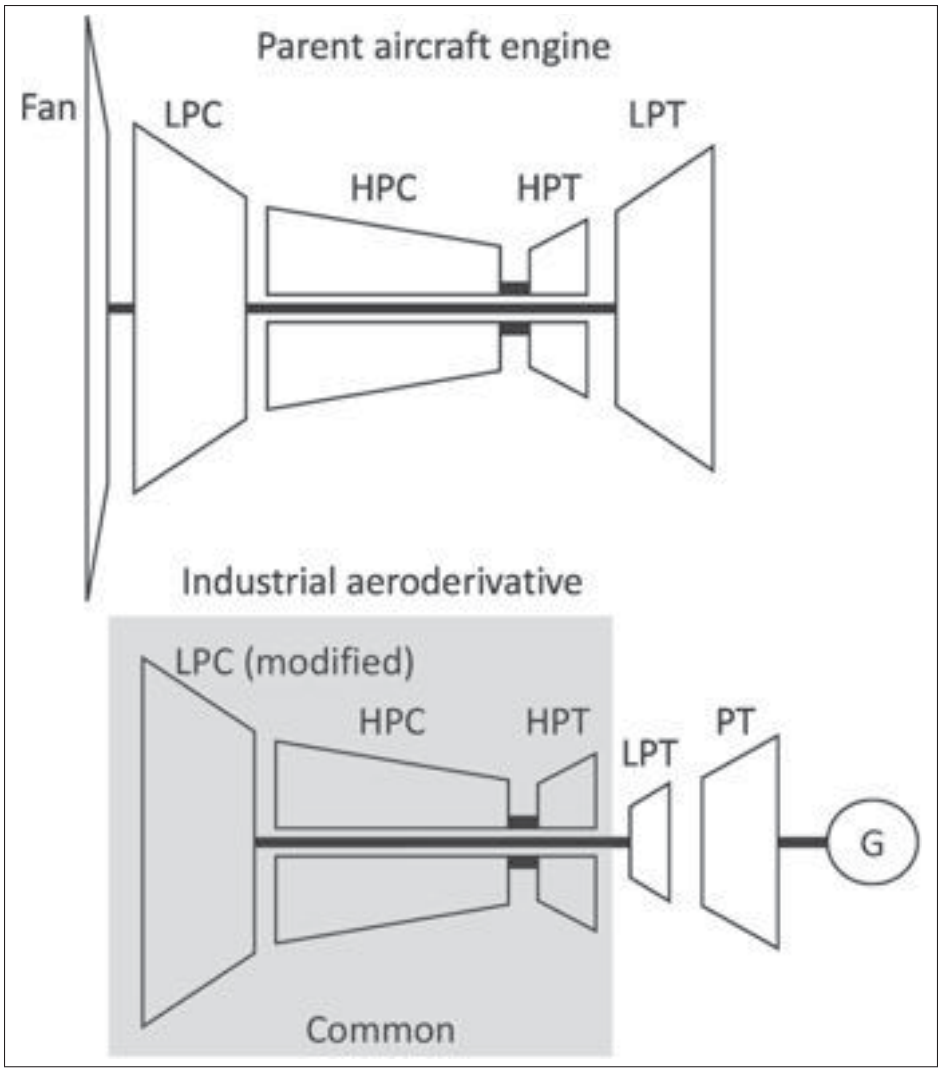

Figure 1.5 Turbofan engine and its aero derivative engine
Taken from Gülen (2019)

achieved. However, the engine control system must also protect the engine from exceeding any design limits under both dynamic and steady-state conditions throughout the operational envelop. These limits include component speeds, temperatures and operating regions which can result in compressor surge. The control strategy normally involves a set point and the control system drives the engine towards the set point. There are two types of controls in ADGTE (Gülen, 2019):

- Speed control (governor).

- Temperature control.

A speed control system can operate in either the isochronous mode or the droop mode. In general, droop mode is applicable to operations when the engine is connected to a grid. On the other hand, isochronous mode is applicable when the engine is not connected to the grid and operates in an isolated or islanded mode (Nguyen, 2000). In the isochronous mode, the control system maintains a constant reference speed regardless of load. When a load change occurs, there is a momentary change in speed during the transient, but the speed will always return to the same reference speed value as shown in Figure 1.6. On the other hand, in the droop mode the reference speed varies with load. Again, during transient conditions, there will be momentary speed change, but after the transient the speed will settle at a new reference speed value determined by the droop % of the generator. The droop % is defined as the ratio of the relative change in system frequency to the relative change in generator power output as shown in Equation (1.1) (Gülen, 2019),

$$d = \frac{\frac{\Delta f}{f}}{\frac{\Delta PW}{PW}} * 100 \tag{1.1}$$

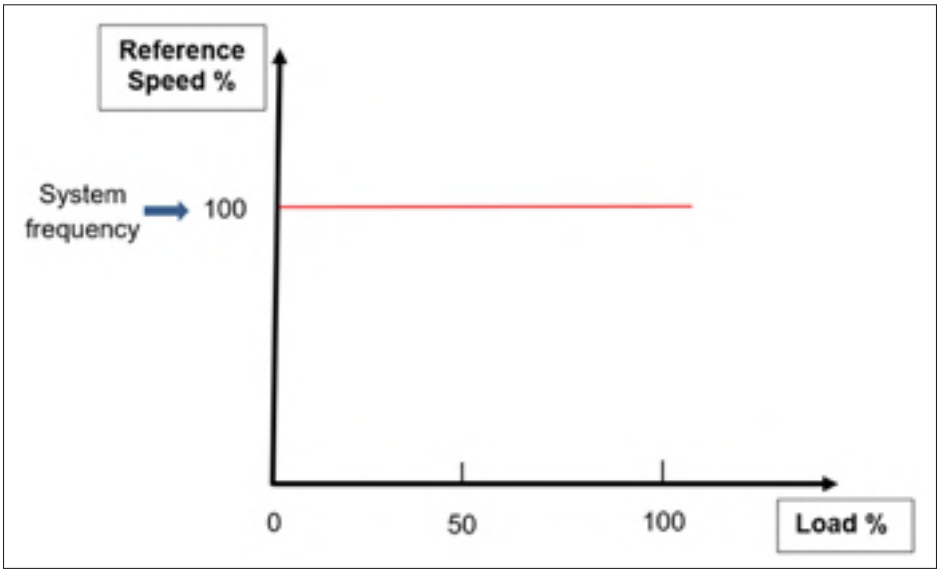

Figure 1.6 Isochronous mode

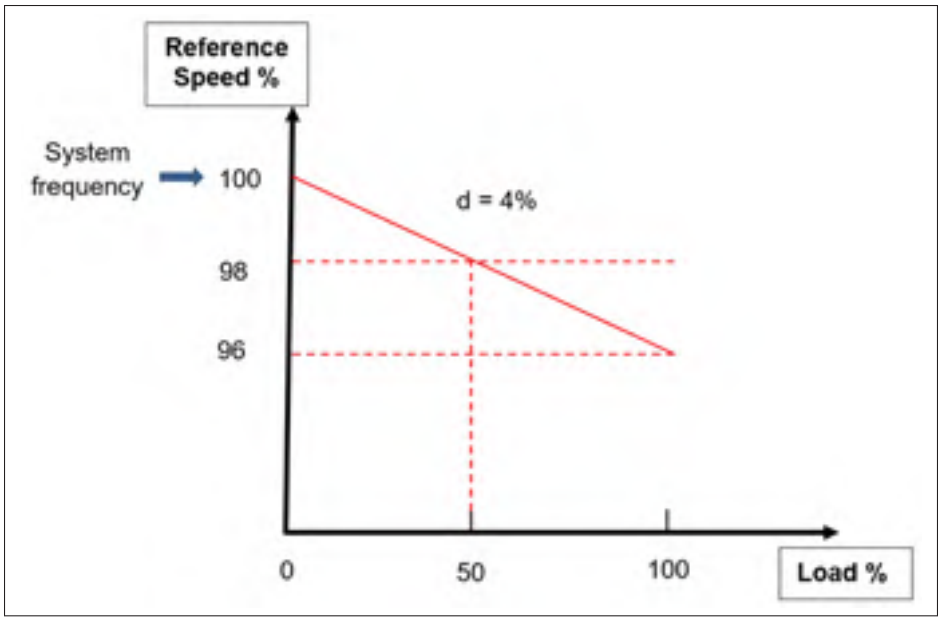

Figure 1.7 Droop mode

As shown in Figure 1.7, speed decreases with an increase in load. If a generator operates at 4% droop, the frequency will decrease 4% when the load is increased from zero to 100%. For a generator set running at 60 Hz at no load, the frequency will drop 4% (3 Hz) to 57 Hz when the load increases from zero to 100%. This mode allows synchronous ADGTEs to run in parallel, so that loads are shared among ADGTEs with the same droop curve in proportion to their power rating. The concept of a droop governor is not intuitive, so that this can be best understood by an analogy to a simple physical system shown in Figure 1.8. Four men pull a 100 unit load, which is analogous to a 50 Hz electric grid. Consequently, the four men are analogous to four ADGTEs. Each man provides a certain fraction of the load. Suddenly, a 20 unit load block falls off. The difference between the force provided by the four men and the load would increase the system speed (for grid analogy, frequency increase by 0.4 Hz). So, in droop mode with $d = 4\%$, each man knows exactly how much load correction he needs to make. As shown in Figure 1.8, for man A, using Equation 1.1, the output correction is 6 units. However, if the men were operated on isochronous mode, they would try to correct the load on their own, which would lead to utter chaos and system breakdown (Gülen, 2019).

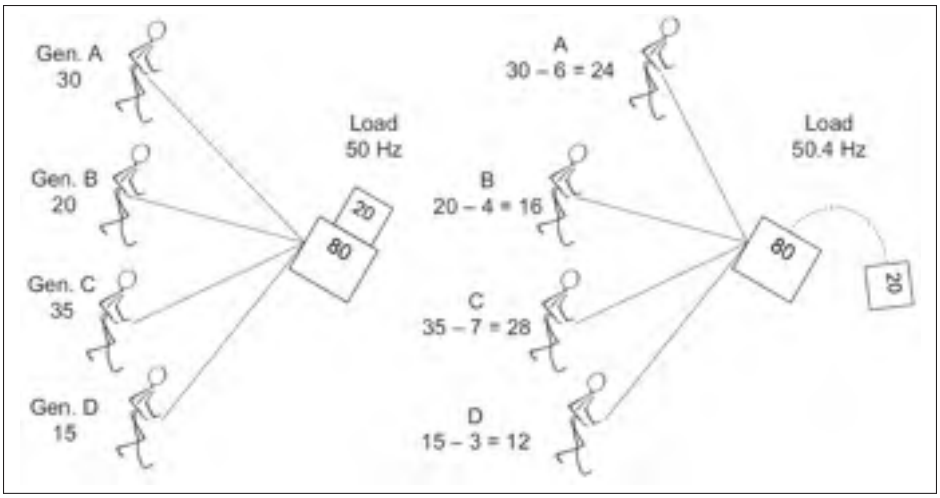

Figure 1.8 Physical analogy to ADGTE with a droop mode
Taken from Gülen (2019)

1.3.1 Siemens SGT-A65 ADGTE - Overview

1.3.1.1 Engine configuration

The Siemens SGT-A65 is one of the world's leading ADGTE used in the power generation and oil-and-gas compression industries. It is the industrial version of the Rolls-Royce Trent 60 high by-pass-ratio aero GTE, which has high efficiency, and in service on the Airbus A330 and Boeing 777. The SGT-A65 is capable of producing 65 MW at thermal efficiency of 42% (H.I.H. Saravanamuttoo, 2017). Figure 1.9 shows the aero and industrial version of the Rolls-Royce Trent 60 engine.

Siemens SGT-A65 DLE three spool ADGTE is used as a case study in this dissertation (Figure 1.10). It has a two-stage low pressure, eight-stage intermediate pressure and six-stage high pressure compressor, with DLE combustion. Furthermore, both high pressure and low pressure turbines consist of a single stage each, and the power turbine has five stages used to drive the low pressure compressor and the power generator at fixed speed (3600 rpm used for power generation at 60 Hz). Figure 1.11 shows a sketch of SGT-A65 ADGTE with its stations numbers. In addition, the engine specifications are illustrated in Table 1.1. To simplify the definition of

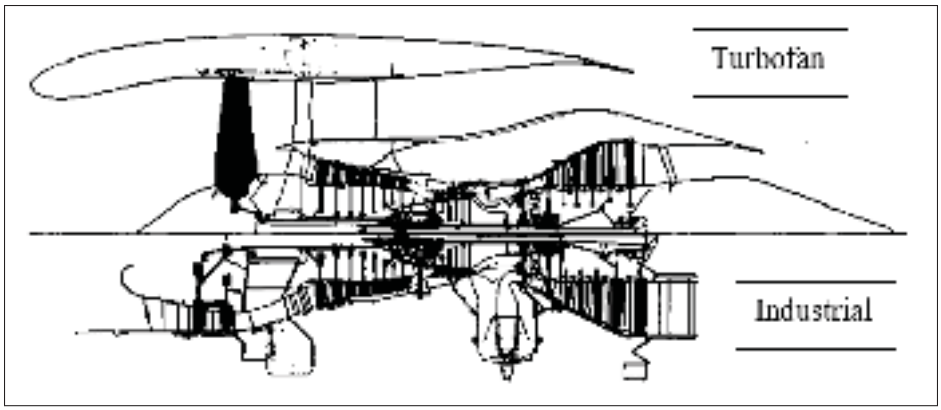

Figure 1.9 Turbofan engine and its aero derivative engine
Taken from H.I.H. Saravanamuttoo (2017)

stations within the gas turbine where performance parameters are quoted, a numbering system is used as shown in Table 1.2.

Table 1.1 Gas turbine technical data

Parameter	**Value**
Exhaust mass flow rate	$171 kg/s$
Output power	$65 MW$
Power turbine speed	$3600 rpm$
Total compression ratio	38 : 1
Exhaust temperature	$437^{o}C$

To prevent the possibility of compressor surge within the LPC when operating at low power and engine transient, spilling compressed air to the atmosphere is used. Low power air spillage is accomplished by means of a modulating low pressure bleed-off valves system. This system comprises of eighteen hinged bleed doors located on the compressor case. All bleed doors are opened in unison to vent LPC exit air, and controlled by means of a modulating four hydraulic arms (actuators). LPBOV represents the opening percentage of low pressure bleed-off valves, it goes from a minimum position of 8% to a maximum position of 105%. Indeed, The LPC variable inlet guide vanes are used to regulate the amount of airflow reaching the engine core. This is necessary due to the fact that the LPC runs at a constant speed, causing a mismatch between the airflow swallowing capacity of the LPC and that of the engine core. The LPC

Table 1.2 Engine station numbering

Station	Description
0	Ambient conditions
20	Engine Intake
22	LPC Inlet
23	LPC Exit
24	IPC Inlet
25	IPC Exit
26	HPC Inlet
30	HPC Exit
31	Combustor Inlet
38	Combustor Exit
40	HPT NGV Inlet
415	HPT Exit
42	IPT NGV Inlet
435	IPT Exit
44	LPT Inlet
454	LPT Exit
5	Gas Turbine Exit / Volute Inlet
52	Volute Exit

variable inlet guide vanes are required to maintain peak performance and an adequate surge margin in the LPC during off-design operating conditions. The VIGV position goes from a minimum (closed) position of 88.088% to a maximum (open) position of 5.65%. To achieve a safe operation of the IPC, three variable stator vanes are modulated to maintain peak performance and an adequate surge margin of IPC during off-design operating conditions. The IPVSV position goes from a minimum position of 1.207% to a maximum position of 95.58%. Intermediate and High pressure bleed off valves are used to maintain an adequate surge margin across the IPC and HPC during partial power conditions. The IPC and HPC bleed systems consist of 4 and 3 ON/OFF valves respectively. NOIPBOV and NOHPBOV represent the number of the opened valves in the IPC and HPC bleed systems.

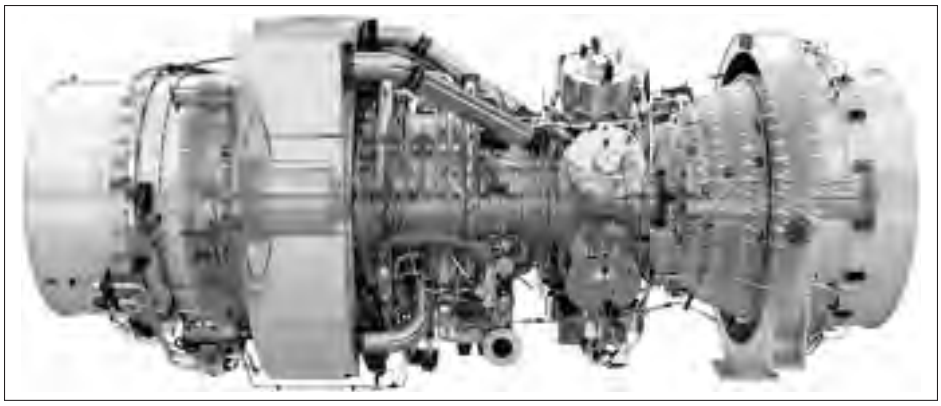

Figure 1.10 Siemens SGT-A65 DLE ADGTE

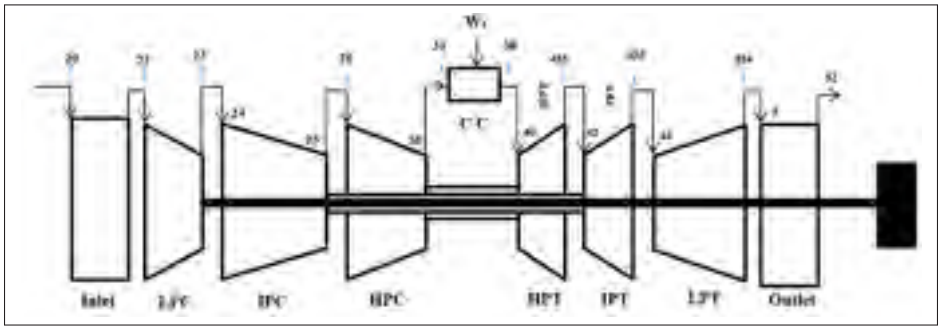

Figure 1.11 Sketch of three spool aero derivative gas turbine engine (SGT-A65)

1.3.1.2 Engine control system

The SGT-A65 ADGTE control system schedules the fuel flow to maintain the engine power or speed at a predetermined speed (3600 rpm). As the electrical load demand on the LPT increases, additional torque is applied on the LPT shaft decreasing its speed. The control system responds to the change in speed by increasing the fuel flow to the combustion chamber, to bring the speed back to the preset value. As the load demand decreases, lowering the torque applied on the LPT, allowing the speed to increase. The control system responds by decreasing the fuel to the combustion chamber, to bring the speed back to the preset value.

The control laws of the engine control system are the algorithms or control logic which govern the operation of the engine. This logic is embedded within software installed in a microproces-

sor based electronic controller. The software handles the processing of all inputs from the various sensors (thermocouples, pressure transducers and speed inputs) laid out across the engine. The software calculates the scheduling of the various gas metering valves, pressure regulating valves, vent valves, air valves, and variable geometry and controls them by outputting signals to multiple actuators via torque motors and solenoids. Figure 1.12 shows schematic drawing of the SGT-A65 engine with its control system.

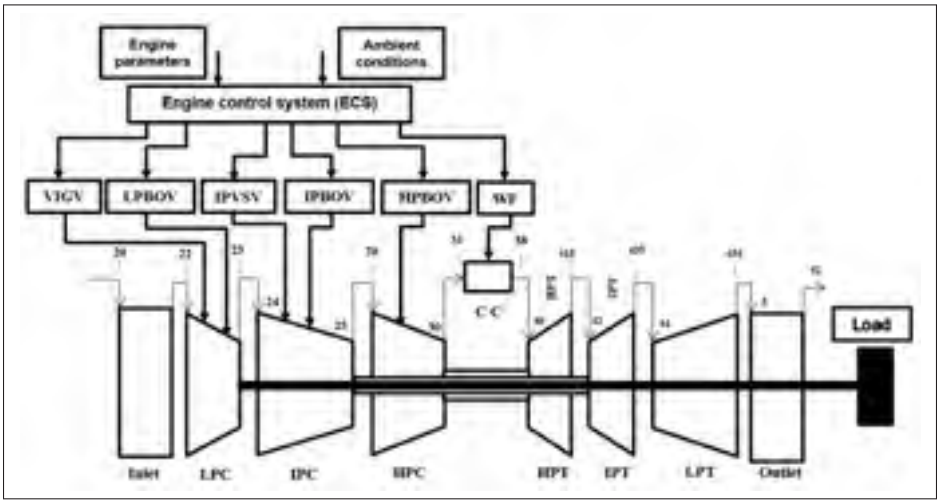

Figure 1.12 The SGT-A65 engine control system

The ECS of SGT-A65 engine in a power generation application carries out three primary functions: Start/stop sequencing, Control, and Protection. Start/Stop sequencing function controls the engine start and stop operation by providing the proper signal required for normal and safe operation. In addition, it is pushing the engine to shut down under all possible abnormal conditions like equipment or control system failure. The start sequence proceeds through five different states before the engine achieves the synch-idle condition: Dry cranking, Purging, Light up, Sub-synchronous idle, and Synch idle. Synch idle is defined as the condition where the LP spool speed matches the frequency of the grid with which it will have to be synchronised (3600 rpm for 60 Hz, 3000 rpm for 50 Hz) while in a no load condition. Figure 1.13 shows rotational speeds versus time for the SGT-A65 engine during starting phase. With respect to the control and protection functions, the ECS controls the engine LP shaft speed or load at

a predetermined value (set point), while at the same time protects the engine from improper operation like over speed, over temperature, and surge. This is done primarily by controlling the fuel flow and the airflow through the engine.

The control function of the ECS is different depending on whether it is in grid mode operation (Droop mode) or in isochronous mode operation. In the isochronous mode the control system controls LP spool speed rather than power. As the load increases, the LP spool will droop from its reference until the engine can produce enough power to match the load and return the LP spool back to its synchronous (steady state) speed. Conversely, if load is removed, the LP spool speed will overshoot its reference and engine power will have to reduce to return the LP spool back to its synchronous (steady state) speed. In the droop mode the steady-state speed varies with load. More details about the engine control architecture will be presented in chapter 4.

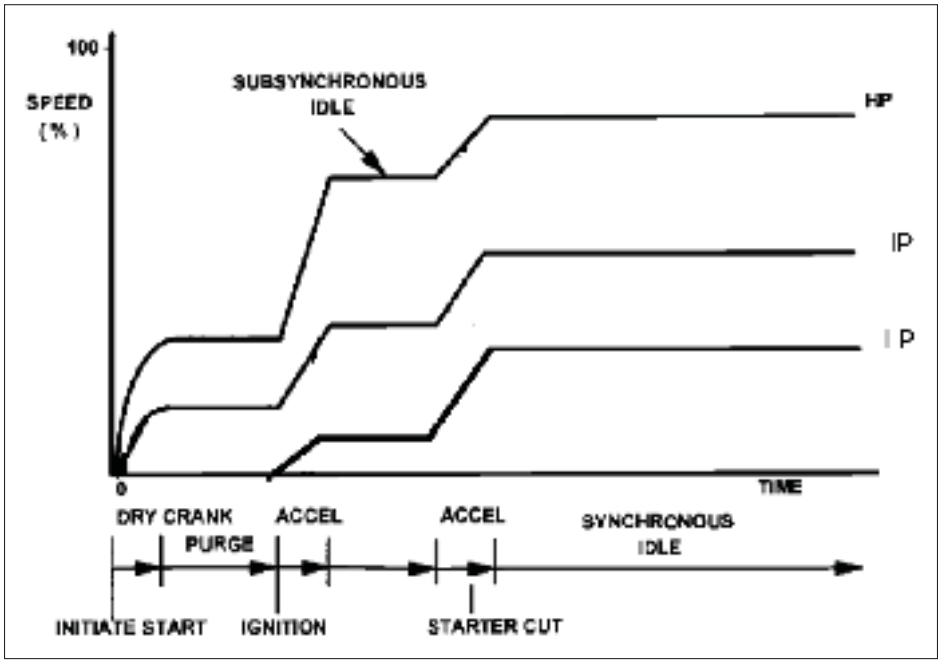

Figure 1.13 The SGT-A65 engine start sequences
Taken from Walsh & Fletcher (2004)

1.3.2 SGT-A65 ADGTE mathematical model

This section presents the mathematical model of Siemens SGT-A65 three spool ADGTE. Although this research is based on the data-driven approaches, part of the data used for the purpose of simulations is generated by Siemens high fidelity thermodynamic simulation program. Thus, it is necessary to review the engine mathematical model.

The ADGTE consists of several key components such as:

- Inlet.
- Compressor.
- Combustor.
- Gas generator turbine.
- Power turbine.
- Exhaust nozzle.

A detailed description of each of these components and ways to model them will be covered in the following parts. In addition, the steady state and transient model will be included.

1.3.2.1 Inlet

The purpose of the engine intake is to transform the inlet free stream flow conditions into the required air conditions at the entrance to the engine compressor. The inlet component is assumed to be a duct and no work was done on the flow through this duct. In addition, the performance of the inlet is defined by the pressure recovery from the free stream to the engine (inlet pressure losses). For a given input parameters to the inlet component P_0 , T_0, and ΔPR_{in}, the total temperature and pressure at the inlet component exit are calculated as shown in the following equations,

$$T_{20} = T_0 * (1 + \frac{\gamma_a - 1}{2} * M^2) \tag{1.2}$$

With M=0

$$T_{20} = T_0 \tag{1.3}$$

$$P22 = (1 - \Delta PR_{in}) * P_{20} \tag{1.4}$$

1.3.2.2 Compressor

The purpose of a compressor is to increase the total pressure of the air to that required value by the engine while absorbing the minimum shaft power possible. Temperature of the incoming air also increases with pressure in the compressor. The work done by the compressor on the gas is extracted from the turbine on the same shaft with the compressor. The compressor characteristics can be obtained from the compressor map, which represents one of the major obstacle in developing a non-linear dynamic model.

Once the compressor geometry has been fixed at the design point, the compressor map may be generated experimentally by the manufacturers to define its performance under all off design conditions. Figure 1.15 shows the form of the compressor map. Pressure ratio and isentropic efficiency are plotted versus corrected flow ($\frac{m^{\bullet}\sqrt{\theta}}{\delta}$) for a series of lines of constant relative speed. The advantage of using a compressor map is that it includes all the losses for a particular design case. However, the compressor map is not always available because the manufacturers prevent publishing of its maps. In order, to overcome this problem, a map scaling technique can be used to scale known published component map into new component map. Map scaling method was developed by Sellers and Daniele during the development of a steady-state and transient performance program called DYNGEN (Sellers & Daniele, 1975). The engine compressor maps should be digitized and loaded to the simulation program in the form of look-up tables, which is the best flexible way to represent a component map in simulation. To facilitate loading compressor map into an engine simulation model beta lines are used. Beta lines are arbitrary lines, which are drawn approximately equispaced and parallel to the surge line on

the map as shown in Figure 1.14. Once the beta line were added to the compressor map, the compressor characteristics could be obtained as function of the relative speed and beta value as shown in the following equations (for example LPC),

$$\pi_{LPC} = fn(\beta_{LPC}, \%N_{LPC}) \tag{1.5}$$

$$\left(\frac{m^{\bullet}\sqrt{\theta}}{\delta}\right)_{LPC} = fn(\beta_{LPC}, \%N_{LPC}) \tag{1.6}$$

$$\eta_{LPC} = fn(\beta_{LPC}, \%N_{LPC}) \tag{1.7}$$

where,

$$\theta = \frac{T_{20}}{288.15} \tag{1.8}$$

$$\delta = \frac{P_{20}}{101325} \tag{1.9}$$

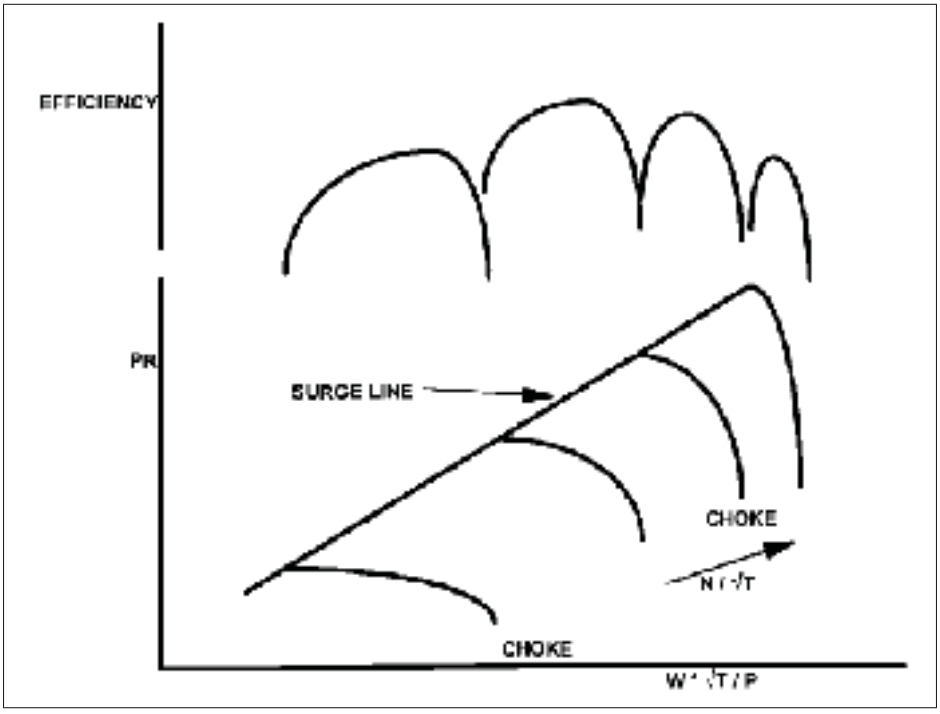

Figure 1.14 The axial compressor map
Taken from Walsh & Fletcher (2004)

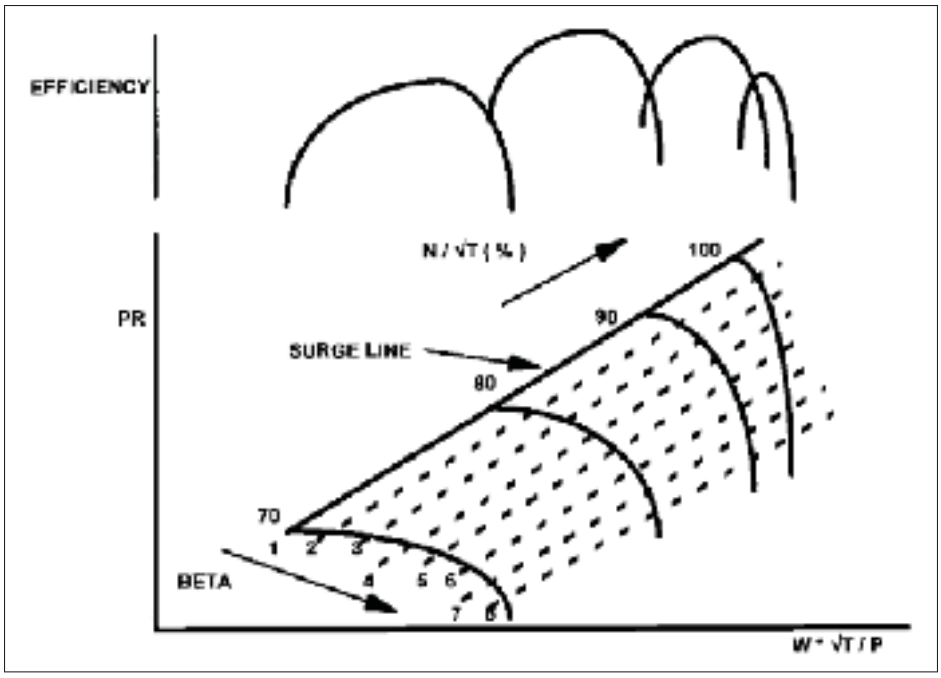

Figure 1.15 The compressor map and beta lines
Taken from Walsh & Fletcher (2004)

Once the compressor characteristics are available, all of the compressor exit conditions can be calculated as follows:

The LPC mathematical model,

$$P_{23} = \pi_{LPC} * P_{22} \tag{1.10}$$

$$T_{23} = T_{22} * \left[1 + \frac{\pi_{LPC}{}^{\left(\frac{\gamma_a - 1}{\gamma_a}\right)} - 1}{\eta_{LPC}} \right] \tag{1.11}$$

$$m^{\bullet}_{22} = \left(\frac{m^{\bullet}\sqrt{\theta}}{\delta} \right)_{LPC} * \frac{\delta}{\sqrt{\theta}} \tag{1.12}$$

$$m^{\bullet}_{32} = m^{\bullet}_{22}(1 - B_{LPC}) \tag{1.13}$$

$$W_{LPC} = m^{\bullet}_{22} * c_{p_a} * (T_{32} - T_{22}) \tag{1.14}$$

These equations can be repeated to IPC and HPC.

1.3.2.3 Combustor

The purpose of the combustor is to further increase the potential energy content of the working fluid through combustion of a gaseous fuel and air mixture. The combustor exit parameters can be calculated based on the combustor inlet conditions, the combustion efficiency, and the combustor total pressure loss as follows:

$$m_{38}^{\bullet} = m_{31}^{\bullet} + WF \tag{1.15}$$

$$T_{38} = \frac{m_{31}^{\bullet} * c_{p_a} * T_{31} + WF * LHV * \eta_{CC}}{m_{38}^{\bullet} * c_{p_g}} \tag{1.16}$$

$$P_{38} = P_{31} * (1 - \Delta PR_{CC}) \tag{1.17}$$

1.3.2.4 Gas generator turbine

Turbine is used to extract sufficient energy from the hot gases of the combustor to drive the compressor and other auxiliary power equipment. As with compressors, to calculate the gas generator turbine exit conditions, it is required to know the turbine inlet conditions and the turbine characteristics (mass flow rate, pressure ratio, and isentropic efficiency) for a given spool speed and beta line value (Turbine map). Once the turbine characteristics are available, all of the turbine exit conditions can be calculated as follows:

The HPT mathematical model,

$$P_{415} = \frac{P_{40}}{\pi_{HPT}} \tag{1.18}$$

$$T_{415} = T_{40} * \left[1 - \eta_{HPT}(1 - \pi_{HPT}^{\left(\frac{\gamma_g - 1}{\gamma_g}\right)})\right] \tag{1.19}$$

$$m_{415}^{\bullet} = m_{40}^{\bullet} + (1 - B_{HPC}) m_{26}^{\bullet} \tag{1.20}$$

$$W_{HPT} = m_{40}^{\bullet} * c_{p_g} * (T_{40} - T_{415}) \tag{1.21}$$

These equations can be repeated to IPT.

1.3.2.5 Power turbine

Power turbine is used to extract sufficient energy from the hot gases of the combustor to drive the LPC and external load (generator for power generation application). All of the power turbine exit conditions can be calculated as follows:

$$P_{454} = \frac{P_{44}}{\pi_{LPT}} \tag{1.22}$$

$$T_{454} = T_{44} * \left[1 - \eta_{LPT}(1 - \pi_{LPT}^{\left(\frac{\gamma_g - 1}{\gamma_g}\right)})\right] \tag{1.23}$$

$$\dot{m}_{454} = \dot{m}_{44} + (1 - B_{HPC\,to\,PT})\dot{m}_{26} + (1 - B_{IPC\,to\,PT})\dot{m}_{24} \tag{1.24}$$

$$W_{PT} = \dot{m}_{44} * c_{p_g} * (T_{44} - T_{454}) \tag{1.25}$$

1.3.2.6 Exhaust nozzle

The purpose of the exhaust duct in the aero derivative gas turbine engines is typically to direct the exhaust gases into the atmosphere, which is different from exhaust nozzles in aero gas turbine engines. There is no work done of the flow through the exhaust duct. In addition, the performance of the exhaust nozzle is defined by the pressure recovery from the engine to the free stream (exhaust nozzle pressure loses). The exhaust nozzle output parameters can be calculated as shown in the following equations,

$$T_5 = T_{52} \tag{1.26}$$

$$P_{52} = (1 - \Delta PR_{ex}) * P_5 \tag{1.27}$$

1.3.2.7 Load

The load characteristic is an important piece of the dynamic modelling because the load applied to the power turbine affects on steady state and transient performance parameters such as surge margins, spool speeds, and turbine inlet temperature.

1.3.2.8 Engine dynamics

The engine is said to be in a steady-state, when the internal state of the GTE (P, T, N) reaches a thermodynamic equilibrium. That means, there is no change in their values and the work generated by the turbine equal to the required work for the engine compressor and external load on the same shaft. However, if there is an imbalance of power on the same engine shaft required to acceleration or deceleration operation, the engine is said to be in a transient state. There are three main phenomena particular to the transient performance of the turbine engine: shaft dynamics caused by the inertial effect, pressure dynamics caused by the mass storage effect, and temperature dynamics caused by the energy storage. Shaft dynamics represents the simplest and the most important dynamic behavior of the GTE. Based on the principle of Newtonian mechanics, the shaft dynamic equations for the three spool ADGTE (SGT-A650) are represented by the following equations,

$$\frac{dN_{LPC}}{dt} = \frac{3600}{4 * \pi^2 * N_{LPC} * J_{LPC}} [W_{LPT} - W_{LPC} - Load] \tag{1.28}$$

$$\frac{dN_{IPC}}{dt} = \frac{3600}{4 * \pi^2 * N_{IPC} * J_{IPC}} [W_{IPT} - W_{IPC}] \tag{1.29}$$

$$\frac{dN_{HPC}}{dt} = \frac{3600}{4 * \pi^2 * N_{HPC} * J_{HPC}} [W_{HPT} - W_{HPC}] \tag{1.30}$$

To capture the pressure and thermal dynamics, a control volume is inserted between each pair of engine modules to allow for the mass and energy storage, which gives rise in pressure and temperature dynamics. Figure 1.16 shows a control volume with temperature, pressure, and density are assumed to be constant throughout the control volume and equal to the outlet

values. In addition, **m** is the mass of air/gas trapped inside the volume, and **V** is the volume of the element. To derive the pressure dynamic equation, assuming that the air/gas within the control volume behaves like a perfect gas (equation (1.31)). So, the rate of change of mass inside the volume is proportional to rate of change of pressure and temperature as shown in equation (1.32).

$$PV = mRT \tag{1.31}$$

$$P_2^{\bullet} = \frac{mR}{V} * T_2^{\bullet} + \frac{RT_2}{V} * m^{\bullet} \tag{1.32}$$

In equation (1.32), the temperature derivative can be neglected in comparison to the mass derivative term (Jaw & Mattingly, 2009). So that, equation (1.32) can be written as,

$$P_2^{\bullet} = \frac{RT_2}{V} * m^{\bullet} \tag{1.33}$$

From the law of conservation of mass, the rate of change of mass **m** trapped inside the control volume is determined by the difference between the amount of mass flow rate entering and leaving the element as shown in equation (1.34),

$$m^{\bullet} = m_1^{\bullet} - m_2^{\bullet} \tag{1.34}$$

Substituting by equation (1.34) into equation (1.33). Then, the rate of change of pressure within the control volume is given by,

$$P_2^{\bullet} = \frac{RT_2}{V} * [m_1^{\bullet} - m_2^{\bullet}] \tag{1.35}$$

With respect to the temperature dynamics, based on the conservation of energy law, the rate of change of the internal energy of the control volume can be given by,

$$U^{\bullet} = m_1^{\bullet} c_p T_1 - m_2^{\bullet} c_p T_1 + E_{net} \tag{1.36}$$

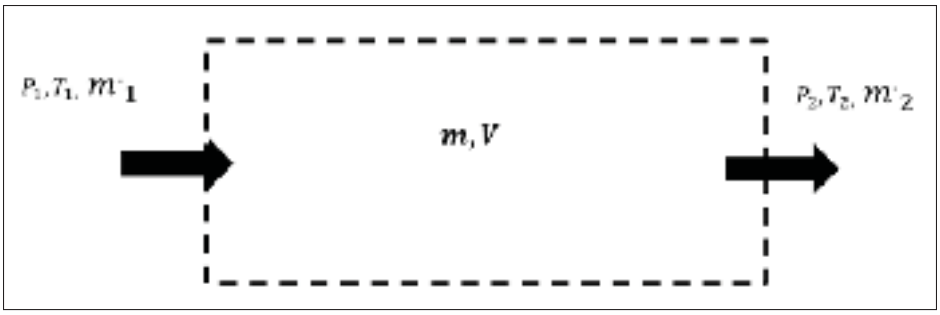

Figure 1.16 An air/gas control volume

where, E_{net} is the net energy entering or leaving the control volume.

From thermodynamics, the internal energy of the control volume is given by equation (1.37). By differentiating equation (1.37) with respect to T and m, the rate of change of internal energy of the control volume can be represented by equation (1.38),

$$U = m * c_v * T \tag{1.37}$$

$$U^{\bullet} = m * c_v * T_2^{\bullet} + c_v * T_2 * m^{\bullet} \tag{1.38}$$

By substituting equation (1.36) and equation (1.34) into equation (1.38), the rate of change of the temperature within the control volume can be given as follows,

$$T_2^{\bullet} = R * T_2 \left[\frac{m_1^{\bullet} c_p T_1 - m_2^{\bullet} c_p T_1 + E_{net} - c_v T_2 \left[m_1^{\bullet} - m_2^{\bullet} \right]}{c_v V * P_2} \right] \tag{1.39}$$

Now, to build a complete dynamic model of the SGT-A65 ADGTE, seven control volumes are inserted between each pair of engine components as shown in Figure 1.17. The dynamics of each control volume can be represented by two state variables: pressure as given by equation (1.35), and temperature as given by equation (1.39). Consequently, the total number of state variables for the seven control volumes is 14. Adding to this number the three state variables representing the LP, IP, and HP shaft speeds, a total of 17 state variables are needed to represent the engine dynamic model. The general non-linear dynamic system is expressed as non-linear

functions of state and input variables as follows,

$$X^{\bullet} = f(X, WF, IPVSV, VIGV, LPBOV, IPBOV, HPBOV) \tag{1.40}$$

where, X is the state variable vector that is represented as follows,

$$X = [N_{LPC}, N_{IPC}, N_{HPC}, P_{24}, P_{26}, P_{31}, P_{40}, P_{42}, P_{44}, P_5, T_{24}, T_{26}, T_{31}, T_{40}, T_{42}, T_{44}, T_5]^T \tag{1.41}$$

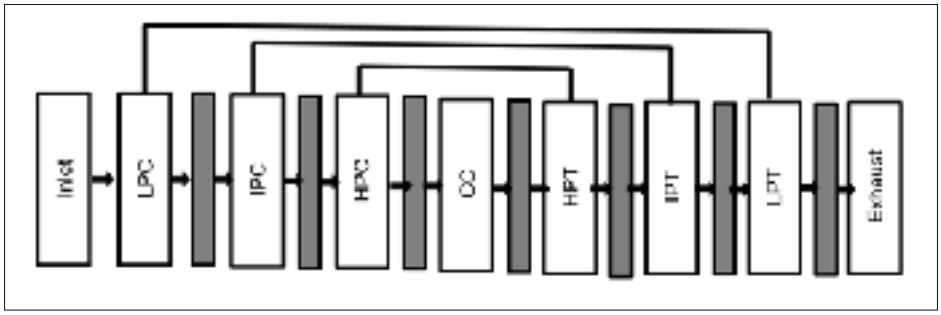

Figure 1.17 Computational flow diagram of a three spool ADGTE

Steady state calculations are obtained when dX/dt=0. The resulting non linear system of algebraic equations may be solved using any iterative method (e.g. the Newton-Raphson method). This iterative method requires guessing a certain number of variables and improving them using the residuals of the same number of error equations. When dynamics are considered the system of non-linear differential equations is to be integrated in time using any integration formula.

1.4 Summary

In this chapter, a review of the gas turbine engine was presented, while focusing on ADGTE construction and principle of operation. It also reviews background information on the SGT-A65 ADGTE including its structure, control system, and its mathematical modelling.

As can be seen, the complete thermodynamic dynamic model of the SGT-A65 ADGTE is very complicated and requires an iterative solution that occurs at the expense of computation time. The purpose of this chapter was to foster a basic understanding of a gas turbine as relevant to this project, and highlight the reason why it is imperative to use a data-driven model of the SGT-A65 three spool engine for real-time model-based applications instead of the highly complicated thermodynamic model.

CHAPTER 2

LITERATURE REVIEW

2.1 Introduction

Modelling and simulation of gas turbines plays a key role in manufacturing and improving performance of gas turbine engines. In recent years, the importance of ADGTEs in the energy industry has sparked a great interest among manufacturers to improve the performance and increase the reliability of the engine, which in turn requires an accurate and real time model to simulate the engine dynamics during the full operating range. This chapter presents a comprehensive overview of the most significant studies in the field of modelling, simulation and control of ADGTEs. It covers both physics based and data driven based models of ADGTEs. This chapter also presents a survey of the historical development of GTE control systems. Besides, it emphasizes on the most significant publications in the field of advanced controller design for industrial GTEs . The concluding remarks from the literature review are presented at the end of this chapter.

2.2 Modelling and simulation of gas turbine engines

Before making a gas turbine engine model, some basic factors should be carefully considered such as modelling objectives, GTE type, GTE configuration, and modelling methods. These factors are considered among the most important criteria at the beginning of the modelling process. There are different objectives for making a GTE model. A GTE can be modelled for condition monitoring, fault detection and diagnosis, sensor validation, system identification, design optimization and improvement of control systems. Thus, a clear statement of the modelling objectives is necessary to make a successful GTE model (Asgari & Chen, 2015). A real-time simulation can be used as a powerful tool in developing, testing and tuning control devices of GTEs (Camporeale *et al.*, 2006). In addition, it can be used to simulate critical transients scenarios that should be avoided on the actual plant due to risk of damage.

The first step of modelling a GTE is defining the type and configuration of the engine which is to be modelled. It is necessary to get enough information about the input/output parameters, engine specifications, and engine configuration. GTEs can be classified according to their applications to aero GTEs and stationary GTEs. More details about the GTEs types and configuration will be mentioned in the next chapter.

Throughout the years many methods were developed to simulate GTE dynamic response. Investigating GTE dynamic response began around the early 1950s, and ranged from a simple linear models (Otto & Taylor III, 1951; Rowen, 1983) to a real time high fidelity non-linear models (Camporeale *et al.*, 2006; Gazzetta Junior *et al.*, 2017; Montazeri-Gh *et al.*, 2018; Petkovic *et al.*, 2019).

GTE modelling methods can be categorized into two main groups including physics based modelling methods (white-box models) and data driven based modelling methods (black-box models). In some cases, the expression of gray-box model may also be used as a combination of the last two methods (Asgari *et al.*, 2014). The next subsections present a comprehensive overview of the most significant studies in white and black box modelling, including their characteristics, benefits, and limitations.

2.2.1 Physics based modelling of GTEs

Physics based models are based on first principles such as the law of physics, chemistry, etc (Nguyen, 2000). This approach has been widely used over many years in order to model gas turbine engines (Ballin, 1988; Duyar *et al.*, 1995; Bettocchi *et al.*, 1996; Saleh, 2017; Tahan *et al.*, 2017; Petkovic *et al.*, 2019). However, this approach can only be used when there is enough information about the physics of the system. In addition, a white box model has traditionally a high number of non linear equations requiring iterative solutions which occur at the expense of computation time. The computation time challenge of the physics based model is a big problem for real time modelling, especially when the system to model consists of a high number of subsystems as in case of three spool GTEs.

Gas turbine physics model consists of both an off-design steady-state model and an off-design dynamic model. Both types of models are derived based on the first principles of physics (Jaw & Mattingly, 2009). When the internal state of an engine reaches a thermodynamic equilibrium, that is, there is no change in the values of state variables, the engine is said to be in a steady state. However, dynamic or transient model determines the time history of engine state and path followed by the engine from its existing steady state to the new steady-state condition because of a disturbance in load demand and/or ambient conditions (Sanghi *et al.*, 2000). Off-design conditions refer to the state where the GTE is operated in conditions which are beyond the standard designed condition.

All off-design steady-state calculations depend on satisfying the essential conditions of matching of mass flow across two adjacent stations, rotational speed and power balance between the compressor, turbine, and load on the same shaft. These are often referred to as component matching calculations (H.I.H. Saravanamuttoo, 2017). To generate an off-design steady-state model of the GTE, a set of non-linear thermodynamic algebraic equations are solved iteratively to ensure that there is a match between each engine components. This iteration can be achieved either via serial nested loops method, or via a matrix method. For both iteration methods, there are several matching guesses, and an equal number of matching constraints (matching of mass flow and work). During iteration the matching guesses are continually updated until the matching constraints are satisfied. For serial nested loops method, the matching guesses parameters and matching constraints are paired and solved in a nested sequence. Whereby for each pass through higher loop, each loop within it is repeated until convergence. This technique is often easier to understand physically, and to implement via personal computer programs. However, this technique becomes computationally inefficient for more than five nested loops (Muir *et al.*, 1989; Kyprianidis & Kalfas, 2008; H.I.H. Saravanamuttoo, 2017; Yazar *et al.*, 2017). On the other hand, in the matrix iteration method, the overall interaction is recognized and the constraint equations are set and solved simultaneously. This requires a numerical method, such as Newton-Raphson, which is utilizing partial derivatives. These partial derivatives represent the effect of changing each matching guess individually on the errors in all the matching con-

straints (Walsh & Fletcher, 2004). The matrix iteration method is now more common and a powerful method for simulation of advanced GTEs (Gaudet, 2008; Gu *et al.*, 2016; Zhou *et al.*, 2020). However, this numerical solver has shown some limits when applied to real time simulation due to the need of calculation of the Jacobian matrix in every iteration. To save some time, the Broyden method may be used to replace the Newton method derivative by a finite difference. So, the Jacobian matrix will be calculated only at the first iteration and to do rank-one updates at other iterations. Even though, the total number of system evaluations is generally much lower and the total computation speed faster than for the Newton-Raphson, the rate of convergence is smaller than for the Newton–Raphson method with a Jacobian determined by difference quotients (Krummrein *et al.*, 2018).

As stated above, steady-state response relied on the fact that compatibility of flow and compatibility of work must be satisfied at all time. However, during transient operations, a mismatch of work between the compressor, turbine, and load is required to allow the engine to accelerate or decelerate. Therefore the assumption of compatibility of work and flow is no longer valid during transient operations (Fawke & Saravanamuttoo, 1971). GTEs have three main types of dynamics which should be considered during dynamics modelling: shaft dynamics, pressure dynamics, and temperature dynamics. To model these dynamics phenomenons, there are two methods for treating flow and work imbalance during dynamic modelling: Constant mass flow iterative (CMF) method (Kong *et al.*, 1999; Thirunavukarasu, 2013; Forhad & Bloomberg, 2015), and Inter-component volume (ICV) method (Camporeale *et al.*, 2006; Petkovic *et al.*, 2019). In the CMF method, shaft dynamics can be modelled only. The CMF approach assumed that the mass flow of the air (or gas) entering an engine component must equal the mass flow leaving the same component (Zhu & Saravanamuttoo, 1992). As stated, the basic assumption in the CMF approach is that flow compatibility is maintained at all times. So that, to predict the engine behavior during a transient, the calculation proceeds as follows: An initial guess is made for certain engine parameters. After that, a single run through the engine calculations is made. The error in mass flows are then noted and progressively minimized by improving the initial guess through a numerical method such as the Newton–Raphson method. So, many

iterations are performed until the error value reached to the required degree of accuracy. Once flow compatibility was achieved, the work imbalance on the engine shaft may be used to represent the shaft dynamics as shown in equation (2.1), and an integration method may be used to predict the shaft speed. On the other hand, to represent the pressure and thermal dynamics of the GTE, the ICV method can be used. The ICV method always assumes flow mismatch and work mismatch between engine components during transient performance. This is done by inserting a control volume between engine components and applying the conservation of mass and energy laws as shown in equations (2.2) and (2.3). A comprehensive expatiation of these equations were presented in the previous chapter. Moreover, the ICV method is considered as a popular and accurate choice for transient performance prediction. In (Tsoutsanis *et al.*, 2013), hybrid CMF-ICV approaches were used to model the dynamic performance of an industrial GTE. The employment of both the ICV and CMF methods improves the computational time and the prediction accuracy of the engine model.

The differential equations that define the engine dynamics (equations (2.1) to 2.3)) may be solved by employing integration methods such as the Euler method (Gaudet, 2008; Wang, 2016), Runge-Kutta method (Kim *et al.*, 2001; Petkovic *et al.*, 2019), etc. However, these integration methods have shown some limits when applied to real time simulation due to constraints on step time. The step time should be no greater than one-tenth the magnitude of the smallest time constant the user wants to observe. Stamatis *et al.* (2001) stated that, the frequency range over which the GTE model is representative can vary between 1 Hz for models with only shaft dynamics to 30-50 Hz with pressure dynamics included, and so integration time step can vary between 50 ms for the lower order models to 1 ms for high order models. Therefore, a larger step time can be used in the CMF method, which decreases the computation time. On the other hand, in the ICV method, a shorter step time is necessary for correct prediction of the transient, which increases the computation time. In order to obtain a real time execution of the model, the integration of this set of differential equations, at each step time, must be completed by the computer within a time shorter than the assumed step time.

$$\frac{dN}{dt} = \frac{3600}{4 * \pi^2 * N * J} [W_T - W_C - Load] \tag{2.1}$$

$$\frac{dP}{dt} = \frac{R*T}{V} * [m^{\bullet}_{in} - m^{\bullet}_{out}] \tag{2.2}$$

$$\frac{dT_{out}}{dt} = R*T_{out}\left[\frac{m^{\bullet}_{in}c_pT_1 - m^{\bullet}_{out}c_pT_{in} + E_{net} - c_vT_{out}\,[m^{\bullet}_{in} - m^{\bullet}_{out}]}{c_vV*P_{out}}\right] \tag{2.3}$$

As can be seen, the physics based model of the GTE consists of a mixed set of non-linear algebraic equations and ordinary differential equations. In order to obtain a real time execution of this model, all the calculations of the iterative procedure and solution of differential equations must be completed by the computer within a time shorter than the assumed time step. Real-time simulation can be used as a powerful tool in developing, testing and tuning control devices of gas turbines. Moreover, it can be possible to simulate critical manoeuvres that should be avoided on the actual engine due to risk of damage. However, a problem that arises when using physical performance model for real time simulation is that the computational time varies at each time step due to the necessary iterations. Furthermore, the iterative method produces noise on the output parameters due to solutions at each time step are falling at random places within the permitted tolerance band. This noise may prevent assessment of system stability, due to the perturbations produced (Walsh & Fletcher, 2004). The fastest achievable sampling rate depends on the complexity of the engine, the degree of detail of the modelling, and on the available computing power. Therefore, to enable calculation in real time, software and hardware approaches have been proposed by many researchers.

For software approaches, in order to reduce the computational time, techniques based on the simplification of the detailed thermal model (physics based model), the utilization of more efficient iteration techniques, and the utilization of more efficient integration techniques may be used. The simplification of the physics model includes the usage of the reduced-order thermal model (Crainic *et al.*, 1997; Rosini *et al.*, 2019). However, this leads to a decreasing of model accuracy. It is also possible to simplify the detailed engine model by linearizing the non-linear model around selected operating points (Rowen, 1983; Montazeri-Gh & Abyaneh, 2017; Chen *et al.*, 2019). However, the linearized models should be used only in the neighbourhood of the working point about which the linearization has been carried out. If simplifications to the non-linear model can't be made easily then one may have to resort to efficient iteration

and numerical methods. The most effective way to keep optimizing the execution time of a simulation is to limit the maximum number of iterations the solver takes through the simulation logic (Lietzau & Kreiner, 2001; Fuksman & Sirica, 2012). Another extremely powerful feature of the iteration method which improves both convergence success rate and time until reach the solution is the selection of the starting point close to the final solution (Gazzetta Junior *et al.*, 2017). Also, the usage of the Broyden method to update the Jacobian matrix in the Newton-Raphson method may reduce the model computation time (Krummrein *et al.*, 2018). With respect to the integration methods, Stamatis *et al.* (2001) developed a real time engine model of two spool GTE. They carried out a comparison between explicit and implicit integration methods in order to study its impact on the execution time. They concluded that no obvious advantage is noticed between explicit and implicit integration. However, for smaller number of fixed iterations implicit integration seems to be faster than explicit integration, while the opposite is valid when increasing the number of fixed iterations. Moreover, one iteration of the code costs about 0.25-0.3 ms using implicit or explicit Euler integration method in Pentium 450 MHz and 2-3 ms in a Pentium 90 MHz. In another effort, Lin *et al.* (1999) presented a hybrid integration method for real time simulation of single spool GTE. The hybrid integration method allowed to enlarge the time step to 20 ms and the integration still remains stable. In some cases, the most desirable approach to achieve real-time simulation is speeding up the calculations though expensive and faster hardware (Sanjawadmath & Suresh, 2017) or parallel processing. Finally, the implementation of real-time models must also balance the constraints of cost and execution time.

As can be seen, the computation time challenge is a big problem for real time modelling of the physics based model, especially when the system to model consists of a high number of subsystems as in our case: (SGT-A65) is a three spool ADGTE, the execution time study for Siemens's high fidelity thermodynamic model resulted in exceeding the sampling time (10 ms) in real time simulation for ramp and step load change using Speedgoat performance real time target machine with Intel Quad-Core i7 3770K @ 3.5 GHz CPU, 4096 MB of RAM. An alternative to white box models is given by data-driven based models.

2.2.2 Data driven based modelling of GTEs

Data-driven based model (or black box model) is one of the modelling approaches which can be used when no or little information is available about the physics of the system. In this case, a data driven model can disclose the relations between system variables using the obtained operational input and output data from the system. Artificial neural network is one of the most significant methods in data-driven based modelling (Asgari *et al.*, 2013). It presents high computation speed, which allows for real time applications. It is a fast-growing method, which has been used in different fields of industry in recent years. It is also being heavily used in machine learning and artificial intelligence applications. The main idea behind ANN is to create a model based on a human brain in order to solve complex scientific and industrial problems in a variety of areas.

Linear NN were first proposed by Widrow and Hoff in the 1960s with the name ADALINE (Widrow & Hoff, 1960), and have been used as the typical NN architecture until the creation of the back propagation algorithm (BP), which provides a tool for training non-linear multi-layer perceptron neural networks (MLP) in the late 1980s Rumelhart *et al.* (1985). Cybenko(Cybenko, 1989) proved that a neural network with one hidden layer of sigmoid or hyperbolic tangent units and an output layer of linear units is capable of approximating any continuous function. The network is described by the magnitude of the weights and biases and is determined by training the network with the operational or simulated data. In the area of modelling and simulation of industrial gas turbine engines, there are many sources in the literature. Asgari et al. (Asgari *et al.*, 2013) presented a general overview of essential basic criteria that need to be considered for making a satisfactory model and control system of a gas turbine engine. It covers both white-box and black box modelling approaches.

Neural networks can be classified into two main categories: static and dynamic neural networks(Ibrahem *et al.*, 2019). Static neural networks are the simplest neural networks, and are characterized by memoryless non linear equations, which means that there are no feedback elements and no delays in the network input. Therefore, the output parameters from the static

NN depend only on the current values of the input parameters as shown in Figure 2.1a. The multi layer feed forward neural networks (MFFNN) are considered as static neural networks because they have only feed forward transformation of the information from the input layer to the output layer. Recently, many research activities have been carried out towards the development of neural models of gas turbine engines used for performance simulation and engine diagnosis (Bettocchi *et al.*, 2004; Khalili & Karrari, 2017; Talaat *et al.*, 2018). In these works, the most common structure of the static NNs used is a feed forward NN, with a single hidden layer, tansig activation function and different numbers of neurons while NN was trained by using trainlm algorithm.

a) Static NN

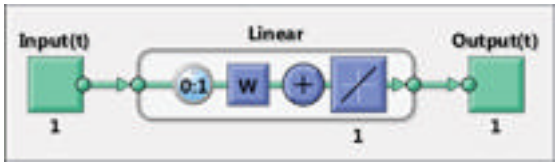

b) Dynamic feed forward NN with input delay

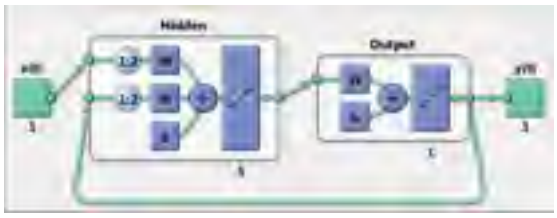

c) Dynamic with feedback NN

Figure 2.1 Neural network types

On the other hand, dynamic neural networks attracted many researchers due to their ability to represent the dynamics of gas turbine engines. In the case of dynamic neural networks, output parameters from the network depend not only on the current input parameters of the network, but also on the previous input and output parameters of the network. Furthermore, dynamic neural networks can be divided into two categories: those that have only feedforward connections (input/output delays) as shown in Figure 2.1b, and those that have feedback or recurrent connections as shown in Figure 2.1c. A significant number of studies across different appli-

cations have stated the advantages of dynamic NNs by introducing different methodologies (Tayarani-Bathaie *et al.*, 2014; Yu & Shu, 2017). Among the existing dynamic NN modelling methods, the non-linear autoregressive network with exogenous inputs (NARX) modelling approach is considered one of the most popular. It has been used in the modelling of gas turbine engines by several researchers Mehrpanahi *et al.* (2018); Salehi & Montazeri-Gh (2018); Tarik *et al.* (2017); Bahlawan *et al.* (2017).

NARX is a recurrent dynamic network with feedback connections enclosing several layers of the network. Note that static neural networks (feed forward) have no feedback elements and contain no delays; the output depends only on the current value of the input to the network. However, in dynamic neural networks, the output depends on the current and previous inputs and outputs of the network. In addition, dynamic networks can be divided into two categories, those that only have a tapped delay line on the input but no feedback connections and those that have feedback or recurrent connections and tapped delay line on the input (such as NARX networks) (Ibrahem *et al.*, 2019). NARX model is based on the linear ARX model, which is commonly used in time-series modelling, and is used in many applications such as multi step ahead prediction and modelling of non-linear dynamic systems. Equation(2.4) defines a NARX model and represents the relation between the model output and its input parameters (Beale *et al.*, 2015),

$$y(t) = f(y(t-1), \cdots, y(t-n_y), u(t-n_k), \cdots, u(t-n_k-n_u+1)) \tag{2.4}$$

where, n_y and n_u are the lags of the output and input of the system respectively. n_k is the system input-output delay and f is a non-linear function.

As can be seen, the major challenge to the application of ANNs is to find the best structure of the network which can represent the system. In this regard, usage of single neural model may not be able to provide accurate prediction when it operates outside the field in which it was trained. Besides, gas turbine engines operate in non-stationary operation conditions which may cause unseen scenarios in the observed data. As a result, this increases the complexity of

the modelling operation since the NN needs to be trained with a data as large enough to cover the entire operation conditions. This in turn increases the training time and the possibility of network over-fitting. To address this problem, we consider to train multiple ANNs in parallel to fit the data instead of a single model. This leads to an ensemble of neural network models.

Ensemble learning approach refers to a set of models working in parallel on tasks such as classification or regression, and they are combined together in some way to obtain the final output (de Sousa *et al.*, 2012). The ensemble development process can be divided into three main steps. The first step is ensemble generation, which refers to generation of ensemble base models. The second step is ensemble pruning, which consists of selecting a subset of the best models from the original set of models based on generalization error. Finally, ensemble integration, a strategy to combine the base models is defined. For regression problems, ensemble integration is done using a linear combination of the base models outputs (de Sousa *et al.*, 2012),

$$f_{en}(x) = \sum_{i=1}^{K} [w_i(x) * f_i(x)] \tag{2.5}$$

where, $w_i(x)$ denotes the weight for the ith model, K is the number of models in the ensemble, $f_i(x)$ denotes the output of the ith model corresponding to input x and $f_{en}(x)$ represents the ensemble output. Diversity is a very important key in the ensemble generation. If all ensemble members provide the same output, there is nothing to be gained from their combination (Zhang & Ma, 2012). Therefore, the ensemble members should be different from each other while each must maintain acceptable accuracy level (Amozegar & Khorasani, 2016). Two different methodologies can be considered for creating diversity among ensemble members. The first method is heterogeneous ensemble in which ensemble members have different architectures(such as number of neurons, training algorithm). The second method is homogeneous ensemble in which ensemble members have the same architectures but trained with different data sets (Brown *et al.*, 2005). The integration of a set of learned models to improve accuracy and generalization is another important step in the ensemble generation. Ensemble integration approaches can be divided into two categories,constant and non-constant weighting functions (Merz & Pazzani, 1999). Examples of the constant weight approach are basic ensemble method

(BEM), generalized ensemble method (GEM), linear regression (LR) and median method. For the second category, the weights vary according to performance of each ensemble member such as dynamic weighting (DW), dynamic weight with selection (DWS)(Rooney & Patterson, 2007) and dynamic and on-line ensemble regression (DOER)(Soares & Araújo, 2015).

In recent years, the ensemble approach attracted many researchers and good results have been reported (de Sousa *et al.*, 2012; Amozegar & Khorasani, 2016). The advantage of ensembles as compared to single models has been presented in terms of increase of robustness and generalization (Zhang & Ma, 2012). In the area of gas turbine engines, (Wang *et al.*, 2014; Wen *et al.*, 2019; Lu *et al.*, 2019; Behera *et al.*, 2019; Li *et al.*, 2019) used ensemble learning for tackling the fault detection identification (FDI) problem and prediction of the RUL of gas turbine engine. (Amozegar & Khorasani, 2016; Xu *et al.*, 2017) developed ensemble of multiple learners to identify the gas turbine engine dynamics. In this thesis, we will focus on the ensemble generation for regression.

2.3 Advanced control of gas turbine engine

Control technology has a key role in development and progressing the performance, reliability, operating life, and safety of modern GTEs. The power output from a GTE is determined by fuel flow, and the control system must ensure that the desired power output is achieved. However, the control system must also protect the engine from exceeding any design limits. These limits include component speeds, temperatures and operating regions which can result in compressor surge (Razak, 2007). So that, the control system for a typical gas turbine in a power generation application carries out three primary functions: Engine staring and shut-down sequencing, Control, and Protection.

The implementation of GTE control systems has changed dramatically over the past half-century. Since 1950s, the computing section and the fuel metering section of the control system were incorporated into a hydro-mechanical system in which fuel passing through the unit provided the necessary hydraulic actuation of a variety of pistons, bellows and levers which me-

tered the required fuel to the combustion system. Of necessity, the implemented control strategies must be fairly simple. As control complexity increased, the traditional hydro-mechanical systems became increasingly bigger, heavier, and relatively expensive. As a result, in the early 1970s, electronic control units (ECU) were designed to replace the hydro-mechanical systems. Such ECU results in higher engine operating efficiency by allowing tighter engine control through the use of higher loop gains and improved strategies to reduce transient overshoot or undershoot. Moreover, it allows implementation of control algorithms which would be difficult to implement mechanically (Spang III & Brown, 1999). Today, almost all modern GTE systems employ a full authority digital electronic control (FADEC) for the fuel control computation function. To give some perspective to this commentary, Figure 2.2 shows some of the major technology milestones regarding the application of electronics in engine fuel control systems.

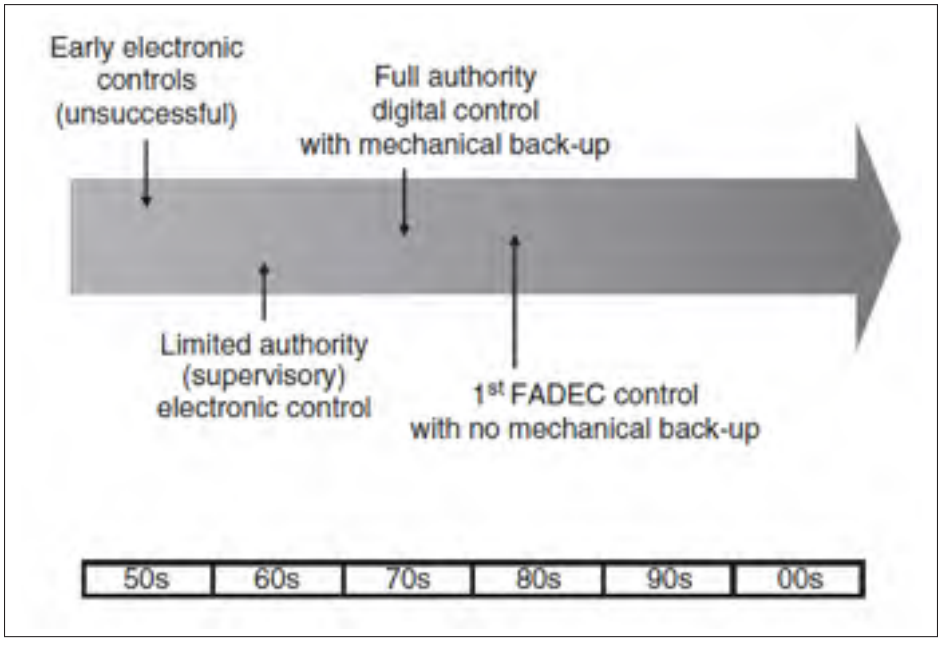

Figure 2.2 History of engine control technology
Taken from MacIsaac & Langton (2011)

New designs and operations of modern GTEs are increasingly complex, where several constraints and control modes should be satisfied simultaneously to achieve a safe and optimal performance for the engine. There are several control strategies proposed to deal with these requirements dating back to 1952. A comprehensive review and analysis on the history of GTEs control strategies could be found in (Jaw & Mattingly, 2009). The Min–Max control strategy is commonly used as the control architecture for GTEs to provide desired power, and prevent the engine from exceeding any safety or operational limits. This strategy is known as a practical algorithm to satisfy all engine control modes simultaneously without any error and malfunction. A min-max controller composed of several control loops (steady state loop, max acceleration loop, max shaft loop speed, max temperature loop, and min deceleration loop), each of which takes the task of observing a different engine controlling mode. These loops are in parallel and at any moment, according to a predefined fuel control strategy, one of them is selected and undertakes the observation (Spang III & Brown, 1999; Montazeri-Gh *et al.*, 2016; Salehi & Montazeri-GH, 2020). Many studies have done for performance improvement of the min-max strategy (Chipperfield & Fleming, 1996; Montazeri-Gh & Jafari, 2011; Esfahani & Montazeri, 2016; Jafari & Nikolaidis, 2018). However, in all these studies the final selection strategy between the transient control loops are kept fixed. Moreover, limit violation may occur for some variables during transient operation. Recent studies have shown that, there is no guarantee for min-max algorithm with linear compensator to protect engine limits during transient state(Imani & Montazeri-Gh, 2017; Montazeri-Gh & Rasti, 2019).

With the desire to have more robustness and flexibility of the next generation of the GTE control systems to achieve ambitious targets and severe limitations set by governments and organizations such as reduction of NOx emission, reduction of fuel consumption, and increase of engine life time, the industry is interested in developing another advanced control strategy that will satisfy the mentioned requirements. MPC is an advanced model-based controller which has attracted the attention of researchers in recent years. The application of MPC to control GTE is introduced by Vroemen and Essen (Vroemen *et al.*, 1999; Van Essen & De Lange, 2001). The philosophy behind the construction of MPC laws is radically different from tra-

ditional error-feedback control approaches. Instead of producing a control action in response to the current and past errors, MPC makes a prediction of future system behavior based on its open loop model, the current system state, the input trajectory, or a disturbance entering the system. Then, it selects the best possible input action according to a cost function. To do this it has to solve an optimization problem, subject to possible constraints. Finally, it applies the first element of the optimal selected input sequence to the plant. At each time step, this procedure is repeated, which introduces the so-called receding horizon principle (Richter, 2011). MPC used in a wide variety of application areas including power plants, chemical industries and etc. The main reason for this is its constraint handling capacity. Unlike most other traditional control strategies, constraints on inputs and outputs can be incorporated into the MPC optimization. Another benefit of MPC is its ability to predict future events as soon as they enter the prediction horizon. Finally, MPC is an essentially multi-variable control strategy, implying that control loops do not need to be decoupled, because all interactions between multiple inputs and outputs are accounted for by the model (Camacho & Alba, 2013).

There are various MPC algorithms only differ among themselves in the onboard model used to represent the controlled process. If a linear model is used for prediction, The MPC approaches which use for prediction linear models are usually named linear MPC algorithm (LMPC) (Mu & Rees, 2004; Ghorbani *et al.*, 2008a; Pandey *et al.*, 2018). However, If a non-linear model is used for prediction, The MPC approaches which use for prediction non-linear models are usually named non-linear MPC algorithm (NMPC) (Brunell *et al.*, 2002; Kim *et al.*, 2013; Pires *et al.*, 2018b). In recent years, there have been extensive interests in the generalized predictive control (GPC) algorithm, which is one of the most popular predictive control algorithms and has been successfully applied in industry, particularly in chemical processes, power, and gas turbines (Mu & Rees, 2004; Aly & Atia, 2012; Ye *et al.*, 2017). The basic idea of GPC is to calculate a sequence of future control signals in such a way that it minimizes a cost function defined over a prediction horizon. The index to be optimized is the expectation of a quadratic function measuring the distance between the predicted system output and some predicted reference sequence over the prediction horizon plus a quadratic function measuring

the control effort (Camacho & Alba, 2013). Moreover, the GPC is applicable to the systems with non-minimal phase, unstable systems in open loop, systems with unknown or varying dead time and systems with unknown order (Pivoňka & Nepevnỳ, 2005).

Ghorbani *et al.* (2008b) used a linear ARX model in a multi-variable MPC strategy for a gas turbine power plant, and the same authors used the same model type in a constrained MPC strategy for a heavy-duty gas turbine power plant (Ghorbani *et al.*, 2008a). Mohamed *et al.* (2016) presented a strategy for implementing LMPC to a large gas turbine power plant. A generalized state space model for that engine was used as an onboard model within the LMPC. Also, Pandey *et al.* (2018) designed a MIMO linear state-space model to simulate the response of 5 MW industrial GTE at certain operating condition, then be used to design a LMPC for this engine. Based on the fact that GTE is inherently non-linear. The inherent non-linearity together with higher product quality specifications, increasing productivity demands, tighter environmental regulations, and demanding economical considerations require to operate systems over a wide range of operating conditions and often near the boundary of the safe region. Under these conditions linear models are often not sufficient to describe the process dynamics adequately and non-linear models must be used. This inadequacy of linear models is one of the motivations for the increasing interest in NMPC.

Pires *et al.* (2018a) designed a NMPC to reduce the NOx emissions of a single-shaft industrial GTE. The non-linear dynamic behavior of the engine is modelled using the academic DESTUR program, a comprehensive first principle computational modelling tool. Four optimization algorithms are used to minimize the objective function, and their performances are compared: differential evolution, particle swarm, genetic algorithm, and pattern search method. The authors concluded that, the computational effort is higher for the MIMO system. However, The four algorithms perform well and are viable for the SISO system implementation.

Kim *et al.* (2013) proposed a NMPC to control the speed and temperature of a 166 MW a single-shaft heavy-duty gas turbine power plant. A reduced order model with 1 sec sampling rate is used to simplify calculations. As can be seen, the usage of a non-linear physics based

model within the NMPC changes the control problem from a convex quadratic program to a nonconvex non-linear problem. Furthermore, in this situation, there is no guarantee that the global optimum can be found especially in real-time control when the optimum has to be obtained in a prescribed time. Besides, the physics based model should be run many times faster than real time to allow usage of this model as model based inside the MPC algorithm.

Therefore, a set of efficient approaches that try to avoid the problems associated to nonconvex optimization has appeared in recent years. One of the simplest ways of dealing with process non-linearities is to perform successive linearization about a nominal operating point. Every sampling period an updated linear model is derived from an underlying non-linear model. In recent years, the successive linearization approach attracted many researchers and good results have been reported (Van Essen & De Lange, 2001; Mu & Rees, 2004; Niu & Liu, 2008; Theoklis *et al.*, 2019; Montazeri-Gh & Rasti, 2019). The advantage of using this method over conventional non-linear design is the avoidance of the problem of local minimums. However, this could result in a large computational load for MIMO systems. Furthermore, the lineraized model is only an approximation of the original non-linear one. Therefore, the obtained control quality may be unsatisfactory for non-linear systems, in particular when the operating point is changed significantly and fast.

As can be seen, the generation of accurate model which can run many times faster than real time, is a big challenge in NMPC design. The use of the ANN in NMPC has been recognized as a effective tool for handling some difficult control process problems, and has recently attracted a great deal of attention (Rusnak *et al.*, 1996; Sørensen *et al.*, 1999), primarily because ANN appear to provide a convenient means for modelling complex non-linear processes with good accuracy and less computational complexity. Two main approaches were used to utilise non-linear neural model in a predictive control scheme (Aly & Atia, 2012). The first idea is to use the non-linear optimization to get the optimum control (Lazar & Pastravanu, 2002). The other is to linearize the non-linear neural model every time step to get the discrete linearized model (Mu & Rees, 2004; Mu *et al.*, 2005). Pivoňka & Nepevnỳ (2005) designed a constrained GPC based on NN model. Authors stated that the designed controller is adaptive, as it based on NN

model which can observe system changes and adapt itself. Rusnak *et al.* (1996) presented the GPC algorithm based on ANN plant model. To obtain the step and the free process responses which are needed in the GPC, the feed-forward ANN model was used to estimate the free and forced responses. The system free response is obtained instantaneously from ANN model while forced response is obtained from instantaneous linearization of the ANN model. This method considered as a trade-off between NMPC and successive linearization approach.

In contrast to LMPC, where convex quadratic programs are mostly solved exactly at each sampling time, NMPC faces an issue: either the non-linear iteration procedure is performed until a pre-specified convergence criterion is met, or the procedure is stopped prematurely with only an approximate solution, so that a pre-specified computation time limit can be met. In (Diehl *et al.*, 2009), the authors gave an overview of Newton type methods for online solution of non-linear optimal control problems. The two big families of Newton type optimization methods, SQP and Interior-point methods were presented. The authors concluded that, NMPC results in improved control performance and allows the direct use of physics based models. However, the consideration of non-linear models also poses challenging theoretical, computational, and implementational problems especially for real time applications. Pires *et al.* (2018b) stated that, computation of the gradient may not be feasible or cost-effective when using a non-linear model within NMPC. Therefore, search methods or heuristic methods become attractive. The maximum number of iteration is an important parameter for theses methods. The control performance could be improved with the increase in the maximum iteration number. However, it will be computationally expensive.

2.4 Conclusion of literature

This chapter presented a comprehensive overview of the literature in the field of modelling, simulation, and control of gas turbines. As it can be seen from the literature, there is a great gain from the research in this field like gas turbine performance evolution and optimization before and after design and manufacture processes. Therefore, the most relevant scientific

sources and significant research activities in this area for different kinds of gas turbines were discussed and summarized. Based on the literature survey, we can note the following issues:

1. There are different approaches to model a dynamic system such as gas turbine. Various kinds of models have been built so far from different perspectives and for different purposes. Mathematical models can be classified according to several different criteria as shown in Figure 2.3.

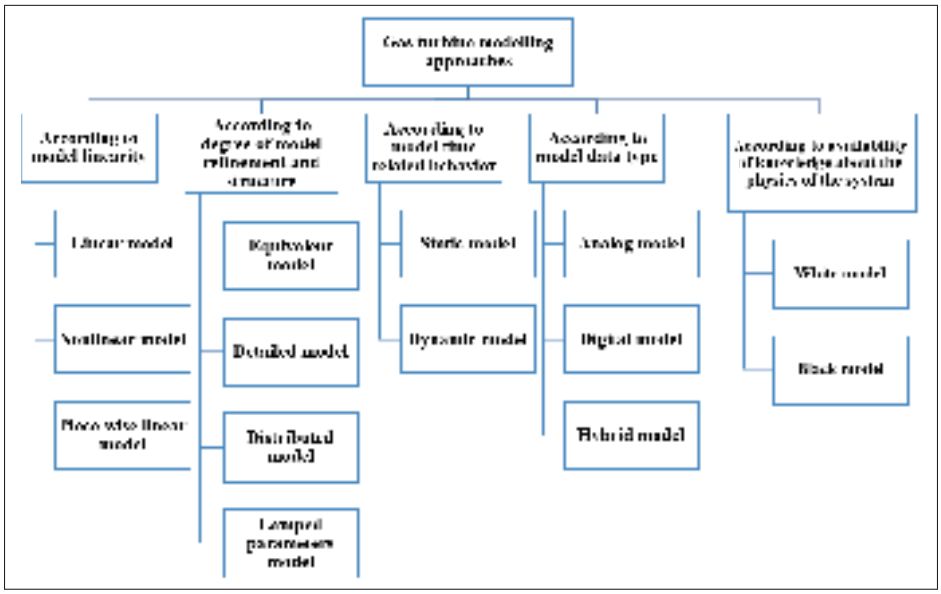

Figure 2.3 Gas turbine modelling approaches

2. The physics based model is very complicated and requires iterative solution, which occurs at the expense of computation time. So that, to enable calculation of the physics based models in real time, software and hardware approaches have been proposed by many researchers:

   - Hardware modification, such as:
     - Application of parallel processing.
     - Utilization of faster computer.

- Software modification, such as:
  - Utilization of more efficient iteration techniques.
  - Utilization of simple models (neglecting the secondary effect parameters).
  - Permitting increased off-line calculation, and thus reducing the required on-line calculations.

3. The computation time challenge is not a big problem for the performance applications. However, this is not the case for the model-based applications. In the case of model based application, the physics based model should be accurate. Besides that, it must run many times faster than real time. An alternative to physics based models is given by data-driven based models, which can represent dynamics of non-linear systems with good accuracy and very low computation effort. So that, the data-driven based models are recommended by many researchers for using in model based applications.

4. Most of static and dynamic ANN research activities on gas turbine engines used a certain structure of neural networks namely, a feed forward neural network, one hidden layer with a number of neurons in this layer ranging from nine to twelve, a tansig activation function in the hidden layer and purelin activation function in the output layer. Finally, Levenberg-Marquardt algorithm is used as a training algorithm. It is important therefore to test other combinations, and to perform an extensive performance comparative study using a combination of different network architectures, training algorithms, activation functions, system order and different number of neurons. This will be done in this study.

5. In the area of MIMO ANN model of gas turbine engines, the research activities used mostly one of the following two methods to generate a nonlinear model for the MIMO engine: Either, by building a neural network model for each output parameter (MISO) with the same structure for each one of them and trained with the same training algorithm (Bahlawan *et al.*, 2017), or by building one block neural model to represent the MIMO system (Tarik *et al.*, 2017; Mehrpanahi *et al.*, 2018; Salehi & Montazeri-Gh, 2018). However, it is more powerful, as will be shown in this study, to use a different neural network's

structure for each output (MISO). The idea of using different NN structures for different outputs comes from analysis of the structure of the human brain based on its function. Human brain consists of many complex biological neural networks; each has to perform a certain function [talk, walk, breath and so on] as shown in Figure 2.4. The main component of these neural networks are neurons. The shape and number of the neurons in each network depend upon the function of the network. For example, a single sensory neuron from your fingertip has an axon that extends the length of your arm, while neurons within the brain may extend only a few millimetres. They also have different shapes depending on their functions (Khan, 2018). Motor neurons that control muscle contractions have a cell body on one end, a long axon in the middle and dendrites on the other end. Sensory neurons have dendrites on both ends, connected by a long axon with a cell body in the middle. Inter-neurons, or associative neurons, carry information between motor and sensory neurons as shown in Figure 2.5. Based on these facts, to generate a neural network model for an ADGTE, we propose to build MISO neural network model for each output. Moreover, the structure of each neural model is different according to the function of the model (output type).

6. As can be seen, the usage of single neural model may not be able to provide accurate prediction when it operates outside the field in which it was trained. Besides, gas turbine engines operate in non-stationary operation conditions, which may cause unseen scenarios in the observed data. This increases the complexity of the modelling operation since the NN needs to be trained with a data as large enough to cover the entire operation conditions. This in turn increases the training time and the possibility of network over-fitting. To address this problem, we consider to train multiple ANNs in parallel to fit the data instead of a single model. This leads to an ensemble of neural network models.

7. According to the literature, most works on ensemble approach focus on classification applications for tackling the FDI problem in gas turbine engines (Wang *et al.*, 2014; Wen *et al.*, 2019; Lu *et al.*, 2019; Behera *et al.*, 2019; Li *et al.*, 2019). However, little research has been done on the use of ensemble approach for gas turbine engine real time perfor-

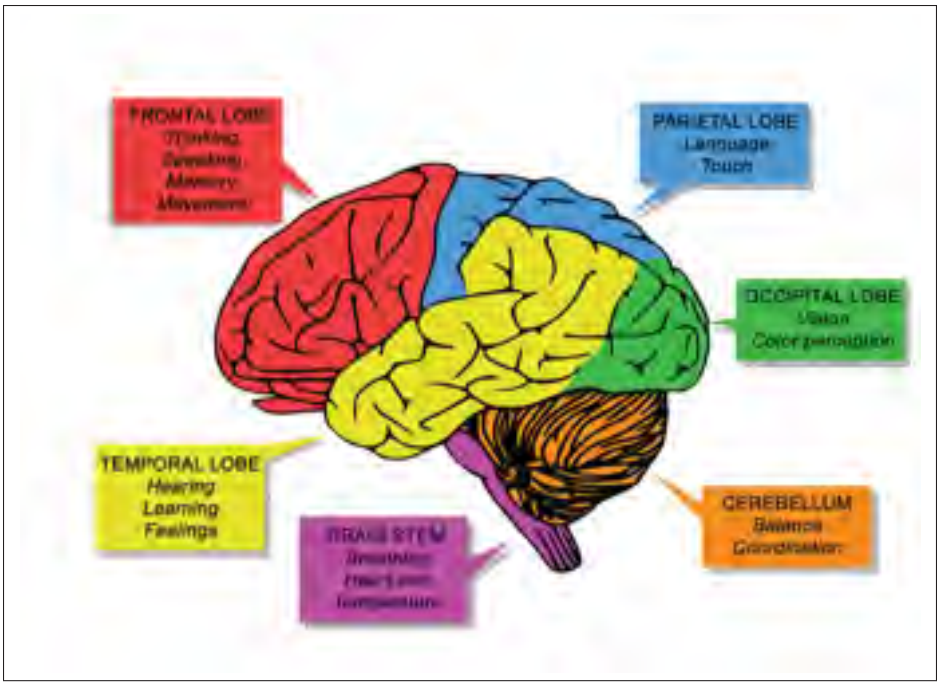

Figure 2.4 Functions of the human brain
Taken from CASTRO (2018)

mance prediction (Amozegar & Khorasani, 2016; Xu *et al.*, 2017). Based on that, this thesis will focus on the ensemble generation for regression. A novel approach for the performance simulation of ADGTE through system identification using ensemble methods is proposed.

8. The Min–Max control strategy is the most widely used control algorithm for industrial GTEs. This strategy uses minimum and maximum mathematical functions to select the winner of different engine control loops at any instantaneous time. However, recent studies (Imani & Montazeri-Gh, 2017; Montazeri-Gh & Rasti, 2019) indicate that this method with linear compensators suffers from lack of safety guarantee in fast load demands. On the other hand, MPC method, which incorporates input/output constraints in its optimization process, has the potential to fulfill the control requirements of an industrial GTEs.

9. The LMPC algorithms are simple to design and are computationally uncomplicated. Unfortunately, the obtained control quality may be unsatisfactory for nonlinear systems, in particular when the operating point is changed significantly and fast. In such cases non-

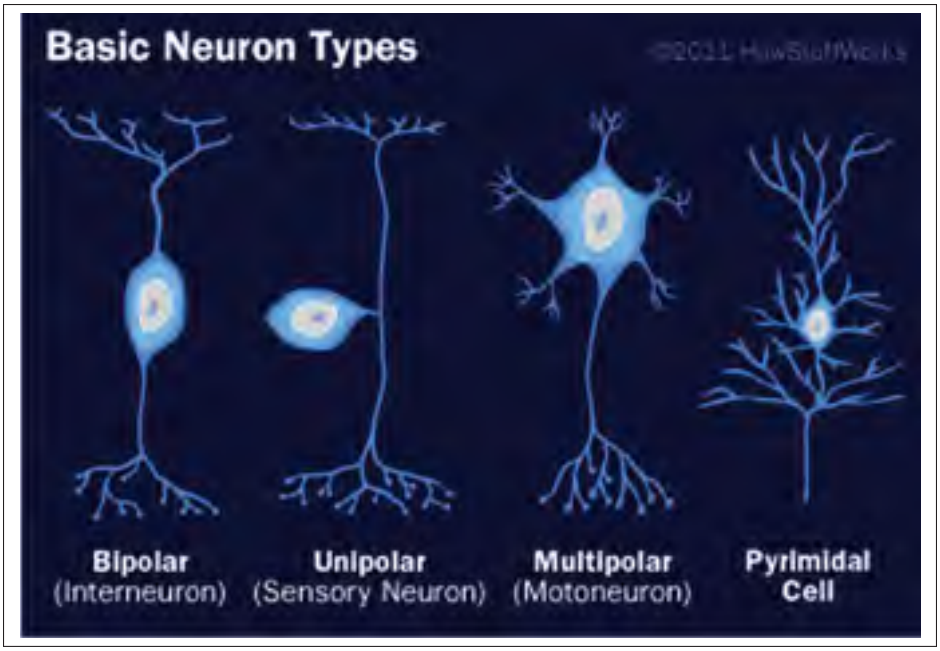

Figure 2.5 Basic neuron types
Taken from Khan (2018)

linear models are straightforward, but their identification is more demanding. Furthermore, complexity of NMPC algorithms is higher than that of the classical linear ones. The implementation of NMPC of ADGTE in real time has two challenges: Firstly, the design of accurate non-linear model which can run many times faster than real time. Secondly, the usage of rapid and reliable optimization algorithm to solve the optimization problem in real time.

10. The resulting implementation of NMPC based on NN model is able to eliminate the most significant obstacles encountered in non-linear predictive control applications by facilitating the development of non-linear models and providing a rapid, reliable solution to the control algorithm.

11. The use of NN models together with the GPC algorithm is a promising technique. Most applications of GPC algorithm based on NN model have used instantaneous linearization of the NN model at each time step. In this thesis, to design an NMPC of ADGTE, a trade-off approach between usage of non-linear model and successive linearization approach is

used in order to reduce the computation effort. In addition, in order to solve this problem, Hildreth's quadratic programming procedure is utilized which offers simplicity and reliability in real-time implementation.

CHAPTER 3

NEURAL NETWORKS MODELLING APPROACH

3.1 Introduction

This chapter embodies the real core of this work, which makes it the most extensive chapter of the thesis. At the next step, ANN model building process including system analysis, data acquisition and preparation, network architecture, as well as network training and validation are explained. The last part of the chapter is focused on the generation of ensembles of NN models.

3.2 Neural network basics

ANN is a non-linear statistical data modelling tool mimicking the neural structure of the human brain. NNs are composed of simple elements operating in parallel. These elements are inspired by biological nervous systems. As in nature, the network function is determined largely by the connections between elements. ANN is trained to perform a particular function by adjusting the values of the connections (weights) between elements. Each such single element is called a neuron. Neurons are arranged in different layers including input layer, hidden layer(s) and output layer. The number of neurons and layers in an ANN model determine the degree of complexity of the network. Figure 3.1 shows a simple structure of a simple NN with four inputs, one output and four neurons in two hidden layers.

3.3 ANN modelling approach

There are many challenges in the building operation of neural networks model, which can be summarized as follows:

- Finding the best neural network type.

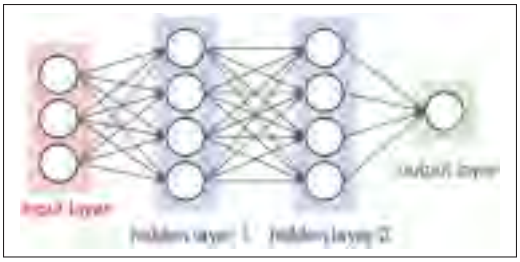

Figure 3.1 A simple structure of an ANN with input, hidden and output layers

- Finding the best training algorithm.
- Finding the best activation function.
- Finding the system order.
- Finding the number of the neurons in the hidden layer.

This thesis presents a novel methodology for modelling ADGTE using ensembles of NARX neural networks. This is a general methodology which can be used in generation of accurate, generalized and real time black box models, and has the advantage of greatly reducing the network training time. The flow diagram of the modelling approach is illustrated in Figure 3.2.

3.3.1 Data acquisition and preprocessing

Data acquisition is the first step and a vital part of ANN modelling approach. The required closed loop engine data can either be collected directly from testing of the actual GT engine (if it is available) or with the help of a high fidelity simulation model that is as realistic as possible. The later possibility is of special interest for collecting data on critical transients scenarios that should be avoided on the actual plant due to risk of damage.

The closed loop datasets which were used in this study are time series datasets consisting of six input parameters (WF, VIGV, LPBOV, IPVSV, IPBOV, and HPBOV) and seven output parameters (N_L, N_I, N_H, PW, T_{30}, P_{30}, and TGT) representing the engine operation from the

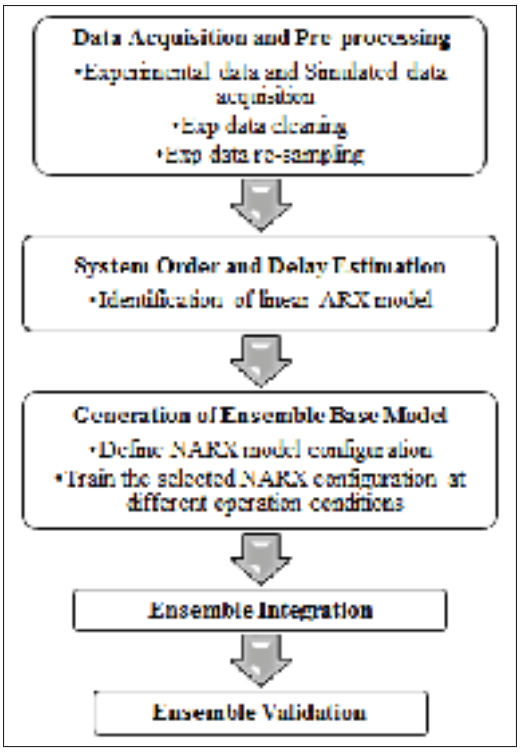

Figure 3.2 The flow diagram of the modelling approach

Synch-Idle or Synch speed (3600 rpm) with no load (unloading) regime to Synch speed with full load regime (loading). The starting and shutdown regimes are not represented in this work.

Note that, these datasets were taken at different operation conditions: ambient temperature T_{amb}[C], ambient pressure P_{amb}[kPa], fuel lower heating value LHV[kJ/kg] and engine's thermal efficiency η_{th}. The thermal efficiency was used to represent the performance degradation of the engine, which is defined as the ratio between the output shaft energy to the added energy as shown in equation (3.1) (H.I.H. Saravanamuttoo, 2017). The only available closed loop experimental data from testing of SGT-A65 engine was collected at a specific operation condition. More data was needed however to train NN models at different operation conditions and use those models to generate the NN ensemble. To generate data at different operation conditions we used Siemens high fidelity thermodynamic model. The accuracy of this model has been well validated by Siemens, so combining experimental data with high fidelity simulated data was the best solution given the limited availability of experimental data. Table 3.1 shows

more details about these datasets, where TR is the training dataset and TS is the testing dataset.

$$\eta_{th} = \frac{PW}{WF * LHV} \tag{3.1}$$

Table 3.1 Time series datasets

Dataset	No of samples	T_{amb}	P_{amb}	LHV	η_{th}
$TR1_{exp}$	21983	26	101.32	48360	0.32
$TS1_{exp}$	8117	26	101.32	48360	0.32
$TS2_{exp}$	17186	26	101.32	48360	0.32
$TS3_{exp}$	3551	26	101.32	48360	0.32
$TR2_{sim}$	15132	30	101.32	47826	0.4231
$TS2_{sim}$	17231	30	101.32	47826	0.4231
$TR3_{sim}$	22480	15	101.32	47826	0.4067
$TS3_{sim}$	12890	15	101.32	47826	0.4067
$TR4_{sim}$	13172	0	101.32	47826	0.4236
$TS4_{sim}$	12067	0	101.32	47826	0.4236
$TR5_{sim}$	16691	-15	101.32	47826	0.4038
$TS5_{sim}$	8816	-15	101.32	47826	0.4038
$TR6_{sim}$	8732	30	101.32	35717	0.3931
$TS6_{sim}$	3700	30	101.32	35717	0.3931
$TR7_{sim}$	8820	15	101.32	35717	0.4061
$TS7_{sim}$	12750	15	101.32	35717	0.4061
$TR8_{sim}$	15044	-15	101.32	35717	0.4092
$TS8_{sim}$	21065	-15	101.32	35717	0.4092

The experimental time series datasets $TR1_{exp}$ and $TS1_{exp}$ are used for pre-processing operation for extracting the most valuable information about the system dynamics to use in identification of ANN models. Firstly, the experimental datasets $TR1_{exp}$ and $TS1_{exp}$ are cleaned by filtering any measurement noise. A simple second order low pass Butterworth digital filter with cut-off frequency 0.5 Hz was used to remove noise from experimental datasets. After that, cleaned datasets [$TR1_{exp}$ and $TS1_{exp}$] were re-sampled at a lower frequency F_s =10 Hz instead of high sampling frequency 20 Hz to avoid aliasing effects and to avoid having the poles of the discrete models being very close to the +1 point on the unit circle. In addition, the lower sampling rate reduces the number of data points which reduces the computation time during training

operation and reduces data collinearity. The selection of the sampling rate was performed based on the Nyquist sampling criterion, which requires setting the sampling rate at least twice the highest frequency of the system.

3.3.2 System order and delay estimation

$TR1_{exp}$ and $TS1_{exp}$ datasets are used in this step after cleaning and re-sampling. Selecting the model order and delay is a key first step towards the goal of identification of non-linear NNs model. A selection procedure is frequently implemented by developing several NN models with different orders and delays and comparing models to evaluate their performance. However, the influence of NN parameters such as number of neurons, training algorithm and activation function may lead to an inappropriate selection. In addition, this method is time consuming. Another approach was used in this thesis, which starts by estimation of the time delays from inputs to outputs n_k by using a non-parametric estimate of the impulse response using MATLAB® routine *impulseest*. This gives good starting points in identification because it requires minimal user specification (Alves *et al.*, 2013). Figure 3.3 represents the impulse response for WF and N_H input-output data. There is a clear indication that the impulse response "takes off" (leaves the confidence region represented by the shaded area in the figure) after one sample (red circle), this points to a delay of one sampling interval.

Secondly, estimation of the system order by generation of a set of candidate MISO ARX models and determining the best model order in the set. The ARX model structure is one of the simplest parametric structures and it is considered a good starting point for identification process because of its simplicity. The general structure of MISO ARX model is shown in equation (3.2).

$$A(q^{-1})y(t) = B_1(q^{-1})u_1(t-n_{k_1}) + \cdots + B_j(q^{-1})u_j(t-n_{k_j}) \tag{3.2}$$

$$A(q^{-1}) = 1 + a_1 q^{-1} + \cdots + a_{n_y} q^{-n_y} \tag{3.3}$$

$$B(q^{-1}) = b_1 + b_2 q^{-1} + \cdots + b_{n_u} q^{-n_u+1} \tag{3.4}$$

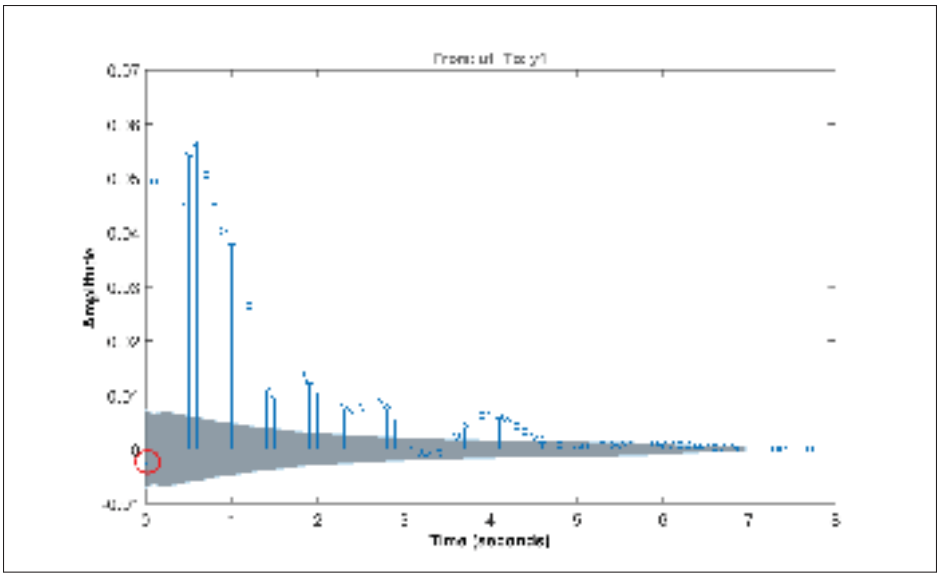

Figure 3.3 Impulse response from WF to N_H used to estimate the input-output delay

where $A(q^{-1})$ and $B(q^{-1})$ are coefficient's polynomials to be estimated by using the prediction error method (PEM). MATLAB® routine *struc* is used to generate a set of model-order combination of MISO ARX model estimation. The routine *struc* changes n_u and n_y for all inputs and outputs from one to five, as higher-order models result in excessive computational effort and pose the risk of losing particular physical meaning of the model, and uses the input-output delay values n_k from delay estimation step. After that, MATLAB® routine *arxstruc* uses the set of model order combination to estimate a set of MISO ARX models based on the $TR1_{exp}$ dataset. The Final Prediction Error (FPE) evaluates model quality, where the model is tested on another dataset $TS1_{exp}$. Such a procedure is known as cross validation. The most accurate model has the smallest FPE. The FPE equation is defined by the following equation:

$$FPE = \frac{1+\frac{d}{N}}{1-\frac{d}{N}}V \tag{3.5}$$

where d is the total number of estimated parameters and N is the length of the data record. V is the loss function (quadratic fit) for the structure in question. Finally, checking Pole-Zero Cancellations for this selected ARX model is performed. MATLAB allows plotting estimated pole-zeroes with their confidence intervals, which allows you to detect any pole-zero cancella-

tions (confidence ellipse overlap). Removing these provides a trimmed model order. Table 3.2 summarizes the results from delay and order estimation process for all MISO models for all output parameters of the engine and uses these results in the non-linear NN identification process. This will be illustrated in the next subsection.

Table 3.2 System order and delay estimation results

Output parameter	n_y	n_u	n_k
N_H	4	[4 4 4 4 4 4]	[1 0 2 0 0 0]
N_I	4	[4 4 4 4 4 4]	[1 1 3 0 0 0]
N_L	4	[4 4 4 4 4 4]	[0 2 1 1 0 0]
PW	4	[2 2 4 4 4 4]	[1 0 3 0 0 0]
TGT	4	[1 4 4 1 1 4]	[1 0 0 0 0 0]
T_{30}	4	[3 1 4 2 1 1]	[6 2 4 3 0 0]
P_{30}	4	[1 2 2 1 1 4]	[0 0 2 1 0 0]

3.3.3 NARX model configuration

This subsection describes the development of multiple MISO NARX models with different configurations to represent each of the engine output parameters. Constructing the MISO NARX model requires determination of network parameters. Such as (i) number of neurons, (ii) number of hidden layers, (iii) hidden layer activation function and (iv) training algorithm. To limit the network complexity, the number of hidden layers is limited to one. Besides, Cybenco Cybenko (1989) proved that NN with one hidden layer of hyperbolic tangent or sigmoid activation function and one output layer of linear activation function could simulate any non-linear system. Another important parameter in the NARX configuration is the training architecture. The NARX network training can be implemented via two architectures: (i) series-Parallel architecture (S&Pr), where the network is trained in open loop mode then transformed to closed loop mode for validation operation, (ii) parallel architecture (Pr), where the network is trained and validated in closed loop mode. In this thesis, to get the optimal NARX model structure which can represent the ADGTE dynamics, we performed an extensive comparative performance study using different combinations of NARX neural network architectures, train-

ing algorithms and activation functions while using different numbers of neurons. As a result, a comprehensive computer program was developed in the MATLAB environment. Figure 3.4 shows the flow diagram of the comprehensive computer program for the MISO NARX model of the ADGTE. This program generates 240 NARX models with different structures by performing the following:

1. Changing of the number of neurons from 1 to 20.
2. Usage of two activation functions logsig and tansig.
3. Usage of three training algorithms trainlm, trainscg and trainbr.
4. Training the network with series-parallel architecture and parallel architecture.

One of the problems that occur during NN training is network over-fitting. The early stopping and cross validation are the default methods for improving network generalization and reduce occurrence of over-fitting during the training operation. When the network begins to over-fit the data, the validation error begins to increase, and after a certain number of iterations, the training is stopped, and the weights and biases at the minimum validation error is fixed.

In this thesis, the network training parameters are defined as: (i) the mean square error (mse) performance function which is minimized until it reaches a sufficiently low cut-off value of (0.01), (ii) the maximum number of training epochs (1000) which represents the number of times that all the training patterns are presented to the NN and (iii) the maximum number of validation increase (100) which represents the number of successive epochs in which the performance function fails to decrease. Training operation was repeated three times for the same neural network with the same input data set to increase the accuracy of the network. The $TR1_{exp}$ dataset is partitioned into 80% used for training the network and 20% used for cross validation. After finishing the network training operation, the $TS1_{exp}$ dataset is used for testing the network and evaluating its generalization performance. (*RMSE*) was used for the evaluation of the network performance in the training and testing operation. It was calculated

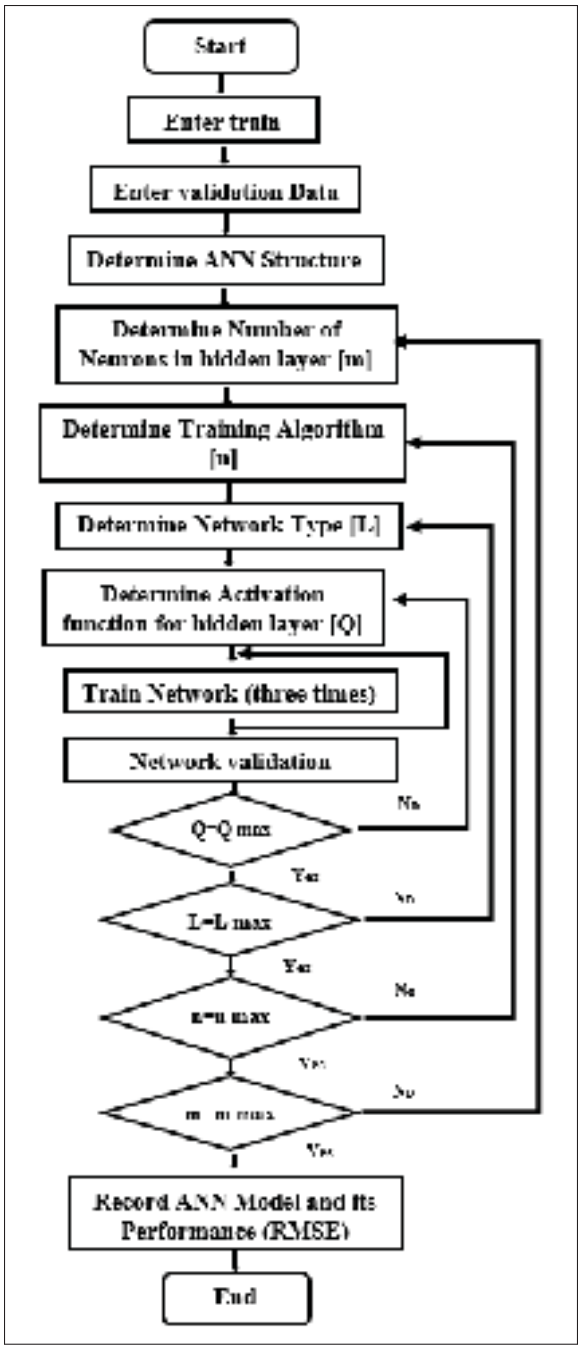

Figure 3.4 Flow diagram of
the generated computer code for
NARX model of the ADGTE

for the whole set of data of each output parameter from the NN, and defined according to equation (3.6),

$$RMSE = \sqrt{\frac{1}{N}\sum_{i=1}^{N}(\frac{y_m - y}{y_{max}})^2} \tag{3.6}$$

where, y_m is the actual output and y is the predicted output. The results of each computation cycle were recorded in a matrix form which includes the network structure, the root mean square error (*RMSE*) for training process, (*RMSE*) for testing process, and training time. The summary of the network constructions for N_H is shown in Table 3.3. Next, the best NN was selected based on the minimum value of (*RMSE*) during testing operation. This will be illustrated in the next subsection.

Table 3.3 Summary of construction of MISO-NARX models for N_H

No of Neurons	**Training Algorithm**	**S & Pr / Pr**	**Activation Function**	**RMSE Train**	**RMSE Test**	**Training Time (s)**
3	trainscg	Pr	tansig	0.3264	0.3251	10.622
3	trainbr	S & Pr	logsig	0	0.0029	2.57
3	trainbr	S & Pr	tansig	0	0.0063	2.6
3	trainbr	Pr	logsig	0.0008	0.0141	22.895
3	trainbr	Pr	tansig	0.9356	0.9644	1.561
4	trainlm	S & Pr	logsig	0	0.0043	3.65
4	trainlm	S & Pr	tansig	0	0.1024	2.851
4	trainlm	Pr	logsig	0.0276	0.0333	1.517
4	trainlm	Pr	tansig	0.0395	0.0479	1.542
4	trainscg	S & Pr	logsig	0.0009	0.1072	11.838
4	trainscg	S & Pr	tansig	0.0009	0.1194	12.356
4	trainscg	Pr	logsig	0.0368	0.0312	21.65
4	trainscg	Pr	tansig	0.0528	0.0389	13.003
4	trainbr	S & Pr	logsig	0	0.0054	2.919
4	trainbr	S & Pr	tansig	0	0.0659	2.916
4	trainbr	Pr	logsig	0.2192	0.258	1.569
4	trainbr	Pr	tansig	0.1241	0.1245	1.565
5	trainlm	S & Pr	logsig	0	0.0056	3.491
5	trainlm	S & Pr	tansig	0	0.0554	3.373

3.3.4 The best model selection process

In order to find the best NN model for the SGT-A65 engine, the output data from the developed computer program was divided into four groups as follows:

First group series-parallel NARX models with tansig activation function, different numbers of neurons, and different training algorithms.

Second group series-parallel NARX models with logsig activation function, different numbers of neurons, and different training algorithms.

Third group parallel NARX models with tansig activation function, different numbers of neurons, and different training algorithms.

Fourth group parallel NARX models with logsig activation function, different numbers of neurons, and different training algorithms.

Finally, the most accurate MISO-NARX model with minimum *RMSE* during testing operation is selected. Table 3.5 to Table 3.11 summarize the results from each group for each output parameters of the SGT-A65 engine. Table 3.4 summarizes the selected MISO NARX models for each output parameters of the SGT-A65 engine. Figure 3.5 and Figure 3.6 show networks structure for all output parameters of SGT-A65 engine.

Table 3.4 The best MISO NARX models configuration

Output parameter	**NO of neurons**	**Training Algorithm**	**S & Pr / Pr**	**Activation Function**	**Training RMSE**	**Testing RMSE**
N_H	2	trainbr	S & Pr	logsig	0	0.0022
N_I	3	trainscg	S & Pr	logsig	0.0002	0.0018
N_L	2	trainlm	Pr	logsig	0.0006	0.0007
PW	15	trainscg	S & Pr	logsig	0.0004	0.0107
TGT	11	trainscg	S & Pr	logsig	0.0002	0.0011
T_{30}	15	trainlm	S & Pr	logsig	0.0002	0.0076
P_{30}	5	trainscg	S & Pr	logsig	0.0041	0.005

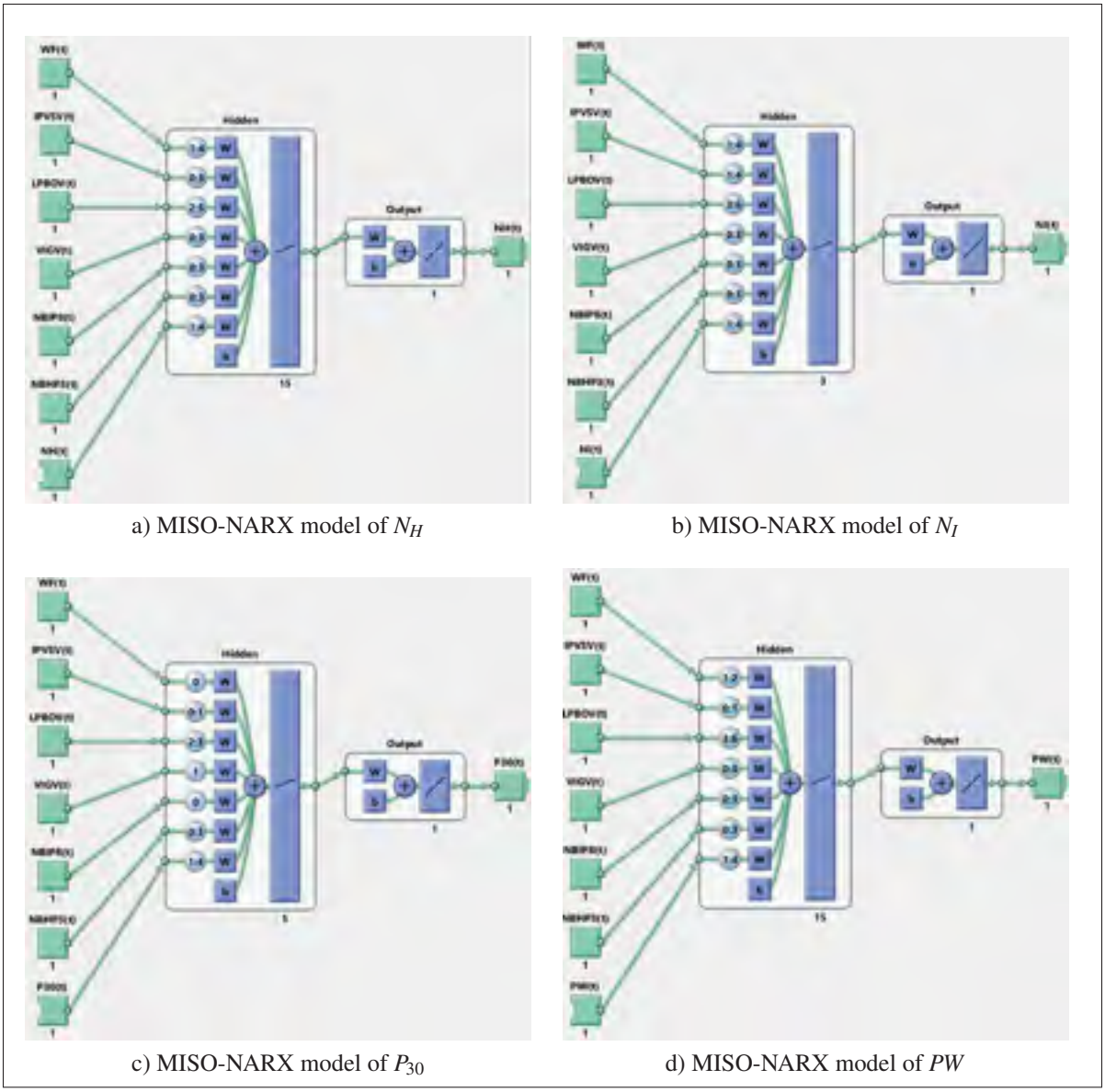

a) MISO-NARX model of N_H

b) MISO-NARX model of N_I

c) MISO-NARX model of P_{30}

d) MISO-NARX model of PW

Figure 3.5 MISO-NARX models of SGT-A65 engine

The comparison between engine output and the selected NN output for all engine output parameters during both training and testing operation are shown in Figure 3.7 through Figure 3.13. As can be seen, the outputs from the MISO-NARX models followed the targets precisely and can predict the reaction of the system to changes in input parameters with high accuracy and reliability. The following subsections summarize the results for each output parameters of the SGT-A65 engine.

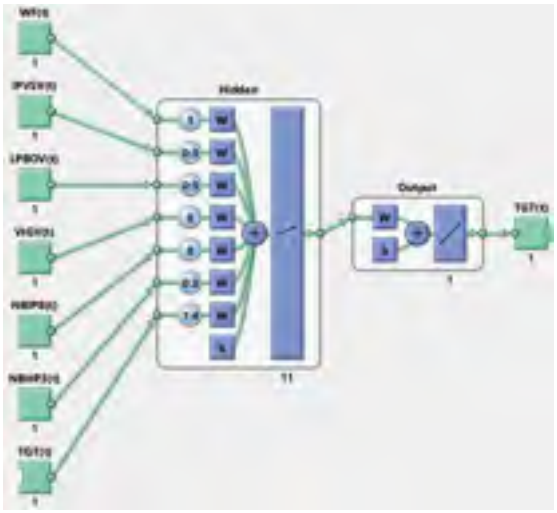

a) MISO-NARX model of TGT

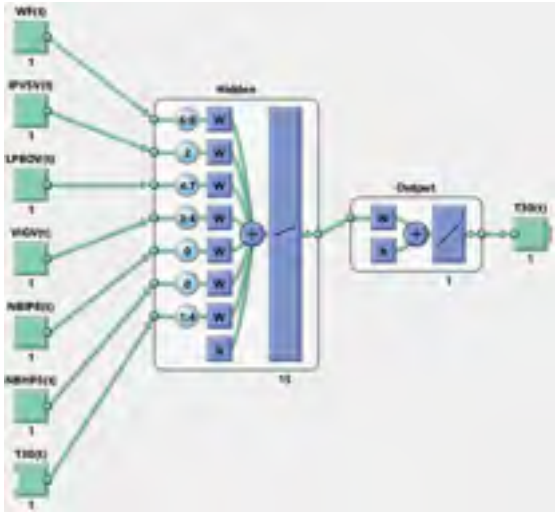

b) MISO-NARX model of T_{30}

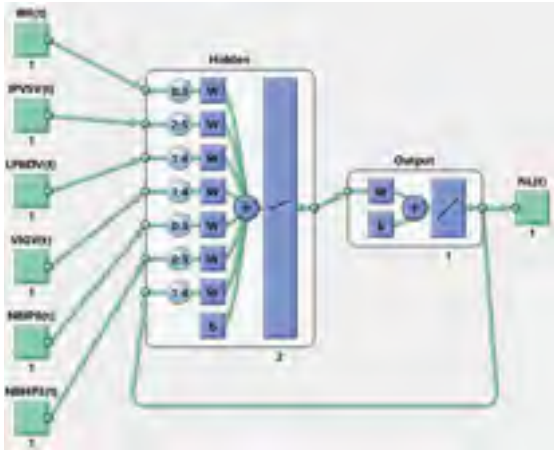

c) MISO-NARX model of N_L

Figure 3.6 MISO-NARX models of SGT-A65 engine

3.3.4.1 MISO-NARX model of N_H

Table 3.5 summarizes the results from each group for N_H during network construction operation. Figure 3.7 shows the comparison between actual engine output and the selected MISO-NARX model output during both training and testing operation. As can be seen, the outputs from the MISO-NARX model followed the targets precisely and can predict the reaction of the system to changes in input parameters with high accuracy.

Table 3.5 The best MISO NARX models configuration for N_H

No of Neurons	Training Algorithm	S & Pr / Pr	Activation Function	RMSE Train	RMSE Test	Training Time
2	trainbr	S & Pr	tansig	0	0.0023	12.031
1	trainlm	S & Pr	tansig	0	0.0024	1.098
12	trainscg	S & Pr	tansig	0.0004	0.0063	1.609
1	trainlm	S & Pr	logsig	0	0.0024	1.114
2	trainbr	S & Pr	logsig	0	0.0022	2.126
1	trainscg	S & Pr	logsig	0.0005	0.0036	0.97
18	trainlm	Pr	tansig	0.0007	0.0028	1544.236
1	trainscg	Pr	tansig	0.0023	0.003	10.138
2	trainbr	Pr	tansig	0.0017	0.0037	17.237
2	trainlm	Pr	logsig	0.0008	0.0028	16.333
19	trainscg	Pr	logsig	0.0009	0.0028	281.202
2	trainbr	Pr	logsig	0.0019	0.0027	15.962

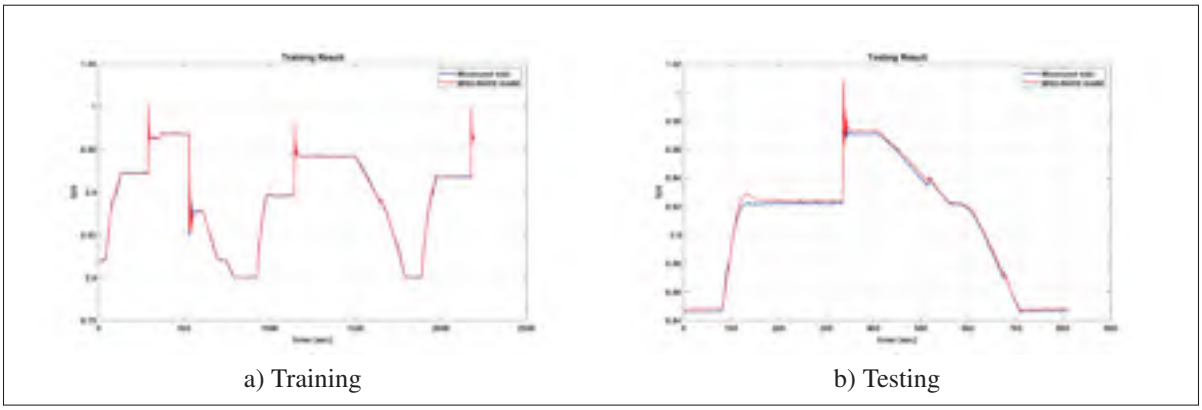

a) Training b) Testing

Figure 3.7 MISO-NARX model prediction and the actual engine output for N_H : (a) Training , (b) Testing

3.3.4.2 MISO-NARX model of N_I

Table 3.6 summarizes the results from each group for N_I during network construction operation. Figure 3.8 shows the comparison between actual engine output and the selected MISO-NARX model output during both training and testing operation. As can be seen, the outputs from the MISO-NARX model followed the targets precisely and can predict the reaction of the system to changes in input parameters with high accuracy.

Table 3.6 The best MISO NARX models configuration for N_I

No of Neurons	Training Algorithm	S & Pr / Pr	Activation Function	RMSE Train	RMSE Test	Training Time
4	trainbr	S & Pr	tansig	0	0.0033	85.258
14	trainlm	S & Pr	tansig	0	0.0045	45.118
19	trainscg	S & Pr	tansig	0.0005	0.0408	4.132
4	trainlm	S & Pr	logsig	0	0.0043	62.661
14	trainbr	S & Pr	logsig	0	0.0038	50.719
3	trainscg	S & Pr	logsig	0.0002	0.0018	1.588
1	trainlm	Pr	tansig	0.0019	0.003	10.798
4	trainscg	Pr	tansig	0.0016	0.0025	152.564
5	trainbr	Pr	tansig	0.0007	0.0019	296.101
3	trainlm	Pr	logsig	0.0007	0.002	21.749
3	trainscg	Pr	logsig	0.0008	0.0018	161.729
20	trainbr	Pr	logsig	0.0005	0.0022	1965.554

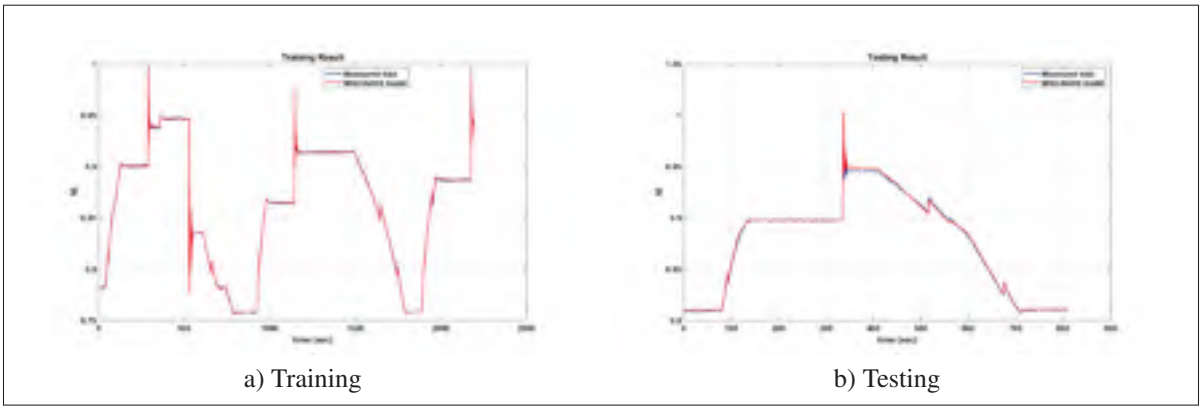

a) Training b) Testing

Figure 3.8 MISO-NARX model prediction and the actual engine output for N_I : (a) Training , (b) Testing

3.3.4.3 MISO-NARX model of N_L

Table 3.7 summarizes the results from each group for N_L during network construction operation. Figure 3.9 shows the comparison between actual engine output and the selected MISO-NARX model output during both training and testing operation. As can be seen, the outputs from the MISO-NARX model followed the targets precisely and can predict the reaction of the system to changes in input parameters with high accuracy.

Table 3.7 The best MISO NARX models configuration for N_L

No of Neurons	Training Algorithm	S & Pr / Pr	Activation Function	RMSE Train	RMSE Test	Training Time
2	trainbr	S & Pr	tansig	0	0.0095	0.032
10	trainlm	S & Pr	tansig	0	0.0695	0.185
1	trainscg	S & Pr	tansig	0.0002	0.0024	0.836
19	trainlm	S & Pr	logsig	0	0.0109	0.04
11	trainbr	S & Pr	logsig	0.0001	0.0128	0.59
15	trainscg	S & Pr	logsig	0.0001	0.0037	1.787
1	trainlm	Pr	tansig	0.0007	0.0009	9.036
9	trainscg	Pr	tansig	0.0013	0.0042	84.208
1	trainbr	Pr	tansig	0.0029	0.0029	10.109
2	trainlm	Pr	logsig	0.0006	0.0007	16.451
4	trainscg	Pr	logsig	0.0011	0.0008	85.18
1	trainbr	Pr	logsig	0.0007	0.0009	10.246

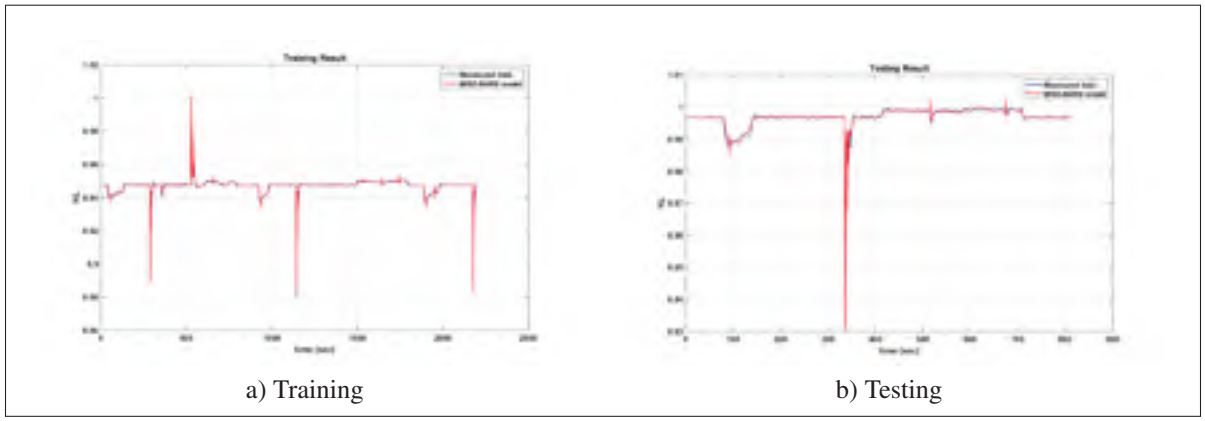

a) Training b) Testing

Figure 3.9 MISO-NARX model prediction and the actual engine output for N_L : (a) Training , (b) Testing

3.3.4.4 MISO-NARX model of *PW*

Table 3.8 summarizes the results from each group for *PW* during network construction operation. Figure 3.10 shows the comparison between actual engine output and the selected MISO-NARX model output during both training and testing operation. As can be seen, the outputs from the MISO-NARX model followed the targets precisely and can predict the reaction of the system to changes in input parameters with high accuracy.

Table 3.8 The best MISO NARX models configuration for *PW*

No of Neurons	Training Algorithm	S & Pr / Pr	Activation Function	RMSE Train	RMSE Test	Training Time
17	trainbr	S & Pr	tansig	0.0014	0.0255	1.439
20	trainlm	S & Pr	tansig	0.0012	0.0169	0.043
19	trainscg	S & Pr	tansig	0.0017	0.0473	1.375
14	trainlm	S & Pr	logsig	0.0016	0.0274	0.12
20	trainbr	S & Pr	logsig	0.0013	0.0115	0.046
15	trainscg	S & Pr	logsig	0.0004	0.0107	0.037
1	trainlm	Pr	tansig	0.0115	0.0151	7.62
1	trainscg	Pr	tansig	0.0116	0.0156	12.332
16	trainbr	Pr	tansig	0.0021	0.0125	11.722
15	trainlm	Pr	logsig	0.0017	0.0107	723.589
9	trainscg	Pr	logsig	0.0041	0.099	19.349
5	trainbr	Pr	logsig	0.0024	0.081	451.322

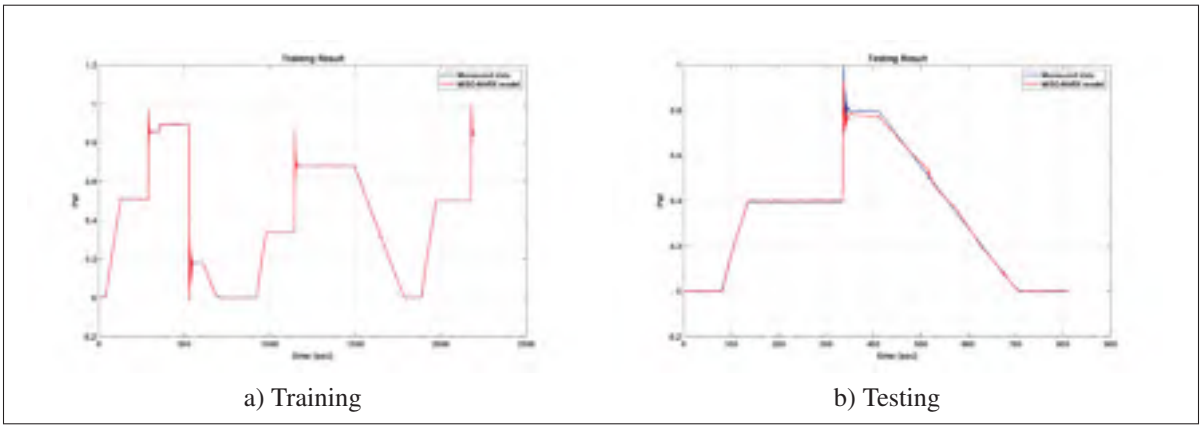

a) Training b) Testing

Figure 3.10 MISO-NARX model prediction and the actual engine output for *PW* : (a) Training , (b) Testing

3.3.4.5 MISO-NARX model of *TGT*

Table 3.9 summarizes the results from each group for *TGT* during network construction operation. Figure 3.11 shows the comparison between actual engine output and the selected MISO-NARX model output during both training and testing operation. As can be seen, the outputs from the MISO-NARX model followed the targets precisely and can predict the reaction of the system to changes in input parameters with high accuracy.

Table 3.9 The best MISO NARX models configuration for TGT

No of Neurons	Training Algorithm	S & Pr / Pr	Activation Function	RMSE Train	RMSE Test	Training Time
6	trainbr	S & Pr	tansig	0.0001	0.0416	0.041
4	trainlm	S & Pr	tansig	0.0002	0.0223	0.496
12	trainscg	S & Pr	tansig	0.0004	0.0288	7.639
7	trainlm	S & Pr	logsig	0.0001	0.0193	0.044
9	trainbr	S & Pr	logsig	0.0001	0.0357	0.031
11	trainscg	S & Pr	logsig	0.0002	0.0011	14.767
3	trainlm	Pr	tansig	0.0039	0.013	163.542
19	trainscg	Pr	tansig	0.0067	0.014	232.231
1	trainbr	Pr	tansig	0.0049	0.0079	5.13
5	trainlm	Pr	logsig	0.0016	0.0047	24.344
13	trainscg	Pr	logsig	0.0054	0.01	44.745
4	trainbr	Pr	logsig	0.003	0.0063	5.908

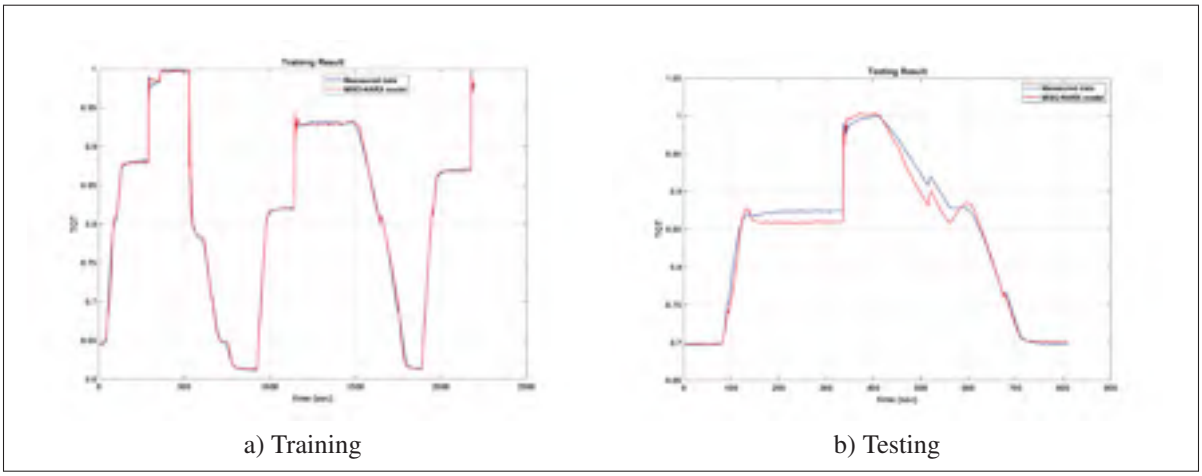

a) Training b) Testing

Figure 3.11 MISO-NARX model prediction and the actual engine output for TGT : (a) Training , (b) Testing

3.3.4.6 MISO-NARX model of T_{30}

Table 3.10 summarizes the results from each group for T_{30} during network construction operation. Figure 3.12 shows the comparison between actual engine output and the selected MISO-NARX model output during both training and testing operation. As can be seen, the outputs

from the MISO-NARX model followed the targets precisely and can predict the reaction of the system to changes in input parameters with high accuracy.

Table 3.10 The best MISO NARX models configuration for T_{30}

No of Neurons	Training Algorithm	S & Pr / Pr	Activation Function	RMSE Train	RMSE Test	Training Time
13	trainbr	S & Pr	tansig	0.0002	0.0299	0.033
15	trainlm	S & Pr	tansig	0.0002	0.028	0.031
10	trainscg	S & Pr	tansig	0.0002	0.0081	2.426
15	trainlm	S & Pr	logsig	0.0002	0.0076	0.034
17	trainbr	S & Pr	logsig	0.0002	0.0134	0.091
10	trainscg	S & Pr	logsig	0.0002	0.0218	9.413
2	trainlm	Pr	tansig	0.0033	0.0079	11.131
2	trainscg	Pr	tansig	0.0147	0.0162	29.046
1	trainbr	Pr	tansig	0.0051	0.0098	8.368
3	trainlm	Pr	logsig	0.0016	0.0087	14.32
1	trainscg	Pr	logsig	0.007	0.0111	105.507
4	trainbr	Pr	logsig	0.0016	0.0083	17.161

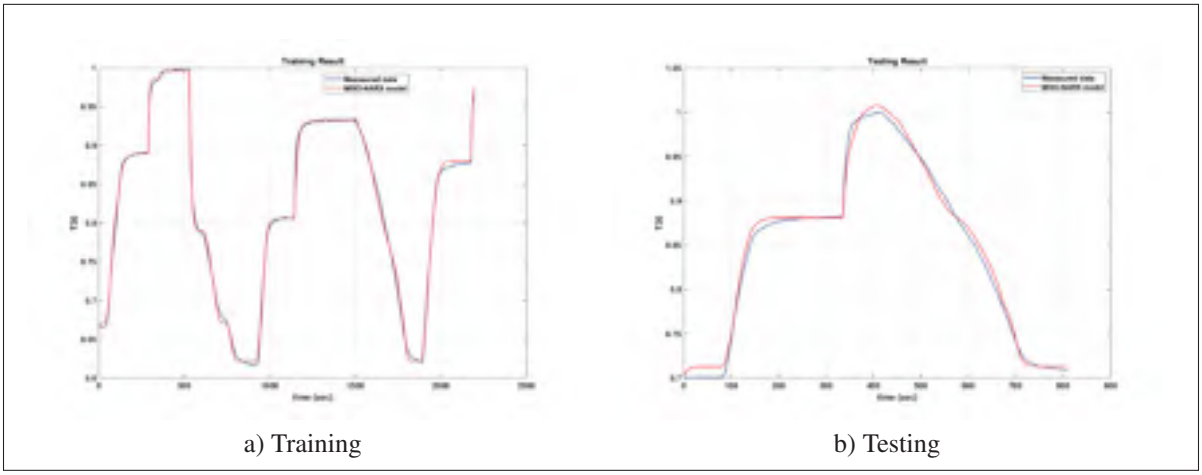

a) Training b) Testing

Figure 3.12 MISO-NARX model prediction and the actual engine output for T_{30} : (a) Training , (b) Testing

3.3.4.7 MISO-NARX model of P_{30}

Table 3.11 summarizes the results from each group for P_{30} during network construction operation. Figure 3.13 shows the comparison between actual engine output and the selected MISO-NARX model output during both training and testing operation. As can be seen, the outputs from the MISO-NARX model followed the targets precisely and can predict the reaction of the system to changes in input parameters with high accuracy.

Table 3.11 The best MISO NARX models configuration for P_{30}

No of Neurons	**Training Algorithm**	**S & Pr / Pr**	**Activation Function**	**RMSE Train**	**RMSE Test**	**Training Time**
11	trainbr	S & Pr	tansig	0.0003	0.0145	0.027
10	trainlm	S & Pr	tansig	0.0003	0.0316	0.029
14	trainscg	S & Pr	tansig	0.0042	0.0276	3.78
19	trainlm	S & Pr	logsig	0.0004	0.0346	0.045
14	trainbr	S & Pr	logsig	0.0004	0.0126	0.045
5	trainscg	S & Pr	logsig	0.0041	0.005	1.749
1	trainlm	Pr	tansig	0.0151	0.0224	10.079
1	trainscg	Pr	tansig	0.0144	0.0214	67.258
1	trainbr	Pr	tansig	0.015	0.0217	7.191
5	trainlm	Pr	logsig	0.0045	0.005	25.666
20	trainscg	Pr	logsig	0.0033	0.0073	284.564
7	trainbr	Pr	logsig	0.0026	0.0077	32.614

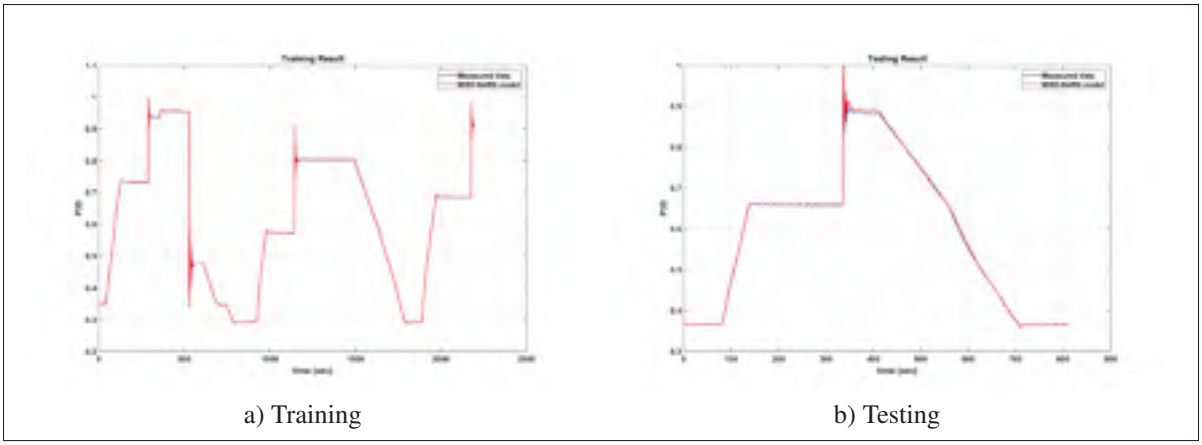

a) Training b) Testing

Figure 3.13 MISO-NARX model prediction and the actual engine output for P_{30} : (a) Training , (b) Testing

3.3.5 Ensemble generation

The generation of ensemble system can be generally divided into three steps as shown in Figure 3.14. It often happens that a number of redundant models are generated during ensemble generation. The next step is ensemble pruning where the pool of generated models are trimmed in order to achieve maximum diversity among the base models. Finally, the selected base models are combined in the ensemble integration step, where the final prediction is formed based on the base models prediction.

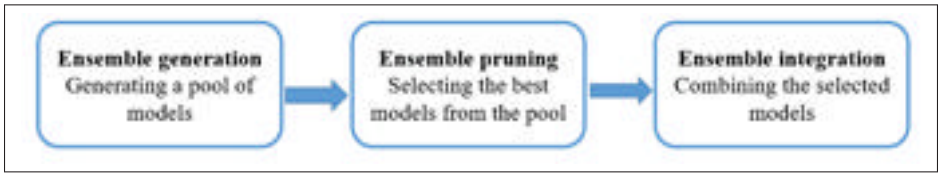

Figure 3.14 Ensemble generation steps
Taken from de Sousa *et al.* (2012)

In this subsection, a homogeneous ensemble for each output parameter of the engine is generated based upon the best selected structure of the MISO-NARX model from the last subsection, and diversity among them is ensured by altering the training datasets which represent differ-

ent operation conditions. Therefore, the ensemble for each output parameter consists of eight MISO NARX models with the same structure. Each model is retrained individually using different training dataset, which represent certain operation condition. In this work, eight operation condition datasets $[TR1 - TR8]$ were generated to represent the ADGTE operation space. The retraining operation is performed in the same way as mentioned before. Figure 3.15 shows inside of each ensemble model. Note that, each model represent certain operation condition.

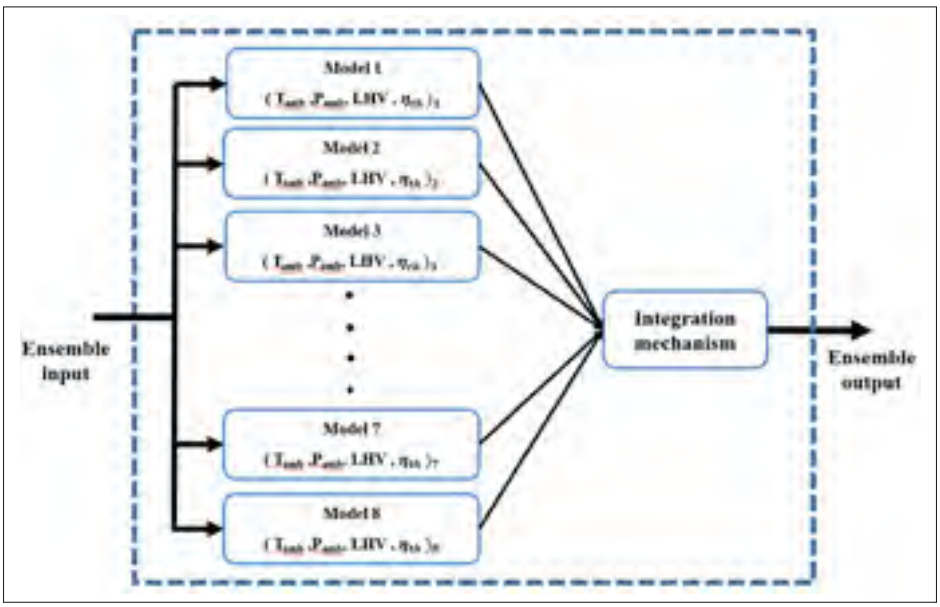

Figure 3.15 Inside of an ensemble model

Figure 3.16 through Figure 3.22 show that, the outputs from each model inside each generated ensemble are different from each other, which explains the ensemble diversity. In this work, the input space is partitioned into eight subspaces, each one represents certain operation conditions, and each model in the ensemble is then assigned to one of these sub-spaces. In another word, we used a mixture of experts to develop a homogeneous ensemble, which can represent the engine at different operation conditions.

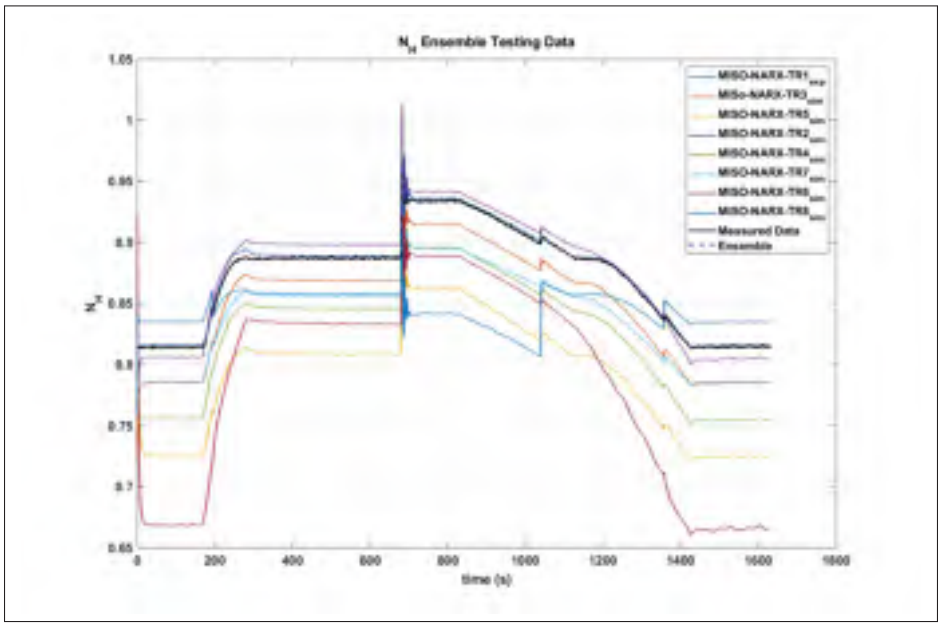

Figure 3.16 N_H ensemble models prediction - $TS1_{exp}$

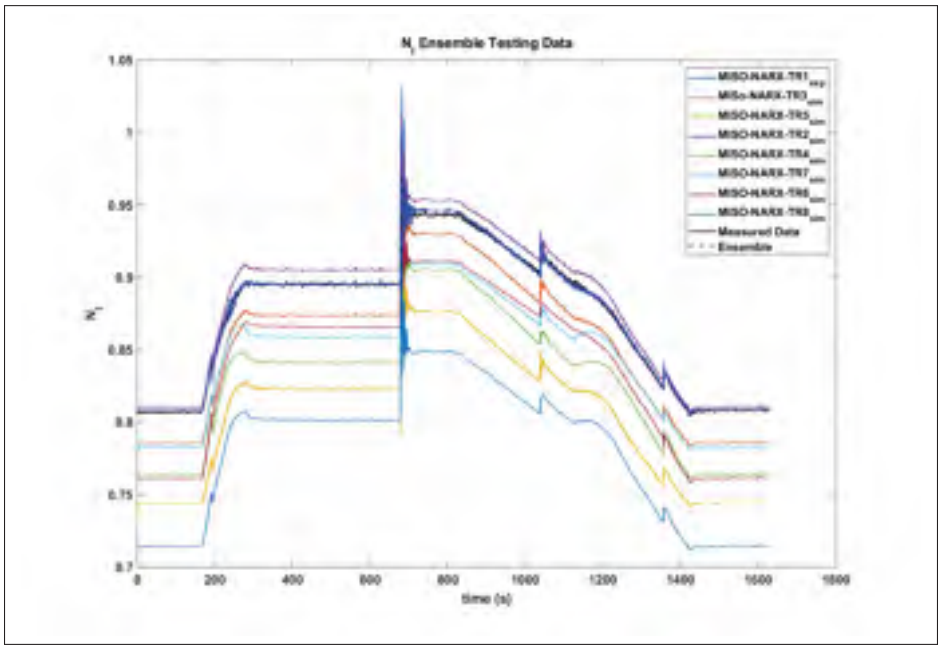

Figure 3.17 N_I ensemble models prediction - $TS1_{exp}$

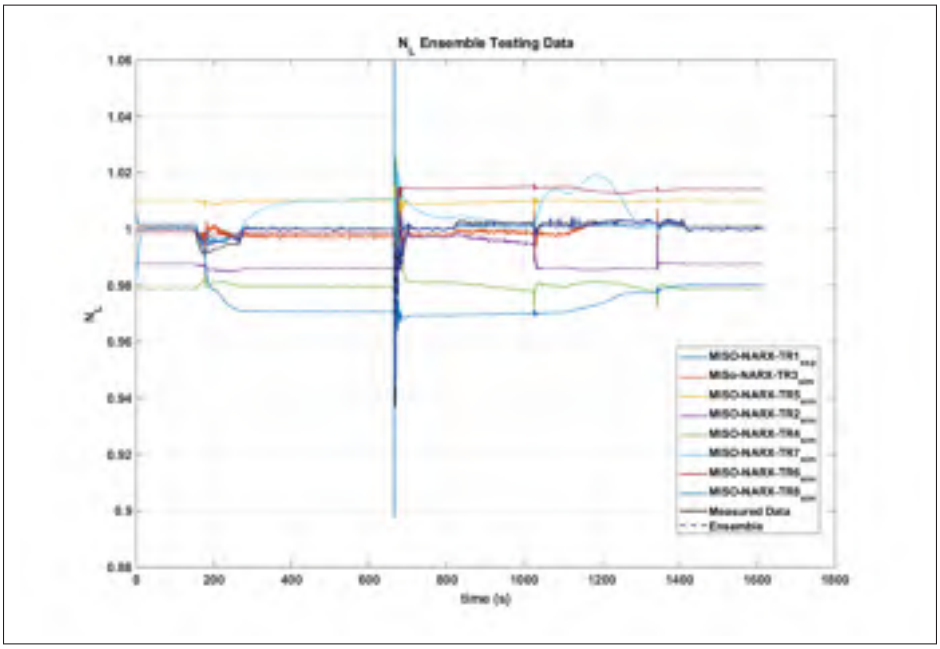

Figure 3.18 N_L ensemble models prediction - $TS1_{exp}$

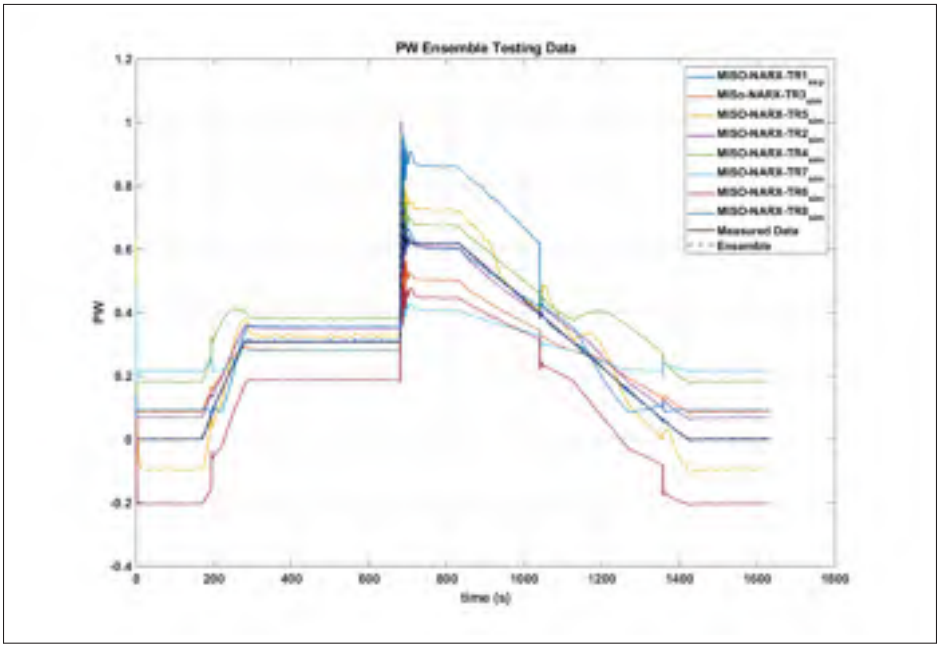

Figure 3.19 PW ensemble models prediction - $TS1_{exp}$

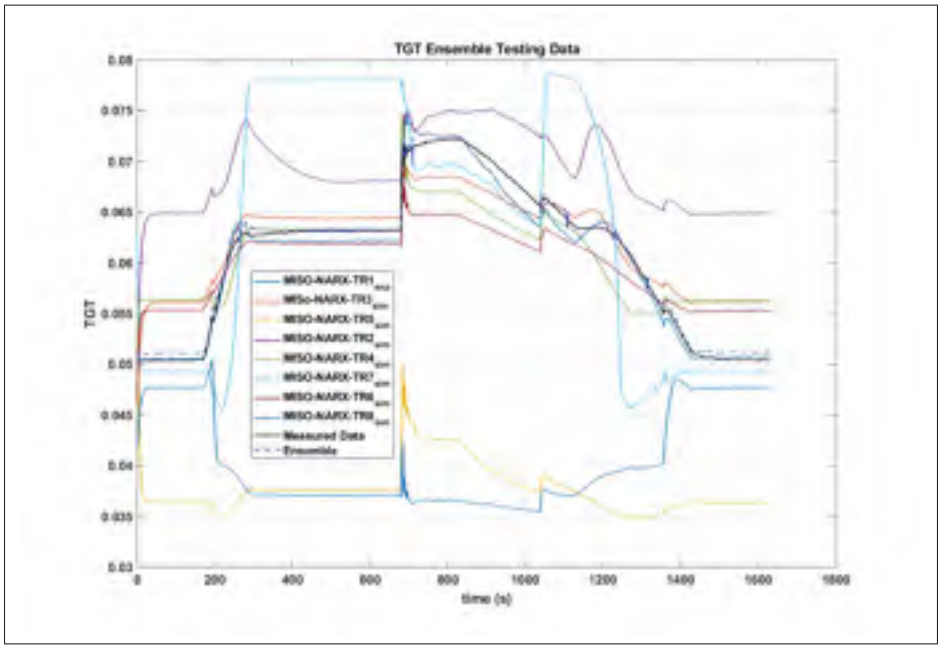

Figure 3.20 TGT ensemble models prediction - $TS1_{exp}$

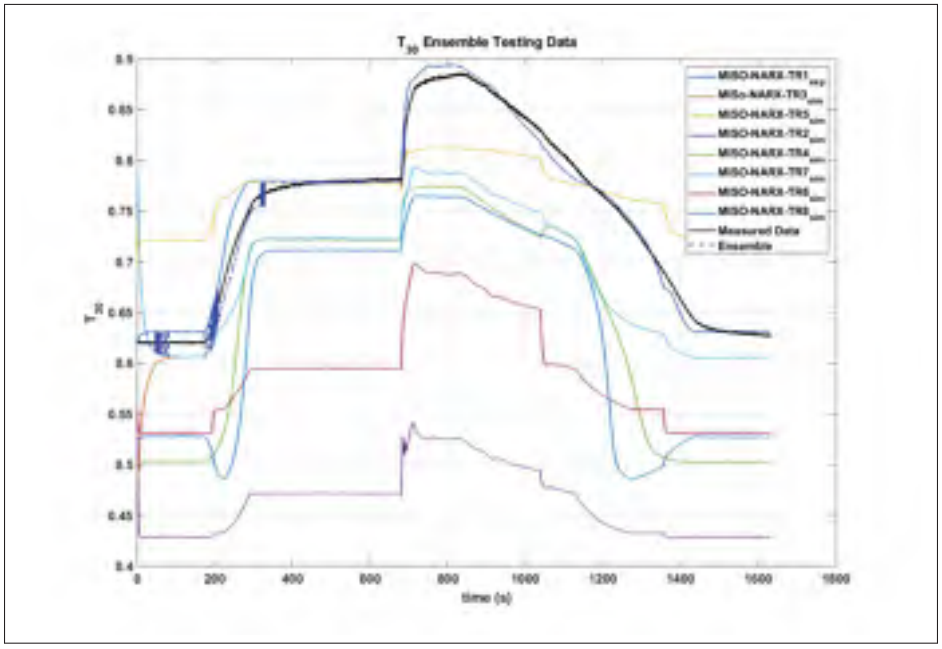

Figure 3.21 T_{30} ensemble models prediction - $TS1_{exp}$

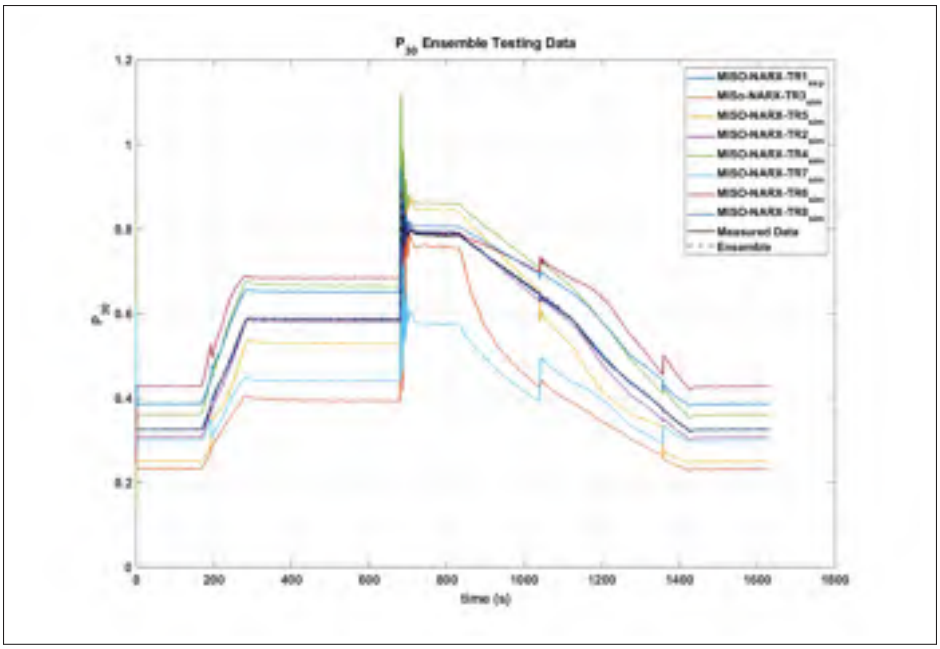

Figure 3.22 P_{30} ensemble models prediction - $TS1_{exp}$

3.3.6 Ensemble integration

Now that we have generated the ensemble for each engine output parameter, we move to the next step. How to combine the identifications that were made for each model in the ensemble and constructing the final output. Four approaches are used to handle the ensemble integration. Firstly, the basic ensemble method (BEM) defined by equation (3.7) below. The BEM is a simple approach to aggregating network outputs by average them together. Secondly, the median method, which is less affected by outliers and skewed data than the mean one. An outlier is an extreme value that differs greatly from other values.

$$f_{BEM} = \frac{1}{K}\sum_{i=1}^{K} f_i(x) \tag{3.7}$$

Thirdly, a dynamic weighting method (DWM) is considered. Note that, the previous two methods are considered as a constant weighting methods, while, DWM is considered as a non-constant weighting method. The weights are adjusted dynamically to be proportional to the

performance of ensemble members (MISO NARX models), a greater weight will be assigned to the ensemble member with better performance. Finally, the proposed HDWM is performed as follows:

1. Calculation of the performance of each ensemble member as described in equation (3.8),

$$e_i = (\frac{y_m - y_i}{y_{max}})^2 \tag{3.8}$$

2. Calculation of the median value of the models' errors

$$MED = median(e_1 e_2 \cdots e_K) \tag{3.9}$$

3. The weight of each model f_i is calculated according to its error as described in Eqn. (3.10), which calculate the weights in such a way: the model i with error e_i around the median value MED receives a weight close to 1. While, models with e_i lower than MED have their weights exponentially increased, and models with e_i larger than MED have their weights exponentially decreased.

$$w_i = \exp(-\frac{e_i - MED}{MED}) \tag{3.10}$$

4. The ensemble output f_{en} is obtained as,

$$f_{en} = \frac{\sum_{i=1}^{K}[w_i(x) * f_i(x)]}{\sum_{i=1}^{K} w_i(x)} \tag{3.11}$$

5. Calculation of the error of the ensemble output with respect to the real output, and comparison this error with the minimum error from the all ensemble members. If $f_{en} < min(e_1 \cdots e_K)$, then the final output will be the ensemble output. Otherwise , the final output will equal to the output from the ensemble member which has the minimum error value.

As we can see, the HDWM is a hybrid method which combines two integration approaches, the fusion approach and the selection approach. The former, combines the ensemble members outputs in order to obtain the final output by weighting each model output based on its performance. The latter, selects from the ensemble the most promising model only.

In order to verify the performance of the proposed ensemble integration method (HDWM), a comparative study was performed between four integration algorithms to measure their impact on the ensemble performance with respect to $TS1_{exp}$ data set. A summary of results of the four integration algorithms presented in Table 3.12. Indeed, Figure 3.23 to Figure 3.29 show estimation of all engine output parameters by ensemble for each output parameter with different integration algorithms and tested with $TS1_{exp}$ data set. As we can see, the proposed HDWM has demonstrated superior performance over the other integration methods.

Table 3.12 *RMSE* of ensemble of MISO NARX models with different integration methods - $TS1_{exp}$

Output parameter	**HDWM**	**DWM**	**BEM**	**Median**
N_H	0.00005	0.00151	0.04283	0.02877
N_I	0.00043	0.01319	0.03669	0.03482
N_L	0.00004	0.00033	0.00534	0.00054
PW	0.00180	0.02960	0.44110	0.07860
TGT	0.00351	0.00926	0.02067	0.03183
T_{30}	0.00389	0.02237	0.05820	0.05870
P_{30}	0.00004	0.00262	0.00240	0.00931

Finally, the Black box model of the SGT-A65 engine is presented by eight homogeneous ensembles of MISO NARX models as shown in Figure 3.30.

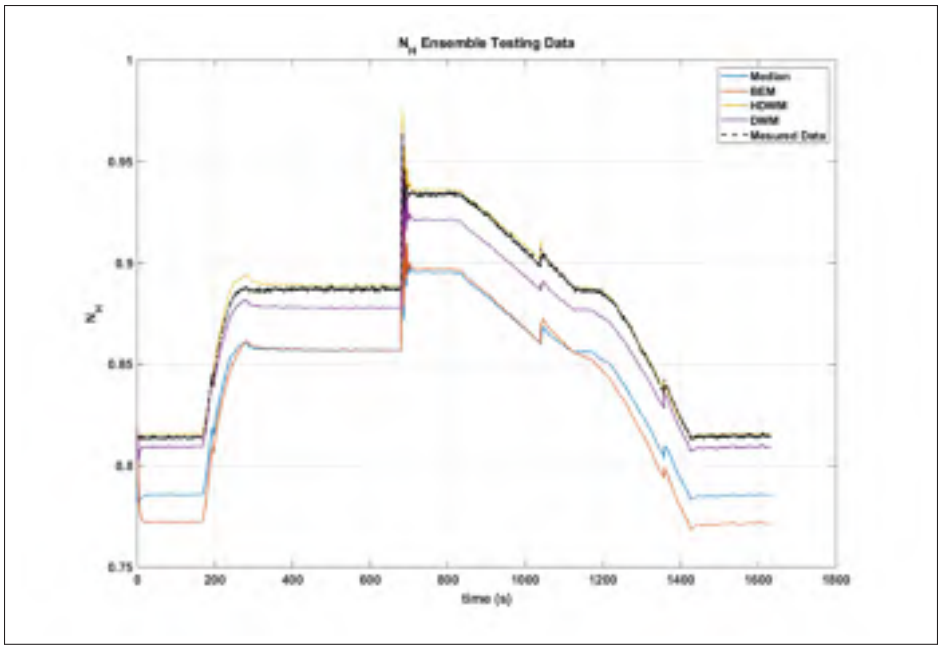

Figure 3.23 N_H ensemble regression with different integration methods - $TS1_{exp}$

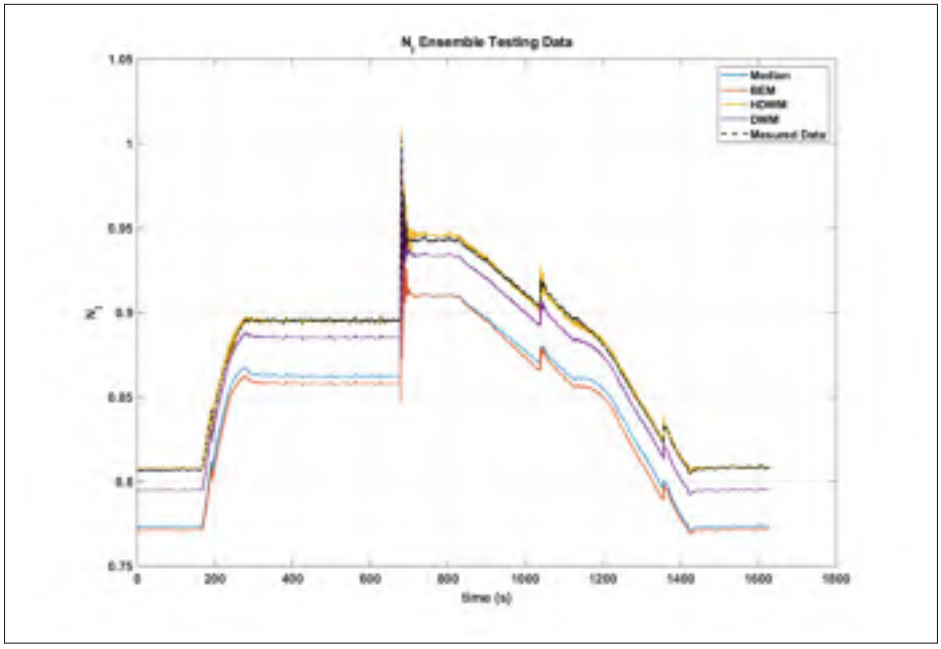

Figure 3.24 N_I ensemble regression with different integration methods - $TS1_{exp}$

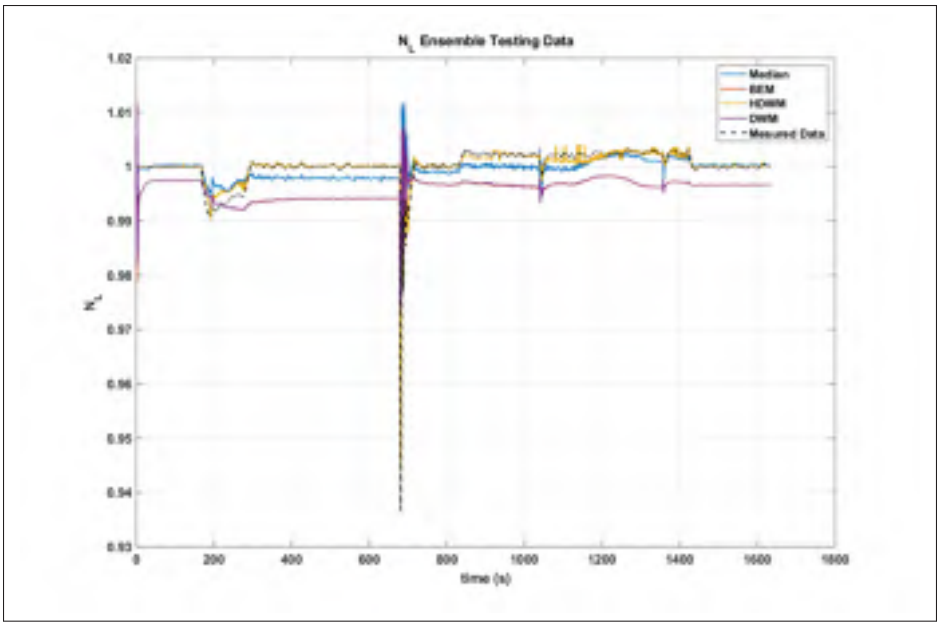

Figure 3.25 N_L ensemble regression with different integration methods - $TS1_{exp}$

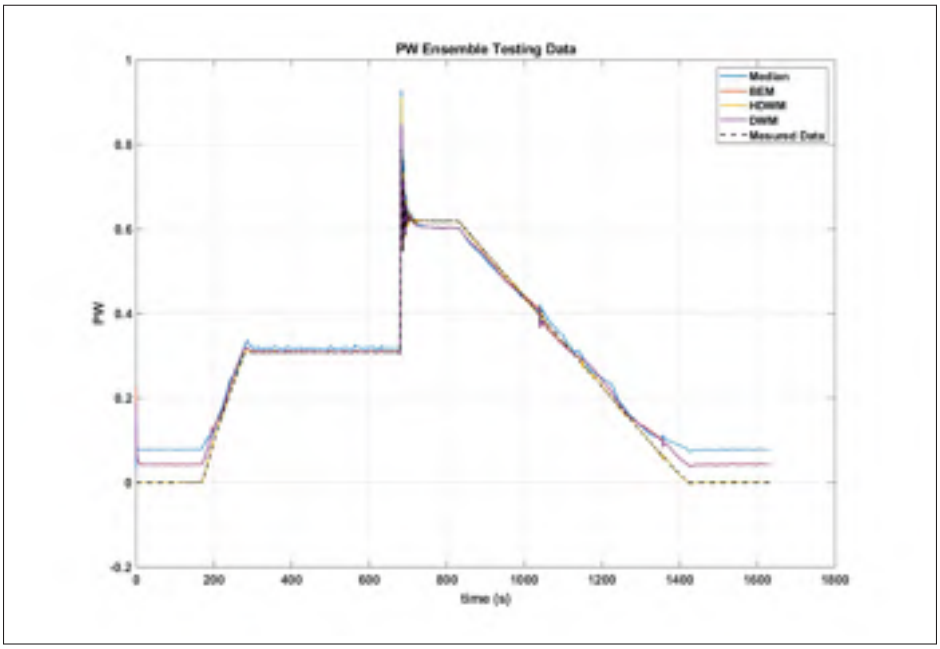

Figure 3.26 PW ensemble regression with different integration methods - $TS1_{exp}$

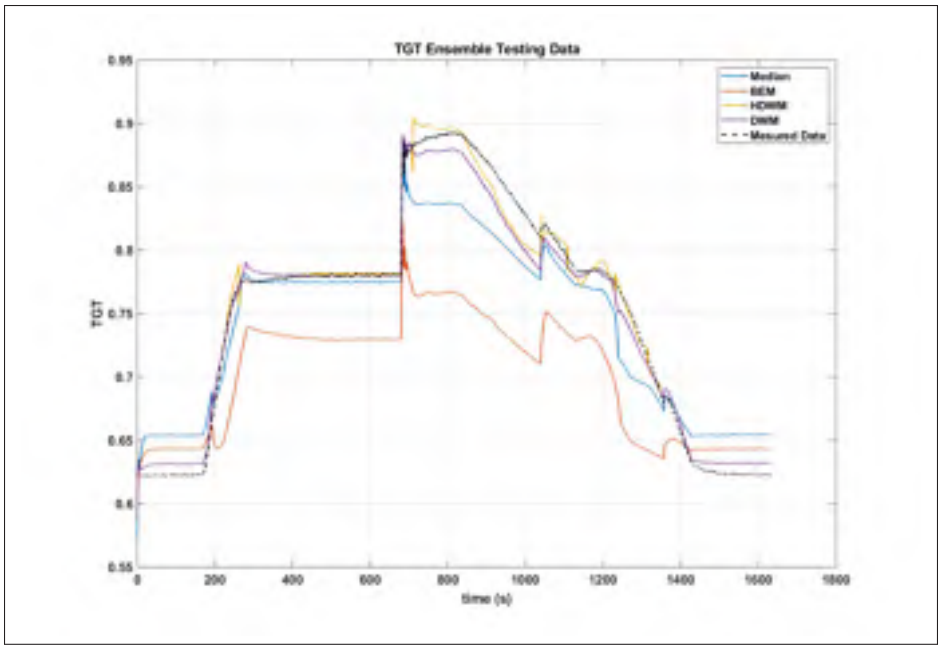

Figure 3.27 TGT ensemble regression with different integration methods - $TS1_{exp}$

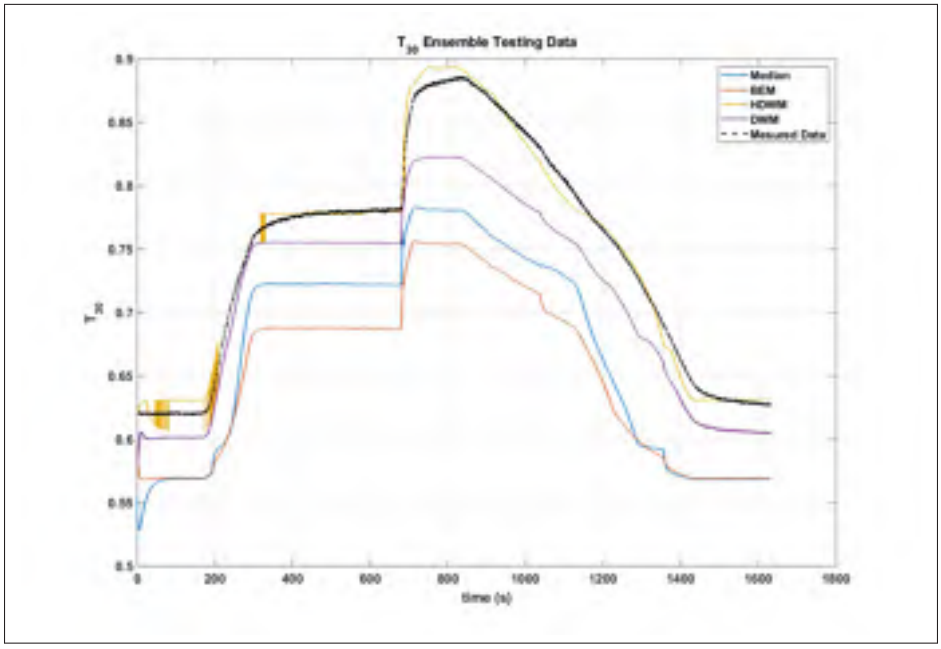

Figure 3.28 T_{30} ensemble regression with different integration methods - $TS1_{exp}$

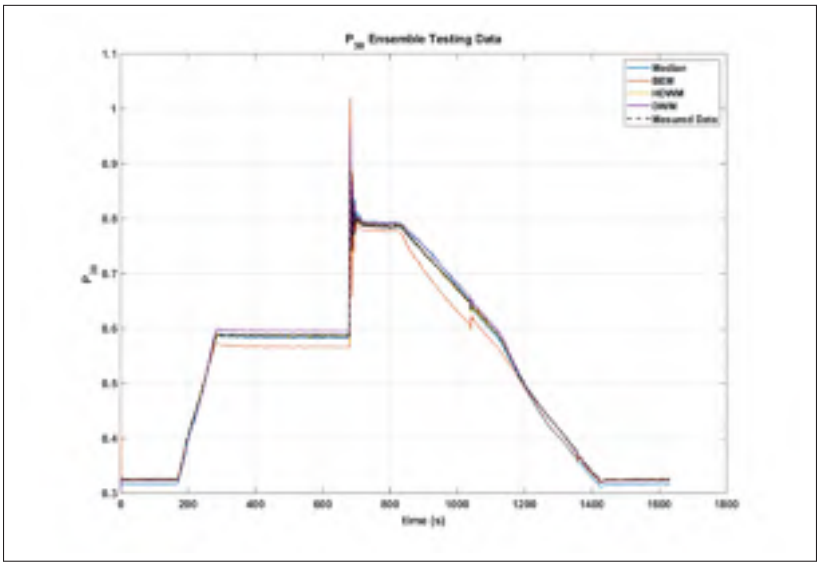

Figure 3.29 P_{30} ensemble regression with different integration methods - $TS1_{exp}$

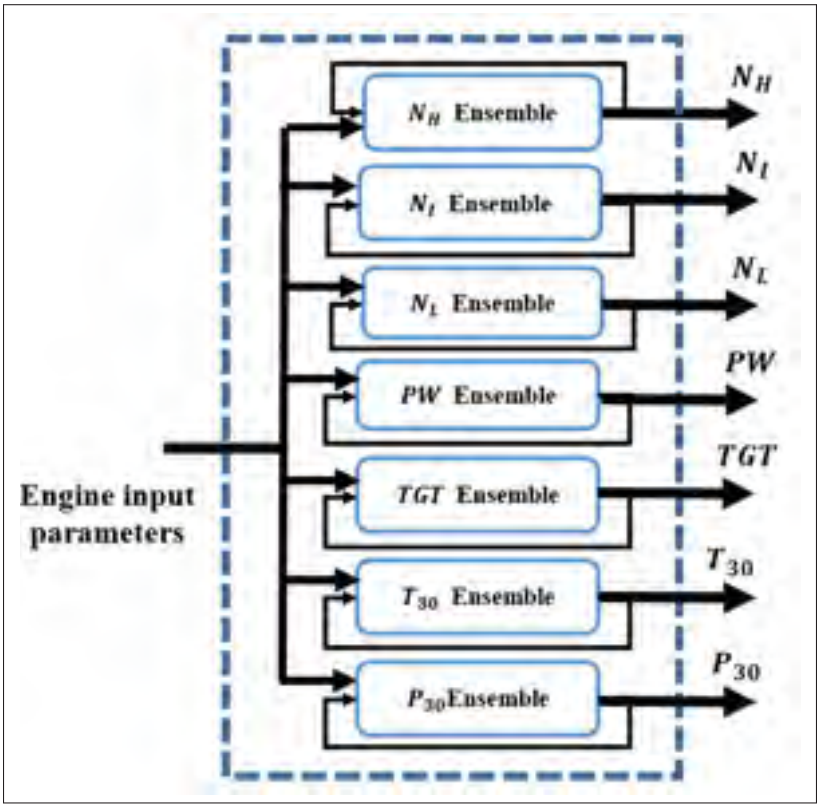

Figure 3.30 Ensemble model of SGT-A65 engine

3.4 Comparison between single MISO-NARX model and ensemble of MISO-NARX models

To show the advantages of using an ensemble in the prediction of engine performance instead of using an individual neural model, we generated a single MISO NARX for each engine output parameters, and trained them with the same approach as mentioned earlier. Indeed, concatenated data from different operation conditions is used for training operation. Figure 3.31 to Figure 3.44 show the comparison between the ensemble of MISO NARX models and the single MISO NARX models for all engine output parameters at different operation conditions. This demonstrates that ensembles of diverse models aggregated with HDWM method can provide higher accuracy and higher robustness in real time than the single MISO NARX neural model approach. One can observe that the ensemble model demonstrates a significantly better performance in identification of the gas turbine engine dynamics than the individual neural model, as it results in an improvement in accuracy of nearly 90%, compared with the single neural model.

3.4.1 Ensemble model of *PW*

Figure 3.31 and Figure 3.32 show the comparison between *PW* estimated by the ensemble of MISO NARX models and the single MISO NARX model. This demonstrates that ensembles of diverse models aggregated with HDWM method can provide higher accuracy and higher robustness in real time than the single MISO NARX neural model approach. A summary of comparison results is shown in Table 3.13.

Table 3.13 Regression performance [*RMSE*] of single MISO NARX model and ensemble of eight MISO NARX models - *PW*

Data set	**Single MISO-NARX model**	**Ensemble of MISO-NARX models**
$TS1_{exp}$	0.0522	0.0018
$TS2_{sim}$	0.0211	0.00045
$TS3_{sim}$	0.0165	0.00081
$TS4_{sim}$	0.0158	0.0020
$TS5_{sim}$	0.0144	0.0029
$TS6_{sim}$	0.0299	0.0097
$TS7_{sim}$	0.0284	0.0090
$TS8_{sim}$	0.0326	0.0010

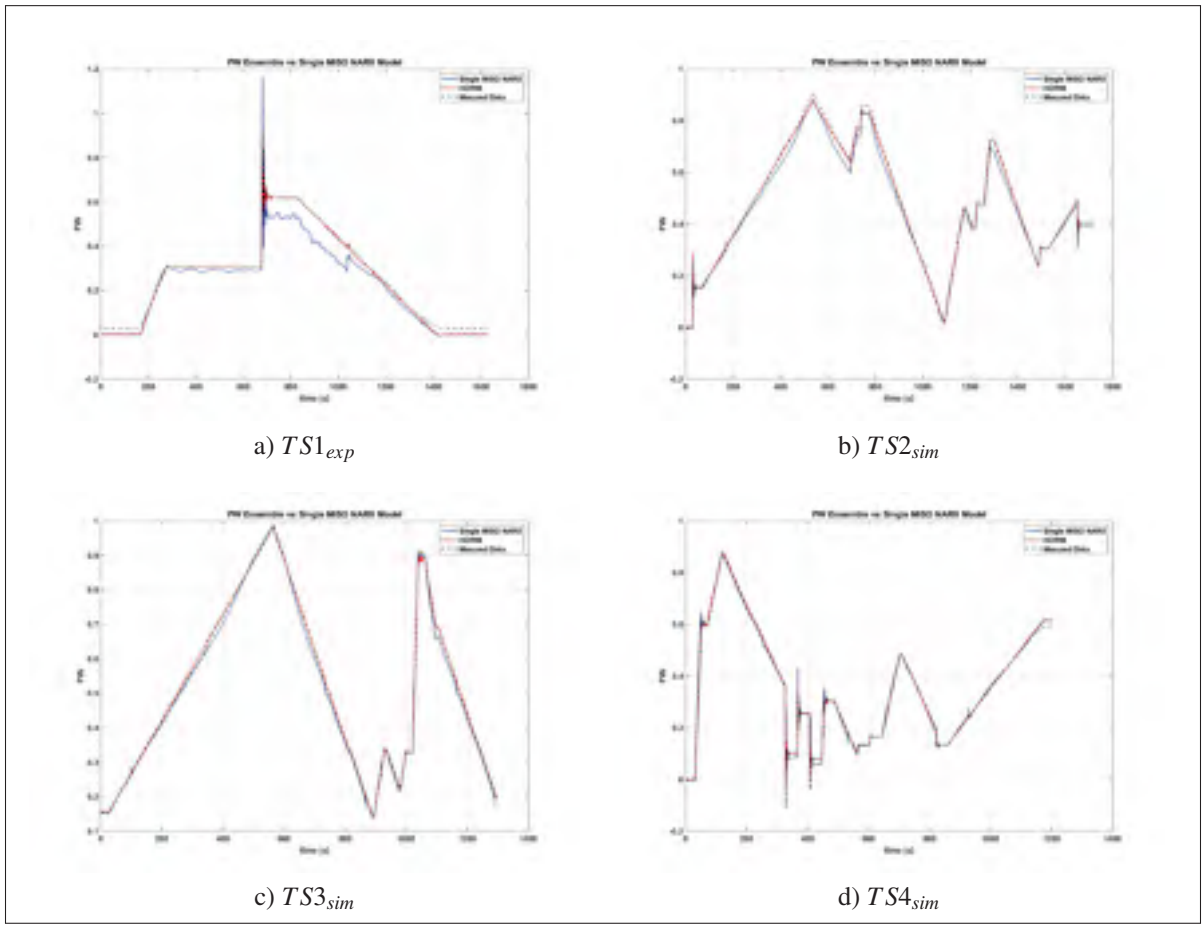

a) $TS1_{exp}$ b) $TS2_{sim}$

c) $TS3_{sim}$ d) $TS4_{sim}$

Figure 3.31 The comparison between the performance of ensemble of MISO NARX models and single MISO NARX model using $TS1_{exp}$ to $TS4_{sim}$ datasets - PW

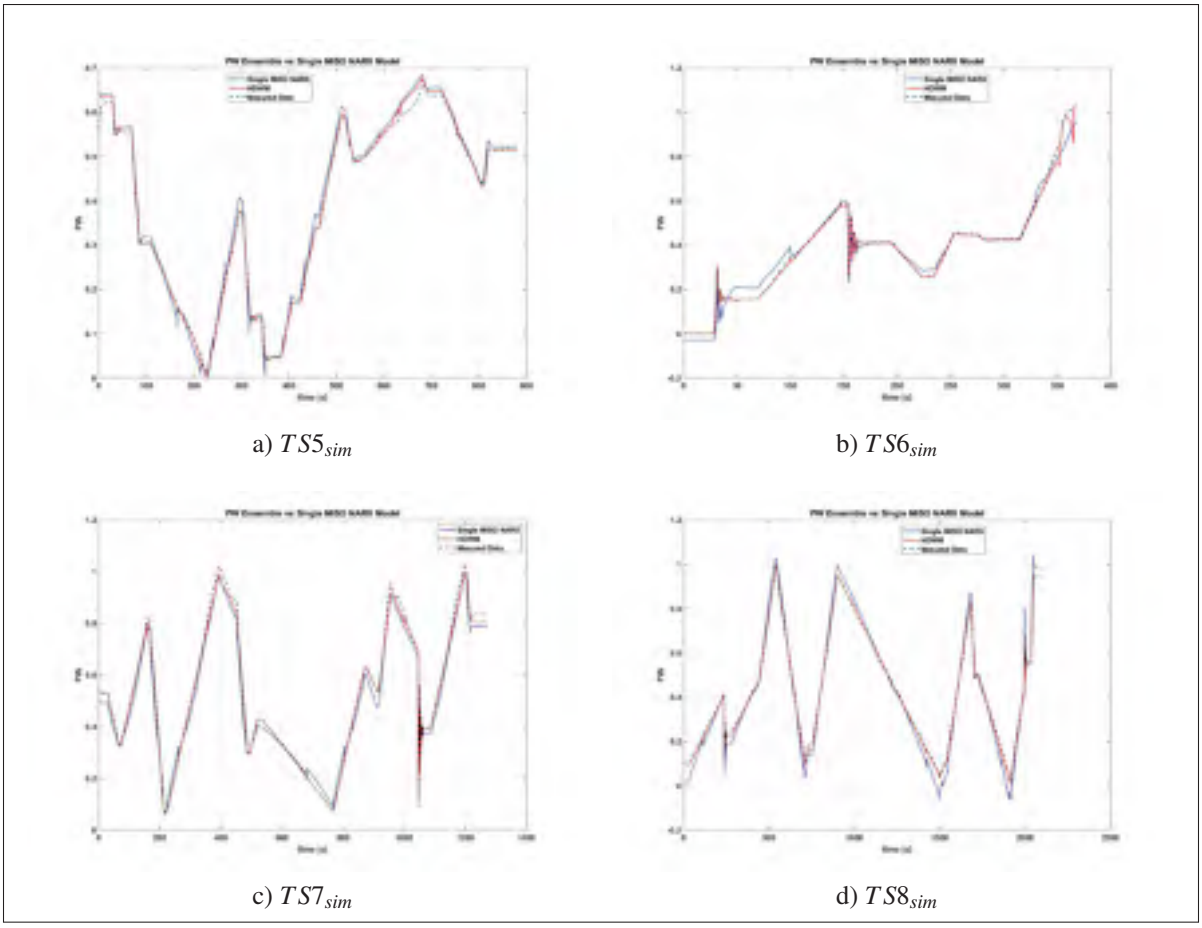

a) $TS5_{sim}$ b) $TS6_{sim}$

c) $TS7_{sim}$ d) $TS8_{sim}$

Figure 3.32 The comparison between the performance of ensemble of MISO NARX models and single MISO NARX model using $TS5_{sim}$ to $TS8_{sim}$ datasets - PW

3.4.2 Ensemble model of N_H

Figure 3.33 and Figure 3.34 show the comparison between N_H estimated by the ensemble of MISO NARX models and the single MISO NARX model. This demonstrates that ensembles of diverse models aggregated with HDWM method can provide higher accuracy and higher robustness in real time than the single MISO NARX neural model approach. A summary of comparison results is shown in Table 3.14.

Table 3.14 Regression performance [$RMSE$] of single MISO NARX model and ensemble of eight MISO NARX models - N_H

Data set	**Single MISO-NARX model**	**Ensemble of MISO-NARX models**
$TS1_{exp}$	0.0056	0.00017
$TS2_{sim}$	0.0024	0.00015
$TS3_{sim}$	0.0020	0.00069
$TS4_{sim}$	0.0038	0.00052
$TS5_{sim}$	0.0028	4.64e-5
$TS6_{sim}$	0.0051	0.00081
$TS7_{sim}$	0.0020	0.00063
$TS8_{sim}$	0.0024	0.00107

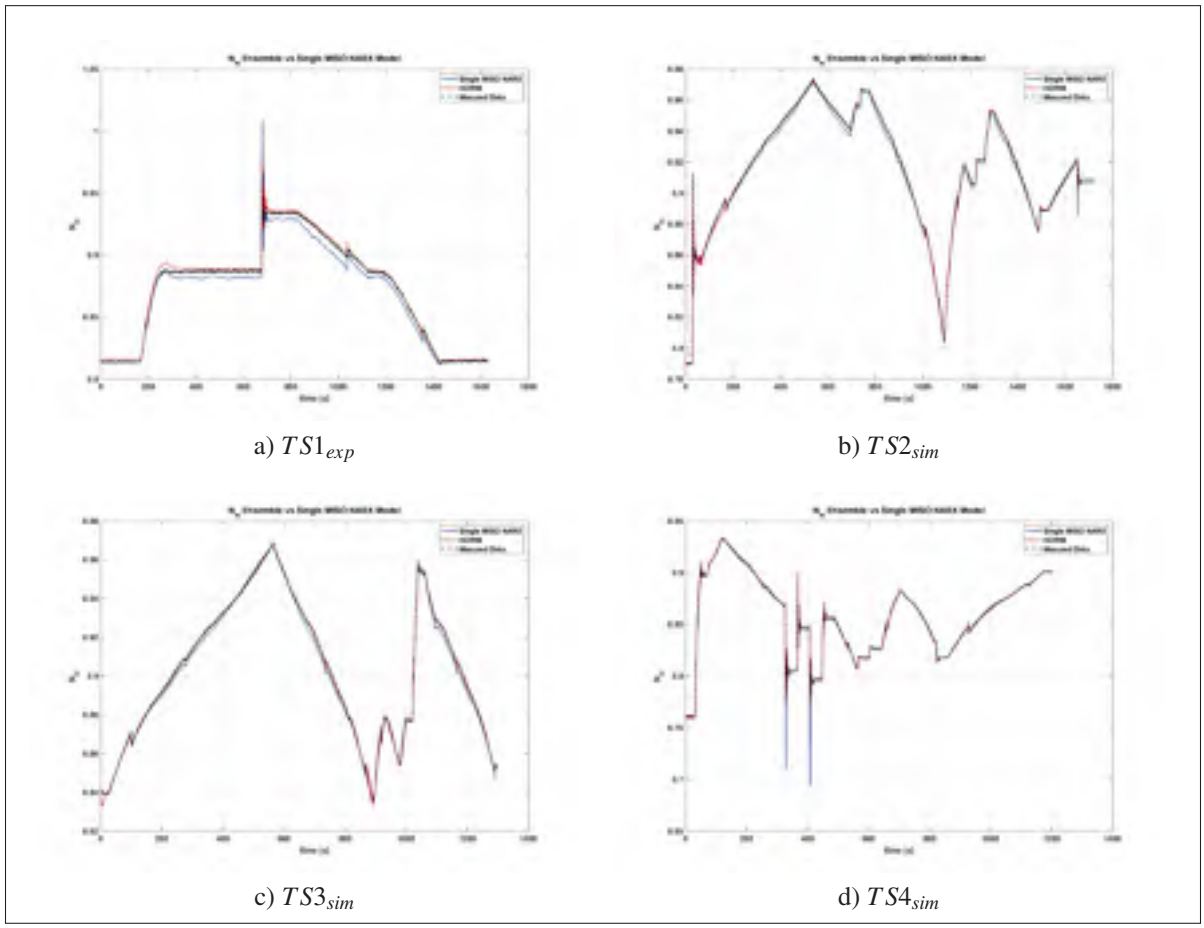

a) $TS1_{exp}$ b) $TS2_{sim}$

c) $TS3_{sim}$ d) $TS4_{sim}$

Figure 3.33 The comparison between the performance of ensemble of MISO NARX models and single MISO NARX model using $TS1_{exp}$ to $TS4_{sim}$ datasets - N_H

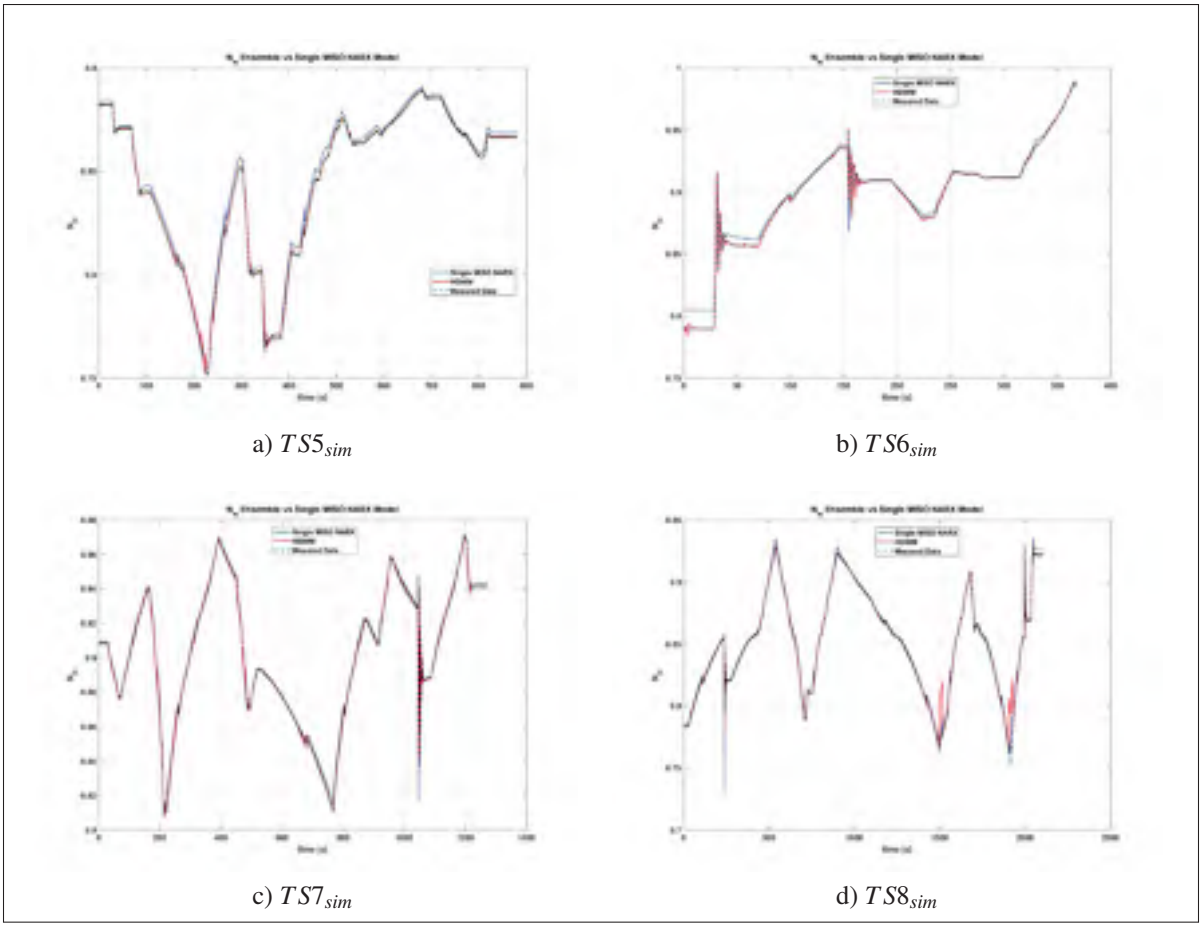

a) $TS5_{sim}$ b) $TS6_{sim}$

c) $TS7_{sim}$ d) $TS8_{sim}$

Figure 3.34 The comparison between the performance of ensemble of MISO NARX models and single MISO NARX model using $TS5_{sim}$ to $TS8_{sim}$ datasets - N_H

3.4.3 Ensemble model of N_I

Figure 3.35 and Figure 3.36 show the comparison between N_I estimated by the ensemble of MISO NARX models and the single MISO NARX model. This demonstrates that ensembles of diverse models aggregated with HDWM method can provide higher accuracy and higher robustness in real time than the single MISO NARX neural model approach. A summary of comparison results is shown in Table 3.15.

Table 3.15 Regression performance [$RMSE$] of single MISO NARX model and ensemble of eight MISO NARX models - N_I

Data set	**Single MISO-NARX model**	**Ensemble of MISO-NARX models**
$TS1_{exp}$	0.0051	0.00088
$TS2_{sim}$	0.0065	0.00061
$TS3_{sim}$	0.0048	0.00026
$TS4_{sim}$	0.0041	4.67e-5
$TS5_{sim}$	0.0107	0.0008
$TS6_{sim}$	0.0036	0.0028
$TS7_{sim}$	0.0038	4.74e-5
$TS8_{sim}$	0.0067	0.00082

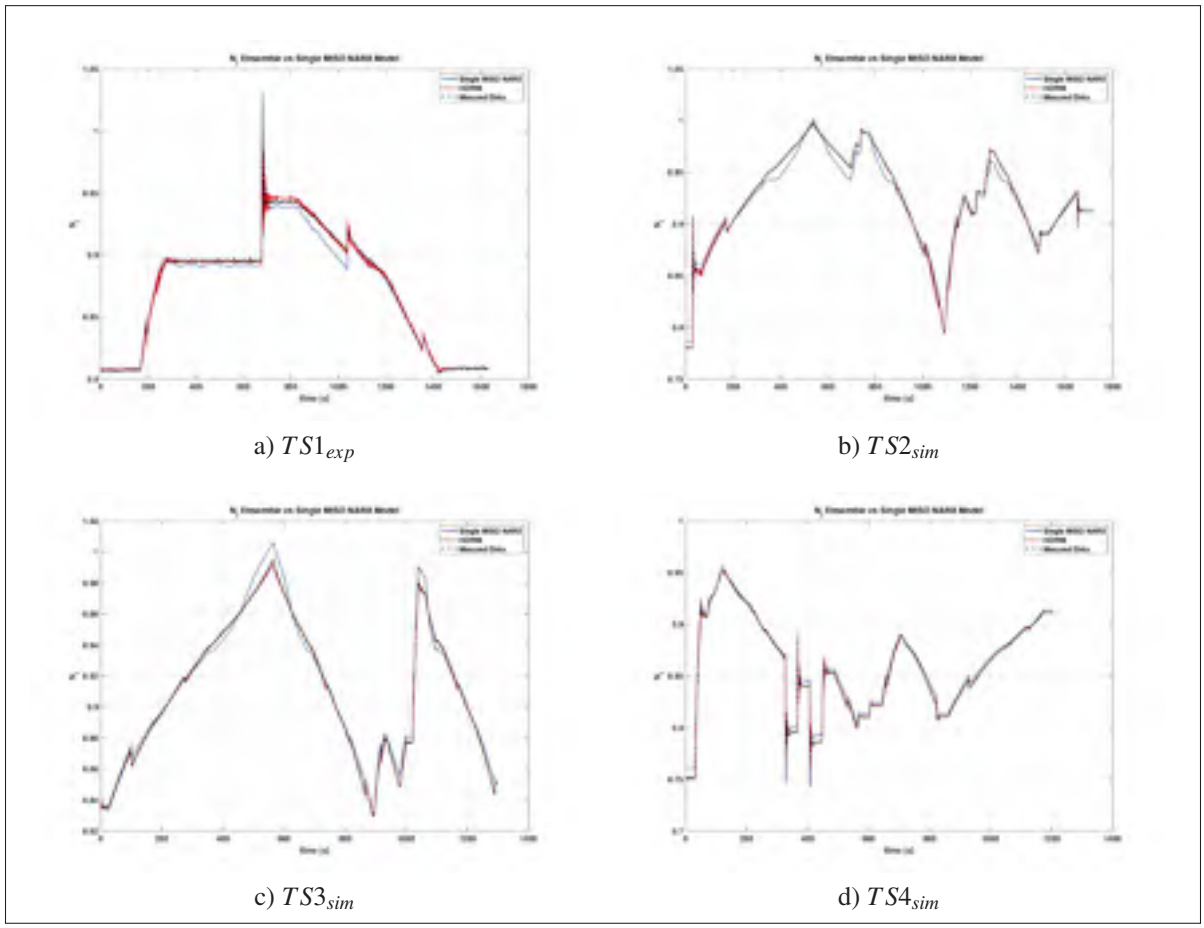

a) $TS1_{exp}$ b) $TS2_{sim}$

c) $TS3_{sim}$ d) $TS4_{sim}$

Figure 3.35 The comparison between the performance of ensemble of MISO NARX models and single MISO NARX model using $TS1_{exp}$ to $TS4_{sim}$ datasets - N_I

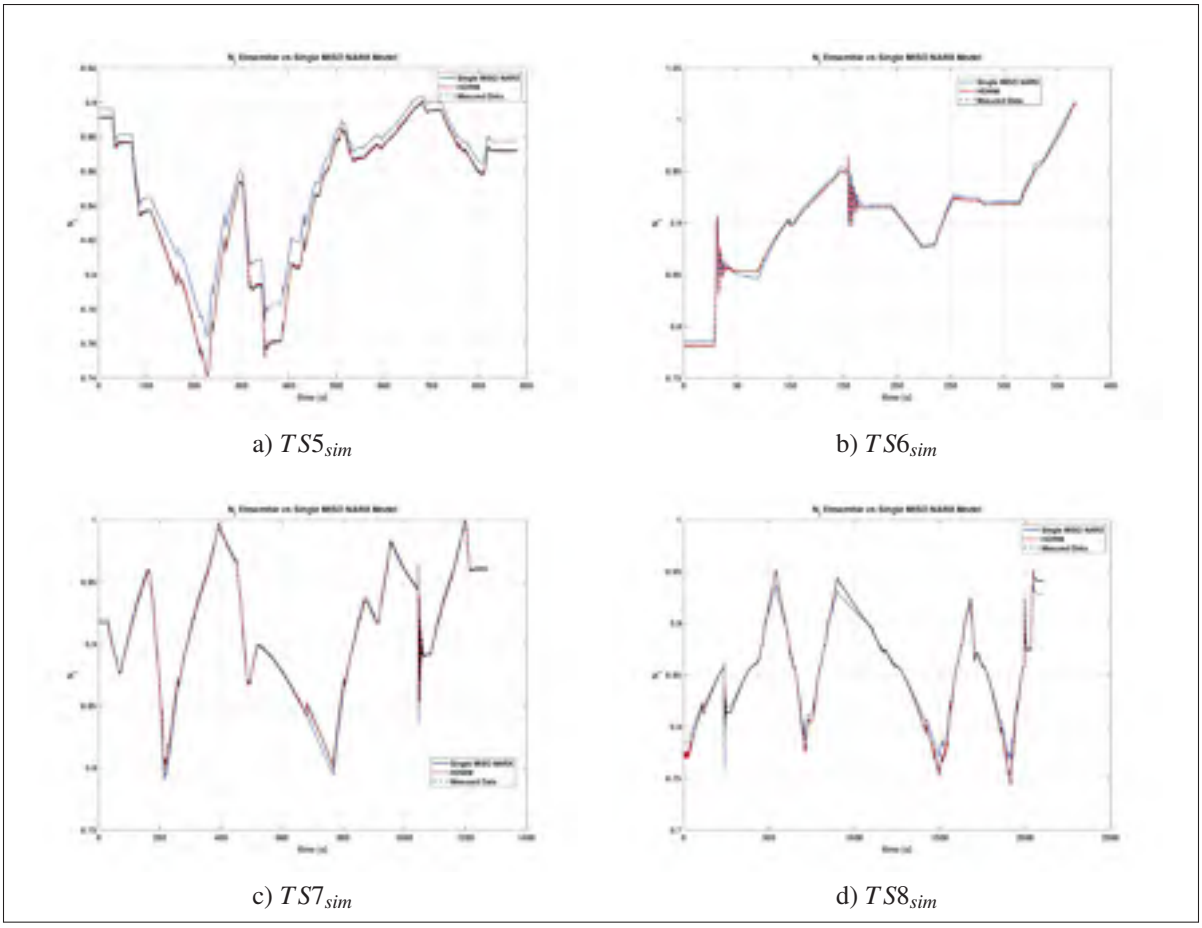

a) $TS5_{sim}$ b) $TS6_{sim}$

c) $TS7_{sim}$ d) $TS8_{sim}$

Figure 3.36 The comparison between the performance of ensemble of MISO NARX models and single MISO NARX model using $TS5_{sim}$ to $TS8_{sim}$ datasets - N_I

3.4.4 Ensemble model of N_L

Figure 3.37 and Figure 3.38 show the comparison between N_L estimated by the ensemble of MISO NARX models and the single MISO NARX model. This demonstrates that ensembles of diverse models aggregated with HDWM method can provide higher accuracy and higher robustness in real time than the single MISO NARX neural model approach. A summary of comparison results is shown in Table 3.16.

Table 3.16 Regression performance [*RMSE*] of single MISO NARX model and ensemble of eight MISO NARX models - N_L

Data set	**Single MISO-NARX model**	**Ensemble of MISO-NARX models**
$TS1_{exp}$	0.0037	8.85e-5
$TS2_{sim}$	0.0074	8.11e-5
$TS3_{sim}$	0.0013	4.77e-5
$TS4_{sim}$	0.0486	0.00026
$TS5_{sim}$	0.0099	3.29e-5
$TS6_{sim}$	0.0147	0.0010
$TS7_{sim}$	0.0103	6.02e-5
$TS8_{sim}$	0.0053	0.00033

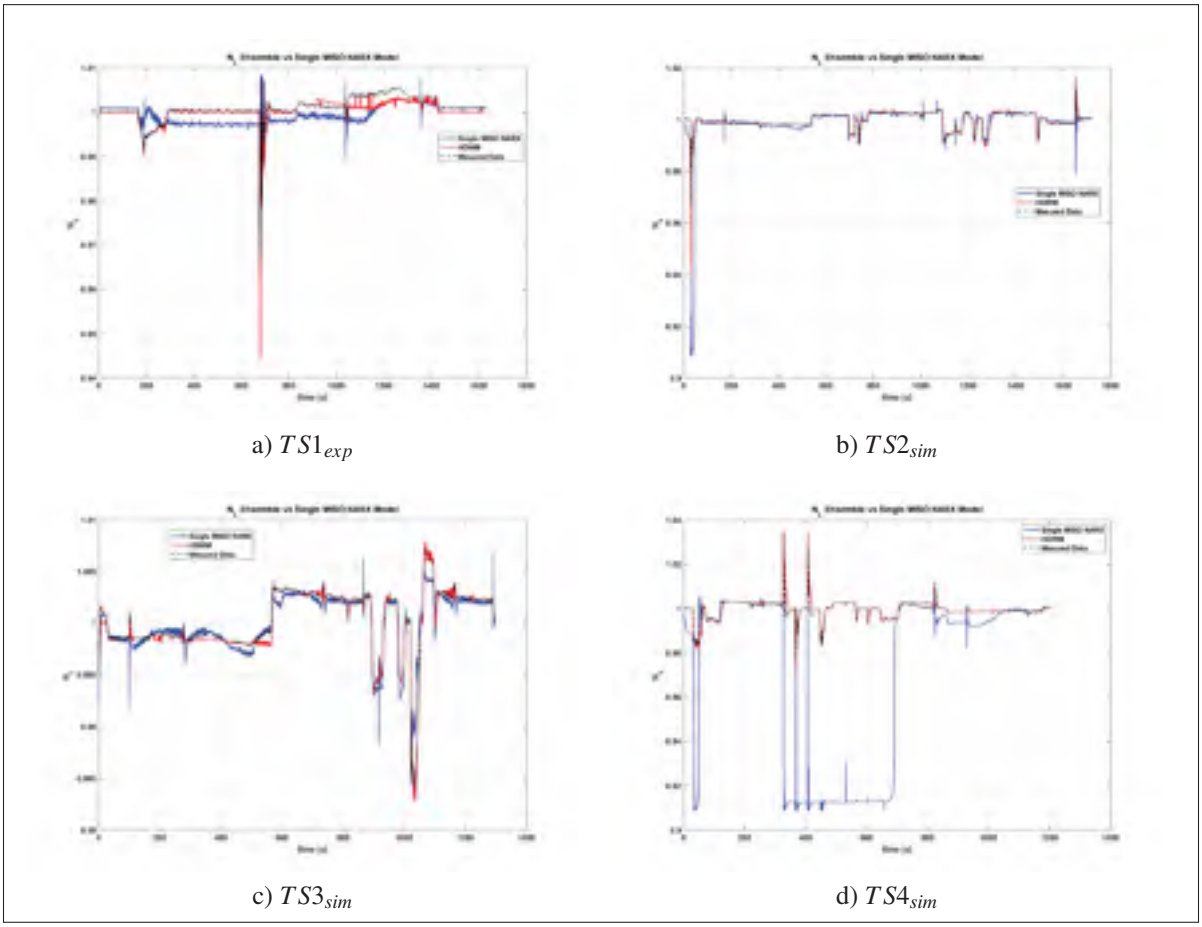

a) $TS1_{exp}$ b) $TS2_{sim}$

c) $TS3_{sim}$ d) $TS4_{sim}$

Figure 3.37 The comparison between the performance of ensemble of MISO NARX models and single MISO NARX model using $TS1_{exp}$ to $TS4_{sim}$ datasets - N_L

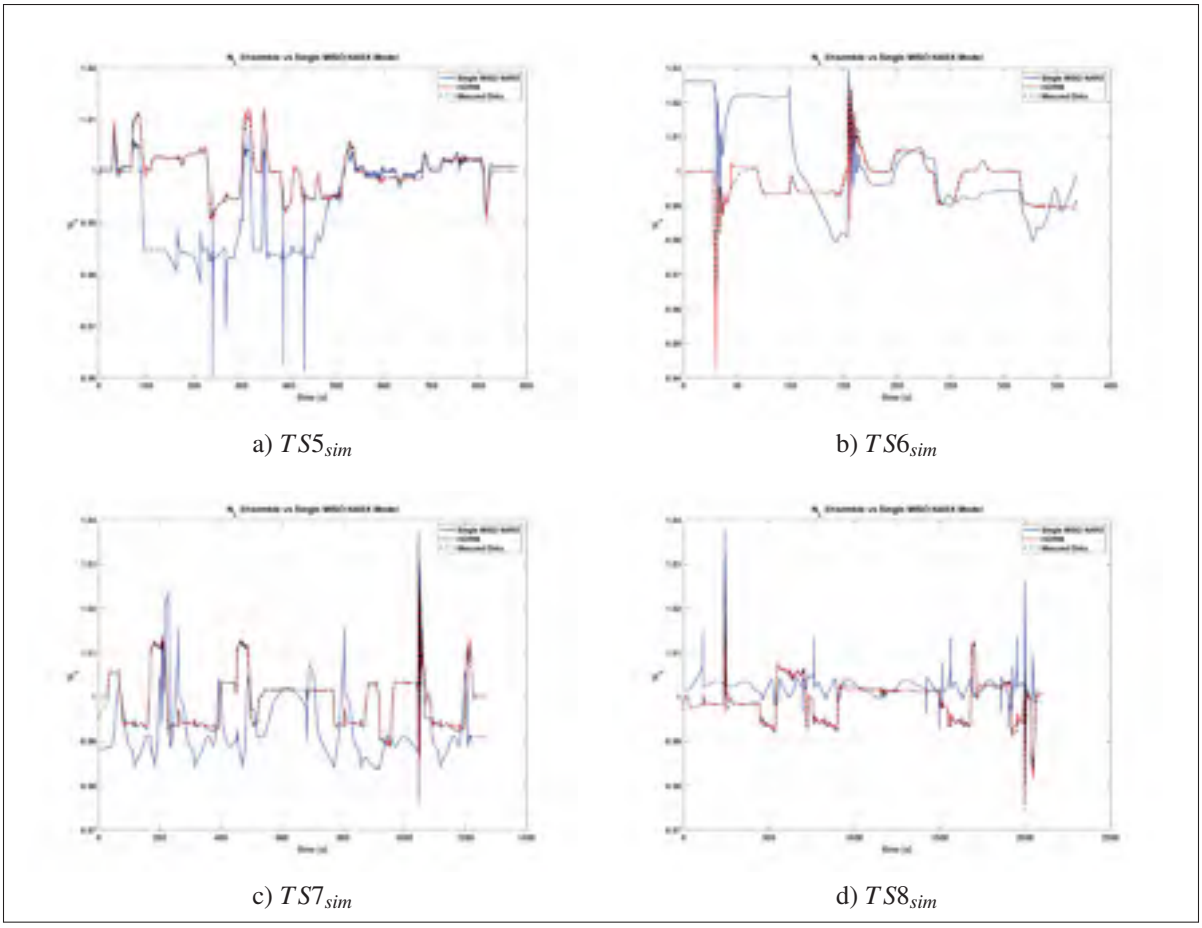

a) $TS5_{sim}$ b) $TS6_{sim}$

c) $TS7_{sim}$ d) $TS8_{sim}$

Figure 3.38 The comparison between the performance of ensemble of MISO NARX models and single MISO NARX model using $TS5_{sim}$ to $TS8_{sim}$ datasets - N_L

3.4.5 Ensemble model of TGT

Figure 3.39 and Figure 3.40 show the comparison between TGT estimated by the ensemble of MISO NARX models and the single MISO NARX model. This demonstrates that ensembles of diverse models aggregated with HDWM method can provide higher accuracy and higher robustness in real time than the single MISO NARX neural model approach. A summary of comparison results is shown in Table 3.17.

Table 3.17 Regression performance [*RMSE*] of single MISO NARX model and ensemble of eight MISO NARX models - *TGT*

Data set	**Single MISO-NARX model**	**Ensemble of MISO-NARX models**
$TS1_{exp}$	0.0202	0.0093
$TS2_{sim}$	0.0302	0.0008
$TS3_{sim}$	0.0257	0.0055
$TS4_{sim}$	0.0274	0.0020
$TS5_{sim}$	0.0320	0.0241
$TS6_{sim}$	0.1044	0.0032
$TS7_{sim}$	0.0377	0.0006
$TS8_{sim}$	0.0400	0.0330

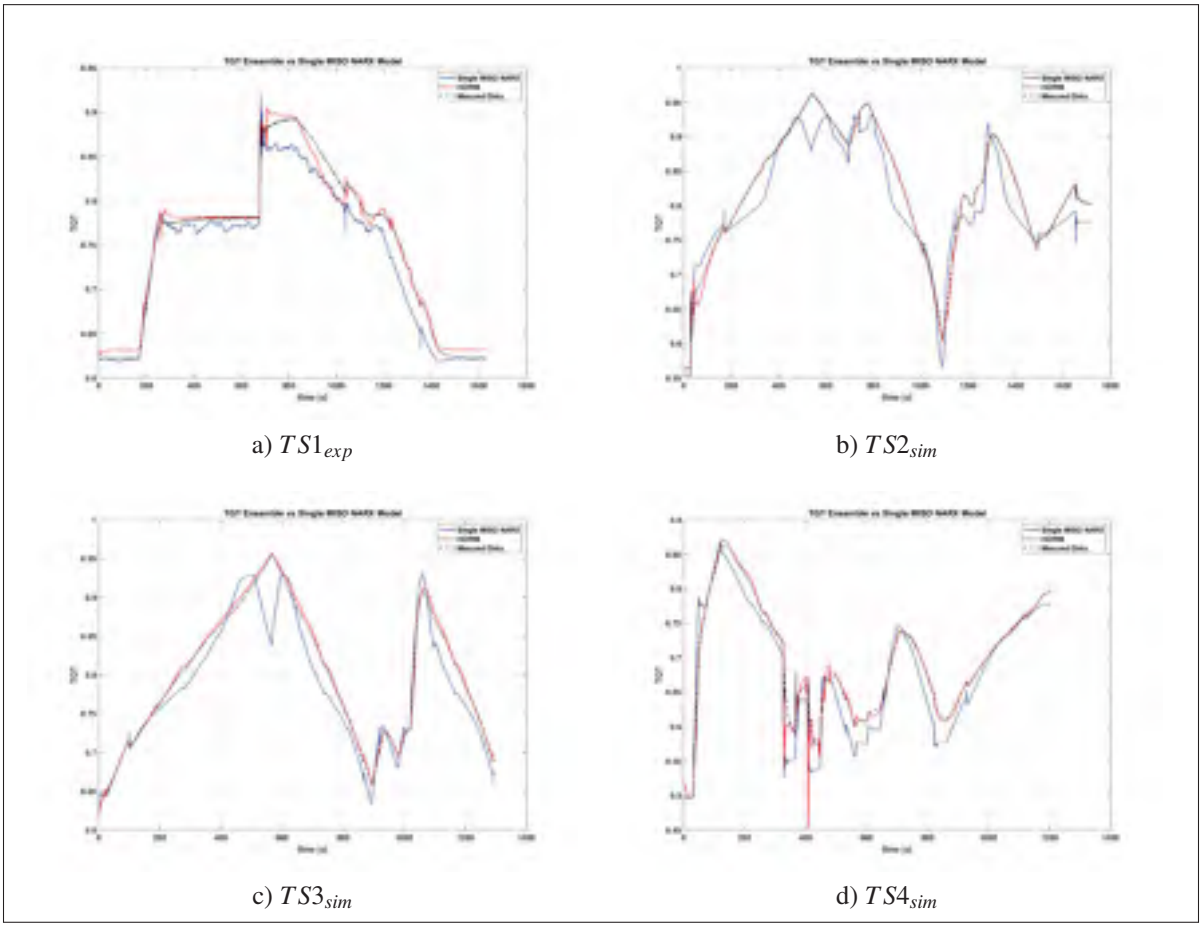

a) $TS1_{exp}$ b) $TS2_{sim}$

c) $TS3_{sim}$ d) $TS4_{sim}$

Figure 3.39 The comparison between the performance of ensemble of MISO NARX models and single MISO NARX model using $TS1_{exp}$ to $TS4_{sim}$ datasets - *TGT*

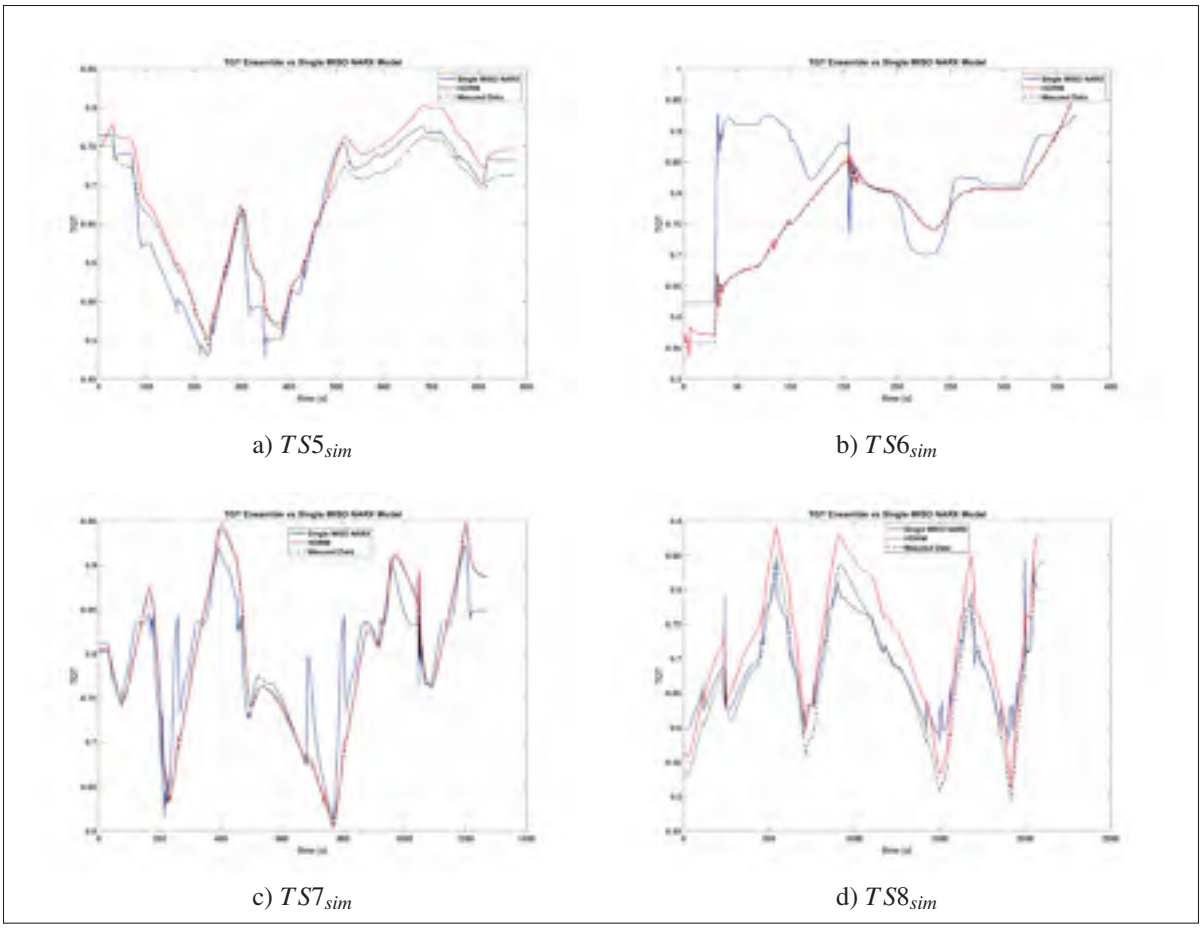

a) $TS5_{sim}$ b) $TS6_{sim}$

c) $TS7_{sim}$ d) $TS8_{sim}$

Figure 3.40 The comparison between the performance of ensemble of MISO NARX models and single MISO NARX model using $TS5_{sim}$ to $TS8_{sim}$ datasets - TGT

3.4.6 Ensemble model of T_{30}

Figure 3.41 and Figure 3.42 show the comparison between T_{30} estimated by the ensemble of MISO NARX models and the single MISO NARX model. This demonstrates that ensembles of diverse models aggregated with HDWM method can provide higher accuracy and higher robustness in real time than the single MISO NARX neural model approach. A summary of comparison results is shown in Table 3.18.

Table 3.18 Regression performance [*RMSE*] of single MISO NARX model and ensemble of eight MISO NARX models - T_{30}

Data set	**Single MISO-NARX model**	**Ensemble of MISO-NARX models**
$TS1_{exp}$	0.0272	0.0031
$TS2_{sim}$	0.0319	0.00021
$TS3_{sim}$	0.0301	0.0054
$TS4_{sim}$	0.0819	0.0001
$TS5_{sim}$	0.1205	0.0007
$TS6_{sim}$	0.0585	0.0012
$TS7_{sim}$	0.0754	0.0001
$TS8_{sim}$	0.1641	0.0013

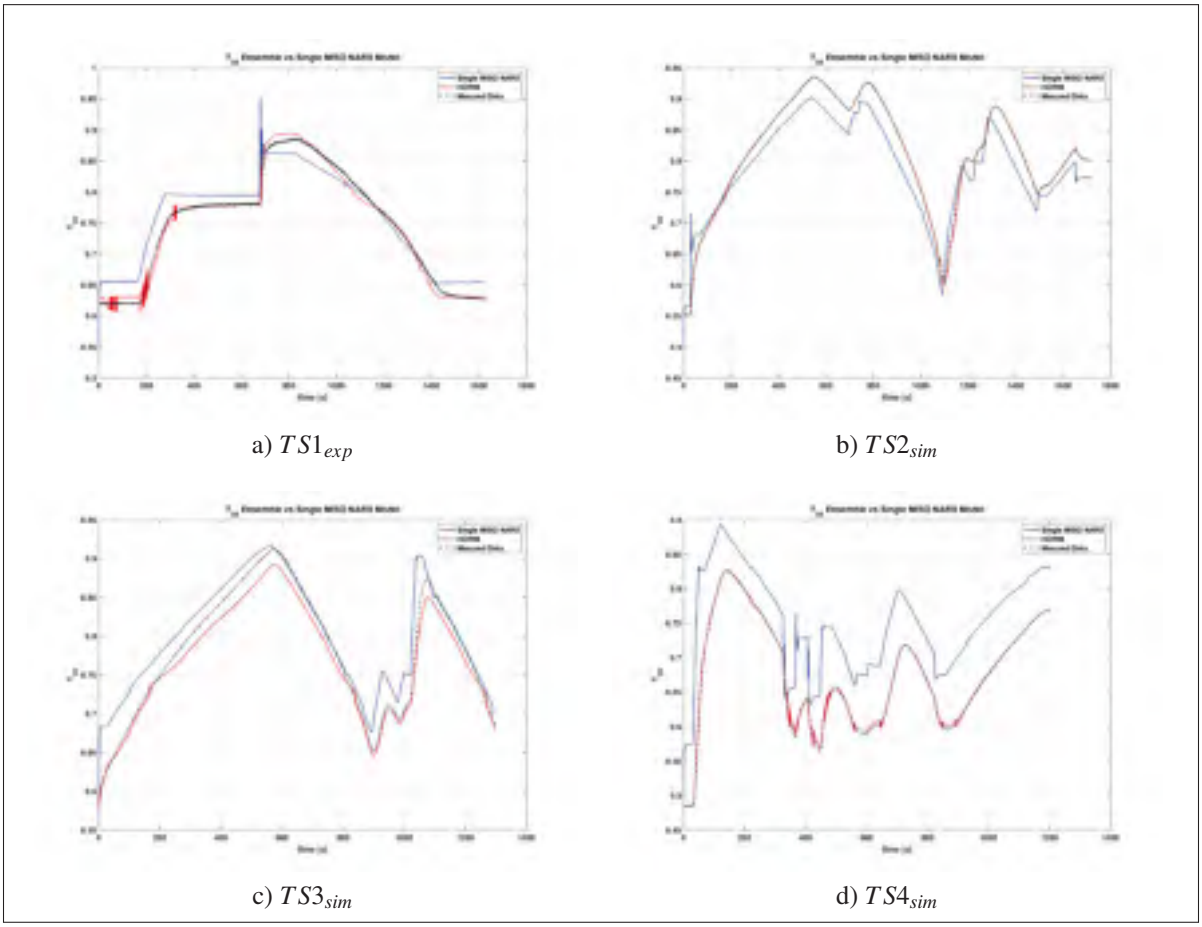

a) $TS1_{exp}$ b) $TS2_{sim}$

c) $TS3_{sim}$ d) $TS4_{sim}$

Figure 3.41 The comparison between the performance of ensemble of MISO NARX models and single MISO NARX model using $TS1_{exp}$ to $TS4_{sim}$ datasets - T_{30}

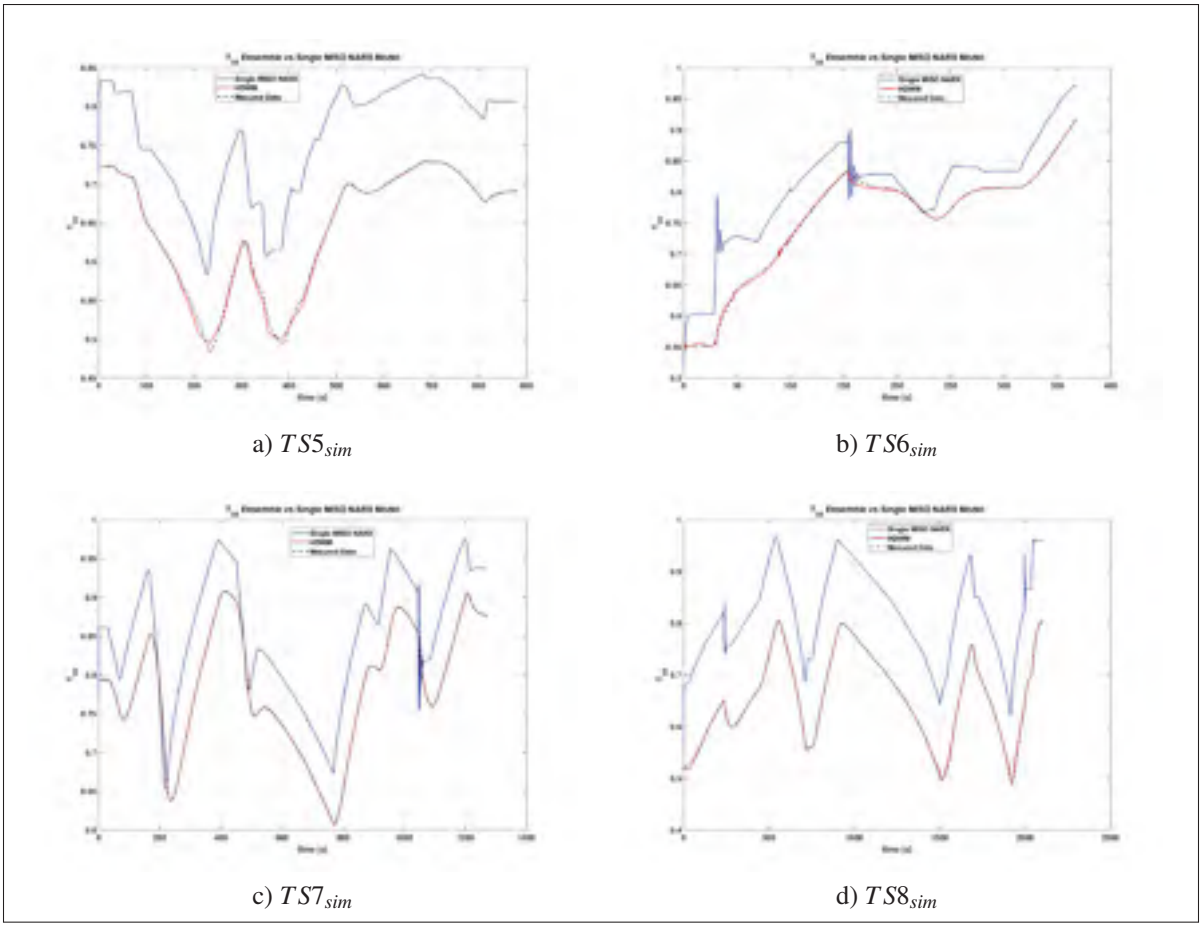

a) $TS5_{sim}$ b) $TS6_{sim}$

c) $TS7_{sim}$ d) $TS8_{sim}$

Figure 3.42 The comparison between the performance of ensemble of MISO NARX models and single MISO NARX model using $TS5_{sim}$ to $TS8_{sim}$ datasets - T_{30}

3.4.7 Ensemble model of P_{30}

Figure 3.43 and Figure 3.44 show the comparison between P_{30} estimated by the ensemble of MISO NARX models and the single MISO NARX model. This demonstrates that ensembles of diverse models aggregated with HDWM method can provide higher accuracy and higher robustness in real time than the single MISO NARX neural model approach. A summary of comparison results is shown in Table 3.19.

Table 3.19 Regression performance [*RMSE*] of single MISO NARX model and ensemble of eight MISO NARX models - P_{30}

Data set	**Single MISO-NARX model**	**Ensemble of MISO-NARX models**
$TS1_{exp}$	0.0796	0.00012
$TS2_{sim}$	0.0134	0.0023
$TS3_{sim}$	0.0125	0.00026
$TS4_{sim}$	0.0282	0.0021
$TS5_{sim}$	0.0400	0.0052
$TS6_{sim}$	0.0419	0.0065
$TS7_{sim}$	0.0220	0.0017
$TS8_{sim}$	0.0383	0.0004

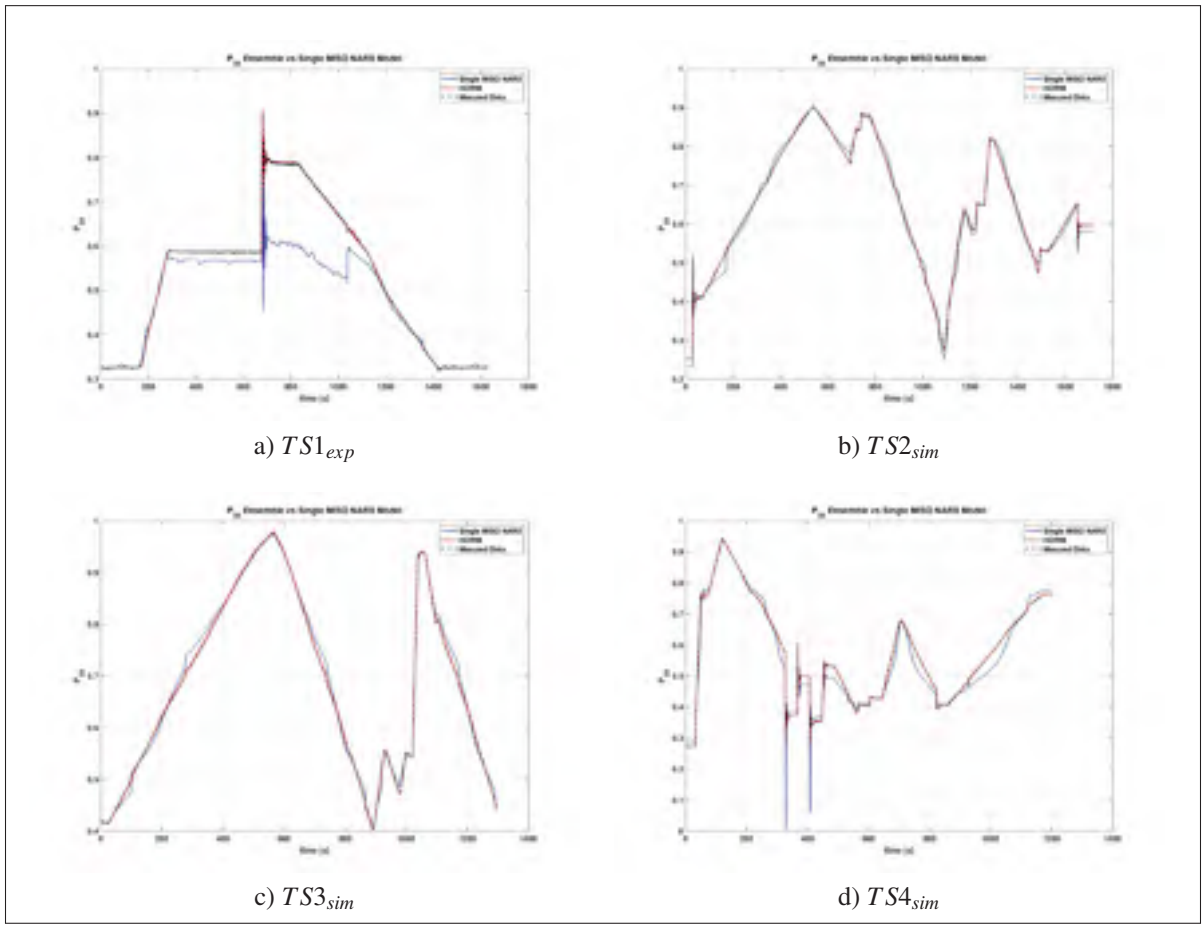

a) $TS1_{exp}$ b) $TS2_{sim}$

c) $TS3_{sim}$ d) $TS4_{sim}$

Figure 3.43 The comparison between the performance of ensemble of MISO NARX models and single MISO NARX model using $TS1_{exp}$ to $TS4_{sim}$ datasets - P_{30}

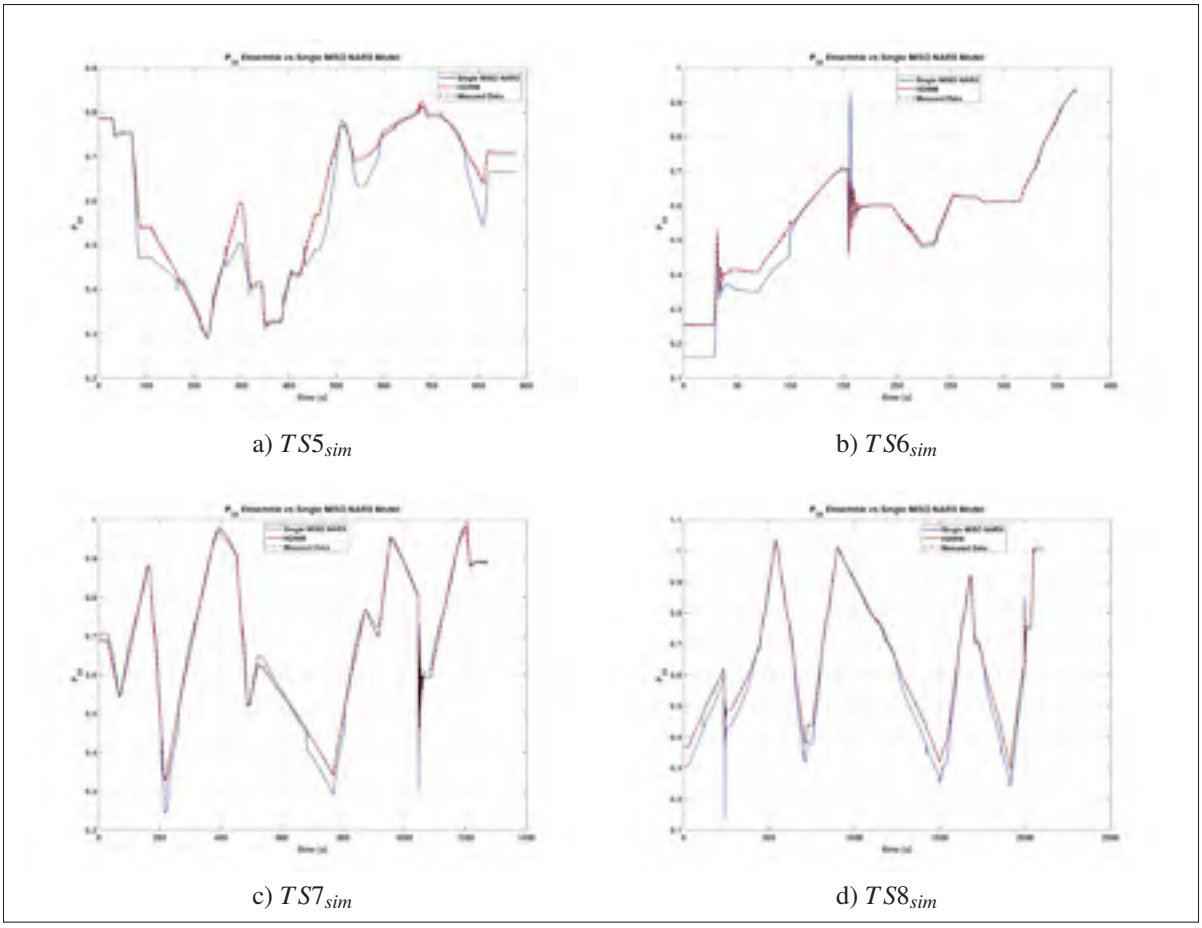

a) $TS5_{sim}$ b) $TS6_{sim}$

c) $TS7_{sim}$ d) $TS8_{sim}$

Figure 3.44 The comparison between the performance of ensemble of MISO NARX models and single MISO NARX model using $TS5_{sim}$ to $TS8_{sim}$ datasets - P_{30}

3.5 Summary

Artificial neural network has been used as a robust and reliable technique for system identification and modelling of complex systems with non-linear dynamics such as gas turbines. It can provide outstanding solutions to the problems that cannot be solved by conventional mathematical methods.

This chapter presents a novel methodology for the development of data driven based model of ADGTE, in order to simulate the dynamic performance of the ADGTE during the full operating range in real time. An ensemble of multiple MISO NARX neural models was introduced to predict the ADGTE output parameters in real time. First, Data collection and preparation

was performed, which includes collection of closed loop data from operational testing of the SGT-A65 ADGTE and the high fidelity simulation program of Siemens at different operation conditions. After that, data cleaning and re-sampling was performed to generate eight datasets for system identification. Secondly, estimation of the system order and delay were done by identification of linear ARX models based on the experimental datasets. This represents a key step before identification of the non-linear neural model. Third, the NARX neural network was chosen to be a base model of the ensemble of ADGTE due to its capability in the simulation and prediction of the response of non-linear systems. Moreover, multiple MISO NARX models for each output parameter from the ADGTE were generated. Each NARX model has a configuration that is different from the other ones and is based on the function of this model. A comprehensive computer program was used to select the best structure of MISO NARX model for each output parameter. After that, retraining operation of the selected MISO-NARX models was performed with training datasets from different operation conditions. As a result, seven homogeneous ensembles each one consisting of eight MISO NARX models were developed to predict the seven output parameters from the ADGTE at different operation conditions. The last and most important step in the ensemble generation is the combination of the outputs from the eight diverse models in each ensemble. A novel hybrid dynamic weighting method (HDWM) was proposed to perform this task, and verification of this method was performed by comparing its outputs with the output from three common integration methods. The results presented a superior performance of the new integration method. Finally, testing of the generated ensembles which use the HDWM method was performed at different operation conditions to measure the prediction accuracy and generalization property of the ensembles.

As shown in the results, the ensemble of MISO-NARX models can represent the ADGTE during the full operating range with a good accuracy even with different input scenarios from different operation conditions which prove the high generalization characteristic of the ensemble. Also, another important gain was the very low execution time (40.5 μs as compared to more than 10 ms using the same real time machine), which can support many real time applications like model based controller design, sensor fault verification and engine health monitoring. In

this study, this model will be used to design a model based controller to improve the performance of the ADGTE.

On the other hand, estimation of the NN model order by generating different ARX models and estimation of the input/output delay, before generation of NN model, are very important steps. These steps save more iterations required to find the best structure of the NN and consequently save more time required for NN model generation. In addition, data cleaning and resampling step significantly reduce training time. The lower sampling rate reduces the number of data points, which reduces the computation time during training operation and reduces data co-linearity. In (Asgari, 2014), in order to find the best model for the gas turbine engine, the generated code was run in MATLAB and 18720 different ANN structures were trained. However, this number was reduced to 240 different ANN structures by using the proposed approach.

CHAPTER 4

NON-LINEAR MODEL PREDICTIVE CONTROLLER

4.1 Introduction

The objective of an ADGTE control system is to provide required power as well as protection against physical and operational limits. NMPC approach is an attractive approach as compared to the classical min-max algorithm, and incorporates input/output constraints in its optimization process to fulfill the control requirements of the engine. However, due to heavy computational burden of NMPC, the real-time implementation of this algorithm is challenging and selection of NMPC design parameters is crucial. A novel method to solve this problem is presented in this chapter. The constrained MIMO GPC strategy based on NN model of a plant is proposed to implement the NMPC of the system. The theoretical foundation of the MPC algorithm is presented as well as the formulation of the unconstrained and constrained GPC algorithm for both SISO and MIMO cases. After that, a detailed derivation of the GPC algorithm based on adaptive non-linear ANN model (NNGPC) is presented in detail, showing the general procedure to obtain the control law and its most outstanding characteristics.

4.2 The Concept of the MPC

The methodology of all the controllers belonging to the MPC family is characterised by the strategies represented in Figure 4.1. Model predictive control is a form of control in which the current control action is obtained by solving, at each sampling instant, a finite horizon open-loop optimal control problem, using the current state of the plant as the initial state; the optimization yields an optimal control sequence and the first control in this sequence is applied to the plant. An important advantage of this type of control is its ability to cope with hard constraints on controls and states. It has, therefore, been widely applied in industrial applications where satisfaction of constraints is particularly important because efficiency demands operating points on or close to the boundary of the set of admissible states and controls.

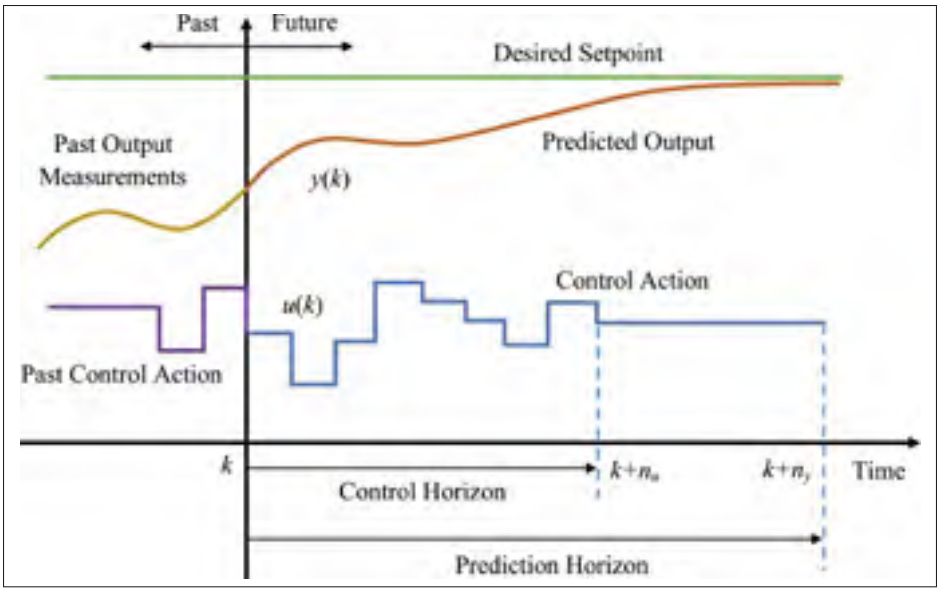

Figure 4.1 The MPC Strategy
Taken from Montazeri-Gh & Rasti (2019)

In order to implement this strategy, the basic structure shown in Figure 4.2 is used. A prediction model is used to predict the future plant outputs over a prediction horizon based on past and current values and on the proposed optimal future control actions. These actions are calculated by the optimizer taking into account the cost function, where the future tracking error is considered as well as the constraints. The objective of the MPC is minimisation of the predicted output errors by adjusting control actions over a given horizon.

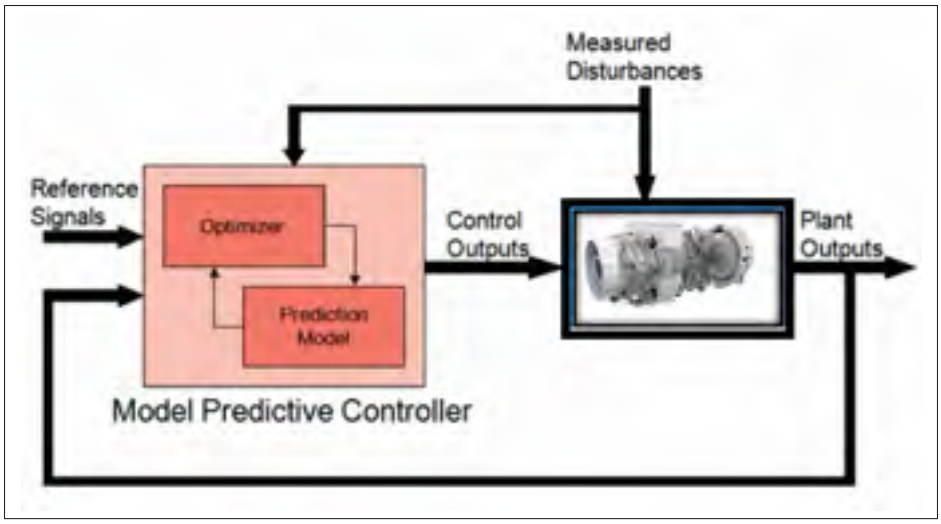

Figure 4.2 Block diagram of a model predictive controller

4.3 Generalized Predictive Control

Generalized Predictive Control (GPC), first introduced by Clarke *et al.* (1987a), is one of a class of MPC algorithms. This method is popular not only in industry, but also in academia. Few advanced control methods have had as much influence, widespread acceptance, and success in industrial applications as the GPC approach. The success of this technique is due to its capabilities of controlling a process with:

- Variable time delay and model order.
- Over-parameterization (plant/model mismatch).
- Unstable zeros (non-minimum phase).
- Unstable poles.
- Load-disturbances.

A model is the center for any kind of model-based control design. The model used in GPC design is the Controlled Autoregressive and Integrated Moving Average (CARIMA) model as

shown in equation (4.1),

$$A(z^{-1})y(t) = B(z^{-1})u(t-1) + C(z^{-1})\frac{e(t)}{\Delta} \tag{4.1}$$

where y(t) is the process output, u(t) is the input , and e(t) is the white noise. The difference operator $\Delta = 1 - z^{-1}$ in the denominator of the noise term is widely assumed, as it forces an integrator into the controller in order to eliminate offset between the measured output and its set point. $A(z^{-1})$, $B(z^{-1})$ and $C(z^{-1})$ are the polynomials in the backward-shift operator z^{-1} with the orders of n_y, n_u and n_k respectively:

$$\begin{aligned} A(z^{-1}) &= 1 + a_1 z^{-1} + a_2 z^{-2} + \cdots + a_{n_a} z^{-n_y} \\ B(z^{-1}) &= b_0 + b_1 z^{-1} + b_2 z^{-2} + \cdots + b_{n_b} z^{-n_u} \\ C(z^{-1}) &= 1 + b_1 z^{-1} + c_2 z^{-2} + \cdots + c_{n_c} z^{-n_k} \end{aligned} \tag{4.2}$$

The GPC strategy is based on applying a control sequence that minimizes a quadratic cost function measuring the control effort and the distance between the predicted system output and desired outputs over the prediction horizon, i.e.

$$J(N_1, N_2, N_u) = \sum_{j=N_1}^{N_2} [\hat{y}(t+j|t) - w(t+j)]^2 + \Lambda \sum_{j=1}^{N_u} [\Delta u(t+j-1)]^2 \tag{4.3}$$

subjected to $\Delta u(t+j) = 0$ when $j > N_u$

where $\hat{y}$ is the predicted output from the system model, and w is the reference output. $u(t+j-1)$ is the sequence of future control action that is to be determined. N_1, N_2 are the minimum, maximum horizon, and N_u is the control horizon. Λ is a weighting factor penalizing changes in the control inputs. The tuning parameters of the GPC are N_1, N_2, N_u, and Λ, which determine the stability and performance of the GPC controller. Notice that, $N_1 \geq 1$, $N_2 \geq N_1$, and $N_2 \geq N_u \geq 1$. In addition, some guidelines for selecting those parameters exist in (Clarke *et al.*, 1987b; Clarke & Mohtadi, 1987).

In order to derive the GPC control law, the optimal prediction of $y(t+j)$ for $N_1 \leq j \leq N_2$ will be obtained first. According to (Camacho & Alba, 2013) the future output value of SISO system is given by equation (4.4),

$$\hat{y}(t+j|t) = G_j(z^{-1})\Delta u(t+j-1) + \Gamma_j(z^{-1})\Delta u^f(t-1) + F_j(z^{-1})y^f(t). \tag{4.4}$$

In equation(4.4), the polynomials $G_j(z^{-1})$, $\Gamma_j(z^{-1})$, and $F_j(z^{-1})$ are calculated by solving the Diophantine equations:

$$\begin{aligned} \frac{C(z^{-1})}{\Delta A(z^{-1})} &= E_j(z^{-1}) + z^{-j}F_j(z^{-1}) \\ \frac{B(z^{-1})E_j(z^{-1})}{C(z^{-1})} &= G_j(z^{-1}) + z^{-j}\frac{\Gamma_j(z^{-1})}{C(z^{-1})} \end{aligned} \tag{4.5}$$

The superscript ^{f} in equation (4.4) denotes filtering by $1/C(z^{-l})$. As can be seen in equation (4.4), the last two terms depend only on the previous states. So that, we can include those terms into one term f. Then, the equation of the predictor can be written in more compact form as follows:

$$\hat{y}(t+j|t) = G_j(z^{-1})\Delta u(t+j-1) + f(t+j) \tag{4.6}$$

where $f(t+j)$ is the **free response** of the system if the input remains constant at the last computed value $u(t-1)$ and $G_j(z^{-1})\Delta u(t+j-1)$ represents the **forced response** of the system which depends on the future control actions yet to be determined. The polynomial $G_j(z^{-1})$ contains the system step response coefficients of the system as shown in equation (4.7),

$$G_j(z^{-1}) = E_j(z^{-1})B(z^{-1}) = g_0 + g_1 z^{-1} + \cdots + g_{j-1}z^{-(j-1)}. \tag{4.7}$$

To simplify the following derivation of the GPC control law, let $N_1 = 1$. Now consider the following set of j step ahead optimal predictions:

$$\begin{aligned} \hat{y}(t+1|t) &= G_1(z^{-1})\Delta u(t) + f(t+1) \\ \hat{y}(t+2|t) &= G_2(z^{-1})\Delta u(t+1) + f(t+2) \\ &\vdots \\ \hat{y}(t+N_2|t) &= G_{N_2}(z^{-1})\Delta u(t+N_2-1) + f(t+N_2) \end{aligned} \tag{4.8}$$

Hence, the predictor in vector notation can be written as:

$$\hat{y} = G\Delta u + f \tag{4.9}$$

where

$$\hat{y} = \begin{bmatrix} \hat{y}(t+1|t) \\ \hat{y}(t+2|t) \\ \vdots \\ \hat{y}(t+N_2|t) \end{bmatrix}_{[N_2X1]}, \qquad \Delta \text{ u} = \begin{bmatrix} \Delta u(t) \\ \Delta u(t+1) \\ \vdots \\ \Delta u(t+N_u-1) \end{bmatrix}_{[N_uX1]},$$

$$f = \begin{bmatrix} f(t+1) \\ f(t+2) \\ \vdots \\ f(t+N_2) \end{bmatrix}_{[N_2X1]} \quad \& \quad \text{G} = \begin{bmatrix} g_0 & 0 & \cdots & 0 \\ g_1 & g_0 & \cdots & 0 \\ \vdots & \vdots & \vdots & \vdots \\ g_{N_u-1} & \cdots & g_1 & g_0 \\ \vdots & \vdots & \vdots & \vdots \\ g_{N_2-1} & g_{N_2-2} & \cdots & g_{N_2-N_u} \end{bmatrix}_{[N_2XN_u]}$$

For SISO systems, the matrix G is a lower triangular matrix of dimension $[N_2XN_u]$. Besides, the first column of G can be calculated as the step response of the system when a unit step is applied to the manipulated variable.

Secondly, the cost function equation (4.3) can be written in matrix form as:

$$J = (\hat{y} - W)^T (\hat{y} - w) + \Lambda \, \Delta u^T \Delta u \tag{4.10}$$

where $w = [w(t+1), w(t+2), \cdots, w(t+N_2)]^T$. Substituting equation (4.9) into equation (4.10) yields:

$$J = (G\Delta u + f - w)^T (G\Delta u + f - w) + \Lambda \, \Delta u^T \Delta u \tag{4.11}$$

Equation (4.11) can be rewritten in matrix form:

$$J = \frac{1}{2} \Delta u^T H \Delta u + b^T \Delta u + f_0 \tag{4.12}$$

where the gradient b and Hessian H are defined as:

$$\begin{aligned} H &= 2(G^T G + \Lambda \, I) \\ b^T &= 2(f - w)^T G \\ f_0 &= (f - w)^T (f - w) \end{aligned} \tag{4.13}$$

For the unconstrained case, the minimization of the cost function (equation (4.12)) can be solved by setting the derivative of J with respect to Δu to zero, which leads to:

$$\Delta u = -H^{-1} b = (G^T G + \Lambda \, I)^{-1} G^T (w - f) \tag{4.14}$$

As the GPC is a receding-horizon control strategy, only the first control increment in Δu (equation (4.14)) is applied to the system and the whole algorithm is recomputed at time $t+1$.

The MIMO version of the GPC is a direct extension of the SISO GPC described above. The matrix and vector elements are not scalars but vectors and matrices themselves. If m-inputs and n-outputs are considered, then matrix $\boldsymbol{G}$ has dimension of $[n * N_2 X m * N_u]$, and it can be

obtained as:

$$\boldsymbol{G} = \begin{bmatrix} G_{11} & G_{12} & \cdots & G_{1m} \\ G_{21} & G_{22} & \cdots & G_{2m} \\ \vdots & \vdots & \ddots & \vdots \\ G_{n1} & G_{n2} & \cdots & G_{nm} \end{bmatrix} \tag{4.15}$$

where each matrix G_{ij} of dimension $[N_2 X N_u]$ contains the coefficients of the ith step response corresponding to the jth input. The vector of predicted outputs, future control signals, free response, and outputs set-point vector are respectively defined as:

$$\hat{\boldsymbol{y}} = \begin{bmatrix} \hat{y}_1(t+1|t) \\ \vdots \\ \hat{y}_1(t+N_2|t) \\ \vdots \\ \hat{y}_n(t+1|t) \\ \vdots \\ \hat{y}_n(t+N_2|t) \end{bmatrix}_{[n*N_2 X 1]}, \qquad \boldsymbol{\Delta u} = \begin{bmatrix} \Delta u_1(t) \\ \vdots \\ \Delta u_1(t+N_u-1) \\ \Delta u_m(t) \\ \vdots \\ \Delta u_m(t+N_u-1) \end{bmatrix}_{[m*N_u X 1]},$$

$$\boldsymbol{f} = \begin{bmatrix} f_1(t+1) \\ \vdots \\ f_1(t+N_2) \\ f_n(t+1) \\ \vdots \\ f_n(t+N_2) \end{bmatrix}_{[n*N_2 X 1]} \quad \& \quad \boldsymbol{w} = \begin{bmatrix} w_1(t+1) \\ \vdots \\ w_1(t+N_2) \\ w_n(t+1) \\ \vdots \\ w_n(t+N_2) \end{bmatrix}_{[n*N_2 X 1]} \tag{4.16}$$

The control weighting matrix $\boldsymbol{\Lambda}$ is with positive elements on its diagonal, i.e.

$$\boldsymbol{\Lambda} = diag(\Lambda_1, \Lambda_2, \cdots, \Lambda_m)$$

As can be seen, one of the advantages of MPC is that multi-variable processes can be handled in a straightforward manner.

4.4 Constrained GPC

The advantages of GPC become evident mainly when constraints are contemplated. The constraints acting on a process can originate from amplitude limits in the control signal, slew rate limits of the actuator, and limits on the output signals. These constraints can be described respectively by:

$$\begin{aligned} u_{min} \leq u(t) \leq u_{max} \\ \Delta u_{min} \leq \Delta u(t) \leq \Delta u_{max} \\ y_{min} \leq y(t) \leq y_{max} \end{aligned} \tag{4.17}$$

where u_{min} and u_{max} are the lower and upper bounds on the manipulated input amplitude. Δu_{min} and Δu_{max} are the lower and upper bounds on the future control increment. y_{min} and y_{max} are the lower and upper bounds on the process output amplitude.

To this end, we need to formulate the predictive control problem (equation (4.9)) as an optimization problem that takes into account the constraints present. Therefore, the key here is to parametrize the constrained variables (equation (4.17)) using the same parameter Δu as the ones used in the design of the GPC control law.

For the input amplitude constraints, we can write the control input predictions in terms of the future control increments as follows:

$$\begin{aligned} u(t) &= \Delta u(t) + u(t-1) \\ u(t+1) &= \Delta u(t+1) + u(t) \\ &= \Delta u(t+1) + \Delta u(t) + u(t-1) \\ u(t+2) &= u(t+1) + \Delta u(t+2) \\ &= \Delta u(t+2) + \Delta u(t+1) + \Delta u(t) + u(t-1) \\ &\vdots \\ u(t+N_u-1) &= \Delta u(t+N_u-1) + \Delta u(t+N_u-2) + \cdots + \Delta u(t) + u(t-1) \end{aligned} \tag{4.18}$$

Now, the input amplitude constraints over the control horizon N_u can be rewritten as follows: The input amplitude constraint at time t is:

$$u_{min} \leq u(t) \leq u_{max} \tag{4.19}$$

Replacing $u(t)$ with $\Delta u(t) + u(t-1)$ from equation (4.18)) and re-arranging the terms yields:

$$u_{min} - u(t-1) \leq \Delta u(t) \leq u_{max} - u(t-1) \tag{4.20}$$

Advancing t by one step gives:

$$\begin{aligned} u_{min} \leq u(t+1) \leq u_{max} \\ u_{min} - u(t-1) \leq \Delta u(t+1) + \Delta u(t) \leq u_{max} - u(t-1) \end{aligned} \tag{4.21}$$

Advancing t+1 by one step once more and performing the same substitution gives:

$$\begin{aligned} u_{min} \leq u(t+2) \leq u_{max} \\ u_{min} - u(t-1) \leq \Delta u(t+2) + \Delta u(t+1) + \Delta u(t) \leq u_{max} - u(t-1) \end{aligned} \tag{4.22}$$

A clear pattern arises, allowing us to write the entire set of input constraints over the control horizon N_u in matrix form as follows:

$$(u_{min} - u(t-1)) \begin{bmatrix} 1 \\ 1 \\ \vdots \\ 1 \end{bmatrix} \leq \begin{bmatrix} 1 & 0 & 0 & \cdots \\ 1 & 1 & 0 & \cdots \\ \vdots & \vdots & \vdots & \vdots \\ 1 & 1 & 1 & \cdots \end{bmatrix} \begin{bmatrix} \Delta u(t) \\ \Delta u(t+1) \\ \vdots \\ \Delta u(t+N_u-1) \end{bmatrix} \leq \begin{bmatrix} 1 \\ 1 \\ \vdots \\ 1 \end{bmatrix} (u_{max} - u(t-1)) \tag{4.23}$$

If the following definitions are introduced:

$$T_u = \begin{bmatrix} 1 & 0 & 0 & \cdots & 0 \\ 1 & 1 & 0 & \cdots & 0 \\ \vdots & \vdots & \vdots & \vdots & \vdots \\ 1 & 1 & 1 & \cdots & 1 \end{bmatrix}_{[N_u X N_u]} , \qquad L_u = \begin{bmatrix} 1 \\ 1 \\ \vdots \\ 1 \end{bmatrix}_{[N_u X 1]} \tag{4.24}$$

then equation (4.23) can be expressed as:

$$d_{u_{min}} \leq T_u \Delta u \leq d_{u_{max}} \tag{4.25}$$

where $d_{u_{min}} = (u_{min} - u(t-1))L_u$ and $d_{u_{max}} = (u_{max} - u(t-1))L_u$. Now, the complete set of input amplitude constraints can be compactly represented as:

$$\begin{aligned} T_u \Delta u &\leq d_{u_{max}} \\ -T_u \Delta u &\leq -d_{u_{min}} \end{aligned} \tag{4.26}$$

A reasonable approach to output constraint handling is the requirement that predicted outputs satisfy the constraints over the prediction horizon N_2. Substituting equation (4.9) in output constraints over N_2 yields:

$$y_{min} L_y \leq G\Delta u + f \leq y_{max} L_y \tag{4.27}$$

where $L_y = [1, 1, 1, \cdots, 1]^T$ is a vector of dimension [N_2 X 1].

The complete set of output constraints can be compactly represented as:

$$\begin{aligned} G\Delta u &\leq y_{max} L_y - f \\ -G\Delta u &\leq -y_{min} L_y + f \end{aligned} \tag{4.28}$$

The complete set of input slew rate constraints over N_u can be expressed as:

$$\begin{aligned} I\Delta u &\leq \Delta u_{max} L_u \\ -I\Delta u &\leq -\Delta u_{min} L_u \end{aligned} \tag{4.29}$$

where I is the identity matrix of dimension $[N_u X N_u]$.

From equations (4.26), (4.28) and (4.29), input and output constraints can be combined in a single inequality on Δu as:

$$M_C \Delta u \leq d_C \tag{4.30}$$

where

$$M_C = \begin{bmatrix} I \\ -I \\ T_u \\ -T_u \\ G \\ -G \end{bmatrix}, \qquad d_C = \begin{bmatrix} \Delta u_{max} L_u \\ -\Delta u_{min} L_u \\ d_{u_{max}} \\ -d_{u_{min}} \\ y_{max} L_y - f \\ -y_{min} L_y + f \end{bmatrix} \tag{4.31}$$

M_C is a matrix representing the constraints with its number of rows equal to the number of constraints and the number of columns equal to the dimension of vector Δu.

For an m-input n-output system with constraints acting over a prediction horizon N_2 and control horizon N_u, the similar mathematical formula can be derived.

The complete set of m-input slew rate constraints over N_u can be expressed as:

$$\begin{aligned} \boldsymbol{I\Delta u} &\leq \boldsymbol{\Delta u_{max} L_u} \\ -\boldsymbol{I\Delta u} &\leq -\boldsymbol{\Delta u_{min} L_u} \end{aligned} \tag{4.32}$$

where

$$\boldsymbol{I} = \begin{bmatrix} I_{[N_u X N_u]} & 0 & 0 & \cdots \\ 0 & I_{[N_u X N_u]} & 0 & \cdots \\ \vdots & \vdots & \ddots & \vdots \\ 0 & 0 & \cdots & I_{[N_u X N_u]} \end{bmatrix}_{[m*N_u X m*N_u]} , \boldsymbol{\Delta u}_{max} = \begin{bmatrix} \Delta u_{1_{max}} \\ \Delta u_{2_{max}} \\ \vdots \\ \Delta u_{m_{max}} \end{bmatrix}_{[mX1]} ,$$

$$\boldsymbol{L_u} = \begin{bmatrix} L_{u_{[N_u X 1]}} & 0 & 0 & \cdots \\ 0 & L_{u_{[N_u X 1]}} & 0 & \cdots \\ \vdots & \vdots & \ddots & \vdots \\ 0 & 0 & 0 & L_{u_{[N_u X 1]}} \end{bmatrix}_{[m*N_u X m]} \& \boldsymbol{\Delta u}_{min} = \begin{bmatrix} \Delta u_{1_{min}} \\ \Delta u_{2_{min}} \\ \vdots \\ \Delta u_{m_{min}} \end{bmatrix}_{[mX1]}$$

The complete set of m-input amplitude constraints over N_u can be expressed as:

$$\begin{aligned} \boldsymbol{T_u \Delta u} &\leq \boldsymbol{d}_{u_{max}} \\ -\boldsymbol{T_u \Delta u} &\leq -\boldsymbol{d}_{u_{min}} \end{aligned} \tag{4.33}$$

where

$$\boldsymbol{T_u} = \boldsymbol{L_u} \begin{bmatrix} T_{u_{[N_u X N_u]}} & 0 & 0 & \cdots \\ 0 & T_{u_{[N_u X N_u]}} & 0 & \cdots \\ \vdots & \vdots & \ddots & \vdots \\ 0 & 0 & \cdots & T_{u_{[N_u X N_u]}} \end{bmatrix}_{[m*N_u X m*N_u]} ,$$

$$\boldsymbol{d}_{u_{max}} = \boldsymbol{L_u} \begin{bmatrix} u_{1_{max}} - u_1(t-1) \\ u_{2_{max}} - u_2(t-1) \\ \vdots \\ u_{m_{max}} - u_m(t-1) \end{bmatrix}_{[mX1]} \& \ \boldsymbol{d}_{u_{min}} = \boldsymbol{L_u} \begin{bmatrix} u_{1_{min}} - u_1(t-1) \\ u_{2_{min}} - u_2(t-1) \\ \vdots \\ u_{m_{min}} - u_m(t-1) \end{bmatrix}_{[mX1]}$$

The complete set of n-output constraints over N_2 can be expressed as:

$$\begin{aligned} \boldsymbol{G\Delta u} &\leq \boldsymbol{y}_{max}\boldsymbol{L_y} - \boldsymbol{f} \\ -\boldsymbol{G\Delta u} &\leq -\boldsymbol{y}_{min}\boldsymbol{L_y} + \boldsymbol{f} \end{aligned} \tag{4.34}$$

where

$$\boldsymbol{L_y} = \begin{bmatrix} L_{y_{[N_2X1]}} & 0 & 0 & \cdots \\ 0 & L_{y_{[N_2X1]}} & 0 & \cdots \\ \vdots & \vdots & \ddots & \vdots \\ 0 & 0 & 0 & L_{y_{[N_2X1]}} \end{bmatrix}_{[n*N_2Xn]} , \boldsymbol{y}_{max} = \begin{bmatrix} y1_{max} \\ y2_{max} \\ \vdots \\ yn_{max} \end{bmatrix}_{[nX1]} \quad \& \boldsymbol{y}_{min} = \begin{bmatrix} y1_{min} \\ y2_{min} \\ \vdots \\ yn_{min} \end{bmatrix}_{[nX1]}$$

From equations (4.32), (4.33), and (4.34) m-input and n-output constraints can be combined in a single inequality on $\boldsymbol{\Delta u}$ as:

$$\boldsymbol{M_C\Delta u} \leq \boldsymbol{d_C} \tag{4.35}$$

where

$$\boldsymbol{M_C} = \begin{bmatrix} \boldsymbol{I} \\ -\boldsymbol{I} \\ \boldsymbol{T_u} \\ -\boldsymbol{T_u} \\ \boldsymbol{G} \\ -\boldsymbol{G} \end{bmatrix}, \qquad \boldsymbol{d_C} = \begin{bmatrix} \boldsymbol{\Delta u}_{max}\boldsymbol{L_u} \\ -\boldsymbol{\Delta u}_{min}\boldsymbol{L_u} \\ \boldsymbol{d}_{u_{max}} \\ -\boldsymbol{d}_{u_{min}} \\ \boldsymbol{y}_{max}\boldsymbol{L_y} - \boldsymbol{f} \\ -\boldsymbol{y}_{min}\boldsymbol{L_y} + \boldsymbol{f} \end{bmatrix} \tag{4.36}$$

4.5 Non-linear model predictive control algorithm (NMPC)

The MPC algorithm based on linear models is a mature control technique with multiple applications in the process industry. The next natural step in this area is the development of predictive control based on non-linear models. The use of controllers that take into account the non-linearities of the plant implies an improvement in the performance of the plant by reducing

the impact of the disturbances and by improving the tracking capabilities of the control system. However, the usage of a non-linear model within the NMPC changes the control problem from a convex quadratic problem to a nonconvex non-linear one. Furthermore, in this situation, there is no guarantee that the global optimum can be found especially in real-time control when the optimum solution has to be obtained in a prescribed time. Therefore, a novel method that tries to avoid these problems has been presented in the following parts of this chapter.

4.5.1 The neural network generalized predictive controller (NNGPC)

An investigation of a novel approach to implement the NMPC based on neural network model is reported in this study. A constrained MIMO NMPC is developed based on the GPC algorithm because of its simplicity, ease of use, and ability to handle problems in one algorithm. Future control actions are determined by minimizing the predicted errors without violating input and output constraints. The NN model, which was generated in the previous chapter, is used as a base model for the GPC controller to predict the future process outputs.

The design of the GPC demands the construction of a predictor (equation (4.9)). Hence, for the calculation of the predicted future output $\hat{y}$ only two characteristics of the system are needed: step (forced) and free responses. To obtain the step and the free process responses which are needed in the generalized predictive control strategy we iteratively use an ensemble of MISO-NARX models as a multi-step-ahead predictor.

The proposed control scheme in Figure 4.3 consists of a non-linear NN model of the system to be controlled in the form of ensembles of MISO-NARX models and the GPC algorithm block. The neural model is trained off-line as shown in the previous chapter. This model works as a predictor which produces the free and forced responses, that are used as an input to the GPC algorithm block. The GPC algorithm produces an output that is either used as an input to the plant or the predictor. The double pole double throw switch, S, is set to the plant when the GPC algorithm has solved for the best control input, $u(k)$, that will minimize a specified cost function. Between samples, the switch is set to the predictor where the GPC algorithm uses

this predictor to calculate the next control input, $u(k+1)$, by making prediction of the response over the prediction horizon N_2 from the predictor. Once the cost function is minimized, this input is passed to the plant. This algorithm is outlined below.

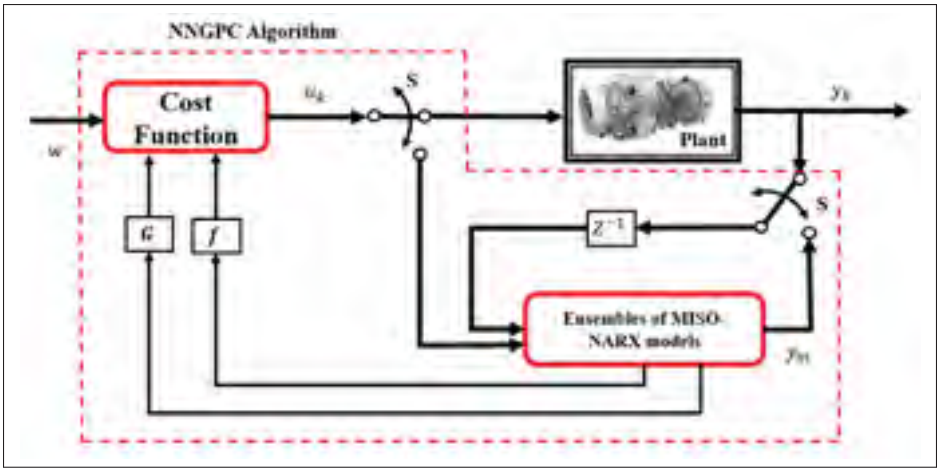

Figure 4.3 Block diagram of NMPC system

An approximation of the predicted future output is given by:

$$\hat{y} = G\Delta u + f \tag{4.37}$$

In this expression at each sampling time the vectors $G(t)$ and $f(t)$ are reconstructed. The free response f depends only on past inputs and outputs. Therefore, to get the free response the prescribed predictor is given a zero increment vector Δu i.e.

$$u(t) = u(t+1) = \cdots = u(t+N_2-1) = u(t-1) \tag{4.38}$$

Hence, the predictor (ensembles of MISO-NARX models) output will be the system free response.

$$\begin{aligned} y_{free}(t+i|t) &= F(y(t+i-1),\cdots,y(t+i-n_y),\cdots,u(t+i-1),\cdots,u(t+i-n_u)) \\ with: u(k) &= \begin{cases} u(t-1), & \text{if } k > t-1 \\ u(k), & \text{otherwise} \end{cases} \end{aligned} \tag{4.39}$$

where $F(.)$ represents the NN response.

The estimation of the step response coefficients to construct G matrix is obtained as follows:

$$\begin{aligned} g_{k-1} &= \frac{y_{step}(t+k|t) - y_{free}(t+k|t)}{\delta u(t)} \\ For\ \ k &= 1,\cdots,N_2 \end{aligned} \tag{4.40}$$

where δu represents the step size, and y_{step} represents the predictor step response which can be obtained by:

$$\begin{aligned} y_{step}(t+k|t) &= f(y(t+k-1),\cdots,y(t+k-n_y),\cdots,u(t+k-1),\cdots,u(t+k-n_u)) \\ with: u(k) &= \begin{cases} u(k), & \text{if } k \leq t-1 \\ u(t-1)+\delta u(t), & \text{if } k > t-1 \end{cases} \end{aligned} \tag{4.41}$$

The main difficulty to obtain an accurate estimate of the step response around some operating point is to select an appropriate value for the amplitude and the sign of the step $\delta u(t)$, because the step response of a non-linear system is determined by the operating point, the size and the sign of the step signal (Oviedo *et al.*, 2006). There are two important requirements that should be taken into consideration during the selection of step δu:

- It is very important that the value $u(t-1)+\delta u(t)$ does not saturate the actuators in the model. Even though the constraints are not taken into account for the optimization, the saturation constraints on the actuators must be taken into account. Failing to consider these sat-

uration points can lead to an underestimated step response and this will generate a response from the controller larger than needed, thereby possibly generating unstable behavior.

- The $\delta u(t)$ should be selected close to the predicted $\Delta u(t)$. Since this value is only known after the optimization, a good choice is to select $\delta u(t)$ equal to $\Delta u(t-1)$ obtained in the previous optimization step $(t-1)$. However, if $\Delta u(t) = 0$ as the system reaches the steady state, equation (4.40) will be badly conditioned. For this reason, a δu_{min} vector should be defined with the minimum value of δu, so that the estimation of step response coefficients is reliable.

Once f and G have been obtained from the response of the predictor (ensemble of MISO-NARX models), the gradient $\mathbf{b}$ and Hessian $\mathbf{H}$ of the GPC quadratic cost function (equation(4.12)) can be calculated based on equation(4.13).

It is important to remark that, the implementation of constrained MIMO NMPC is achieved by the usage of a NNGPC algorithm. In this algorithm, the estimation of free and forced response of the GPC predictor was derived from the non-linear model instead of linear CARIMA model or instantaneous linearization of the non-linear model. Therefore, by using this approach, the optimization problem can be solved as a linear optimization problem instead of a nonconvex and non-linear programming problem and this will improve the computation time and reliability of the solution. In the next subsection , we will talk about the optimization algorithm used in solving this quadratic optimization problem.

4.5.2 Numerical solutions using quadratic programming

A significantly important part of MPC with constraints are algorithms of numerical optimization. Reduction of the computational complexity of the optimization methods has been widely researched. The reason is that in certain cases of predictive control of fast dynamics processes, an optimization algorithm may not be feasible within the sampling period time. This situation occurs particularly when requirements on control are more complex, e.g. in the multivariable control. The Active Set method, Primal-Dual Interior Point method, and Hildreth's QP proce-

dure are some examples of QP methods that handle optimisation solutions involving constraints (Wang, 2009; Luenberger & Ye, 2016).

In the Active Set method, the active constraints (constraints that meet the condition $M_C \Delta u = d_C$) need to be identified along with optimal control decision variable Δu. The Active Set method requires an iterative updating procedure to test the constraint conditions (active or inactive) before solving for optimal decision variable. The main drawback of the Active Set method is that it produces quite a high computation load if many constraints are imposed on the optimisation problem.

A Primal-Dual method systematically identifies the constraints that are not active. They can then be eliminated in the solution. The Hildreth's method is based on numerical iterations, in which particular subresults are gradually improving. This method can be categorized as a dual optimization method, which manipulates with the Lagrangian multipliers. In this study, Hildreth's quadratic programming procedure is utilized which offers simplicity and reliability in real-time implementation (Wang, 2009). Furthermore, Hildreth's method may be useful to implement on non-PC platforms like programmable logic controllers or embedded machine which do not support linear algebra libraries.

From equations (4.13) and (4.30) the NNGPC optimization problem can be expressed as a quadratic cost function with linear inequality constraints as:

$$\begin{aligned} J &= \frac{1}{2}\Delta u^T H \Delta u + b^T \Delta u + f_0 \\ subject\ to & \\ M_C \Delta u &\leq d_C \end{aligned} \tag{4.42}$$

where H, b, f_0, M_C, and d_C are defined in equations (4.12) and (4.31).

For the unconstrained case, the minimization of the cost function (equation (4.42)) can be found by setting the derivative of J with respect to Δu to zero, which leads to:

$$\Delta u = -H^{-1}b = (G^T G + \Lambda I)^{-1} G^T (w - f) \tag{4.43}$$

In order to minimise the objective function (equation (4.43)) subject to inequality constraints, the following Lagrange expression is considered::

$$J = \frac{1}{2}\Delta u^T H \Delta u + b^T \Delta u + f_0 + \lambda^T (M_C \Delta u - d_C) \tag{4.44}$$

where λ is a column vector called Lagrange multiplier. The number of its components is equal to the number of inequality equations. The Lagrange Multiplier λ indicates whether a constraint is either active or inactive. Based on Karush-Kuhn-Tucker conditions (Gill *et al.*, 2019), if the element in the Lagrange Multiplier vector λ_i is strictly positive, the corresponding i^{th} constraint is active. In contrast, if the element is λ_i is zero then the i^{th} constraint is inactive (which indicates that a solution has satisfied the constraint condition $M_C \Delta u \leq d_C$).

A dual method can be used to identify the constraints that are not active as proposed in (Wang, 2009). Assuming feasibility (i.e. there is a Δu that satisfies $M_C \Delta u \leq d_C$), the dual problem to the original QP problem can be derived as follows:

$$\max_{\lambda \geq 0} \min_{\Delta u} \quad [\frac{1}{2}\Delta u^T H \Delta u + b^T \Delta u + f_0 + \lambda^T (M_C \Delta u - d_C)] \tag{4.45}$$

The minimization over Δu is assumed unconstrained and the optimal solution is given by:

$$\Delta u = -H^{-1}b - H^{-1} M_C^T \lambda \tag{4.46}$$

Substituting equation (4.46) into equation (4.45), the dual problem becomes:

$$\max_{\lambda \geq 0} \quad [-\frac{1}{2}\lambda^T L \lambda - \lambda^T Z - \frac{1}{2} b^T H^{-1} b] \tag{4.47}$$

where the matrices L and Z are given by:

$$L = M_C H^{-1} M_C^T \tag{4.48}$$

$$Z = M_C H^{-1} b + d_C \tag{4.49}$$

Thus, equation (4.47) is also a QP problem with λ as the decision variable. So, equation (4.47) is equivalent to:

$$\min_{\lambda \geq 0} \quad [\frac{1}{2}\lambda^T L\lambda + \lambda^T Z + \frac{1}{2} d_C^T H^{-1} d_C] \tag{4.50}$$

The set of optimal Lagrange multipliers that minimize the dual objective function equation (4.50) are denoted as $\lambda^\star$. Using the value of $\lambda^\star$, the decision variable Δu is obtained for the NNGPC control using equation (4.46) where λ is replaced by $\lambda^\star$.

In order to obtain $\lambda^\star$, the Hildreth's quadratic programming procedure can be used to solve the dual problem (equation (4.50)). The iteration expression of Hildreth's Quadratic Programming Procedure is given in the following equation:

$$\lambda_i^{k+1} = max(0, \omega_i^{k+1}) \tag{4.51}$$

where,

$$\omega_i^{k+1} = \frac{-1}{Z_{ii}} [L_i + \sum_{j=1}^{i-1} Z_{ij} \lambda_j^{k+1} + \sum_{j=i+1}^{n} Z_{ij} \lambda_j^k] \tag{4.52}$$

and k is the k^{th} iteration, the scalars Z_{ij} and Z_{ii} are the ij^{th} elements and the diagonal of the matrix Z respectively, while the scalar L_i is the i^{th} element in the vector L.

Now, The Hildreth's algorithm procedure used in this study can be summarized as follows:

1. The program finds the global optimal solution (equation (4.43)) and checks if all the constraints are satisfied. If so, the program returns the optimal solution. If not, the program begins to calculate the dual variable (Go to step 2).

2. At $k = 0$ and $\lambda_i^k = 0$

3. $k = k+1$

4. Compute ω_i^{k+1} using equation (4.52)

5. $\lambda_i^{k+1} = max(0, \omega_i^{k+1})$, (equation (4.51))

6. If $||\lambda^{k+1} - \lambda^k|| \geq \xi$ Go to step 2
   else $\Delta u = -H^{-1}b - H^{-1}M_C^T\lambda^\star$, Stop

The iteration of Hildreth's QP procedure converges monotonically to an optimal Lagrange multiplier $\lambda^\star$ (contains either zero for inactive constraints or positive values for active constraints) over a finite number of iterations. The requirements for the dual variables $\lambda^\star$ to converge to a set of fixed values are based on the conditions that the active constraints are linearly independent and their number remains less than or equal to the number of decision variables Δu (Wang, 2009). However, If these conditions are violated, the iteration will terminate when the loop reaches its predefined maximum value.

4.6 Summary

In this chapter, the theoretical foundation of the NNGPC algorithm was presented. This algorithm was proposed in order to overcome the computational limitation of the NMPC. Different components of the NNGPC algorithm such as: the predictor, formulation of the free and forced responses by using the onborad NN model, optimisation and constraints handling of the MPC algorithm were discussed. The association of the GPC algorithm NN model is computationally simple and suitable for control of nonlinear and complex processes. In the next chapter, the simulation results of the proposed system NNGPC algorithm are presented to validate the feasibility of the NNGPC algorithm in controlling an ADGTE used for power generation application.

CHAPTER 5

SGT-A65 ENGINE ADVANCED CONTROLLER DESIGN

5.1 Introduction

This chapter presents the validation results of the proposed NNGPC based on the NN model discussed in Chapter 4. The algorithm is implemented in MATLAB/Simulink with the perspective of future implementation on a Programmable Logic Controller (PLC). In this chapter, different components of the NNGPC algorithm such as: the predictor, formulation of the free and forced responses by using the onborad NN model, optimisation and constraints handling of the NNGPC algorithm are discussed. Moreover, an ensemble of MISO-NARX models with seven input parameters including power demand are generated to simulate the actual engine during the NNGPC controller testing. In addition, several tests have been conducted in the early parts of controller development to identify the control tuning parameters such as N_2, N_u, and Λ, that would produce satisfactory control performance. In addition, a brief introduction to the structures of current controller of the SGT-A65 engine is introduced. Finally, to verify the performance, a comparison between the performance of NNGPC controller and the performance of the existing controller is performed.

5.2 SGT-A65 engine current min-max control system architecture

The Industrial Trent (SGT-A65) engine control system schedules the fuel flow to maintain the engine power or speed to the desired level (3600 rpm). While, maintaining the other parameters of the engine, such as spool speeds, temperatures and pressures within its operating limits at all times. The min-max controller with PI compensator in each loop is currently used for the SGT-A65 ADGTE.

The overall control architecture of the SGT-A65 engine is shown in Figure 5.1. As can be seen, the fuel control system is based on multiple SISO independent loops all vying for control of the engine fuel flow (WF) through the loop selection logic, which is a series of highest and

lowest wins gates (min-max algorithm). The basis of this algorithm is to control a main output using a single control input while maintaining the other intended outputs within their limits. The min-max controller gives PI control action for all the loops in the selector algorithm. The proportional and integral gains are taken from a lookup tables. These gains are tuned in order to provide the required bandwidth and stability margins across the operating envelope.

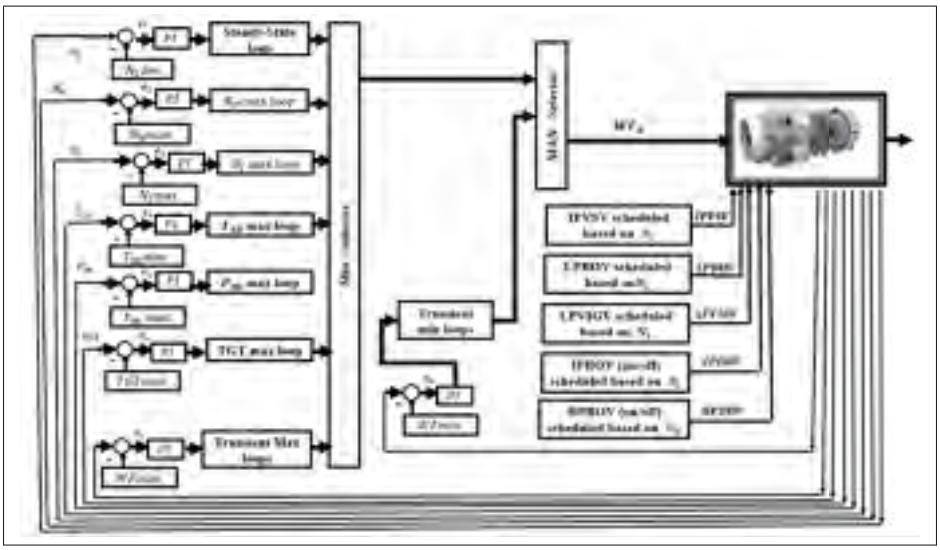

Figure 5.1 Engine fuel control system using min-max controller

In addition, to protect the engine during the acceleration or deceleration operation, five manipulated parameters were used by the ECS to protect engine as shown in Figure 5.1. These manipulated parameters are defined as follows:

- IPVSV is scheduled as a function of corrected shaft speed N_I to maintain peak performance and adequate surge margin during off-design operating conditions.
- LPVIGV and LPBOV are scheduled as a function of corrected shaft speed N_L and corrected power to prevent the possibility of compressor surge within the LPC.
- IPBOV and HPBOV consist of 4 and 3 ON/OFF valves respectively. Each of the bleed valves is commanded closed when the corrected shaft sped (N_I for IPBOV and N_H for HP-

BOV) exceeds the individual thresholds at which the valves are commanded to close. They are required to maintain an adequate surge margin across the IPC and HPC respectively.

As can be seen, the min-max controller solves the non-linear constrained problem using multiple SISO loops to protect against engine limits. However, the strong non-linearity of the engine can not always be handled adequately by the min-max controller with linear compensator especially during the fast load change Imani & Montazeri-Gh (2017); Montazeri-Gh & Rasti (2019). In this study, we propose solving this problem using MIMO NMPC method, which handles the MIMO non-linearities and constraints explicitly and in a single control formulation.

5.3 NNGPC design for SGT-A65 engine

In this work, The NNGPC is implemented in MATLAB®/SIMULINK environment. As shown in Figure 5.2, the NNGPC controller substitutes the seven control loops in the min-max controller by one NNGPC multi-variable controller. The first objective of the NNGPC is to maintain the low pressure spool speed N_L at a certain set point (3600 rpm) as the generator load changes. The second objective considered is to ensure that N_H, N_I, TGT, and P_{30} stay below their maximum limits so as not to damage the gas turbine. These two objectives are achieved by manipulating three controlling variables: WF, $IPVSV$, and $LPBOV$. Table 5.1 illustrates the input and output parameters cross-correlation based on $TR1_{exp}$ data set. The highest correlation among input and output parameters of the SGT-A65 ADGTE is observed between the input parameters (WF, $IPVSV$, and $LPBOV$) and the output parameters (N_H, N_I, N_L, TGT, P_{30}, PW, and T_{30}). However, the input parameters ($VIGV$, $IPBOV$, and $HPBOV$) do not have a strong correlation with the output parameters.

In addition to these two objectives, we also introduce input constraints on amplitude and slew rate of the controlling variables (WF, $IPVSV$, and $LPBOV$) to ensure safe acceleration and deceleration of the engine. In practice, input and output constraints are not necessarily fixed values. It is possible that constraints change with a certain parameter variable. Acceleration

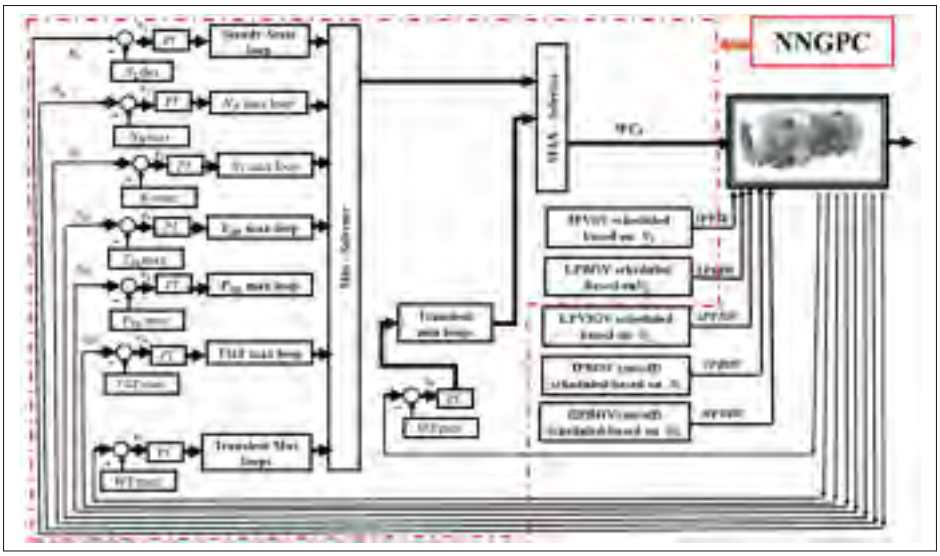

Figure 5.2 The NNGPC for SGT-A65

Table 5.1 Input and output parameters cross correlation

	N_H	N_I	N_L	TGT	P_{30}	PW	T_{30}
WF	0.9767	0.9811	-0.1811	0.9711	0.9907	0.9870	0.9531
$IPVSV$	0.9908	0.9881	-0.1464	0.9800	0.9681	0.9611	0.9517
$LPBOV$	0.9457	0.9494	-0.0690	0.9377	0.9493	0.9520	0.9197
$VIGV$	-0.2152	-0.2265	0.0152	-0.2257	-0.2490	-0.1937	-0.2563
$IPBOV$	-0.9125	-0.8953	0.0578	-0.9059	-0.8864	-0.8880	-0.8967
$HPBOV$	0.0043	-0.0036	0.2541	0.0359	-0.0151	-0.0147	0.0534

is limited by a WF/P_{30} schedule according to N_H. The maximum WF/P_{30} schedule is simply multiplied by the current value of P_{30} to obtain the maximum allowable fuel flow request WF_{max}. In addition, deceleration is limited by a WF/P_{30} schedule according to N_H. The minimum WF/P_{30} schedule is simply multiplied by the current value of P_{30} to obtain the minimum allowable fuel flow request WF_{min}. WF_{min} and WF_{max} are used as the lower and upper limits respectively of the fuel flow demand inside the NNGPC controller. Beside that, the TGT_{max} is scheduled according to ambient temperature and relative humidity. This value is used as the upper limit of the TGT inside NNGPC controller. Table 5.2 summarizes the input and output parameters constraints.

Table 5.2 Input and output parameters constraints

Parameter	Lower limit	Upper limit
WF	WF_{min}	WF_{max}
$IPVSV$	1.2067 %	95.5823 %
$LPBOV$	8 %	105.05 %
ΔWF	-100 pph/s	200 pph/s
$\Delta IPVSV$	-2 %/s	4 %/s
$\Delta LPBOV$	-2 %/s	3 %/s
N_H	-	10531 rpm
N_I	-	6833.74 rpm
TGT	-	TGT_{max}
P_{30}	-	580 psi

In practical situations such as our case, the controlled variables may not be subject to constraints, and the constrained outputs may not need to be controlled. Based on that, three actuators are used to control a single output, namely N_L. Four other variables, namely N_H, N_I, TGT, and P_{30} are considered as constrained outputs. This implies that different sets of G and f matrices must be used, according to whether an output is controlled or constrained. So that, the input vector, incremental input vector, the controlled outputs vector, and the constrained output vector are defined as follows:

$$\begin{aligned} \boldsymbol{u} &= [WF, IPVSV, LPBOV]^T \\ \boldsymbol{\Delta u} &= [\Delta WF, \Delta IPVSV, \Delta LPBOV]^T \\ y_{contr} &= [N_L] \\ \boldsymbol{y}_{constr} &= [TGT, N_H, P_{30}, N_I]^T \end{aligned} \tag{5.1}$$

The free response of the controlled parameter N_L can be expressed as:

$$f_{contr} = \begin{bmatrix} f_{N_L}(t+1) \\ f_{N_L}(t+2) \\ \vdots \\ f_{N_L}(t+N_2) \end{bmatrix}_{[N_2 X 1]} \tag{5.2}$$

where f_{N_L} is the output from the N_L ensemble due to input $\boldsymbol{u}$ as explained in equation (4.39). On the other hand, the free-response of the constrained parameters can be expressed as:

$$f_{constr} = \begin{bmatrix} f_{TGT}(t+1) \\ \vdots \\ f_{TGT}(t+N_2) \\ f_{N_H}(t+1) \\ \vdots \\ f_{N_H}(t+N_2) \\ f_{P_{30}}(t+1) \\ \vdots \\ f_{P_{30}}(t+N_2) \\ f_{N_I}(t+1) \\ \vdots \\ f_{N_I}(t+N_2) \end{bmatrix}_{[n_c * N_2 X 1]} \tag{5.3}$$

where n_c = 4 is the number of constrained outputs, and f_{TGT}, f_{N_H}, $f_{P_{30}}$, and f_{N_I} are the output from the TGT, N_H, P_{30}, and N_I ensembles respectively due to input $\boldsymbol{u}$ as explained in equation (4.39).

The step response matrix of the controlled parameter N_L can be expressed as:

$$\boldsymbol{G}_{contr} = \begin{bmatrix} G_{N_{L_{WF}}} & G_{N_{L_{IPVSV}}} & G_{N_{L_{LPBOV}}} \end{bmatrix}_{[N_2 X m * N_u]} \tag{5.4}$$

where $m = 3$ is the number of the controlling parameters, and $G_{N_{L_{WF}}}$, $G_{N_{L_{IPVSV}}}$, and $G_{N_{L_{LPBOV}}}$ are the N_L step response matrices due to step input in WF, $IPVSV$, and $LPBOV$ respectively. Indeed, the $G_{N_{L_{WF}}}$ matrix can be defined as follows:

$$G_{N_{L_{WF}}} = \begin{bmatrix} g_{N_{L_{WF_0}}} & 0 & \cdots & 0 \\ g_{N_{L_{WF_1}}} & g_{N_{L_{WF_0}}} & \cdots & 0 \\ \vdots & \vdots & \vdots & \vdots \\ g_{N_{L_{WF_{N_u-1}}}} & \cdots & g_{N_{L_{WF_1}}} & g_{N_{L_{WF_0}}} \\ \vdots & \vdots & \vdots & \vdots \\ g_{N_{L_{WF_{N_2-1}}}} & g_{N_{L_{WF_{N_2-2}}}} & \cdots & g_{N_{L_{WF_{N_2-N_u}}}} \end{bmatrix}_{[N_2 X N_u]} \tag{5.5}$$

where the step response coefficients of the $G_{N_L WF}$ matrix are obtained as follows:

$$\begin{aligned} g_{N_{L_{WF_{k-1}}}} &= \frac{NL_{WF_{step}}(t+k|t) - f_{N_L}(t+k|t)}{\delta WF(t)} \\ &For\ \ k = 1, \cdots, N_2 \end{aligned} \tag{5.6}$$

where $NL_{WF_{step}}$ represents the NL ensemble step response due to input $\boldsymbol{u}$ (equation (5.7)) with a step input in WF of magnitude δWF. Note that, $\delta WF(t)$ equals to $\Delta WF(t-1)$, which was obtained in the previous optimization step $(t-1)$. However, if $\Delta WF(t) = 0$, as the system reaches the steady state, $\delta WF(t)$ will be equal to $\delta WF_{min} = 0.01 * WF_{min}$.

$$\boldsymbol{u}(k) = \begin{cases} [WF(k), IPVSV(k), LPBOV(k)]^T, & \text{if } k \leq t-1 \\ [WF(t-1) + \delta WF(t), IPVSV(t-1), LPBOV(t-1)]^T, & \text{if } k > t-1 \end{cases} \tag{5.7}$$

The $G_{N_L IPVSV}$, and $G_{N_L LPBOV}$ matrices are calculated in the same way like the $G_{N_L WF}$ matrix. However, we use the input $\boldsymbol{u}$ with a step input in $IPVSV$ of magnitude $\delta IPVSV$ when calculating $G_{N_L IPVSV}$, and the input $\boldsymbol{u}$ with a step input in $LPBOV$ of magnitude $\delta LPBOV$ when calculating $G_{N_L LPBOV}$. Note that, $\delta IPVSV_{min} = 0.01 * IPVSV_{min}$, and $\delta LPBOV_{min} = 0.01 * LPBOV_{min}$.

With respect to the step response matrix of the constrained parameters, it can be presented as follows:

$$\boldsymbol{G}_{constr} = \begin{bmatrix} G_{TGT_{WF}} & G_{TGT_{IPVSV}} & G_{TGT_{LPBOV}} \\ G_{N_{H_{WF}}} & G_{N_{H_{IPVSV}}} & G_{N_{H_{LPBOV}}} \\ G_{P_{30_{WF}}} & G_{P_{30_{IPVSV}}} & G_{P_{30_{LPBOV}}} \\ G_{N_{I_{WF}}} & G_{N_{I_{IPVSV}}} & G_{N_{I_{LPBOV}}} \end{bmatrix}_{[n_c * N_2 X m * N_u]} \tag{5.8}$$

where $G_{TGT_{WF}}$, $G_{TGT_{IPVSV}}$, and $G_{TGT_{LPBOV}}$ are the TGT step response matrices due to step input in WF, $IPVSV$, and $LPBOV$ respectively. $G_{N_{H_{WF}}}$, $G_{N_{H_{IPVSV}}}$, and $G_{N_{H_{LPBOV}}}$ are the N_H step response matrices due to step input in WF, $IPVSV$, and $LPBOV$ respectively. $G_{P_{30_{WF}}}$, $G_{P_{30_{IPVSV}}}$, and $G_{P_{30_{LPBOV}}}$ are the P_{30} step response matrices due to step input in WF, $IPVSV$, and $LPBOV$ respectively. $G_{N_{I_{WF}}}$, $G_{N_{I_{IPVSV}}}$, and $G_{N_{I_{LPBOV}}}$ are the N_I step response matrices due to step input in WF, $IPVSV$, and $LPBOV$ respectively. Each step response matrix in the $\boldsymbol{G}_{constr}$ matrix is calculated in the same way that it was used in calculation of $G_{N_{L_{WF}}}$ matrix.

As mentioned earlier, the NNGPC is implemented in MATLAB®/SIMULINK environment. Figure 5.3 presents the SIMULINK block of the NNGPC controller. This block consists of two main components: the predictor SIMULINK block which is used to generate the required $\boldsymbol{f}$ and $\boldsymbol{G}$ matrices to solve the quadratic optimization problem, and the optimizer MATLAB function, which presents the optimization algorithm. This optimization algorithm is solved by using Hildreth's QP. The outputs from the optimizer MATLAB function are the optimum control actions (WF, $IPVSV$, and $LPBOV$) required to achieve the NNGPC objectives.

Figure 5.4 shows more details about the predictor block. The predictor block consists of four main blocks, which are iterated N_2 times each sampling time by using the For-iteration block. The first block inside the predictor is the f-block, which is used to calculate the free response for each controlled and constrained parameters as shown in Figure 5.5. In addition, the MATLAB function in the f-block is used to store the output from the ensemble (the onboard model) at each iteration and arranged them in the form of column vector of dimension [N_2 X 1] (for example f_{N_L} in equation (5.2)). Indeed, to align the onboard model (MISO-NARX ensembles) with the actual engine, the S switch allows feedback from output of the actual engine every sampling

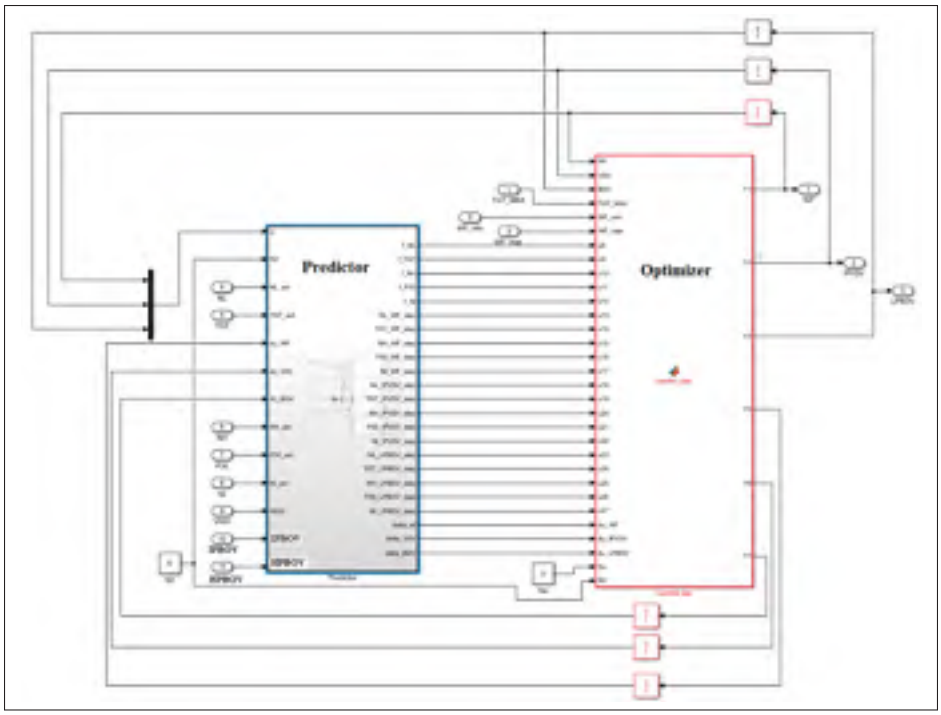

Figure 5.3 The NNGPC SIMULINK block

time. However, between samples, S switch allows feedback from output of the onboard model as shown in Figure 5.6. The other three blocks inside the predictor block calculate the step response for each controlled and constrained parameters. The $G-WF$ block, the $G-IPVSV$ block, and the $G-LPBOV$ block calculate the step response due to step input in WF, $IPVSV$, and $LPBOV$ respectively. All of the step response blocks have the same structure like free response block. However, the step response blocks have input incremental block to generate a step input in controlling variables each sampling time as shown in Figure 5.7.

On the other hand, for the simulation of NNGPC controller, two different engine models have to be implemented, one representing the actual engine and one representing the onboard engine model. The usage of two identical models would mean a perfect matching between the engine and the onboard model and would thus not lead to realistic results. Therefore, another ensemble of MISO NARX models was generated in the same approach as mentioned earlier in chapter 4 to simulate the actual engine during the controller testing phase. However, this actual engine model differs from the onboard model in terms of the number of input parameters. the actual

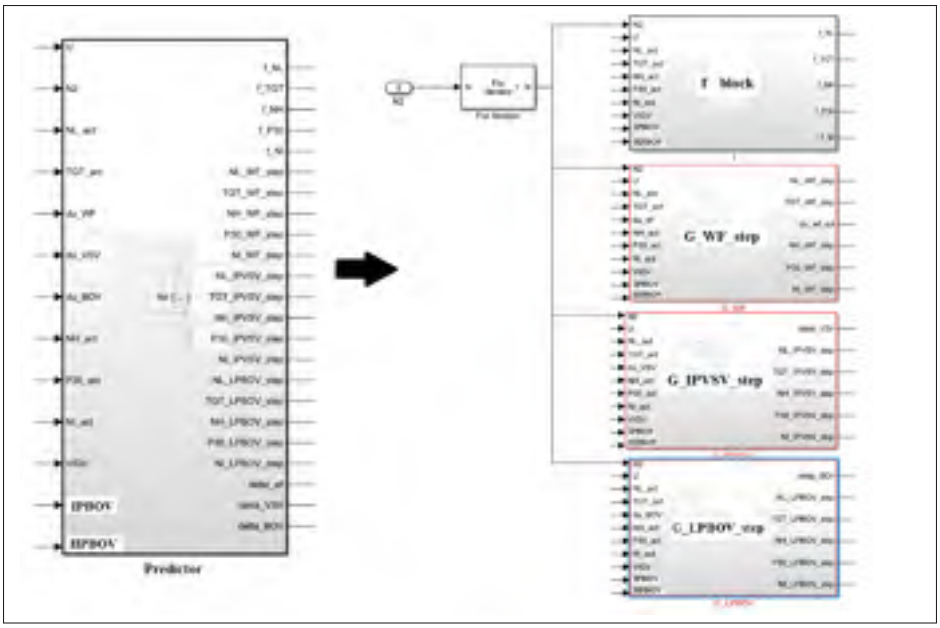

Figure 5.4 The Predictor block

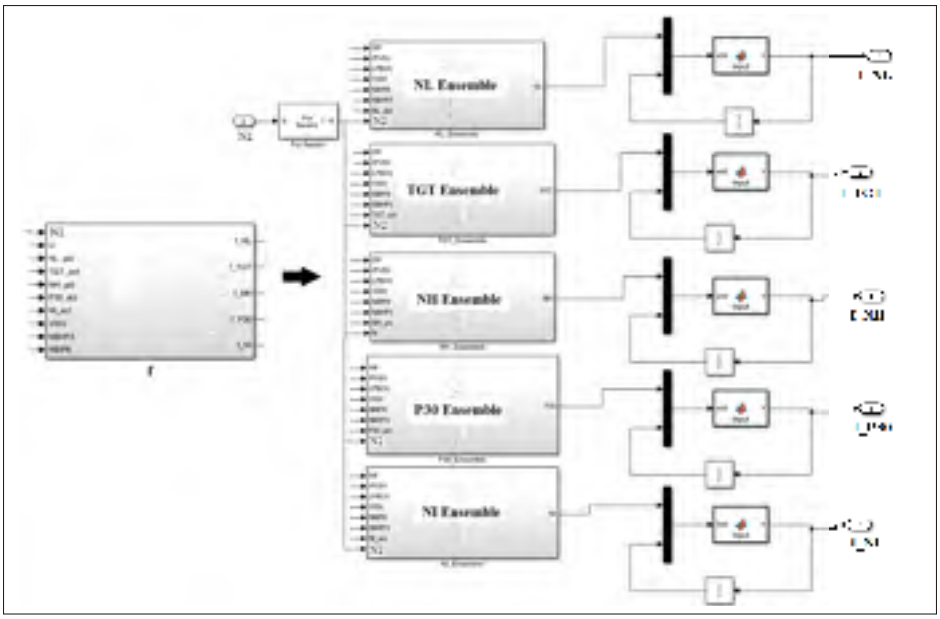

Figure 5.5 The free response block

engine model has a seven input parameters: WF, $IPVSV$, $LPBOV$, $VIGV$, $IPBOV$, $HPBOV$, and PW_{dem} as shown in Figure 5.8. Figure 5.9 through Figure 5.15 present the testing results of the actual engine model by using experimental dataset $TS2_{exp}$. As can be seen, the outputs

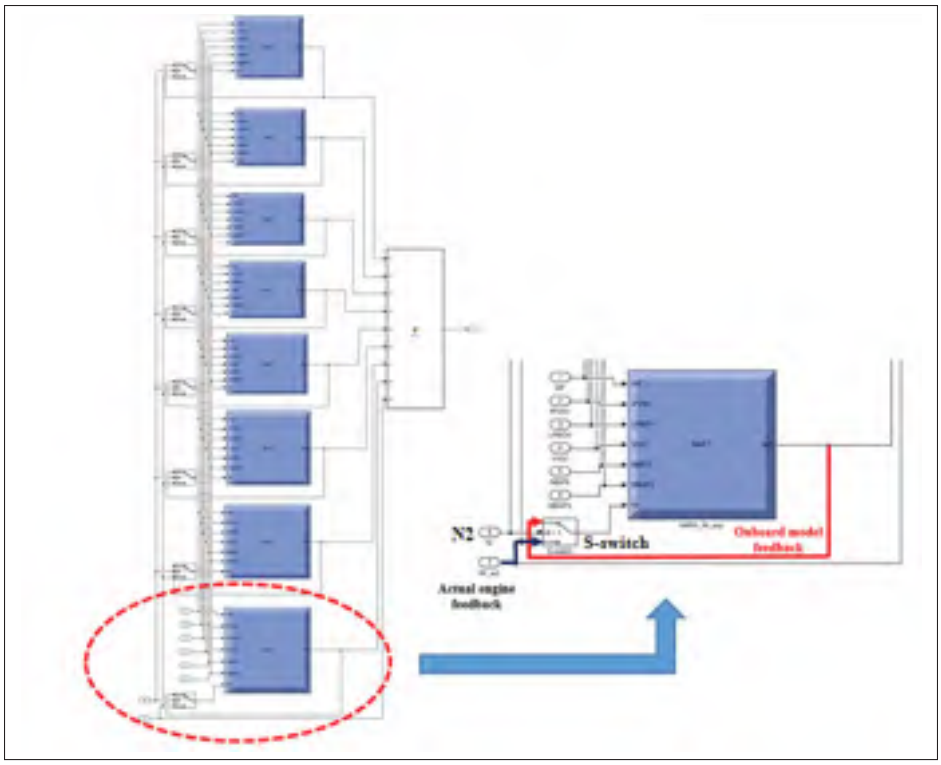

Figure 5.6 The N_L ensemble block

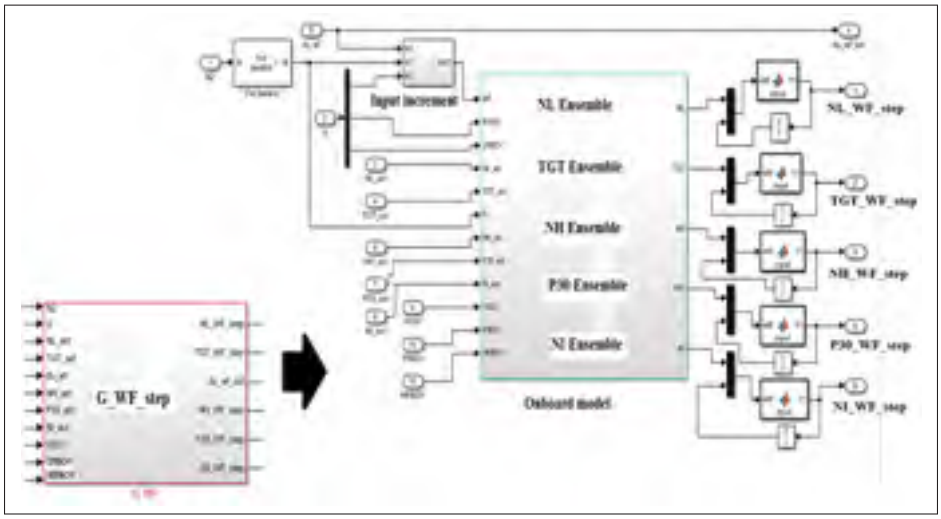

Figure 5.7 The step response block

from the actual engine model followed the targets precisely and can predict the reaction of the system to load changes with high accuracy and reliability.

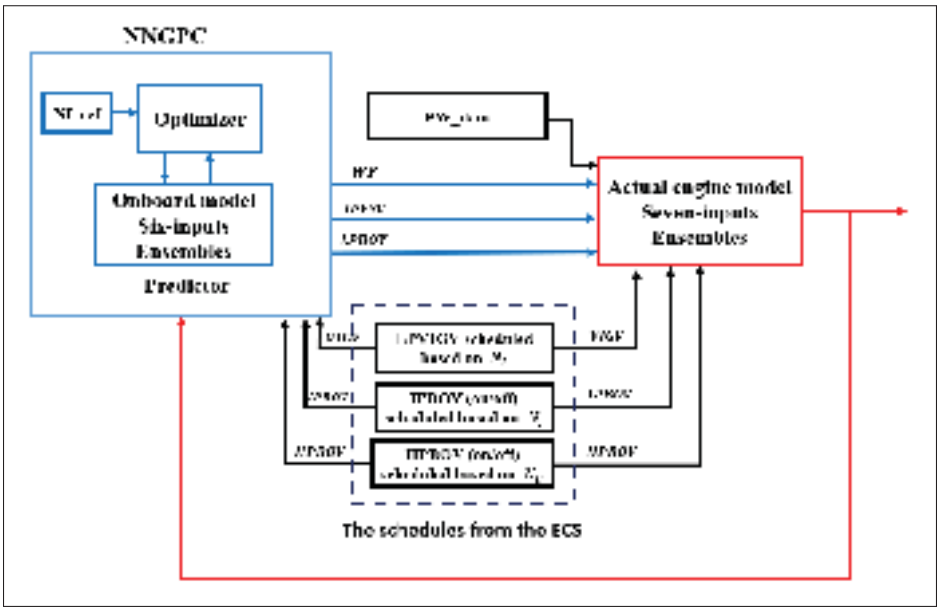

Figure 5.8 Integration of onboard model and actual engine model

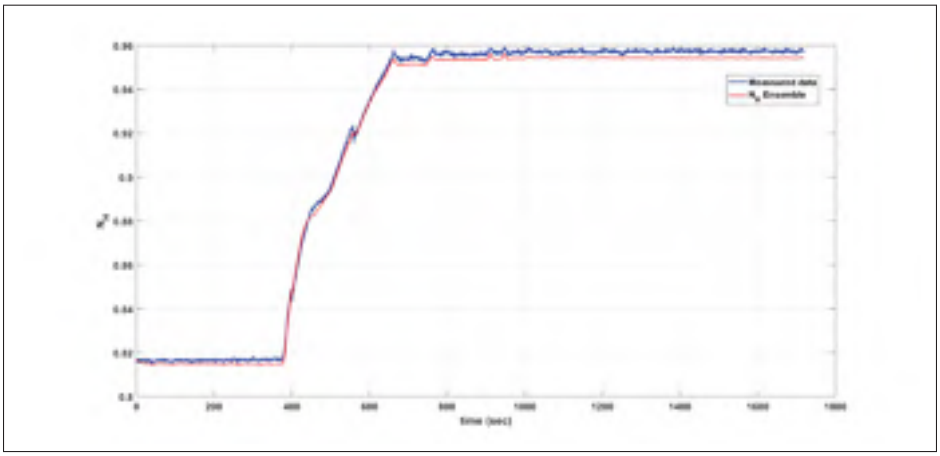

Figure 5.9 The actual engine model testing results: N_H

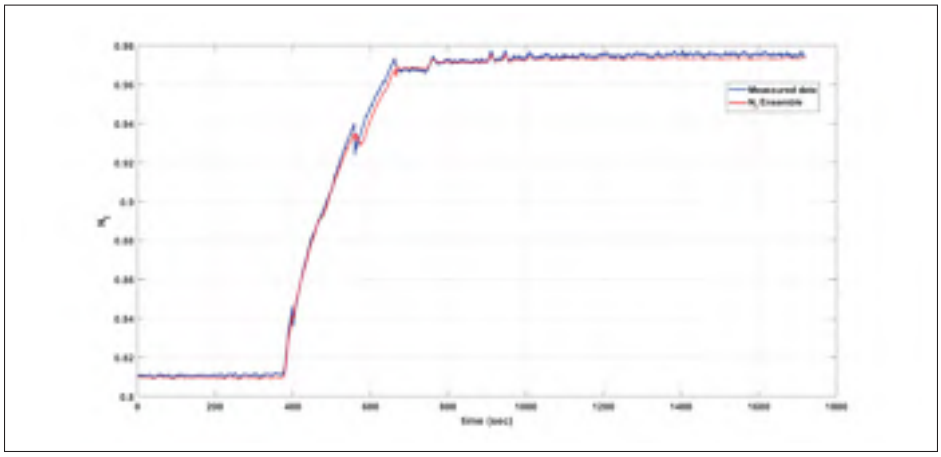

Figure 5.10 The actual engine model testing results: N_I

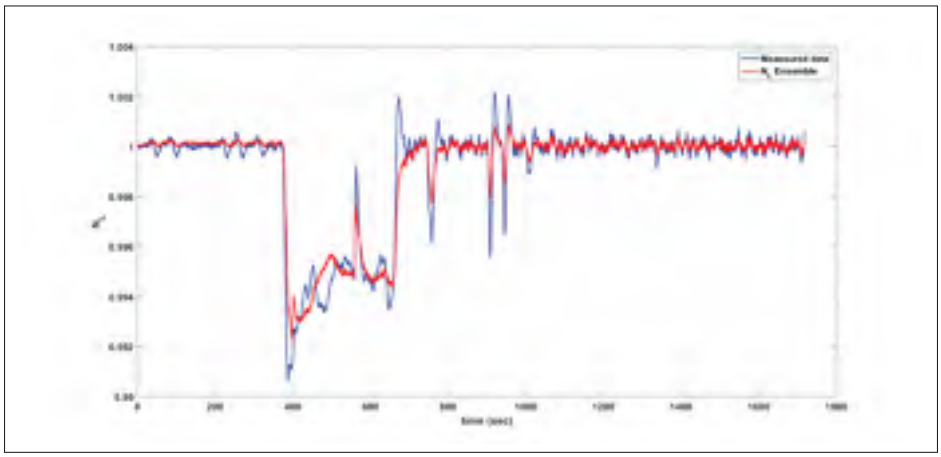

Figure 5.11 The actual engine model testing results: N_L

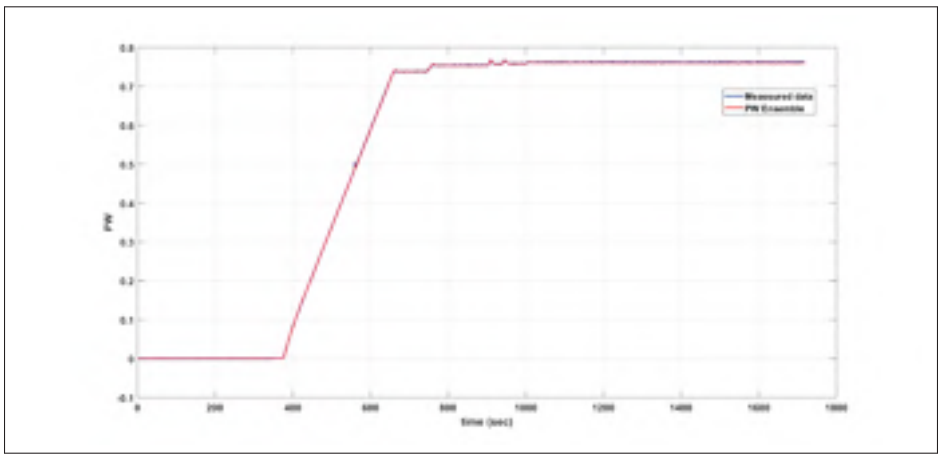

Figure 5.12 The actual engine model testing results: PW

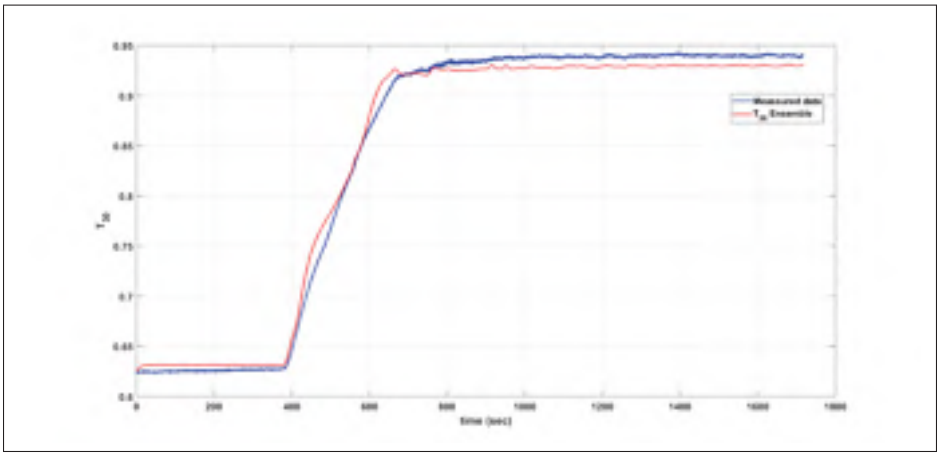

Figure 5.13 The actual engine model testing results: T_{30}

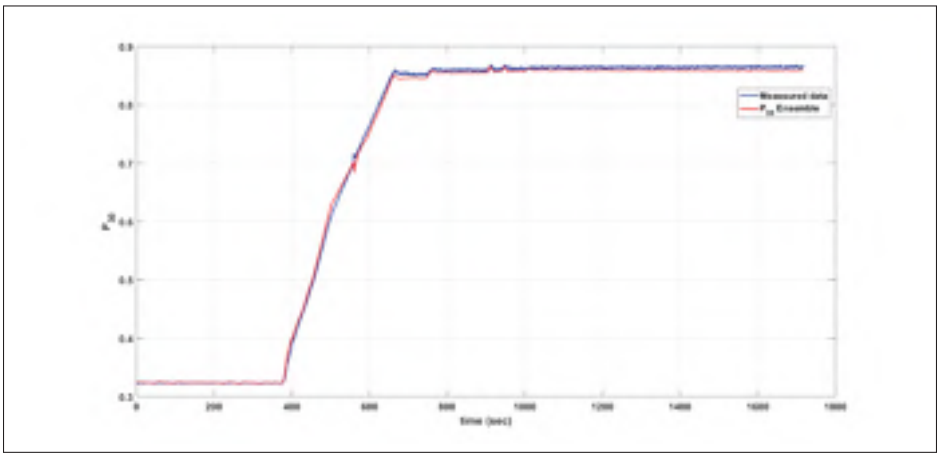

Figure 5.14 The actual engine model testing results: P_{30}

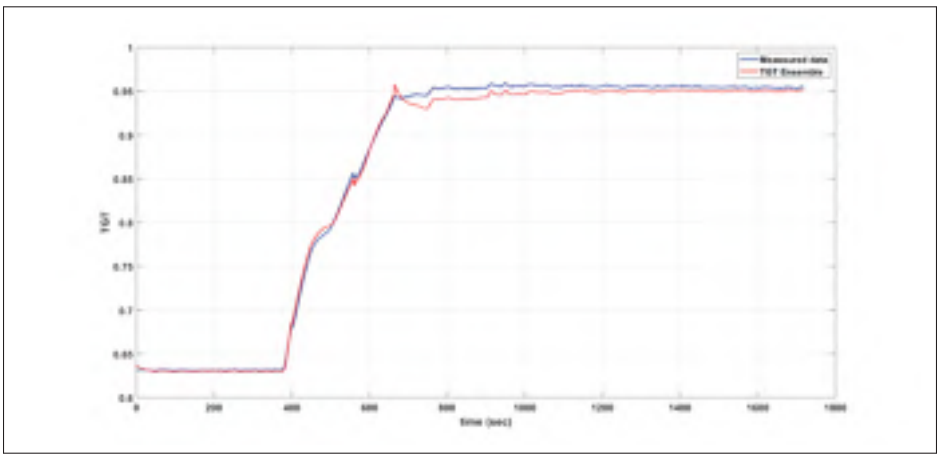

Figure 5.15 The actual engine model testing results: TGT

5.4 The NNGPC tuning

The proposed NNGPC design consists of three tuning parameters that need to be properly tuned to achieve good controller performance. The tuning parameters that influence the closed loop response of the system include the prediction horizon N_2, the control horizon N_u, and the weighting factor Λ. In this study, the NNGPC tuning parameters are obtained by trial and error. The selection of MPC tuning parameters in gas turbine application has already been studied in previous studies (Ghorbani *et al.*, 2008b; Richter, 2011). A higher N_2 and N_u can result in better performance of the plant. However, it results in increasing of computation time, which makes the implementation of NNGPC in real time more difficult. In addition, changes in Λ have a strong influence on the simulation outcome. Low values tend to produce faster responses with actuator saturation, and very high values may penalize control activity excessively, resulting in poor transient response. In order to measure the computational efforts required for the NNGPC, the CPU time that is required to execute the calculations of the controller, is used as the characterization of computational efforts. In addition, all simulation cases run on the same computer, which is composed of 3.31 GHz Intel(R) Xeon (R) CPU E3-1225 v6 machine with 64 GB RAM running Microsoft Windows 10. The Matlab/Simulink version is Matlab R2018b. It is assumed that the simulation time is 100 s for all cases, and T_s = 0.01 s.

Figure 5.16 through Figure 5.20 show the effect of changing N_2 for fixed values of $N_u = 3$ and $\Lambda = [0.5\ 15\ 65]$ with the summary of controller performance given in Table 5.3. It is observed that performance improvement is initially obtained by increasing N_2 , but further changes have no effect beyond N_2 = 10. However, the computational efforts increases about 85 % when the N_2 is increased from 5 to 10. Indeed, N_u is selected at 3 sample steps. However, no detectable improvement occurs beyond N_u equal 3.

Changes in Λ have a strong influence on the simulation outcome. Low values tend to produce faster responses with controlling parameters saturation, and very high values may penalize control activity excessively, resulting in slow transient response. Finally, the best controller performance was obtained with N_2 = 5, N_u = 3 and Λ= [0.5 15 65].

Table 5.3 The control performance comparison with various N_2 values

Output parameter	N_2	Settling time (s)	Overshoot (%)	Computation time (s)
PW	3	18.63	4.1	15.39
	5	7.6	4	35.34
	10	7.5	15.7	245.68
N_L	3	10.27	9.4	15.39
	5	3.7	4	35.34
	10	3.61	3.8	245.68

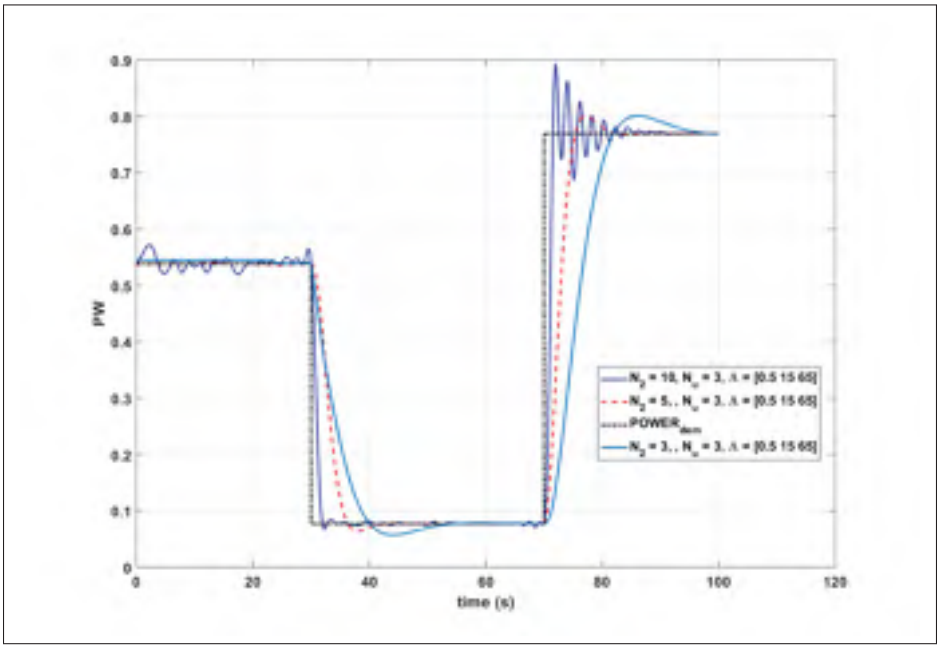

Figure 5.16 Effect of prediction horizon on PW

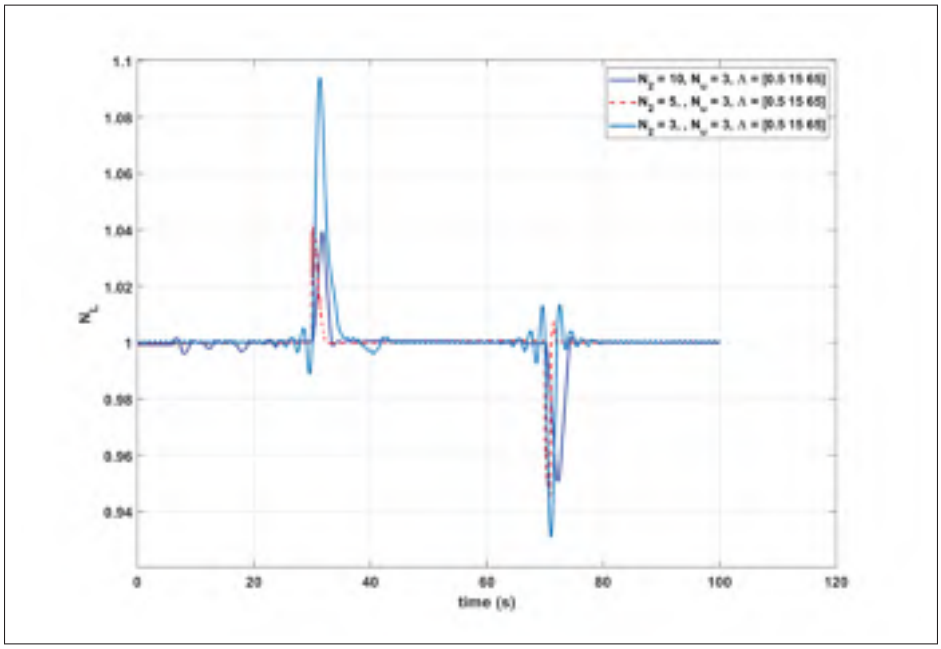

Figure 5.17 Effect of prediction horizon on N_L

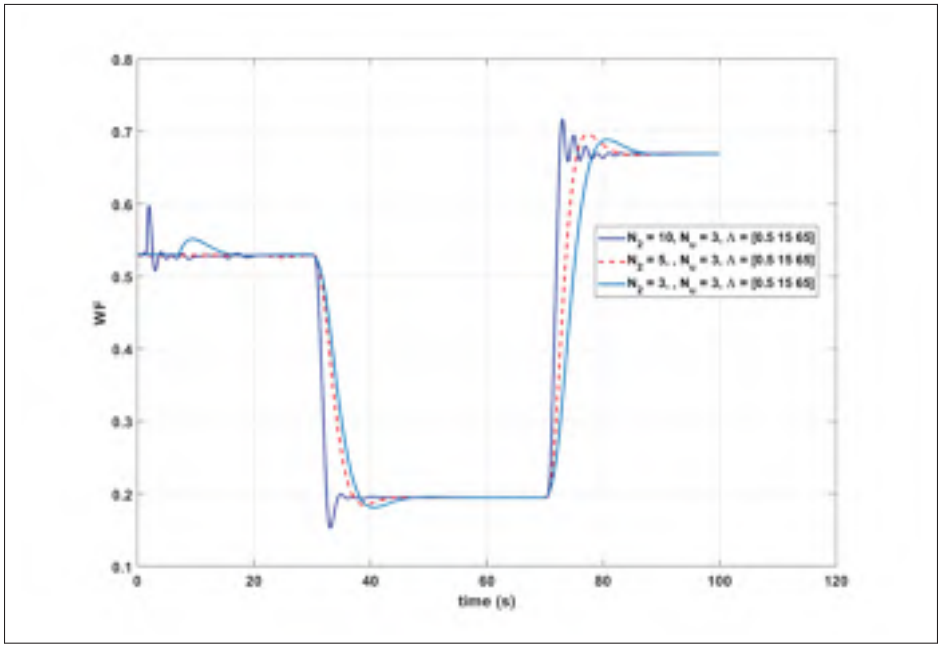

Figure 5.18 Effect of prediction horizon on WF

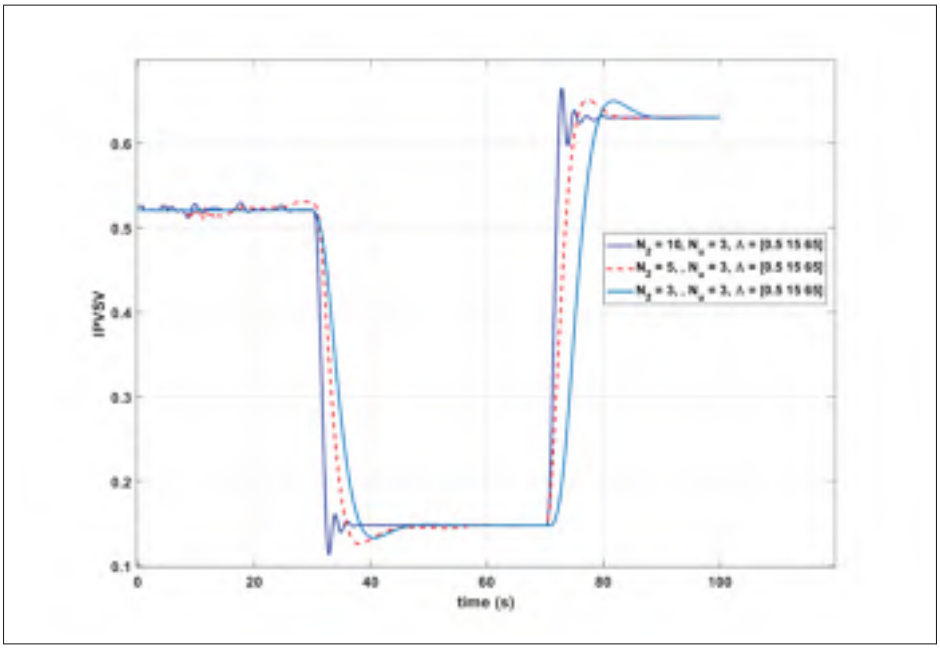

Figure 5.19 Effect of prediction horizon on *IPVSV*

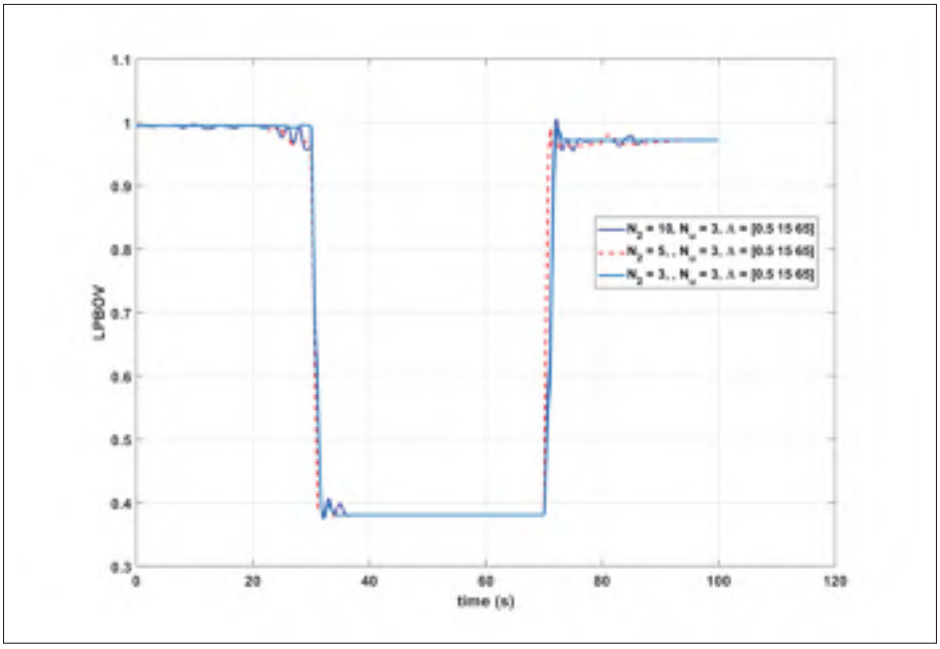

Figure 5.20 Effect of prediction horizon on *LPBOV*

5.5 Results

To demonstrate the performance of the NNGPC controller, we have simulated its response to a load rejection disturbance, i.e., a sudden load fall related to power failure due to a lightning strike or mechanical failure, and sudden load acceptance disturbance, i.e., a sudden increase in load demand. The operation conditions during this test are $T_{amb} = 15^{o}C$, $P_{amb} = 101.325\ kPa$, $LHV = 47826\ kJ/kg$, and $\eta_{th} = 0.4$. For this test, we will change the generator load and look at the corresponding changes in the input and output parameters. The generator load profile is indicated in Figure 5.21. This load change will be applied to the actual engine model.

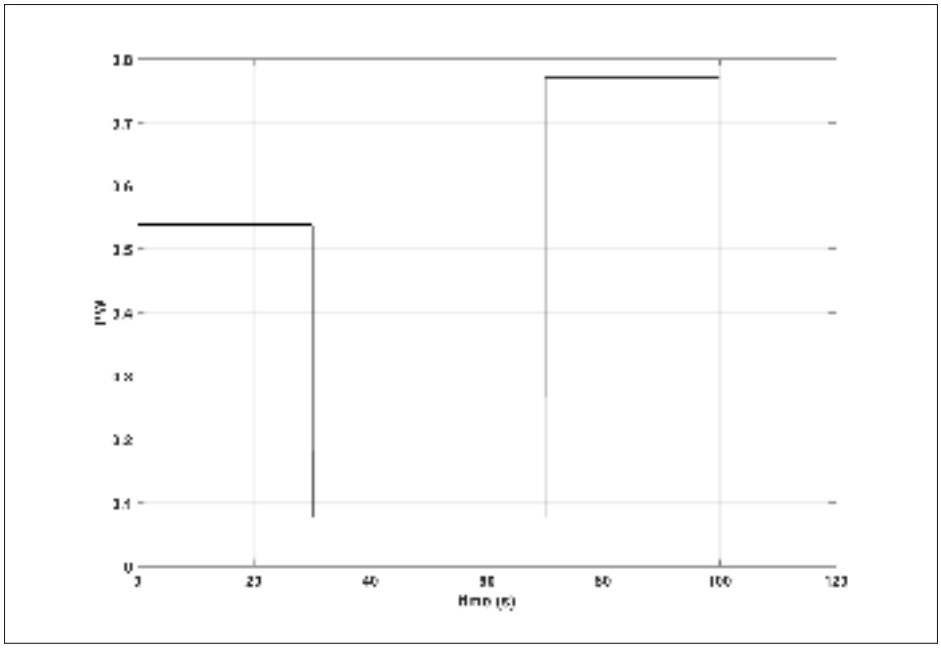

Figure 5.21 The generator load profile

The simulation results with the above operation conditions are presented in Figure 5.22 through Figure 5.31. As can be seen, the NNGPC controller realizes the control objectives. Figure 5.22 shows demand load and produced power changes. As the figure indicates, response overshoot during load accept is 4.2 % and the NNGPC controller could bring the response to the desired value in about 9.12 s settling time (the settling time is calculated when the response settles

within the 2 % settling time threshold). Indeed, the response undershoot during load reject is 2.1 % and the NNGPC controller could bring the response to the desired value in about 5.15 s settling time.

The low pressure turbine speed N_L changes is shown in Figure 5.23. As seen, the maximum overshoot and undershoot of the N_L is about 4.1 % during load reject disturbance and 5.45 % during load accept disturbance respectively. As the figure indicates, the NNGPC controller could bring the response to the set point value (3600 rpm) with deviation of $\pm 0.02\%$ in about 4.21 s. Figure 5.24 through Figure 5.28 show all output parameters variation during load change, which indicate that all constrained variables were maintained below the predetermined maximum limits even when a large disturbance was introduced to the system instantaneously.

On the other hand, the variations of controlling parameters are shown in Figure 5.29 through Figure 5.31. In Figure 5.29, the load dependent maximum and minimum fuel flow constraints are indicated. As can be seen, the NNGPC controller could keep WF within the predetermined constraints during engine acceleration and deceleration. In addition, Figure 5.30 and Figure 5.31 show the $IPVSV$ and $LPBOV$ variation respectively. The figures show both controlling parameters are within the predetermined minimum and maximum constraints.

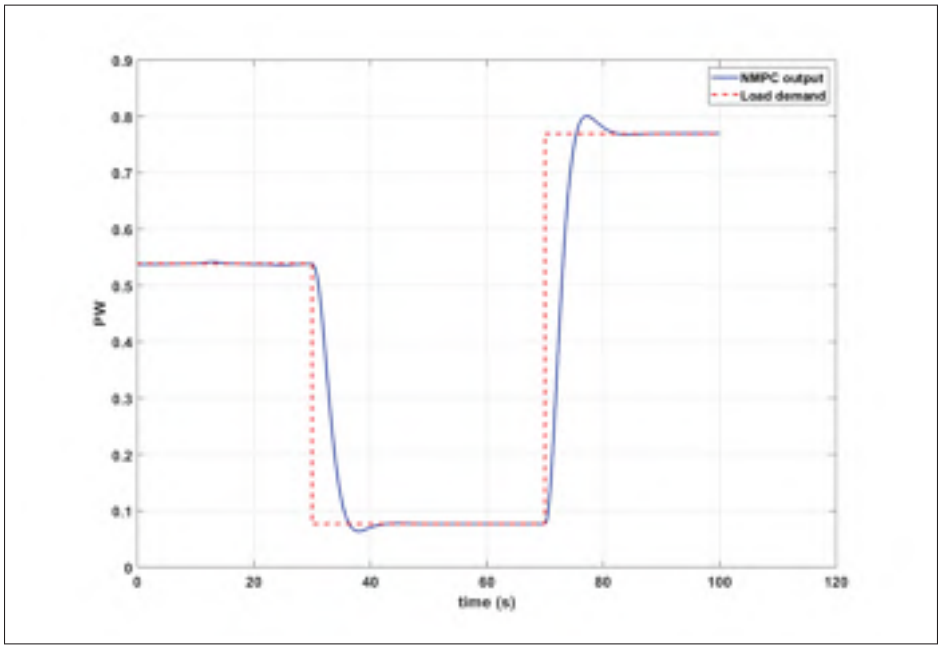

Figure 5.22 The *PW* response during load change

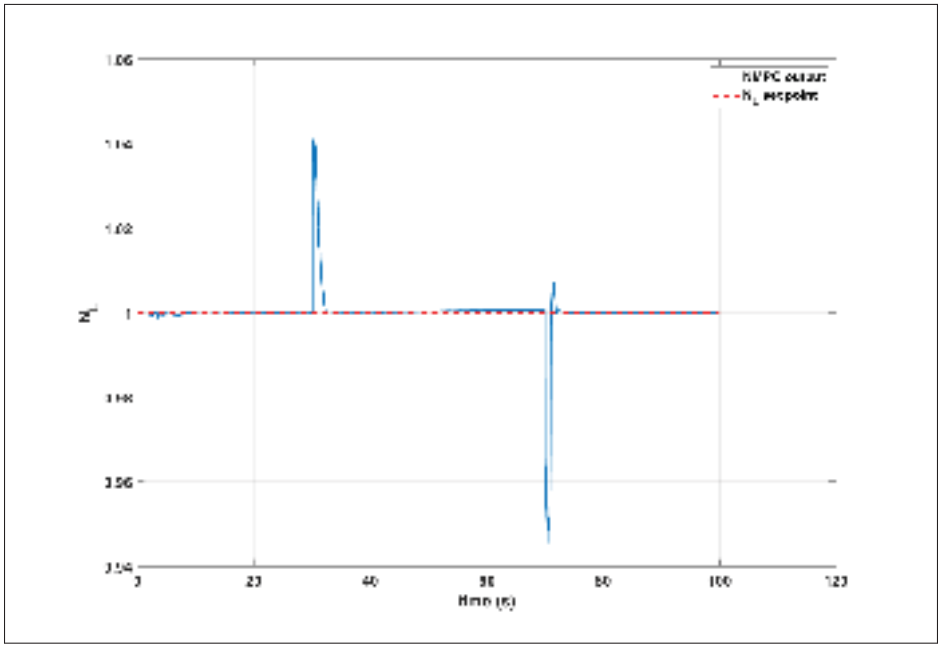

Figure 5.23 The N_L response during load change

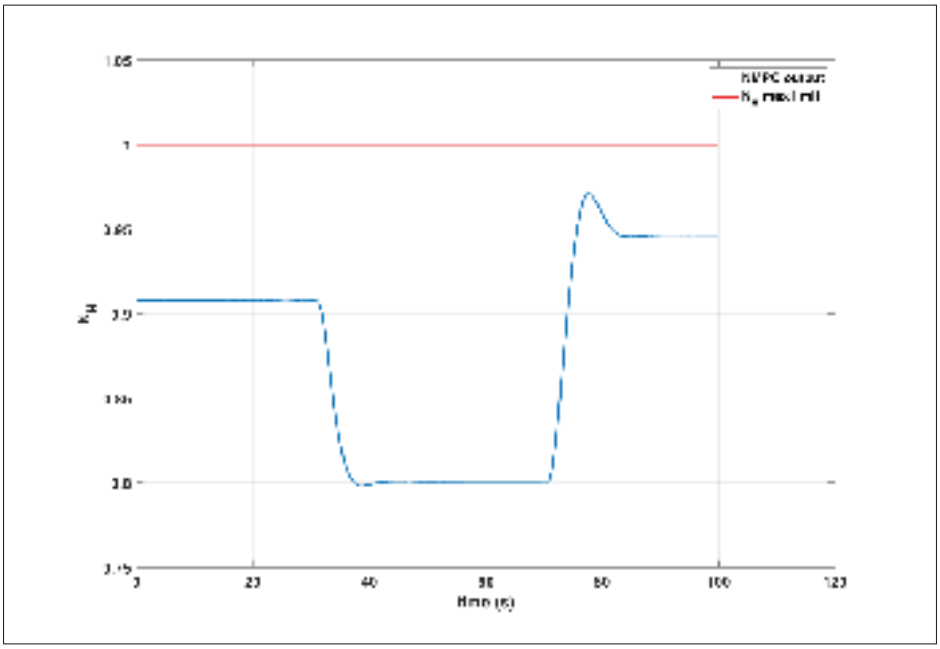

Figure 5.24 The N_H response during load change

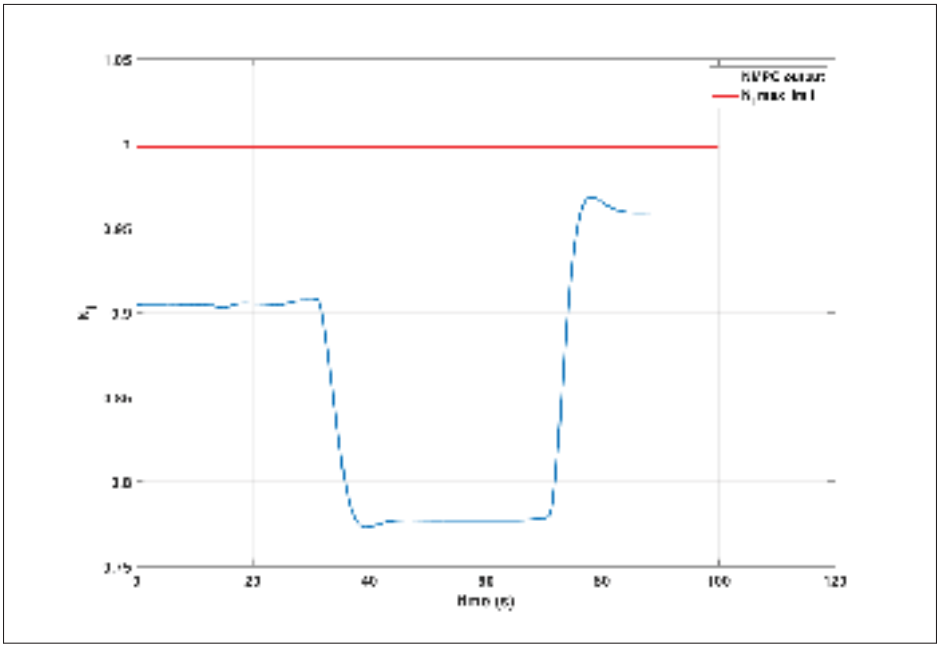

Figure 5.25 The N_I response during load change

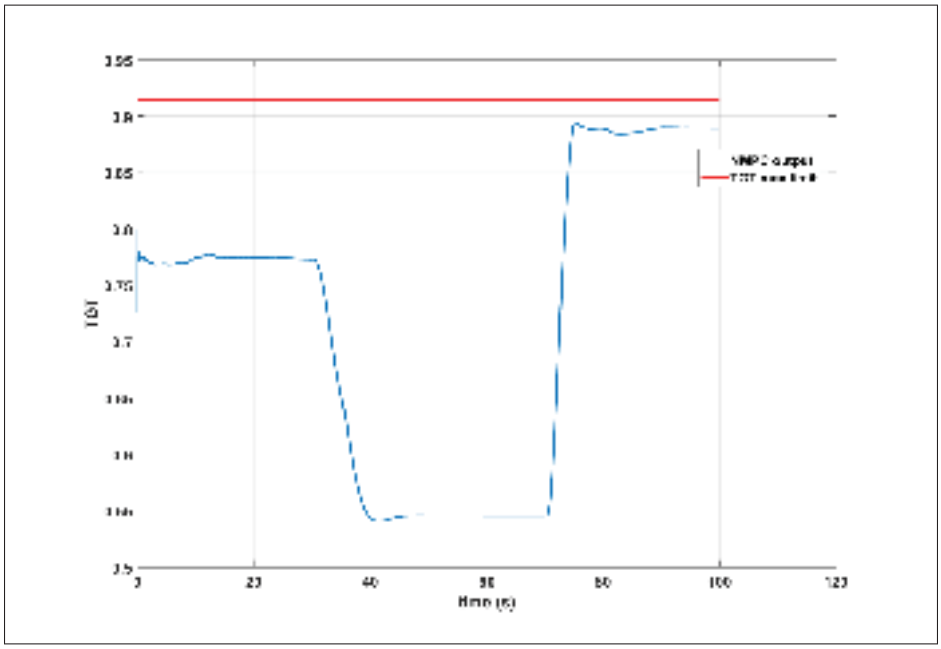

Figure 5.26 The TGT response during load change

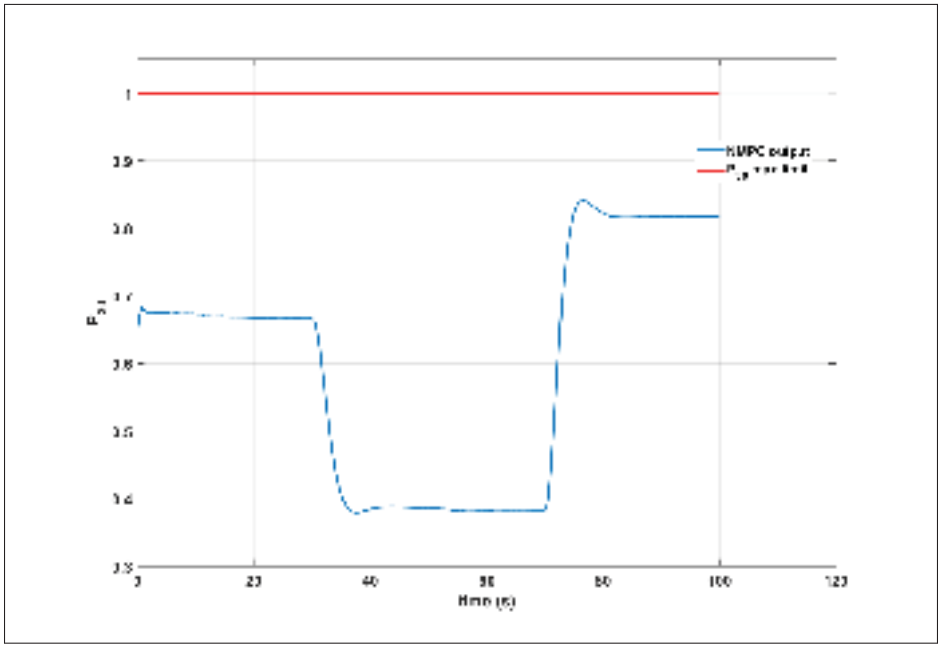

Figure 5.27 The P_{30} response during load change

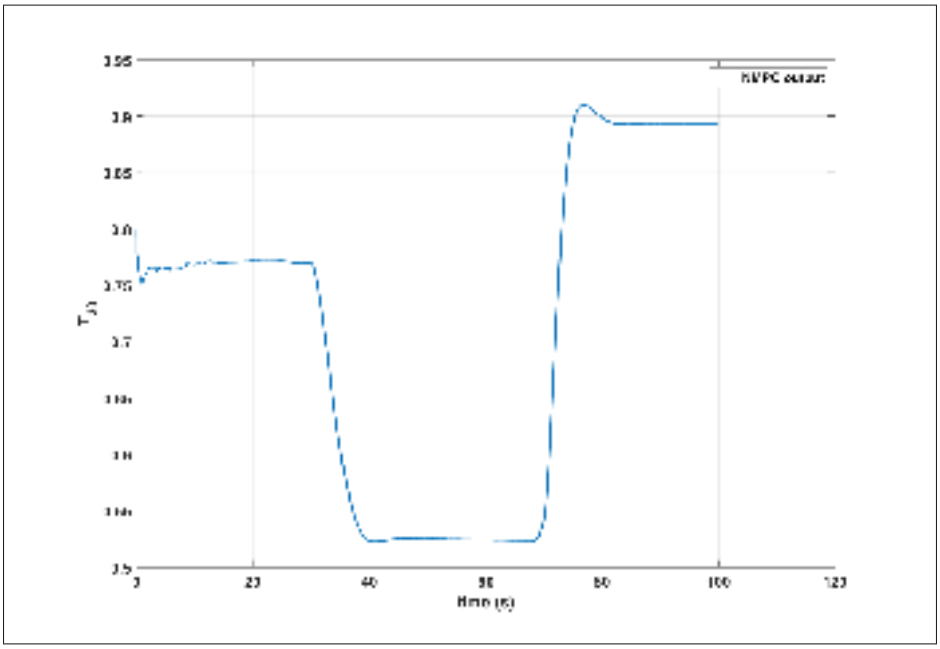

Figure 5.28 The T_{30} response during load change

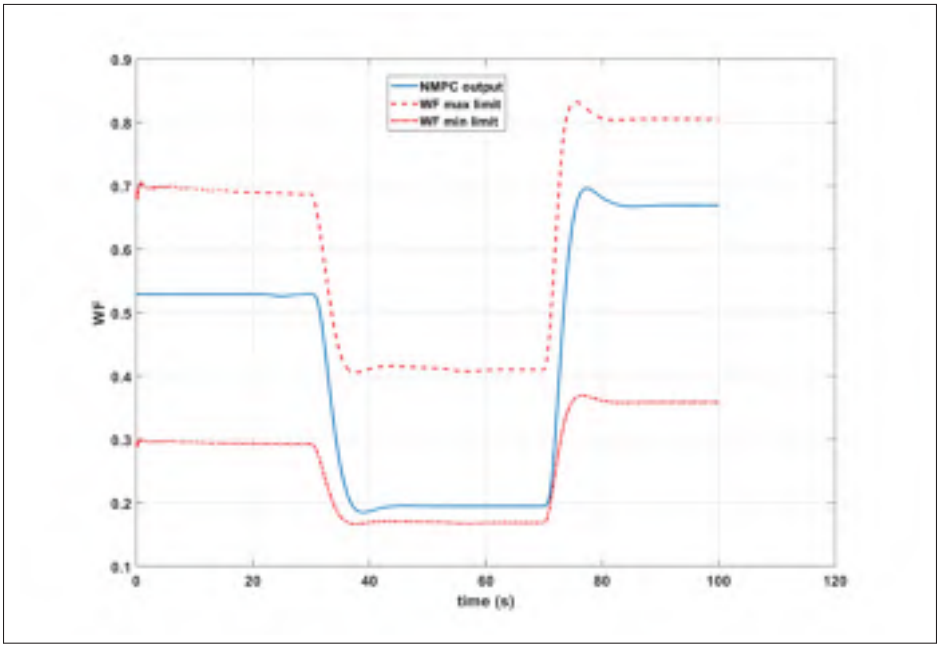

Figure 5.29 The WF response during load change

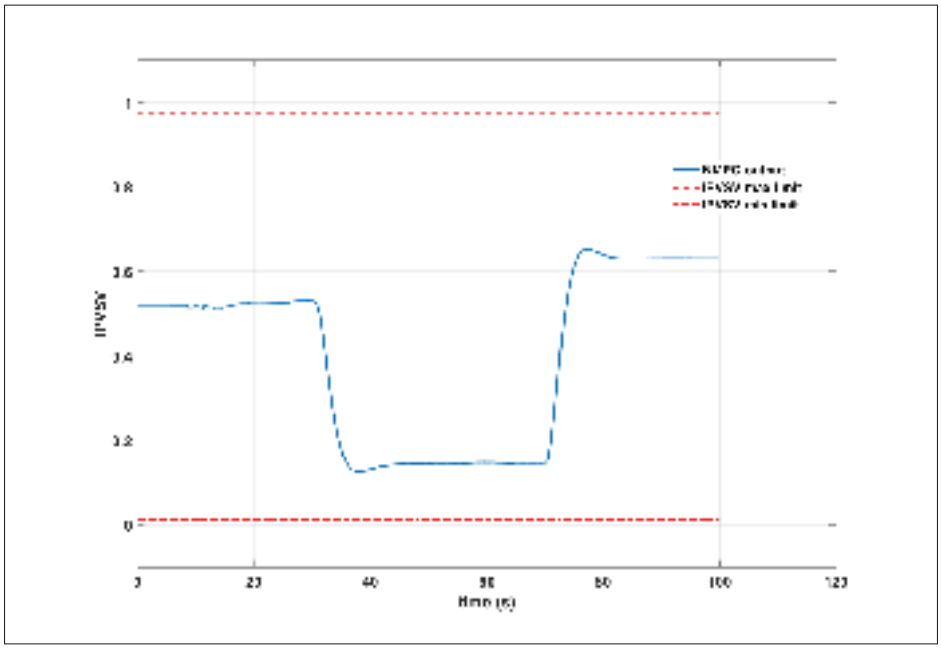

Figure 5.30 The *IPVSV* response during load change

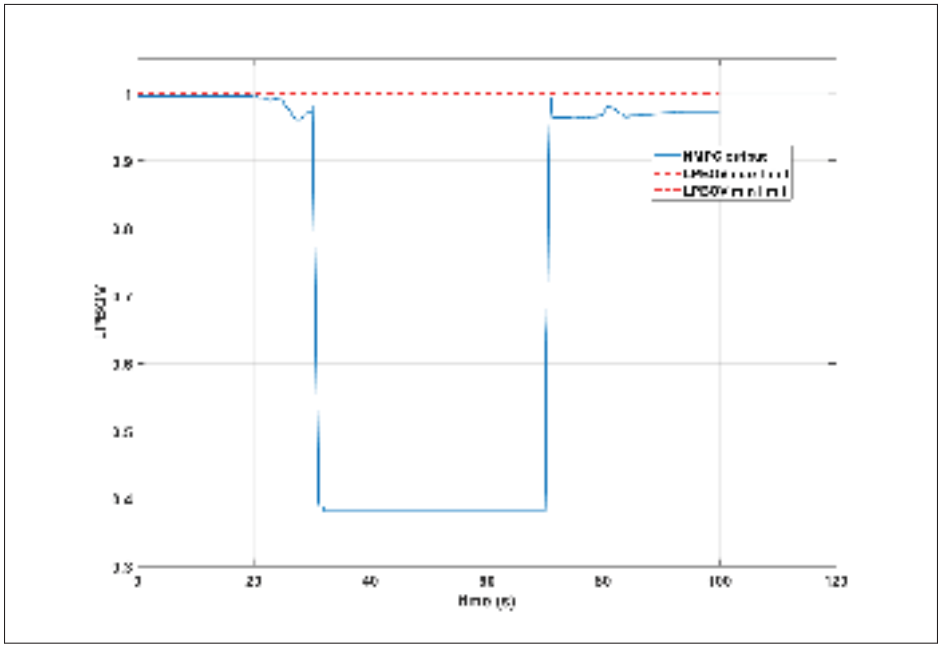

Figure 5.31 The *LPBOV* response during load change

To assess the performance of the NNGPC developed in this study, we have compared the response of the NNGPC controller to that of the existing min-max controller due to the same load disturbance. For this comparison, the experimental dataset $TS3_{exp}$ has been used. The simulation results of this test are presented in Figure 5.32 through Figure 5.41 with the summary of comparison results given in Table 5.4. As can be seen, The NNGPC has demonstrated output responses with less oscillatory behaviour and smoother control actions to the sudden variation in the electric load than those observed in the existing min-max controller. In addition, both controllers have the ability to maintain all constrained parameters below the predetermined maximum limits. However, the time constant of min-max controller response is lower than that of the NNGPC controller, which resulted in faster response by using min-max controller.

In Figure 5.33, the *NL* achieves 1.087 (overshoot is 8.7 %) with the NNGPC controller, which is within % 10 of its nominal value, in accordance with the load rejection test criterion. In addition, the NNGPC controller brought back *NL* to its set point value in the course of 4.2 s. However, the min-max controller could bring the response to the set point value in about 12.79 s with overshoot of 8.4 %.

Table 5.4 The controller performance comparison under load rejection test

Output parameter	**Controller**	**Settling time (s)**	**Overshoot (%)**	**Time constant (s)**
PW	NNGPC	3.22	2.6	1.16
	min-max	3.01	11.2	0.01
N_H	NNGPC	4.99	n/a	2.7
	min-max	3.1	6.17	0.19
N_I	NNGPC	3.76	1.2	2.68
	min-max	3.12	5.94	0.17
TGT	NNGPC	4.66	1.75	3.18
	min-max	9.24	n/a	1.62
P_{30}	NNGPC	1.5	2.97	0.31
	min-max	4.1	23.56	0.23
T_{30}	NNGPC	6.1	3.59	2.25
	min-max	12.91	n/a	3.1

As shown in Figure 5.39 through Figure 5.41, the control movements resulted from the NNGPC controller show smoother variations in WF, $IPVSV$, and $LPBOV$ parameters than those resulting from the min-max controller. As a consequence of that, the NNGPC controller requires less control effort than the min-max controller to achieve the desired objectives. The minimization of controller effort has significant practical repercussions because it reduces the intensity of mechanical wear of the actuators. Therefore, the minimization of control effort indicators has an impact on the increase of the functional safety, life time, and economics of the controlled process.

Moreover, Figure 5.39 shows that the fuel flow rate WF calculated by the min-max controller exceeds the minimum fuel limit during the load rejection test. This is because the bleed valves are opened very rapidly and hence all of a sudden much less air gets to the combustion chamber. So, if the fuel flow was not reduced quick enough, we will have a rich flameout. In addition, The minimum fuel flow limit violation by the min-max controller may occur as a result of the strong non-linearity of the engine, which can not always be handled adequately by the classical controller especially during the fast load change. In fact, this result coincides with the opinion found in recent studies, which have shown that there is no guarantee for min-max algorithm with linear compensator to protect engine limits during fast transient state (Imani & Montazeri-Gh, 2017; Montazeri-Gh & Rasti, 2019). However, the NNGPC controller could keep WF within the minimum and maximum fuel flow limits.

Finally, the computational efforts required for the NNGPC to execute the calculations of the controller during this test is 5.153 s, knowing that, the test simulation time is 35.5 s. Therefore, the computation time required to solve an optimization problem was sufficiently faster than the sampling rate (T_s = 0.01 s) by applying Hildreth's quadratic programming algorithm. This efficient algorithm would allow NNGPC to be implemented via real-time optimization for gas turbine power plants in a fast and robust manner.

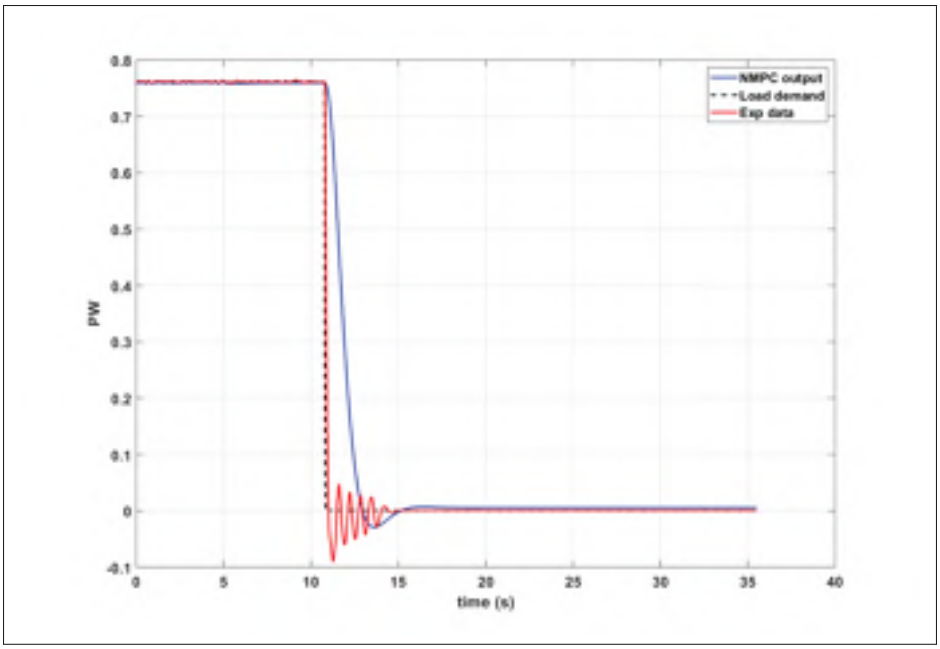

Figure 5.32 Comparison between NNGPC controller and min-max controller performance during load disturbance - *PW*

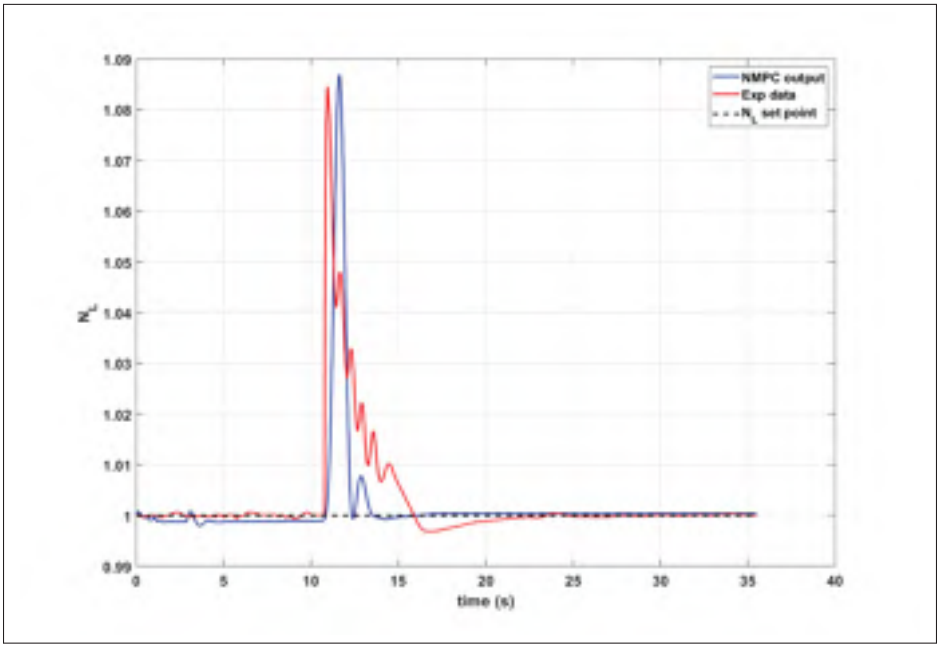

Figure 5.33 Comparison between NNGPC controller and min-max controller performance during load disturbance - N_L

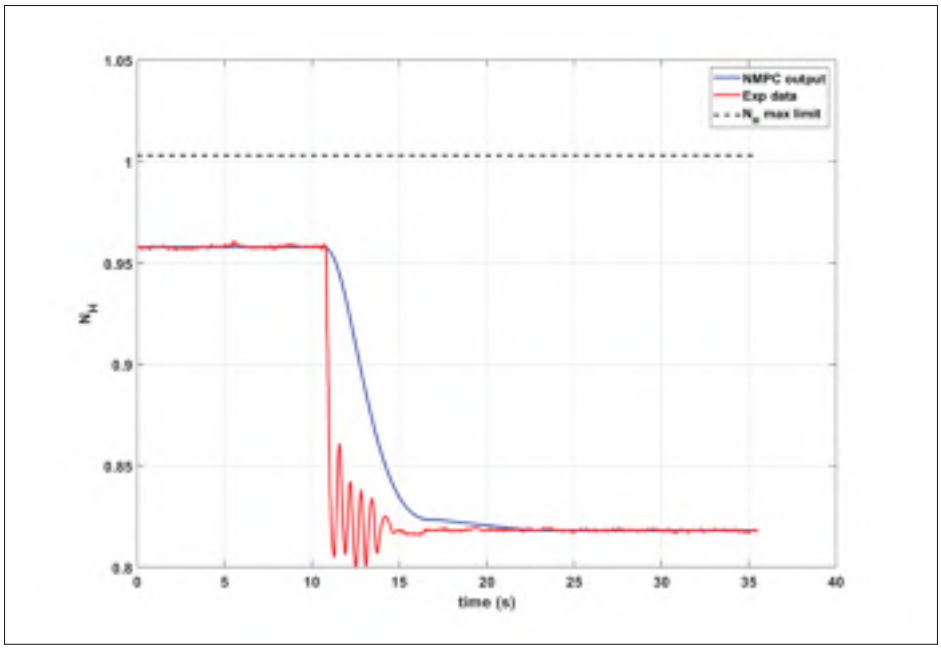

Figure 5.34 Comparison between NNGPC controller and min-max controller performance during load disturbance - N_H

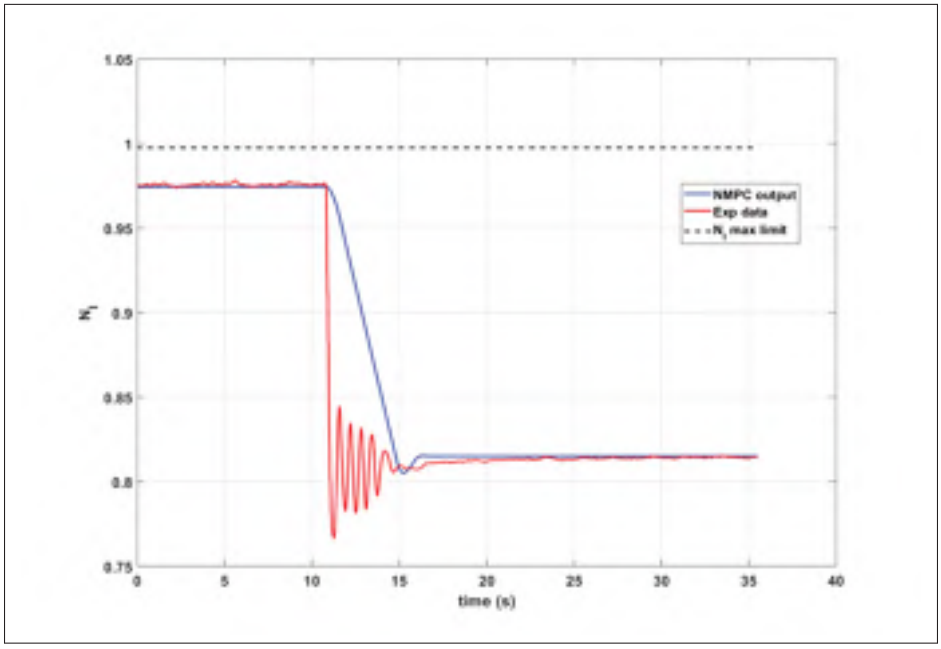

Figure 5.35 Comparison between NNGPC controller and min-max controller performance during load disturbance - N_I

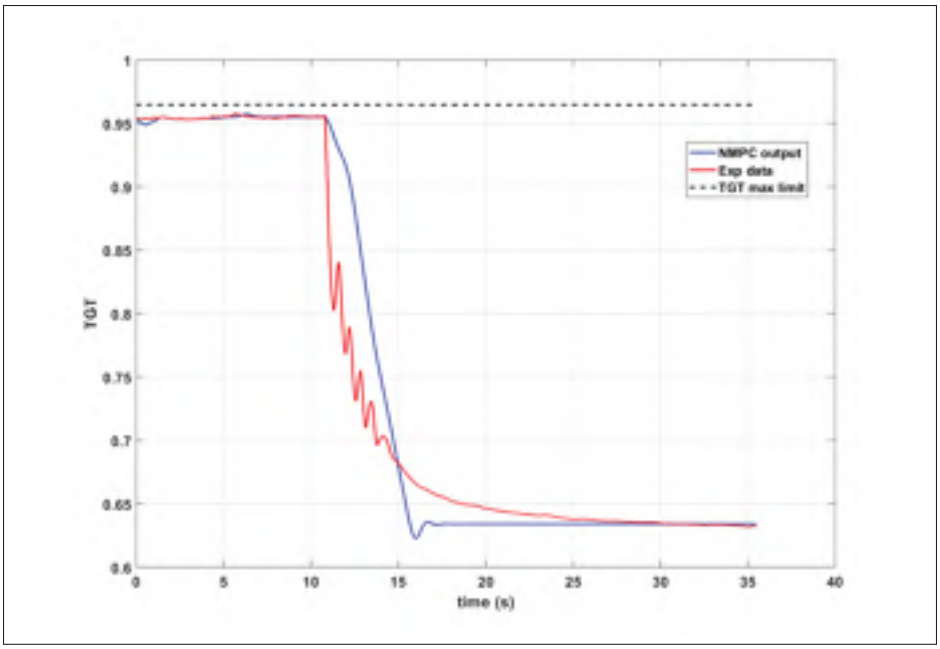

Figure 5.36 Comparison between NNGPC controller and min-max controller performance during load disturbance - TGT

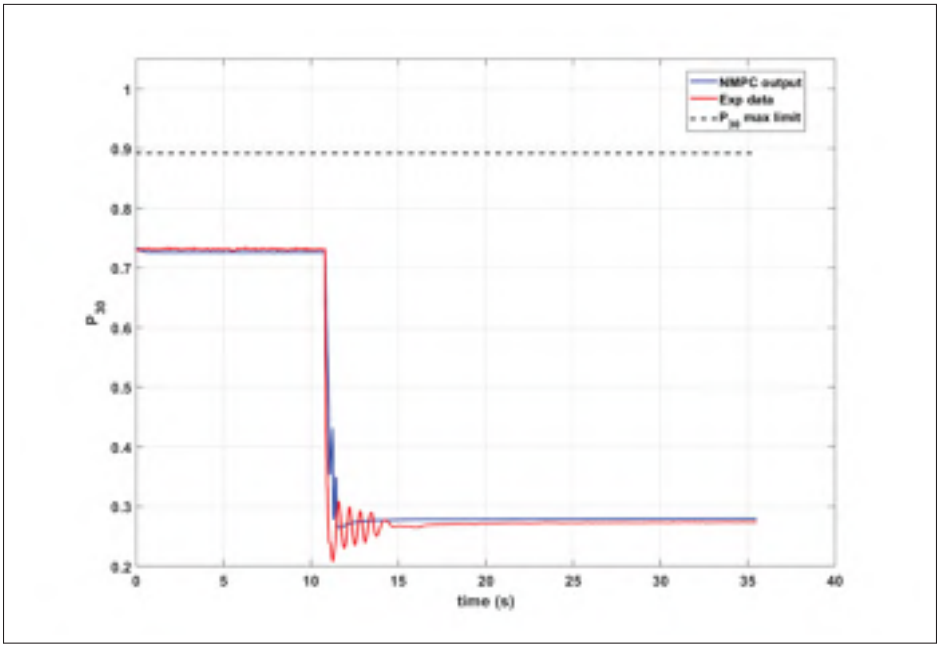

Figure 5.37 Comparison between NNGPC controller and min-max controller performance during load disturbance - P_{30}

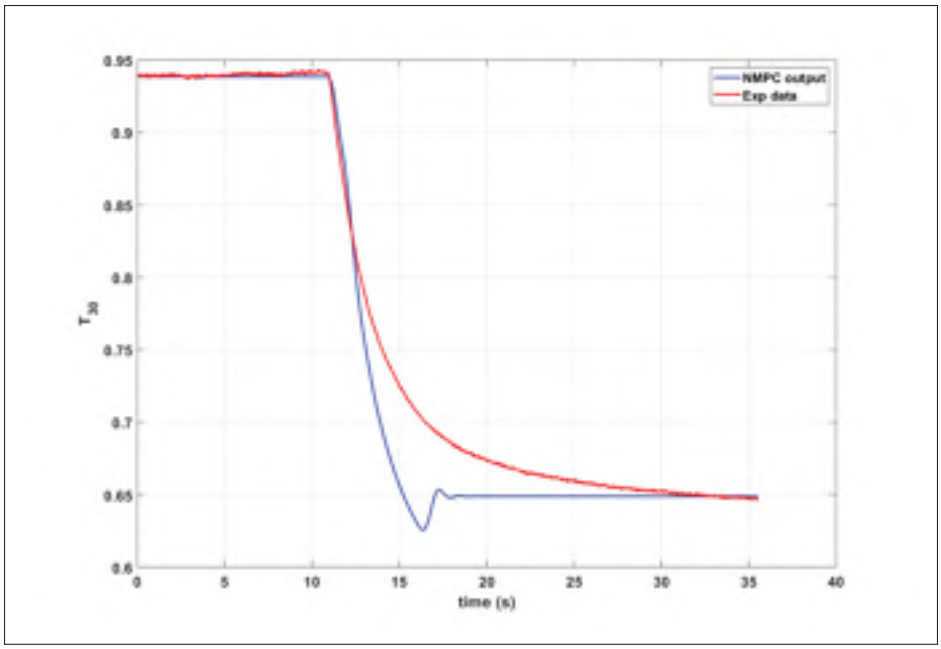

Figure 5.38 Comparison between NNGPC controller and min-max controller performance during load disturbance - T_{30}

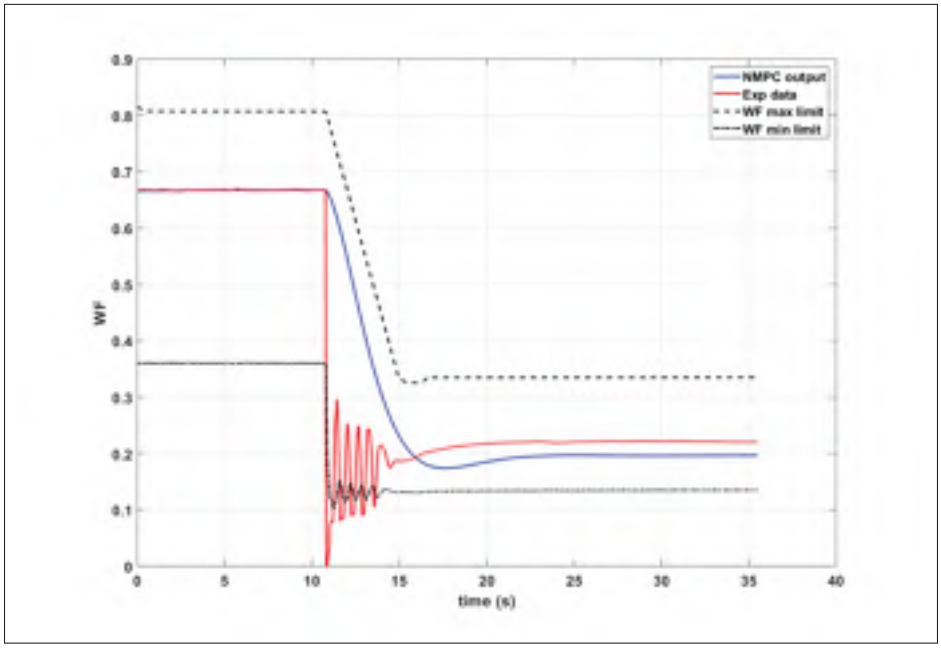

Figure 5.39 Comparison between NNGPC controller and min-max controller performance during load disturbance - WF

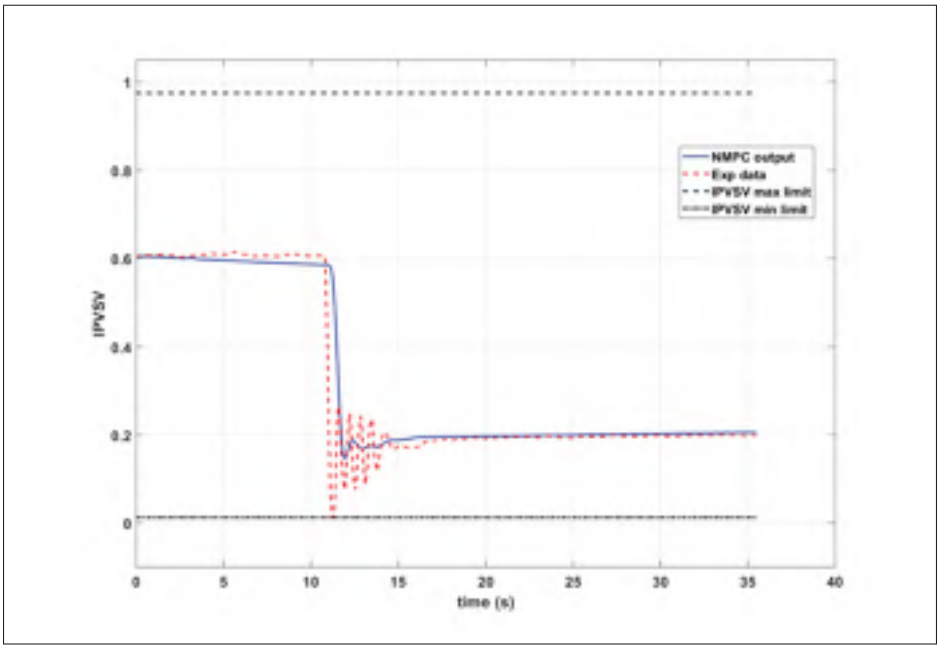

Figure 5.40 Comparison between NNGPC controller and min-max controller performance during load disturbance - *IPVSV*

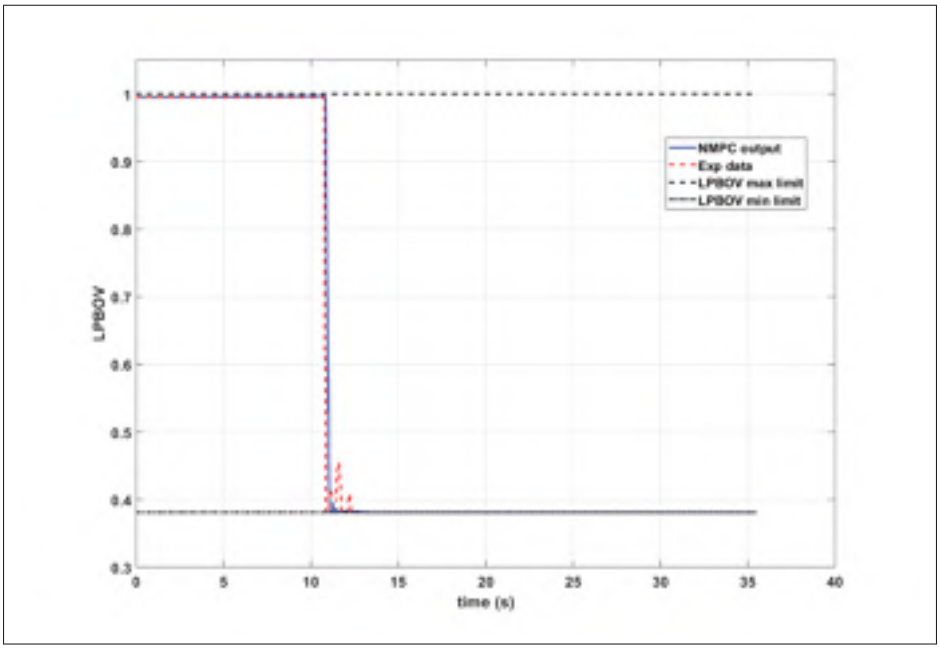

Figure 5.41 Comparison between NNGPC controller and min-max controller performance during load disturbance - *LPBOV*

5.6 Summary

The simulation results for the SGT-A65 engine controlled by the NNGPC controller was presented in this chapter. As can be seen, the simulation results show that although NNGPC can not produce faster response, in terms of time constant, than min-max controller, it resulted in less oscillatory behaviour and smoother control actions to the sudden variation in the electric load than those observed in the existing min-max controller. In addition, computation time required to solve an optimization problem was sufficiently faster than the sampling rate that allow a real time implementation of the NNGPC controller. Moreover, the use of controllers that take into account the non-linearities of the plant implies an improvement in the performance of the plant by reducing the impact of the disturbances and by improving the tracking capabilities of the control system.

In addition, a larger prediction horizon can make a faster response and better control quality. However, it will also greatly increase the calculation and affect real time performance of NNGPC controller. So that, as an indication of forthcoming research, it is intended to use an optimization approach to perform NMPC tuning and find the best tuning parameters based on the desired performance characteristics.

CONCLUSIONS AND RECOMMENDATIONS

6.1 Conclusions

This thesis focuses on solving important challenges in the area of gas turbine engine's controller design to ensure the safe operation of the engine and at the same time get the maximum performance. The system identification and advanced control algorithms based on NN methodology were developed to control an ADGTE used in power generation application under loading and unloading condition. The main results can be summarized as follows;

1. A novel methodology for the development of real time data driven based model of ADGTE was presented in Chapter 3 to address the first objective. An ensemble of multiple MISO-NARX neural models was introduced to predict the ADGTE output parameters in real time. Inspired by the way biological neural networks process information and by their structure which changes depending on their function, multiple-input single-output (MISO) NARX models with different configurations were used to represent each of the ADGTE output parameters with the same input parameters.

2. Estimation of the NN model order by generating different ARX models and estimation of the input/output delay, before generation of NN model, are very important steps. These steps save more iterations required to find the best structure of the NN and consequently saving more time required for NN model generation. In addition, data cleaning and resampling step significantly reduced training time. The lower sampling rate reduces the number of data points, which reduces the computation time during training operation and reduces data collinearity.

3. Usage of a single neural network to represent each of the system output parameters may not be able to provide an accurate prediction for unseen data and as a consequence, provides poor generalization. To overcome this problem, an ensemble of MISO NARX models was

used to represent each output parameter. The major challenge of the ensemble generation is to decide how to combine results produced by the ensemble's components. A novel hybrid dynamic weighting method (HDWM) was proposed to perform this task.

4. A comparison between the ensemble of MISO NARX models and the single MISO NARX models for all engine output parameters at different operation conditions showed that, the ensemble of MISO-NARX models can represent the ADGTE during the full operating range with a good accuracy even with different input scenarios from different operation conditions which prove the high generalization characteristic of the ensemble. Also, another important gain was the very low execution time (40.5 μs), which can support many real time applications like model based controller design, sensor fault verification and engine health monitoring. Moreover, one can observe that the ensemble model demonstrates a significantly better performance in identification of the gas turbine engine dynamics than the individual neural model, as it resulted in an improvement in accuracy of nearly 90%, compared with the single neural model.

5. With the desire to have more robustness and flexibility of the next generation of the GTE control systems to achieve ambitious targets and severe limitations set by governments and organizations, Chapter 4 outlined the NMPC controller design problem.

6. One of the key features of the NNGPC algorithm is the novel approach used to estimate the free and forced responses of the GPC algorithm based on NN model. It reduces the NMPC based optimization problem to a linear optimization problem at each sampling step. That will improve the computation time and reliability of the solution.

7. In addition, a significantly important part of the constrained NNGPC controller is the numerical optimization algorithm. The Hildreth's QP procedure was utilized which offers simplicity and reliability in real-time implementation (Wang, 2009). Furthermore, Hil-

dreth's method may be useful to implement on non-PC platforms like programmable logic controllers or embedded machine which do not support linear algebra libraries.

8. A comparison between the performance of NNGPC controller and the performance of the existing min-max controller was performed. The NNGPC has demonstrated superior output responses with less oscillatory behaviour and smoother control actions to the sudden variation in the electric load than those observed in the existing min-max controller. In addition, computation time required to solve an optimization problem was sufficiently faster than the sampling rate that allow a real time implementation of the NNGPC controller.

6.2 Recommendations

Some recommendations for further studies are outlined below:

1. As the only available experimental data from the real engine testing was collected at a specific operation conditions, future work will involve looking at the NNGPC controller performance over a different operation conditions and different transient scenarios and determining what modifications are required to obtain acceptable robust performance. Once the control algorithm is proven, we will focus on implementing the controllers we showcased here on Programmable Logic Controller (PLC) with the aim of eventually being able to test it in a real life test bed environment. This process will involve converting the NNGPC algorithm to structured text for implementation on a PLC.

2. In this thesis we studied the homogeneous ensemble models, where source of diversity was the variation in the training data. An alternative would be studying heterogeneous ensemble in which ensemble members have different architectures such as number of neurons, number of layers, and training algorithm.

3. In this thesis, off-line learning techniques are applied for identifying the GTE dynamics. A potential future work is to study the on-line ensemble learning to identify the GTE dynamics while the engine is operating.

4. In this thesis, the max number of iterations in the Hildreth's QP procedure was fixed to 100 iterations. In addition, we used the Lagrange multipliers values to identify the active and inactive constrains. An investigation would be needed to study the effect of iteration number and the significance of the Lagrange multipliers values obtained in the proposed approach on the convergence speed and solution stability.

5. In this thesis the tuning of the NNGPC controller was performed by using the trial and error method. However, there is still a need for a more systematic approach to perform MPC tuning and find the best tuning parameters based on the desired performance characteristics. MPC tuning is usually performed ad-hoc based on some experience. Most of the time, several simulation runs are performed to check if the chosen tuning parameters are suitable. Automated tuning procedures using genetic algorithm can be applied to reduce the manual operations.

LIST OF PUBLICATION

The contributions of this work have been presented in two journals and three conference publications. The complete list of publications associated with this research work is presented below.

Journals

1. Ibrahem, I. A., Akhrif., O., Moustapha., H. & Staniszewski., M. (2020b). An ensemble of recurrent neural networks for real time performance modelling of three-spool aero-derivative gas turbine engine, Submitted for publication in the ASME Journal of Engineering for Gas Turbines and Power; July 2020. (**Accepted**)

   This paper is summarized in Chapter 3. It presents a novel methodology for the development of data driven based model of ADGTE.

2. Ibrahem, I. A., Akhrif., O., Moustapha., H. & Staniszewski., M. Nonlinear Generalized Predictive Controller Based on Ensemble of NARX Models for Industrial Gas Turbine Engine, Submitted for publication in the Elsevier Journal of Energy; July 2020. (**Under review**)

   This paper is summarized in Chapters 4 and 5. It presents a novel approach used in the development of a constrained MIMO NMPC for an ADGTE used for power generation.

   Conferences

   Published:

3. Ibrahem, I. A., Akhrif., O., Moustapha., H. & Staniszewski., M. (2019). Neural Networks Modelling of Aero-derivative Gas Turbine Engine: A Comparison Study.

Proceedings of the 16th International Conference on Informatics in Control, Automation and Robotics - Volume 1: ICINCO,, pp. 738-745.

This paper is summarized in Chapter 2. It represents a preliminary investigation based on a literature survey of a data-driven based modelling approach, which is needed to select the best type of neural network to represent the ADGTE during the full operating range.

4. Ibrahem, I. A., Akhrif., O., Moustapha., H. & Staniszewski., M. (2020c). An ensemble of recurrent neural networks for real time performance modelling of three-spool aero-derivative gas turbine engine. *ASME Turbo Expo 2020: Power for Land, Sea, and Air*.

   This paper is summarized in Chapter 3. Based on the recommendation from the third paper, a single MISO NARX neural model was introduced to predict the ADGTE output parameters in real time. However, the single MISO NARX neural model may not be able to provide accurate prediction when it operates outside the field in which it was trained.

5. Ibrahem, I. A., Akhrif., O., Moustapha., H. & Staniszewski., M. (2020a). Real-time modelling and Hardware in the loop simulation of an aero-derivative gas turbine engine. *Proceedings of Global Power and Propulsion Society*.

   This paper is summarized in Chapter 3. Based on the recommendation from the forth paper, an ensemble of multiple MISO NARX neural models was introduced to predict the ADGTE output parameters in real time.

BIBLIOGRAPHY

Administration, F. A. (2011). *Airplane Flying Handbook (FAA-H-8083-3A)*. Skyhorse Publishing Inc.

Alves, V. A. O., de Godoy, R. J. C. & Garcia, C. (2013). Optimal time delay estimation for System Identification. *2013 American Control Conference*, pp. 95–100.

Aly, A. & Atia, I. (2012). Neural Modeling and Predictive Control of a Small Turbojet Engine (SR-30). *10th International Energy Conversion Engineering Conference*, pp. 4242.

Amozegar, M. & Khorasani, K. (2016). An ensemble of dynamic neural network identifiers for fault detection and isolation of gas turbine engines. *Neural Networks*, 76, 106–121.

Asgari, H. (2014). Modelling, Simulation and control of gas turbines using artificial neural networks.

Asgari, H. & Chen, X. (2015). *Gas turbines modeling, simulation, and control: using artificial neural networks*. CRC Press.

Asgari, H., Chen, X. & Sainudiin, R. (2013). Modelling and simulation of gas turbines. *International Journal of Modelling, Identification and Control*, 20(3), 253–270.

Asgari, H., Venturini, M., Chen, X. & Sainudiin, R. (2014). Modeling and simulation of the transient behavior of an industrial power plant gas turbine. *Journal of Engineering for Gas Turbines and Power*, 136(6), 061601.

Bahlawan, H., Morini, M., Pinelli, M., Spina, P. R. & Venturini, M. (2017). Development of Reliable NARX Models of Gas Turbine Cold, Warm and Hot Start-Up. *ASME Turbo Expo 2017: Turbomachinery Technical Conference and Exposition*.

Ballin, M. G. (1988). A high fidelity real-time simulation of a small turboshaft engine.

Beale, M. H., Hagan, M. T. & Demuth, H. B. (2015). Neural Network Toolbox™ User's Guide.

Behera, S., Choubey, A., Kanani, C. S., Patel, Y. S., Misra, R. & Sillitti, A. (2019). Ensemble trees learning based improved predictive maintenance using IIoT for turbofan engines. *Proceedings of the 34th ACM/SIGAPP Symposium on Applied Computing*, pp. 842–850.

Bettocchi, R., Pinelli, M., Spina, P., Venturini, M. & Burgio, M. (2004). Set up of a robust neural network for gas turbine simulation. *ASME Turbo Expo 2004: Power for Land, Sea, and Air*, pp. 543–551.

Bettocchi, R., Spina, P. R. & Fabbri, F. (1996). Dynamic modeling of single-shaft industrial gas turbine. *ASME 1996 International Gas Turbine and Aeroengine Congress and Exhibition*.

Brown, G., Wyatt, J., Harris, R. & Yao, X. (2005). Diversity creation methods: a survey and categorisation. *Information Fusion*, 6(1), 5–20.

Brunell, B. J., Bitmead, R. R. & Connolly, A. J. (2002). Nonlinear model predictive control of an aircraft gas turbine engine. *Proceedings of the 41st IEEE Conference on Decision and Control, 2002.*, 4, 4649–4651.

Camacho, E. F. & Alba, C. B. (2013). *Model predictive control*. Springer Science & Business Media.

Camporeale, S., Fortunato, B. & Mastrovito, M. (2006). A modular code for real time dynamic simulation of gas turbines in simulink.

CASTRO, E. (2018). Diagram Of How the Brain Works Elegant Gemütlich Diagram Brain Parts and Functions Bilder Menschliche. Consulted at http://www.dreamdiving-resort.com/diagram-of-how-the-brain-works.

Chen, Q., Huang, J., Pan, M. & Lu, F. (2019). A Novel Real-Time Mechanism Modeling Approach for Turbofan Engine. *Energies*, 12(19), 3791.

Chipperfield, A. & Fleming, P. (1996). Multiobjective gas turbine engine controller design using genetic algorithms. *IEEE Transactions on Industrial Electronics*, 43(5), 583–587.

Clarke, D. W., Mohtadi, C. & Tuffs, P. (1987a). Generalized predictive control—Part I. The basic algorithm. *Automatica*, 23(2), 137–148.

Clarke, D. W., Mohtadi, C. & Tuffs, P. (1987b). Generalized predictive control—part II extensions and interpretations. *Automatica*, 23(2), 149–160.

Clarke, D. & Mohtadi, C. (1987). Properties of generalized predictive control. *IFAC Proceedings Volumes*, 20(5), 65–76.

Crainic, C., Harvey, R. & Thompson, A. (1997). Real Time Thermodynamic Transient Model for Three Spool Turboprop Engine. *ASME 1997 International Gas Turbine and Aeroengine Congress and Exhibition*.

Cybenko, G. (1989). Approximation by superpositions of a sigmoidal function. *Mathematics of control, signals and systems*, 2(4), 303–314.

de Sousa, J. F., Moreira, J. M., Soares, C. M. & Jorge, A. (2012). Ensemble approaches for regression: A survey.

Diehl, M., Ferreau, H. J. & Haverbeke, N. (2009). Efficient numerical methods for nonlinear MPC and moving horizon estimation. In *Nonlinear model predictive control* (pp. 391–417). Springer.

Duyar, A., Gu, Z. & Litt, J. S. (1995). A simplified dynamic model of the T700 turboshaft engine. *Journal of the American Helicopter Society*, 40(4), 62–70.

Effiom, S. O., Abam, F. I. & Nwankwojike, B. N. (2017). Performance evaluation of aeroderivative gas turbine models derived from a high bypass turbofan for industrial power generation. *Cogent Engineering*, 4(1), 1301235.

Esfahani, M. A. & Montazeri, M. (2016). Designing and Optimizing Multi-Objective Turbofan Engine Control Algorithm Using Min-Max Method. *International Journal of Computer Science and Information Security*, 14(8), 1040.

Fawke, A. & Saravanamuttoo, H. (1971). Digital computer methods for prediction of gas turbine dynamic response. *SAE Transactions*, 1805–1813.

Fletcher, A. H. (1963). The Avon aircraft engine and its industrial power applications. *Proceedings of the Institution of Mechanical Engineers*, 177(1), 1068–1074.

Forhad, M. M. I. & Bloomberg, M. (2015). Drive Train Over-Speed Prediction for Gas Fuel Based Gas Turbine Power Generation Units. *Turbo Expo: Power for Land, Sea, and Air*, 56758, V006T05A024.

Fuksman, I. & Sirica, S. (2012). Real-time execution of a high fidelity aero-thermodynamic turbofan engine simulation. *Journal of engineering for gas turbines and power*, 134(5).

Gaudet, S. R. (2008). *Development of a dynamic modeling and control system design methodology for gas turbines*. (Ph.D. thesis, Carleton University).

Gazzetta Junior, H., Bringhenti, C., Barbosa, J. R. & Tomita, J. T. (2017). Real-time gas turbine model for performance simulations. *Journal of Aerospace Technology and Management*, 9(3), 346–356.

Ghorbani, H., Ghaffari, A. & Rahnama, M. (2008a). Constrained model predictive control implementation for a heavy-duty gas turbine power plant. *WSEAS Transactions on Systems and Control*, 3(6), 507–516.

Ghorbani, H., Ghaffari, A. & Rahnama, M. (2008b). Multivariable model predictive control for a gas turbine power plant. *Proceedings of the 10th WSEAS International Conference on Automatic Control, Modelling & Simulation*, pp. 275–281.

Gill, P. E., Murray, W. & Wright, M. H. (2019). *Practical optimization*. SIAM.

Gu, C.-w., Wang, H., Ji, X.-x. & Li, X.-s. (2016). Development and application of a thermodynamic-cycle performance analysis method of a three-shaft gas turbine. *Energy*, 112, 307–321.

Gülen, S. C. (2019). *Gas Turbines for Electric Power Generation*. Cambridge University Press.

Haaser, F. & Casper, R. (1991). Development of the LM 6000: the World's Most Efficient Simple Cycle Industrial Gas Turbine. *Pmc. ASME COGEN 1991*, 177–188.

H.I.H. Saravanamuttoo,G.F.C. Rogers, P. S. H. C. A. (2017). *Gas Turbine Theory* (ed. 7). Pearson. Consulted at http://gen.lib.rus.ec/book/index.php?md5=e522f34d4e94f04313d3074c1e7ef784.

Horlock, J. (1997). Aero-engine derivative gas turbines for power generation: thermodynamic and economic perspectives. *Journal of engineering for gas turbines and power*, 119(1).

Ibrahem, I. A., Akhrif., O., Moustapha., H. & Staniszewski., M. Nonlinear Generalized Predictive Controller Based on Ensemble of NARX Models for Industrial Gas Turbine Engine.

Ibrahem, I. A., Akhrif., O., Moustapha., H. & Staniszewski., M. (2019). Neural Networks Modelling of Aero-derivative Gas Turbine Engine: A Comparison Study. *Proceedings of the 16th International Conference on Informatics in Control, Automation and Robotics - Volume 1: ICINCO,*, pp. 738-745.

Ibrahem, I. A., Akhrif., O., Moustapha., H. & Staniszewski., M. (2020a). Real-time modelling and Hardware in the loop simulation of an aero-derivative gas turbine engine. *Proceedings of Global Power and Propulsion Society*.

Ibrahem, I. A., Akhrif., O., Moustapha., H. & Staniszewski., M. (2020b). An ensemble of recurrent neural networks for real time performance modelling of three-spool aero-derivative gas turbine engine.

Ibrahem, I. A., Akhrif., O., Moustapha., H. & Staniszewski., M. (2020c). An ensemble of recurrent neural networks for real time performance modelling of three-spool aero-derivative gas turbine engine. *ASME Turbo Expo 2020: Power for Land, Sea, and Air*.

Imani, A. & Montazeri-Gh, M. (2017). Improvement of Min–Max limit protection in aircraft engine control: An LMI approach. *Aerospace Science and Technology*, 68, 214–222.

Jafari, S. & Nikolaidis, T. (2018). Turbojet Engine Industrial Min–Max Controller Performance Improvement Using Fuzzy Norms. *Electronics*, 7(11), 314.

Jaw, L. & Mattingly, J. (2009). Aircraft Engine Controls. American Institute of Aeronautics and Astronautics, Inc.

Khalili, R. & Karrari, M. (2017). Modeling and identification of an industrial gas turbine using classical and non-classical approaches. *Electrical Engineering (ICEE), 2017 Iranian Conference on*, pp. 667–672.

Khan, K. (2018). Surprising Discovery of Genetic Mosaic in Brain. Consulted at http://aboutislam.net/science/health/surprising-discovery-genetic-mosaic-brain/.

Kim, J., Song, T., Kim, T. & Ro, S. (2001). Model development and simulation of transient behavior of heavy duty gas turbines. *J. Eng. Gas Turbines Power*, 123(3), 589–594.

Kim, J. S., Powell, K. M. & Edgar, T. F. (2013). Nonlinear model predictive control for a heavy-duty gas turbine power plant. *2013 American control conference*, pp. 2952–2957.

Kong, C., Ki, J. & Koh, K. (1999). Steady-State and Transient Performance Simulation of a Turboshaft Engine with Free Power Turbine. *ASME 1999 International Gas Turbine and Aeroengine Congress and Exhibition*.

Krummrein, T., Henke, M. & Kutne, P. (2018). A highly flexible approach on the steady-state analysis of innovative micro gas turbine cycles. *Journal of Engineering for Gas Turbines and Power*, 140(12).

Kyprianidis, K. & Kalfas, A. I. (2008). Dynamic performance investigations of a turbojet engine using a cross-application visual oriented platform. *The Aeronautical Journal*, 112(1129), 161–169.

Lazar, M. & Pastravanu, O. (2002). A neural predictive controller for non-linear systems. *Mathematics and Computers in Simulation*, 60(3-5), 315–324.

Li, Z., Goebel, K. & Wu, D. (2019). Degradation modeling and remaining useful life prediction of aircraft engines using ensemble learning. *Journal of Engineering for Gas Turbines and Power*, 141(4), 041008.

Lietzau, K. & Kreiner, A. (2001). Model based control concepts for jet engines. *ASME Turbo Expo 2001: Power for Land, Sea, and Air*.

Lin, S.-T., Lu, J.-H., Hong, M.-C. & Hsu, K.-W. (1999). Real-Time Dynamic Simulation of Single Spool Turboj et Engines. *Simulation*, 73(6), 352–361.

Lu, F., Wu, J., Huang, J. & Qiu, X. (2019). Aircraft engine degradation prognostics based on logistic regression and novel OS-ELM algorithm. *Aerospace Science and Technology*, 84, 661–671.

Luenberger, D. G. & Ye, Y. (2016). Basic properties of linear programs. In *Linear and Nonlinear Programming* (pp. 11–31). Springer.

MacIsaac, B. & Langton, R. (2011). *Gas turbine propulsion systems*. John Wiley & Sons.

Mehrpanahi, A., Hamidavi, A. & Ghorbanifar, A. (2018). A novel dynamic modeling of an industrial gas turbine using condition monitoring data. *Applied Thermal Engineering*, 143, 507–520.

Merz, C. J. & Pazzani, M. J. (1999). A principal components approach to combining regression estimates. *Machine learning*, 36(1-2), 9–32.

Mohamed, O., Wang, J., Khalil, A. & Limhabrash, M. (2016). Predictive control strategy of a gas turbine for improvement of combined cycle power plant dynamic performance and efficiency. *SpringerPlus*, 5(1), 980.

Montazeri-Gh, M. & Abyaneh, S. (2017). Real-time simulation of a turbo-shaft engine's electronic control unit. *Mechanics & Industry*, 18(5), 503.

Montazeri-Gh, M. & Jafari, S. (2011). Evolutionary optimization for gain tuning of jet engine min-max fuel controller. *Journal of Propulsion and Power*, 27(5), 1015–1023.

Montazeri-Gh, M. & Rasti, A. (2019). Comparison of model predictive controller and optimized min-max algorithm for turbofan engine fuel control. *Journal of Mechanical Science and Technology*, 33(11), 5483–5498.

Montazeri-Gh, M., Abyaneh, S. & Kazemnejad, S. (2016). Hardware-in-the-loop simulation of two-shaft gas turbine engine's electronic control unit. *Proceedings of the Institution of Mechanical Engineers, Part I: Journal of Systems and Control Engineering*, 230(6), 512–521.

Montazeri-Gh, M., Fashandi, S. A. M. & Abyaneh, S. (2018). Real-time simulation test-bed for an industrial gas turbine engine's controller. *Mechanics & Industry*, 19(3), 311.

Mu, J. & Rees, D. (2004). Approximate model predictive control for gas turbine engines. *Proceedings of the 2004 American Control Conference*, 6, 5704–5709.

Mu, J., Rees, D. & Liu, G. (2005). Advanced controller design for aircraft gas turbine engines. *Control Engineering Practice*, 13(8), 1001–1015.

Muir, D. E., Saravanamuttoo, H. I. & Marshall, D. (1989). Health monitoring of variable geometry gas turbines for the Canadian Navy.

Nguyen, T. V. (2000). *A method to identify the parametric dynamic model of a single-shaft gas turbine engine*. (Ph.D. thesis, Colorado State University).

Niu, L. & Liu, X. (2008). Multivariable generalized predictive scheme for gas turbine control in combined cycle power plant. *2008 IEEE Conference on Cybernetics and Intelligent Systems*, pp. 791–796.

Otto, E. W. & Taylor III, B. L. (1951). Dynamics of a turbojet engine considered as a quasi-static system.

Oviedo, J. J. E., Vandewalle, J. P. & Wertz, V. (2006). *Fuzzy logic, identification and predictive control*. Springer Science & Business Media.

Pandey, A., de Oliveira, M. & Moroto, R. H. (2018). Model predictive control for gas turbine engines. *ASME Turbo Expo 2018: Turbomachinery Technical Conference and Exposition*.

Petkovic, D., Banjac, M., Milic, S., Petrovic, M. V. & Wiedermann, A. (2019). Modelling the Transient Behaviour of Gas Turbines. *Turbo Expo: Power for Land, Sea, and Air*, 58554, V02AT45A014.

Pires, T. S., Cruz, M. E., Colaço, M. J. & Alves, M. A. (2018a). Application of nonlinear multivariable model predictive control to transient operation of a gas turbine and NOX emissions reduction. *Energy*, 149, 341–353.

Pires, T. S., Cruz, M. E., Colaço, M. J. & Alves, M. A. (2018b). Nonlinear model predictive control applied to transient operation of a gas turbine. *Journal of Sustainable Development of Energy, Water and Environment Systems*, 6(4), 770–783.

Pivoňka, P. & Nepevnỳ, P. (2005). Generalized predictive control with adaptive model based on neural networks. *Proceedings of the 6th WSEAS international conference on Neural networks*, pp. 1–4.

Razak, A. (2007). *Industrial gas turbines: performance and operability*. Elsevier.

Richter, H. (2011). *Advanced control of turbofan engines*. Springer Science & Business Media.

Rooney, N. & Patterson, D. (2007). A weighted combination of stacking and dynamic integration. *Pattern recognition*, 40(4), 1385–1388.

Rosini, A., Palmieri, A., Lanzarotto, D., Procopio, R. & Bonfiglio, A. (2019). A Model Predictive Control Design for Power Generation Heavy-Duty Gas Turbines. *Energies*, 12(11), 2182.

Rowen, W. I. (1983). Simplified mathematical representations of heavy-duty gas turbines.

Royce, R. (2015). *The jet engine*. John Wiley & Sons.

Rumelhart, D. E., Hinton, G. E. & Williams, R. J. (1985). *Learning internal representations by error propagation*.

Rusnak, A., Fikar, M., Najim, K. & Mészáros, A. (1996). Generalized predictive control based on neural networks. *Neural Processing Letters*, 4(2), 107–112.

Saleh, E. B. E. (2017). *Modeling and Simulation of A Double Spool Turbofan Engine Using SIMULINK®*. (Ph.D. thesis, Zagazig University Zagazig).

Salehi, A. & Montazeri-Gh, M. (2018). Black box modeling of a turboshaft gas turbine engine fuel control unit based on neural NARX. *Proceedings of the Institution of Mechanical Engineers, Part M: Journal of Engineering for the Maritime Environment*.

Salehi, A. & Montazeri-GH, M. (2020). Design and HIL-based verification of the fuel control unit for a gas turbine engine. *Proceedings of the Institution of Mechanical Engineers, Part G: Journal of Aerospace Engineering*, 0954410020910593.

Sanghi, V., Lakshmanan, B. & Sundararajan, V. (2000). Survey of advancements in jet-engine thermodynamic simulation. *Journal of Propulsion and Power*, 16(5), 797–807.

Sanjawadmath, V. & Suresh, R. (2017). Model based verification and validation of digital controller performance of a developmental aero gas turbine engine. *2017 Second International Conference on Electrical, Computer and Communication Technologies (ICECCT)*, pp. 1–6.

Sellers, J. F. & Daniele, C. J. (1975). *DYNGEN: A program for calculating steady-state and transient performance of turbojet and turbofan engines*. National Aeronautics and Space Administration.

Soares, S. G. & Araújo, R. (2015). A dynamic and on-line ensemble regression for changing environments. *Expert Systems with Applications*, 42(6), 2935–2948.

Sørensen, P. H., Nørgaard, M., Ravn, O. & Poulsen, N. K. (1999). Implementation of neural network based non-linear predictive control. *Neurocomputing*, 28(1-3), 37–51.

Spang III, H. A. & Brown, H. (1999). Control of jet engines. *Control Engineering Practice*, 7(9), 1043–1059.

Stamatis, A., Mathioudakis, K., Ruiz, J. & Curnock, B. (2001). Real time engine model implementation for adaptive control and performance monitoring of large civil turbofans. *ASME Turbo Expo 2001: Power for Land, Sea, and Air*.

Tahan, M., Muhammad, M. & Karim, Z. A. (2017). Performance evaluation of a twin-shaft gas turbine engine in mechanical drive service. *Journal of Mechanical Science and Technology*, 31(2), 937–948.

Talaat, M., Gobran, M. & Wasfi, M. (2018). A hybrid model of an artificial neural network with thermodynamic model for system diagnosis of electrical power plant gas turbine. *Engineering Applications of Artificial Intelligence*, 68, 222–235.

Tarik, M., Omar, M., Abdullah, M. & Ibrahim, R. (2017). Modelling of dry low emission gas turbine using black-box approach. *Region 10 Conference, TENCON 2017-2017 IEEE*, pp. 1902–1906.

Tayarani-Bathaie, S. S., Vanini, Z. S. & Khorasani, K. (2014). Dynamic neural network-based fault diagnosis of gas turbine engines. *Neurocomputing*, 125, 153–165.

Theoklis, N., Jafari, S. & Li, Z. (2019). Advanced constraints management strategy for real-time optimization of gas turbine engine transient performance.

Thirunavukarasu, E. (2013). Modeling and simulation study of a dynamic gas turbine system in a virtual test bed environment.

Tsoutsanis, E., Meskin, N., Benammar, M. & Khorasani, K. (2013). Dynamic performance simulation of an aeroderivative gas turbine using the matlab simulink environment. *ASME 2013 International Mechanical Engineering Congress and Exposition*.

Van Essen, H. & De Lange, H. (2001). Nonlinear model predictive control experiments on a laboratory gas turbine installation. *J. Eng. Gas Turbines Power*, 123(2), 347–352.

Vroemen, B., Van Essen, H., Van Steenhoven, A. & Kok, J. (1999). Nonlinear model predictive control of a laboratory gas turbine installation.

Walsh, P. P. & Fletcher, P. (2004). *Gas turbine performance*. John Wiley & Sons.

Wang, C. (2016). Transient performance simulation of gas turbine engine integrated with fuel and control systems.

Wang, L. (2009). *Model predictive control system design and implementation using MATLAB®*. Springer Science & Business Media.

Wang, W., Xu, Z., Tang, R., Li, S. & Wu, W. (2014). Fault detection and diagnosis for gas turbines based on a kernelized information entropy model. *The Scientific World Journal*, 2014.

Wen, L., Dong, Y. & Gao, L. (2019). A new ensemble residual convolutional neural network for remaining useful life estimation. *Math. Biosci. Eng*, 16, 862–880.

Widrow, B. & Hoff, M. E. (1960). *Adaptive switching circuits*.

Xu, Y., Xu, R. & Yan, W. (2017). Power plant performance modeling with concept drift. *2017 International Joint Conference on Neural Networks (IJCNN)*, pp. 2096–2103.

Yazar, I., Yasa, T. & Kiyak, E. (2017). Simulation-based steady-state aero-thermal model for small-scale turboprop engine. *Aircraft Engineering and Aerospace Technology*.

Ye, Q., Lou, X. & Sheng, L. (2017). Generalized predictive control of a class of MIMO models via a projection neural network. *Neurocomputing*, 234, 192–197.

Yu, B. & Shu, W. (2017). Research on Turbofan Engine Model above Idle State Based on NARX Modeling Approach. *IOP Conference Series: Materials Science and Engineering*, 187(1), 012002.

Zhang, C. & Ma, Y. (2012). *Ensemble machine learning: methods and applications*. Springer.

Zhou, Q., Yin, Z., Zhang, H., Wang, T., Sun, W. & Tan, C. (2020). Performance analysis and optimized control strategy for a three-shaft, recuperated gas turbine with power turbine variable area nozzle. *Applied Thermal Engineering*, 164, 114353.

Zhu, P. & Saravanamuttoo, H. (1992). Simulation of an advanced twin-spool industrial gas turbine.